UDC 520/524 (082)

YU ISSN 0373-3742
YU ISBN 86-80019-01-1

ПУБЛИКАЦИЈА АСТРОНОМСКЕ ОПСЕРВАТОРИЈЕ У БЕОГРАДУ
PUBLIKACIJA ASTRONOMSKE OPSERVATORIJE U BEOGRADU
No. 73

PROCEEDINGS OF THE THIRD BULGARIAN-SERBIAN ASTRONOMICAL METING

May 13-15, 2002, Gjolechitsa, Bulgaria

Edited by G. Ivanov, M. S. Dimitrijević and P. Jovanović

БЕОГРАД
2002

PUBL. ASTRON. OBS. BELGRADE No. 73, 1-286 BELGRADE JULY 2002

PUBLICATIONS OF THE ASTRONOMICAL OBSERVATORY OF BELGRADE

FOUNDED IN 1947

Published and copyright © by Astronomical Observatory, Volgina 7, 11000 Belgrade, Yugoslavia

Director of the Astronomical Observatory: Dr Milan S. Dimitrijević
Internet address `http://www.aob.bg.ac.yu`

The publication of this issue is financially supported by the Ministry of Sciences and Technology of Serbia and by the Federal Ministry of Development, Science and Environmental Protection.

Number of copies / тираж : 300

Production: INKA d. o. o., Tikveška 16, Beograd

UDC 520/524 (082)

YU ISSN 0373-3742
YU ISBN 86-80019-01-1

ПУБЛИКАЦИЈЕ АСТРОНОМСКЕ ОПСЕРВАТОРИЈЕ У БЕОГРАДУ
PUBLICATIONS OF THE ASTRONOMICAL OBSERVATORY OF BELGRADE

Св. 73 No. 73

PROCEEDINGS OF THE THIRD BULGARIAN-SERBIAN ASTRONOMICAL MEETING

May 13-15, 2002, Gjolechitsa, Bulgaria

Edited by G. Ivanov, M. S. Dimitrijević and P. Jovanović

БЕОГРАД
2002

PUBL. ASTRON. OBS. BELGRADE No. 73, 1–286 BELGRADE JULY 2002

Contents

Publ. Astron. Obs. Belgrade. No. 73 (2002), 5 - 5

ПРИВЕТСТВИЕ

Уважаеми гости,

Дами и господа,

Позволете ми най-сърдечно да ви поздравя с добре дошли в Научната станция на Софийския университет "Св. Климент Охридски" в планината Рила на Третия българо-сръбски симпозиум. Първият симпозиум бе проведен в гр. Белоградчик. Той бе много успешен. В отпечатания от Астрономическата обсерватория – Белград "PROCEDINGS OF THE FIRST BULGARIAN-YUGOSLAV ASTRONOMICAL MEETING", редактиран от проф. Милан Димитриевич, Лука Попович и Милчо Цветков, бяха публукувани 7 доклада от български и 8 от югославски астрономи. Обаче общият брой на участниците в първия симпозиум бе 27 души. На третия симпозиум, поради финансови трудности, са поканени само 4 доклада, по два от българска и сръбска страна, но приоритет е даден на постерната сесия. Надяваме се, че по този начин ще имаме възможност да осъществим по-добри и по-ефективни научни контакти между българските и сръбските астрономи. Катедрата по астрономия е много щаслива, че в нейно лице Софийския университет "Св. Климент. Охридски" е един от инициаторите за провеждането на този симпозиум. Катедрата по астрономия се надява, че провеждането на регулярни българо-сръбски симпозиуми през две години ще се превърне в традиция, което ни дава увереност за перспективно научно сътрудничество между българските и сръбските астрономи. Катедрата по астрономия е убедена, че географската близост на България и Сърбия е допълнително условие за ползотворно научно сътруничество в астрономията.

Проф. дфн Георги Иванов,
ръководител на Катедра Астрономия
при Софийския университет "Св. Кл. Охридски"

Publ. Astron. Obs. Belgrade. No. 73 (2002), 7 - 8

ПРИВЕТСТВИЕ

Уважаеми колеги, скъпи приятели,

През средата на май 1998 г. Милчо Цветков и аз в София мечтаехме да организираме българо - сръбска конференция. Аз му разказвах, че докато в Югославия имаше единствена телевизия всички ние – сърби, македонци, словенци се разбирахме, а сега за нашите деца македонският и словенският са чужди езици. Аз му казвах, че ако нашите младежи общуват, бързо биха се разбрали. Говорихме си, че между отделни колеги – сърби и българи има контакти, но младите нямат полза от това. Нашата цел беше да съберем младите да общуват и за в бъдеще да стане както до 1974 год. в Югославия, когато всички астрономи говореха на своите езици и се разбираха. Защото ние, за разлика от румънците и гърците, можем с малко усилия от двете страни да се разбираме. Ние се договорихме тази първа среща да бъде в Белоградчик и през август 1998 г. аз докарах пълен автобус с всички млади хора от Белградската обсерватория. Винаги ще запомним пристигането си, когато Милчо ме прегърна и каза "Направихме го". Това е третата среща и се надявам тези срещи да станат традиция. Тези конференции ни позволиха да се запознаем, да дискутираме съвместно научните проблеми, с които се занимаваме и заедно да ги публикуваме. Освен това имахме удоволствието да разширим кръга на приятелите си. Аз бих използвал този момент да благодаря на Милчо Цветков, без който тези конференции не биха станали, и на Катя, която направи всичко възможно дружбата между българските и сръбските астрономи да се реализира. Искам да благодаря на Александър и Ренада Антови, които оказаха безрезервна подкрепа и организираха незабравима среща в Белоградчик. Искам да благодаря на проф. Иванов, който от началото подкрепи нашето начинание и организира тази среща. Искам да благодаря на Васил Попов за безрезервната подкрепа за реализиране на нашата мечта, и още на Валери Голев. Когато попитах проф. Иванов и Милчо и Катя Цветкови кой е вложил най-много време и труд за да се организира тази конференция, без колебание те ми отговориха – това е Анеля Станева, на която искам да изразя голямата си благодарност. Когато попитах: кой още е вложил своя ентусиазъм , време и труд, те ми отговориха "Радостин Куртев", на когото също искам да изкажа благодарност.

Искам да благодаря на Лука Попович, който още от самото начало вложи много труд и ентусиазъм за организирането на трите конференции и за реализирането на моята и Милчова идея. Искам да благодаря и на моя приятел Миодраг Дачич.

Големият руски поет Александър Блок е казал:"Ако нямате исторически източници, значи нямате и история." Миодраг Дачич, чиито фотографии от миналите конференции имаме в сборниците, осигури източниците за историята на балканската астрономия, чиито страници днес пишем.

Ние сме засяли семената на приятелство, любов и сътрудничество. За да пораснат и наберат сила, те трябва да се пазят. Нека нашите спомени за радостта и удоволствието от съвместните срещи ги защитават и развиват.

Желая на всички успешна работа, много удоволствие и радост и разширяване на нашето приятелство.

Милан Димитриевич
Директор на Белградската обсерватория

Publ. Astron. Obs. Belgrade No. 73 (2002), 9 - 10

ПОЗДРАВНИ ГОВОР

Уважене колеге, драги пријатељи.

Половином маја 1998. године, Милчо Цветков и ја смо у Софији маштали о томе да организујемо Бугарско - српску астрономску конференцију. Ја сам причао да док је у Југославији била јединствена телевизија било је нормално да Словенац, Македонац и Србин говоре на својим језицима и да се разумеју, а да су данас, за нашу децу, македонски и словеначки страни језици. Говорио сам да ако би се наши млади мало дружили, врло брзо би се међусобно разумели.

Разговарали смо о томе да је између српских и бугарских астронома било појединачних посета и сарадње, али да млади од тога нису имали користи. Наш циљ је био да доведемо младе да међусобно разговарају и да у будућности, као у Југославији до 1974, српски и бугарски астрономи говоре сваки на своме језику и да се разумеју. Јер ми, за разлику од Румуна или Грка, можемо са мало напора то да учинимо.

Договорили смо се да прва конференција буде исте 1998. године у Белоградчику и ја сам у августу довео пун аутобус и све маладе са Опсерваторије. Увек ћу памтити када ме је на доласку Милчо загрлио и радосно рекао - Направихме го.

Ово је трећа конференција и надам се да ће овакви сусрети постати традиција. Ове конференције омогућиле су нам да се упознамо, заједнички продискутујемо научне проблеме којима се бавимо и заједнички публикујемо своје радове. Осим тога, дале су нам велико задовољство, као и могућност да проширимо круг пријатеља.

Ја бих искористио ову прилику да се захвалим Милчи Цветкову, без кога ових конференција не би било и Катји која је учинила све да се наш заједнички сан о дружењу младих бугарских и српских астронома реализује.

Хтео бих да се захвалим и Александру и Ренади Антовим, који су нас безрезервно подржали и организовали незаборавно дружење у Белоградчику.

Хтео бих да се захвалим професору Георги Иванову, који је од почетка подржавао нашу идеју и организовао ову конференцију.

Хтео бих да се захвалим Василу Попову за безрезервну подршку у реализацију нашег маштања. За безрезервну подршку желим да се захвалим и Валерију Голеву.

Када сам питао професора Иванова, Милчу и Катју Цветкове, ко је највише

времена и труда уложио да се организује ова конференција, без оклевања су ми рекли да је то Анелија Станева, којој желим да изразим велику захвалност.

Када сам их питао ко је још уложио свој ентузијазам, време и труд, рекли су ми да је то Радостин Куртев коме желим да се захвалим.

желео бих да се захвалим и Луки Поповићу, који је у организацију све три конференције уложио велики труд и који је на остварењу ове наше идеје са великим ентузијазмом радио од почетка.

Хтео бих да се захвалим и моме пријатељу Миодрагу Дачићу. Велики руски песник Александар Блок је рекао: "Ако немате историјске изворе, немате историју." Дачић, чије фотографије са претходних конференција имамо у књигама, обезбеђује историјске изворе за историју астрономије Балкана чије странице данас исписујемо.

Посејали смо семе пријатељства, љубави и сарадње. Да би биљка порасла и ојачала, треба да се негује. Нека је штите и развијају наше успомене на радост заједничког дружења на овим конференцијама. желим вам свима успешан рад, пуно задовољства и радости и продубљивање нашег пријатељства.

Милан С. Димитријевић
Директор Београдске астрономске опсерваторије

Publ. Astron. Obs. Belgrade. No. 73 (2002), 11 - 12

ПРИВЕТСТВИЕ ОТ НАЦОНАЛНИЯ АСТРОНОМИЧЕСКИ СЪЮЗ И ОТ СЪЮЗА НА АСТРОНОМИТЕ В БЪЛГАРИЯ

Уважаеми колеги,

За мен е особена чест от името на Националния комитет по астрономия и от името на Съюза на астрономите в България да поздравя Вас участниците в Третия българо-сръбски семинар с добре дошли и да Ви пожелая успешна работа през следващите три дни.

Тази среща ми напомня далечната 1981 година. Тогава в Дубровник, на брега на Адриатика установихме първите лични контакти между нас и вас, колегите от Белградската астрономическа обсерватория. Това стана по време на поредната *ERMA-6.*След закриването на симпозиума *проф. Телеки (светла му памет)* ни покани да посетим Белградската астрономическа обсерватория. Неколкодневното посещение беше действително едно великолепно преживяване. От сутрин до вечер обсъждахме различни проблеми, разглеждахме обсерваторията, посетихме Белградския университет и някои забележителности на Белград. Групата, която се образува спонтанно притежаваше особена колоритност. В нея участваха и двама известни американски астрономи: проф. Елеонор Хелин и д-р Рон Хелин от JPL и Паломарската обсерватория. Те бяха поканени от Българската академия на науките да посетят Националната астрономическа обсерватория – Рожен и съчетаваха участието си в *ERMA-6* с посещението си у нас. Тук ще си позволя да покажа една снимка от онова време на част от спонтанно образувалата се група.

Темите на разговорите естествено бяха най-разнообразни – от чисто теоретични до нааблюдателни. Последните бяха свързани с възможностите на новата обсерватория у нас както и с планирания по това време строеж на обсерватория на територията на тогавашната Югославия с 1,5 м. телескоп.

Дискусиите по времето на това кратко посещение позволиха едно принципно договаряне за бъдещо сътрудничество. Договорихме се през следващата 1982 г. да се съберем отново и продължим дискусиите относно бъдещата съвместна работа.

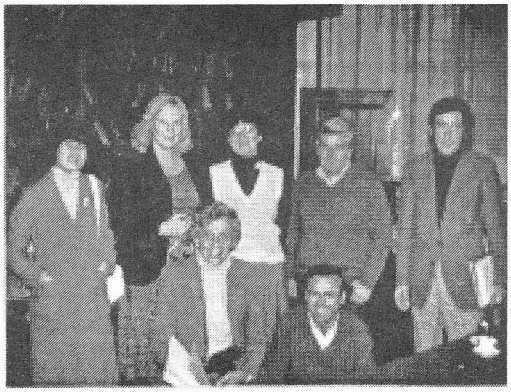

БЕЛГРАД – 1981 г.

А. Стоящи от ляво на дясно:
Виолета Иванова – България,
Елеонор Хелин – САЩ,
Войслава Протич – Югославия,
Иван Паквор - Югославия,
Мике Кузманоски - Югославия;

В. Седящи:
Владимир Шкодрав –България,
Драгомир Олевич - Югославия.

Срещата отново се състоя в Белградската астрономическа обсерватория. Отново, и по-детайлно обсъдихме възможностите на току що откритата Национална астрономическа обсерватория – Рожен, както и областите , в които бихме могли да си сътрудничим. По време на последното обсъждане беше решено да подготвим проект на рамков договор за сътрудничество, който да бъде подписан от ръководствата на двете институции.

Скоро след приключване на разговорите договорът беше подписан, но за съжаление така съставен, че не можа да проработи. Тук не бих искал да обсъждам обективните и субективни причини за това.

Ще отбележа, че през цялото време разговорите бяха изключително колегиални, духът беше приятелски и дружелюбен. Надявам се , че този дух на близост и приятелство ще продължи и сега по време на на тази среща.

Всички знаем, че астрономията е интернационална наука и отклонението от този аспект не би било полезен за самата нея. Иска ми се контактите и разговорите да продължат и да се развиват. Това се налага още повече в наше време, когато съществуват определени условия Националната астрономическа обсерватория-Рожен със своето обурудване се превърне в общ астрономически център в Югоизточна Европа, което е и в действителност.

Проф. дфн Владимир Шкодров
Председател на Националния комитет по астрономия в България,
Председател на Съюза на астрономине в България

Publ. Astron. Obs. Belgrade No. 73 (2002), 13 - 26 *Invited lecture*

APPROXIMATE METHODS FOR STARK BROADENING CALCULATIONS FOR ASTROPHYSICALLY IMPORTANT SPECTRAL LINES

MILAN S. DIMITRIJEVIĆ, LUKA Č. POPOVIĆ, MIODRAG DAČIĆ, ZORICA CVETKOVIĆ
Astronomical Observatory, Volgina 7, 11160-Belgrade 74, Serbia, Yugoslavia
E-mail mdimitrijevic@aob.aob.bg.ac.yu
E-mail lpopovic@aob.oab.bg.ac.yu
E-mail mdacic@aob.oab.bg.ac.yu
E-mail zcvetkovic@aob.aob.bg.ac.yu

Abstract. A review of approximate methods for calculation of spectral line profiles in hot stellar plasma has been presented. We have discussed in detail the modified semiempirical method for Stark broadening parameters determination as well as the regularities and systematic trends for interpolation of new data and critical evaluation of existing ones.

1. INTRODUCTION

Since the atmospheric composition of a star is not known *a priori*, and many interesting groups of stars exist with very peculiar abundances as compared to the Sun, stellar spectroscopy depends on very extensive list of elements and line transitions with their atomic and line broadening parameters.

The interest for a very extensive list of line broadening data is additionally stimulated by the development of space astronomy, since with instruments like Goddhard High Resolution Spectrograph (GHRS) on Hubble Space Telescope, an extensive amount of high quality spectroscopic information over large spectral regions of all kind of celestial objects has been and will be collected, stimulating the spectral–line–shape research. The dramatic increase of accuracy and resolution is well illustrated in Fig. 1 where the χ Lupi UV spectrum obtained by IUE and GHRS are compared

Development of computers also stimulates the need for a large amount of atomic and spectroscopic data. Particularly large number of data is needed for example for opacity calculations. An illustrative example might be the article on the calculation of opacities for classical Cepheid models (Iglesias et al. 1990), where 11 996 532 spectral lines have been taken into account (45 lines of H, 45 of He, 638 of C, 54 of N, 2 390 of O, 16 030 of Ne, 50 170 of Na, 105 700 of Mg, 145 200 of Al, 133 700 of Si, 12 560 of Ar and 11 530 000 of Fe), and where Stark broadening is included. Another good

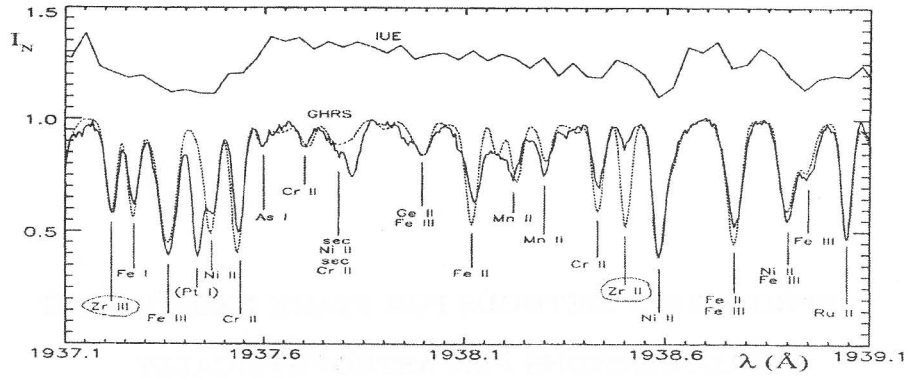

Fig. 1: The UV spectrum of χ Lupi obtained with GHRS and with IUE satellite (Leckrone et al. 1993). The resolution of GHRS spectrum is 0.0023 nm and the maximal signal to noise ratio is 95 (Brandt et al. 1999). The full line at GHRS spectrum is observed and the dotted synthesized one.

example for the need of an extensive set of atomic and spectroscopic data including Stark broadening is the modeling of stellar atmospheres. For example, PHOENIX (see Hauschildt and Baron, 1999 and references therein) computer code for the stellar modelling includes a database containing 42 x 10^6 atomic/ionic spectral lines.

Interesting investigations which shows the possibilities opened with the development of computer technology and indicating the need for as much as possible larger amount of spectroscopic and atomic data, are calculations of equivalent width changes with the age in starburst stellar clusters and galaxies (Gonzales-Delgado et al. 1999). In this research the change of particular hydrogen and helium lines equivalent widths during 500 milion years, has been calculated and compared with observations of stellar clusters and starburst galaxies. Calculations have been done in two steps. First, the population of stars of different spectral types, as a function of age are calculated, and then the profiles of the lines are synthesized by adding the different contributions from stars. For spectral line profiles synthesis the effects of natural, Stark, neutral atom impact and thermal Doppler broadening have been taken into account.

We draw attention here, that for temperatures of around 10 000 K or higher, hydrogen is mainly ionized and Stark broadening is the principal pressure broadening mechanism of spectral lines. Consequently, astronomers often need Stark broadening data for a large amount of spectral lines. In spite of the fact that very sophysticated methods for Stark broadening calculations exist, as e.g. quantum mechanical strong coupling method (see e.g. Dimitrijević et al. 1981, Dimitrijević 1996 and references therein) or semiclassical approach (see e.g. Jones et al. 1971, Benett and Griem 1971, Griem 1974, Sahal–Bréchot 1969ab), approximate approaches are often the unique way to obtain the needed information. Moreover, they may be used for the critical evaluation of existing theoretical and experimental data. The aim of this lecture is to present some of such methods, in particular methods developed in Serbia.

2. MODIFIED SEMIEMPIRICAL METHOD FOR STARK BROADENING AND ASTROPHYSICAL APPLICATIONS

It is twenty two years from the formulation of the modified semiempirical (MSE) approach (Dimitrijević and Konjević 1980) for the calculation of Stark broadening parameters for non-hydrogenic ion spectral lines. Within this period the considered method has been applied successfully many times for different problems in astrophysics and physics. According to the modified semiempirical (MSE) approach (Dimitrijević and Konjević 1980, 1981, 1987, Dimitrijević and Kršljanin 1986, Dimitrijević and Popović 1993, 2001, Popović and Dimitrijević 1996a) the electron impact full width (FHWM) of an isolated ion line is given as

$$W_{MSE} = N\frac{8\pi}{3}\frac{\hbar^2}{m^2}\left(\frac{2m}{\pi kT}\right)^{1/2}\frac{\pi}{\sqrt{3}}\frac{\lambda^2}{2\pi c}\cdot\{\sum_{\ell_i\pm1}\sum_{A_{i'}J_{i'}}\vec{\Re}^2[n_i\ell_iA_iJ_i,n_i(\ell_i\pm1)A_{i'}J_{i'}]\widetilde{g}(x_{\ell_i,\ell_i\pm1})+$$

$$+\sum_{\ell_f\pm1}\sum_{A_{f'}J_{f'}}\vec{\Re}^2[n_f\ell_fA_fJ_f,n_f(\ell_f\pm1)A_{f'}J_{f'}]\widetilde{g}(x_{\ell_f,\ell_f\pm1})+\left(\sum_{i'}\vec{\Re}^2_{ii'}\right)_{\Delta n\neq0}g(x_{n_i,n_i+1})+ \tag{1}$$

$$+\left(\sum_{f'}\vec{\Re}^2_{ff'}\right)_{\Delta n\neq0}g(x_{n_f,n_f+1})\},$$

and the corresponding Stark shift as

$$d_{MSE} = N\frac{4\pi}{3}\frac{\hbar^2}{m^2}\left(\frac{2m}{\pi kT}\right)^{1/2}\frac{\pi}{\sqrt{3}}\frac{\lambda^2}{2\pi c}\cdot\{\sum_{A_{i'}J_{i'}}\sigma_{J_iJ_{i'}}\vec{\Re}^2[n_i\ell_iA_iJ_i,n_i(\ell_i+1)A_{i'}J_{i'}]\widetilde{g}_{sh}(x_{\ell_i,\ell_i+1})-$$

$$-\sum_{A_{i'}J_{i'}}\sigma_{J_iJ_{i'}}\vec{\Re}^2[n_i\ell_iA_iJ_i,n_i(\ell_i-1)A_{i'}J_{i'}]\widetilde{g}_{sh}(x_{\ell_i,\ell_i-1})$$

$$-\sum_{A_{f'}J_{f'}}\sigma_{J_fJ_{f'}}\vec{\Re}^2[n_f\ell_fA_fJ_f,n_f(\ell_f+1)A_{f'}J_{f'}]\widetilde{g}_{sh}(x_{\ell_f,\ell_f+1})+$$

$$+\sum_{A_{f'}J_{f'}}\sigma_{J_fJ_{f'}}\vec{\Re}^2[n_f\ell_fA_fJ_f,n_f(\ell_f-1)A_{f'}J_{f'}]\widetilde{g}_{sh}(x_{\ell_f,\ell_f-1})+\left(\sum_{i'}\vec{\Re}^2_{ii'}\right)_{\Delta n\neq0}g_{sh}(x_{n_i,n_i+1})-$$

$$-2\sum_{i'(\Delta E_{ii'}<0)}\sum_{A_{i'}J_{i'}}\vec{\Re}^2(n_i\ell_iA_iJ_i,n_i\ell_{i'}A_{i'}J_{i'})g_{sh}(x_{\ell_i,\ell_{i'}})-\left(\sum_{f'}\vec{\Re}^2_{ff'}\right)_{\Delta n\neq0}g_{sh}(x_{n_f,n_f+1})+ \tag{2}$$

$$+2\sum_{f'(\Delta E_{ff'}<0)}\sum_{A_{f'}J_{f'}}\vec{\Re}^2(n_f\ell_fA_fJ_f,n_f\ell_{f'}A_{f'}J_{f'})g_{sh}(x_{\ell_f,\ell_{f'}})+\sum_k\delta_k\}$$

where the initial level is denoted as i and the final one as f and the square of the matrix element
$\{\vec{\Re}^2[n_k\ell_k A_k J_k, (\ell_k \pm 1)A_{k'}J_{k'}], \quad k = i, f\}$ is

$$\vec{\Re}^2[n_k\ell_k A_k J_k, n_k(\ell_k \pm 1)A'_k J'_k] = \frac{\ell_>}{2J_k+1} Q[\ell_k A_k, (\ell_k \pm 1)A'_k] Q(J_k, J'_k)[R^{n^*_k(\ell_k\pm1)}_{n^*_k\ell_k}]^2 \tag{3}$$

Also,
$\ell_> = \max(\ell_k, \ell_k \pm 1)$ and

$$(\sum_{k'} \vec{\Re}^2_{kk'})_{\Delta n\neq 0} = (\frac{3n^*_k}{2Z})^2 \frac{1}{9}(n^{*2}_k + 3\ell^2_k + 3\ell_k + 11) \tag{4}$$

In Eqs. (1) and (2)

$$x_{\ell_k,\ell_{k'}} = \frac{E}{\Delta E_{\ell_k,\ell_{k'}}}, \quad k = i, f;$$

and $E = \frac{3}{2}kT$
is the electron kinetic energy and $\Delta E_{\ell_k,\ell_{k'}} = |E_{\ell_k} - E_{\ell_{k'}}|$ is the energy difference between levels ℓ_k and $\ell_k \pm 1$ $(k = i, f)$,

$$x_{n_k,n_k+1} \approx \frac{E}{\Delta E_{n_k,n_k+1}},$$

where for $\Delta n \neq 0$, the energy difference between energy levels with n_k and n_k+1, $\Delta E_{n_k,n_k+1}$ is estimated as $\Delta E_{n_k,n_k+1} \approx 2Z^2 E_H/n^{*3}_k$, $n^*_k = [E_H Z^2/\ (E_{ion} - E_k)]^{1/2}$ is the effective principal quantum number, Z is the residual ionic charge (for example Z=1 for neutrals) and E_{ion} is the appropriate spectral series limit.

If we have an oscillator strength, e.g. from literature, the corresponding matrix element may be calculated as

$$\vec{\Re}^2_{k,k'} \approx 3\frac{E_H}{E_{k'} - E_k} \cdot f_{k'k} \qquad (E_{k'} > E_k), \quad k = i, f$$

or

$$\vec{\Re}^2_{k,k'} \approx 3\frac{E_H}{E_k - E_{k'}} \frac{2k'+1}{2k+1} \cdot f_{kk'} \qquad (E_{k'} < E_k), \quad k = i, f \tag{5}$$

where $f_{k'k}$ (for $E_{k'} > E_k$) and $f_{kk'}$ (for $E_{k'} < E_k$) are oscillator strengths and E_H is the hydrogen ionization energy.

Possible configuration mixing may be taken into account (see e.g. Dimitrijević and Popović 1993) if one represents $\vec{\Re}^2_{\alpha\beta}$ as

$$\vec{\Re}^2_{\alpha\beta} = K_\alpha \cdot \vec{\Re}^2_{\alpha\alpha'} + K_\beta \cdot \vec{\Re}^2_{\beta\beta'}, \tag{6}$$

where K_α and K_β are mixing coefficients for two configurations and $K_\alpha + K_\beta = 1$.

In Eqs. (1 - 4) N and T are electron density and temperature, respectively, while $Q(\ell A, \ell' A')$ and $Q(J, J')$ are multiplet and line factors. The value of A depends on the coupling approximation (see e.g. Dimitrijević and Popović 1996a). In the case of the LS coupling approximation, applied here, $A = L$, for the jK approximation $A = K$ and for the jj approximation $A = j$. The $[R^{n_k^* \ell_k \pm 1}_{n_k^* \ell_k}]$ is the radial integral, and with $g(x)$ (Griem 1968), $\widetilde{g}(x)$ (Dimitrijević and Konjević 1980) and $g_{sh}(x)$ (Griem 1968), $\widetilde{g}_{sh}(x)$ (Dimitrijević and Kršljanin 1986) are denoted the corresponding Gaunt factors for width and shift, respectively. The factor $\sigma_{kk'} = (E_{k'} - E_k)/|E_{k'} - E_k|$, where E_k and $E_{k'}$ are the energy of the considered and its perturbing level. The sum $\sum_k \delta_k$ is different from zero only if perturbing levels with $\Delta n \neq 0$ strongly violating the assumed approximations exist, so that they should be taken into account separately, and may be evaluated as

$$\delta_i = \pm \vec{\Re}^2_{ii'} [g_{sh}(\frac{E}{\Delta E_{i,i'}}) \mp g_{sh}(x_{n_i, n_i+1})], \tag{7}$$

for the upper level, and

$$\delta_f = \mp \vec{\Re}^2_{ff'} [g_{sh}(\frac{E}{\Delta E_{f,f'}}) \mp g_{sh}(x_{n_f, n_f+1})], \tag{8}$$

for the lower level. In eqs. (7) and (8) the lower signs correspond to $\Delta E_{kk'} < 0$, $k = i, f$.

In comparison with the full semiclassical approach (Sahal-Bréchot 1969ab, Griem 1974) and the Griem's semiempirical approach (Griem 1968) who needs practically the same set of atomic data as the more sophysticated semiclassical one, the modified semiempirical approach (Dimitrijević and Konjević 1980, 1981, 1987, Dimitrijević and Kršljanin 1986, Dimitrijević and Popović 1993, 2001, Popović and Dimitrijević 1996a) needs a considerably smaller number of such data. In fact, if there are no perturbing levels strongly violating the assumed approximation, for *e.g.* the line width calculations, we need only the energy levels with $\Delta n = 0$ and $\ell_{if} = \ell_{if} \pm 1$, since all perturbing levels with $\Delta n \neq 0$, needed for a full semiclasical investigation or an investigation within the Griem's semiempirical approach (Griem 1968), are lumped together and approximately estimated. Here, n is the principal and ℓ the orbital angular momentum quantum numbers of the optical electron and with i and f are denoted the initial and final state of the considered transition.

Due to the considerably smaller set of needed atomic data in comparison with the complete semiclassical (Sahal-Bréchot 1969ab, Griem 1974) or Griem's semiempirical (Griem 1968) methods, the MSE method is particularly useful for stellar spectroscopy depending on very extensive list of elements and line transitions with their atomic and line broadening parameters where it is not possible to use sophysticated theoretical approaches in all cases of interest.

The MSE method is also very useful whenever line broadening data for a large number of lines are required, and the high precision of every particular result is not so important like e.g. for opacity calculations or plasma modeling. Moreover, in the case of more complex atoms or multiply charged ions the lack of the accurate atomic data needed for more sophysticated calculations, makes that the reliability of the semiclassical results decreases. In such cases the MSE method might be very interesting as well.

3. SYMPLIFIED MSE FORMULA

For the astrophysical purposes, of particular interest might be the simplified semiempirical formula (Dimitrijević and Konjević 1987) for Stark widths of isolated, singly, and multiply charged ion lines applicable in the cases when the nearest atomic energy level ($j' = i'$ or f') where a dipolly allowed transition can occur from or to initial (i) or final (f) energy level of the considered line, is so far, that the condition $x_{jj'} = E/|E_{j'} - E_j| \leq 2$ is satisfied. In such a case full width at half maximum is given by the expression (Dimitrijević and Konjević 1987):

$$W(\mathring{A}) = 2.2151 \times 10^{-8} \frac{\lambda^2(\mathrm{cm}) N(\mathrm{cm}^{-3})}{T^{1/2}(\mathrm{K})} (0.9 - \frac{1.1}{Z}) \sum_{j=i,f} (\frac{3n_j^*}{2Z})^2 (n_j^{*2} - \ell_j^2 - \ell - 1). \quad (15)$$

Here, N and T are the electron density and temperature respectively, $E = 3kT/2$ is the energy of perturbing electron, $Z - 1$ is the ionic charge and n the effective principal quantum number. This expression is of interest for abundance calculations, as well as for stellar atmospheres research, since the validity conditions are often satisfied for stellar plasma conditions.

Similarly, in the case of the shift

$$d(\mathring{A}) = 1.1076 \times 10^{-8} \frac{\lambda^2(\mathrm{cm}) N(\mathrm{cm}^{-3})}{T^{1/2}(\mathrm{K})} (0.9 - \frac{1.1}{Z}) \frac{9}{4Z^2} \times$$

$$\times \sum_{j=i,f} \frac{n_j^{*2} \varepsilon_j}{2\ell_j + 1} \{(\ell_j + 1)[n_j^{*2} - (\ell_j + 1)^2] - \ell_j (n_j^{*2} - \ell_j^2)\}. \quad (16)$$

If all levels $\ell_{i,f} \pm 1$ exist, an additional summation may be performed in Eq. (16) to obtain

$$d(\mathring{A}) = 1.1076 \times 10^{-8} \frac{\lambda^2(\mathrm{cm}) N(\mathrm{cm}^{-3})}{T^{1/2}(\mathrm{K})} (0.9 - \frac{1.1}{Z}) \frac{9}{4Z^2} \sum_{j=i,f} \frac{n_j^{*2} \varepsilon_j}{2\ell_j + 1} (n_j^{*2} - 3\ell_j^2 - 3\ell_j - 1), \quad (17)$$

where $\varepsilon = +1$ for $j = i$ and -1 for $j = f$.

4. TESTS AND APPLICATIONS FOR DETERMINATION OF STARK BROADENING PARAMETERS

The modified semiempirical approach has been tested several times on numerous examples (Dimitrijević 1990a). In order to test this method, selected experimental data for 36 multiplets (7 different ion species) of triply–charged ions were compared with theoretical linewidths. The averaged values of the ratios of measured to calculated widths are as follows (Dimitrijević and Konjević 1980): for doubly charged ions 1.06 ± 0.32 and for triply–charged ions 0.91 ± 0.42. The assumed accuracy of the MSE approximation is about $\pm 50\%$, but it has been shown in Popović and Dimitrijević (1996b, 1998) and, Dimitrijević and Popović (2001) that the MSE approach, even in the case of the emitters with very complex spectra (e.g. Xe II and Kr II),

gives very good agreement with experimental measurements (in the interval ±30%). For example for Xe II, $6s - 6p$ transitions, the averaged ratio between experimental and theoretical widths is 1.15 ± 0.5 (Popović and Dimitrijević 1996b).

In order to complete as much as possible the needed Stark broadening data, Belgrade group (Milan S. Dimitrijević, Luka Č. Popović, Vladimir Kršljanin, Dragana Tankosić, Nenad Milovanović, Zoran Simić, Miodrag Dačić, Zorica Cvetković, Predrag Jovanović) used the modified semiempirical method to obtain the Stark width and in some cases shift data for a large number of spectral lines for the different atom and ion species. Up to now:

6 Fe II, 4 Pt II, 16 Bi II, 12 Zn II, 8 Cd II, 18 As II, 10 Br II, 18 Sb II, 8 I II, 20 Xe II, 138 Ti II, 3 La II, 16 Mn II, 14 V II, 6 Eu II, 37 Kr II, 6 Y II, 6 Sc II, 4 Be III, 4 B III, 13 S III, 8 Au II, 8 Zr II, 53 Ra II, 3 Mn III, 10 Ga III, 8 Ge III, 4 As III, 3 Se III, 6 Mg III, 6 La III, 5 Sr III, 8 V III, 210 Ti III, 9 C III, 7 N III, 11 O III, 5 F III, 6 Ne III, 8 Na III, 10 Al III, 5 Si III, 3 P III, 16 Cl III, 6 Ar III, 30 Zr III, 20 Co III 2 B IV, Cu IV, 30 V IV, 14 Ge IV, 7 C IV, 4 N IV, 4 O IV, 2 Ne IV, 4 Mg IV, 7 Si IV, 3 P IV, 2 S IV, 2 Cl IV, 4 Ar IV, 3 C V, 50 O V, 12 F V, 9 Ne V, 3 Al V, 6 Si V, 11 N VI, 28 F VI, 8 Ne VI, 7 Na VI, 15 Si VI, 6 P VI, and 1 Cl VI transitions have been calculated (see Dimitrijević and Popović 2001 and references therein). The shift data for 16 Bi II, 12 Zn II, 8 Cd II, 18 As II, 10 Br II, 18 Sb II , 8 I II, 20 Xe II, 5 Ar II, 6 Eu II, 14 V II, 8 Au II, 14 Kr II and 138 Ti II transitions have been calculated (see Dimitrijević and Popović 2001 and references therein). Moreover, 286 Nd II Stark widths have been calculated (Popović et al. 2001b) within the symplified modified semiempirical approach.

Calculations within the modified semiempirical approach, for comparison with experimental data or testing of the theory have been performed also for Stark widths for 14 Al I, 46 Al II, 12 Al III (Heading et al. 1997), 1 C IV, 1 N V, 1 O VI (Böttcher et al. 1988, Glenzer et al. 1992), 1 Ne VIII (Glenzer et al. 1992), 3 N III, 3 O IV, 3 F V, 2 Ne VI (Glenzer et al. 1994), 12 C IV (Ackermann et al. 1985), 4 C II, 5 N II, 3 O II, 4 F II, 3 Ne II (Blagojević et al. 1999), 1 N II (Milosavljević et al. 1999), 8 S II (Djeniže et al. 1990), 2 Ne VII (Wrubel et al. 1996), 4 N III, 2 F V (Blagojević et al. 1996), 2 Ne III, 2 Ar III, 2 Kr III, 2 Xe III (Konjević 1995), 3 Si III (Dimitrijević 1983), 3 Ne III, 2 Ar III, 2 Kr III, 2 Xe III (Konjević and Pittman 1987) transitions. Moreover, in Kobilarov and Konjević (1990) Stark widths and shifts for 2 Cl II and 6 Ar III lines have been calculated.

5. APPLICATION TO THE INVESTIGATION OF "ZIRCONIUM CONFLICT" IN χ LUPI STAR ATMOSPHERE

The electron-impact broadening is the main broadening mechanism in A and B type star atmospheres (see e.g. Popović et al. 1999). The electron-impact broadening data are needed for various problems in astrophysics, as e.g. for diagnostic and modeling of stellar plasma, investigation of its physical properties and for abundance determination. These investigations provide us with useful information for modeling of stellar evolution. As an example, the abundances study in stellar atmospheres provides evidences for the chemical composition of the stellar primordial cloud, processes occurring within the stellar interior, and the dynamical processes in stellar atmosphere.

The available abundance analysis for early-type stars show that about 10% - 20% of A and B stars have abundance anomalies, including anomalies in isotopic compositions

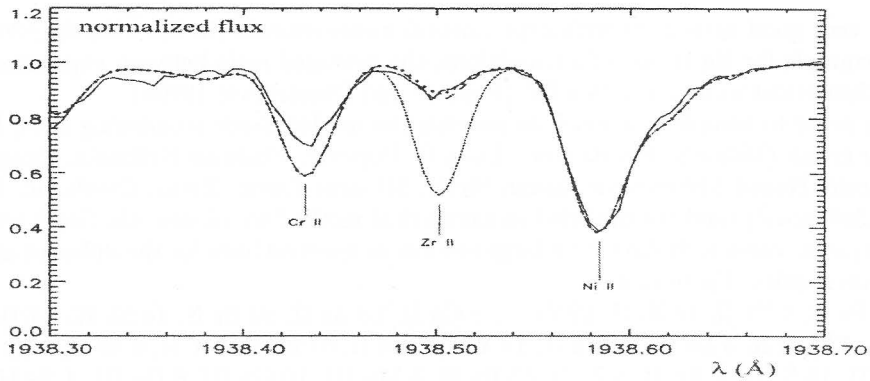

Fig. 2: The UV spectrum of the χ Lupi star within the 193.83 nm - 193.87 nm wavelength range. With the full line is denoted the spectrum obtained by GHRS. With the dotted line is shown the synthesized Zr II 4d5s5p $v^2D^o_{3/2}$ - $4d^25s$ $a^2D_{3/2}$ $\lambda = 193.85$ nm line obtained for zirconium abundance $\log(N_{Zr}/N_H) = -8.12$. These abundance value is obtained from Zr III lines. With - - - is denoted synthesized spectrum for zirconium abundance $\log(N_{Zr}/N_H) = -9.1$, and with larger dots for $\log(N_{Zr}/N_H) = -9.0$ (Leckrone et al. 1993).

(Leckrone et al. 1993). The abundance anomalies in these stars, called CP stars, have been caused by different hydrodynamical processes in the outer stellar layers (aided and mitigated by magnetic fields, weak stellar winds, turbulence, rotation mixing, etc.). In order to investigate these processes, atomic data for numerous lines of numerous emitters are needed.

For example the zirconium lines are present in spectra of HgMn stars (Cowley and Aikman 1975, Heacox 1979, Leckrone et al. 1993, Sikström et al. 1999). It is interesting that the zirconium abundance determination from weak Zr II optical lines and strong Zr III lines (detected in UV) is quite different (see Leckrone et al. 1993, Sikström et al. 1999) in HgMn star χ Lupi. This is illustrated in Fig. 2, where the UV spectrum of the χ Lupi star within the 193.83 nm - v 193.87 nm wavelength range is shown. With the full line is denoted the spectrum obtained by GHRS. With the dotted line is shown the synthesized Zr II 4d5s5p $v^2D^o_{3/2}$ - $4d^25s$ $a^2D_{3/2}$ $\lambda = 193.85$ nm line obtained for zirconium abundance $\log(N_{Zr}/N_H) = -8.12$. These abundance value is obtained from Zr III lines. With - - - is denoted synthesized spectrum for zirconium abundance $\log(N_{Zr}/N_H) = -9.1$, and with larger dots for $\log(N_{Zr}/N_H) = -9.0$ (Leckrone et al. 1993).

It is so called "zirconium conflict" and it was supposed by Sikström et al. (1999) that this difference is probably due to non adequate use of stellar models, e.g. if the influence of non-LTE effects or if diffusion is not taken into account.

Zirconium, often overabundant in HgMn stars (see Heacox 1979), is one member of Sr-Y-Zr triad, which is vital for the study of s-process nucleosynthesis and has been pointed as presenting a non-nuclear abundance pattern in HgMn stars. The most obvious interpretations of this anomaly are with the help of diffusion theory or with inclusion of non-LTE effects. However, it is of interest also to investigate the

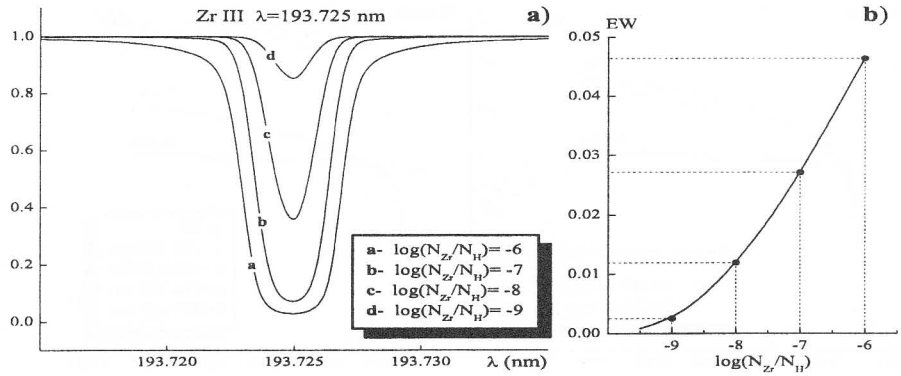

Fig. 3: The change of the Zr III $4d^2\ ^3P_1$ - $4d5p\ ^3P^o_0$ $\lambda = 193.725$ line profile due to the change of the zirconium abundance $\log(N_{\rm Zr}/N_{\rm H})$ for stellar atmospheres model with $T_{eff} = 10500$ K, $\log g = 4.0$ and the turbulence velocity $V_t = 0.0$ km s^{-1} (**a**). In (**b**), the equivalent width as a function of the zirconium abundance is shown.

contribution of the differences of Zr II and Zr III Stark broadening parameters to the zirconium conflict.

In Popović et al. (2001a), the electron-impact broadening parameters calculation of two astrophysically important Zr II and 34 Zr III lines has been performed, in order to test the influence of this broadening mechanism on determination of equivalent widths and to discuss its possible influence on zirconium abundance determination.

Atomic energy levels needed for calculations have been taken from Reader and Acquista (1997) and from Charro *et al.* (1999). Obtained results have been used to see how much the electron-impact broadening can take part in so called "zirconium conflict" in the HgMn star χ Lupi. In order to test the importance of the electron-impact broadening effect in determination of zirconium abundance, Popović et al. (2001a) have synthesized the line profiles of Zr II, λ=193.8 nm and Zr III, λ=194.0 nm using SYNTH code (Piskunov 1992) and the Kurucz's ATLAS9 code for stellar atmosphere model (Kurucz 1993) $T_{\rm eff} = 10500$ K, $\log g$ =4.0 and the turbulence velocity $V_t = 0.0$ km s^{-1} , i.e. with the stellar models with similar characteristics as in the case of χ Lupi ($T_{\rm eff}$ =10650 K and $\log g$ =3.8, see e.g. Leckrone et al. 1999). These lines have been choosen, because they have been usually used for abundance determination. The reason is that the lines have small wavelength displacement and they are well resolved (Leckrone et al. 1993). The change of the Zr III $4d^2\ ^3P_1$ - $4d5p\ ^3P^o_0$ $\lambda = 193.725$ line profile due to the change of the zirconium abundance is shown in Fig. 3a, while in Fig. 3b the equivalent width as a function of the zirconium abundance is shown.

Popović et al. (2001a) have calculated the equivalent widths with the electron-impact broadening effect and without it for different abundances of zirconium. The obtained results for ZrIII[194.0nm] and ZrII[193.8nm] lines show that the electron-broadening effect is more important in the case of higher abundance of zirconium. The equivalent width increases with abundance for both lines, but the equivalent width for ZrIII[194.0nm] line is more sensitive than for ZrII[193.8nm] line. It may cause error in abundance determination in the case when the electron-impact broadening

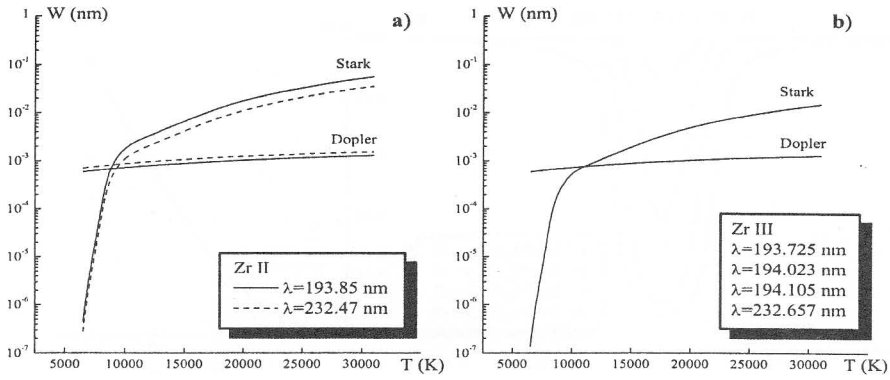

Fig. 4: The behaviour of Stark and Doppler widths (FWHM) with temperature, for stellar atmosphere model with T_{eff} =10500 K, $\log g$=4.0 and V_t = 0.0 km s^{-1} for a) Zr II 4d5s5p v^{2}D$^o_{3/2}$ - 4d^{2}5s a^{2}D$_{3/2}$ λ = 193.85 nm (full line—) and Zr II 4d5s5p v^{2}F$^o_{5/2}$ - 4d^{2}5s b^{2}G$_{7/2}$ λ = 232.47 nm (broken line) and b) Zr III 4d^2 ^{3}P$_1$ - 4d5p ^{3}P$^o_0$ λ = 193.725 nm, Zr III 4d^2 ^{1}G$_4$ - 4d5p ^{1}F$^o_3$ λ = 194.023 nm, Zr III 4d^2 ^{3}P$_2$ - 4d5p ^{3}P$^o_2$ λ = 194.105 nm i Zr III 4d^2 ^{3}P$_1$ - 4d5p ^{3}P$^o_1$ λ = 194.657 nm. In Fig. 4b, dependence for all indicated lines is not shown since it is approximately the same.

effect is not taken into account. In any case synthesizing of these two lines in order to measure the zirconium abundance without taking into account the electron-impact widths will give that with the ZrIII[194.0nm] the abundance of zirconium is higher than with the ZrII[193.8nm] line. However, this effect cannot cause the difference of one order of magnitude in abundance.

Although the "zirconium conflict" in HgMn star χ Lupi cannot be explained only by this effects, one should take into account that this effect may cause errors in abundance determination. Moreover in Fig 4 is demonstrated that Stark broadening is comparable with Doppler broadening or dominant broadening mechanisms for temperatures around 10 000 K and higher.

6. OTHER ASTROPHYSICAL APPLICATIONS

The modified semiempirical method and Stark broadening parameters calculated within this approach have been applied in astrophysics e.g. for the determination of carbon, nitrogen and oxygen abundances in early B-type stars (Gies and Lambert 1992) magnesium, aluminium and silicon abundances in normal late-B and HgMn stars, from co-added IUE spectra (Smith 1993) and elemental abundances in hot white dwarfs (Chayer et al. 1995ab), investigations of abundance anomalies in stars (Michaud and Richer 1992), elemental abundance analyses with DAO spectrograms for 15 - Vulpeculae and 32 - Aquarii (Bolcal et al 1992), radiative acceleration calculation in stellar envelopes (LeBlanc and Michaud 1995, Gonzales et al. 1995ab, Alecian et al. 1993, Seaton 1997), consideration of radiative levitation in hot white dwarfs (Char et al. 1995, Chayer et al. 1995ab), quantitative spectroscopy of hot stars (Kudritzki and Hummer 1990), non - LTE calculations of silicon - line strengths in B - type stars (Lennon et al. 1986), stellar opacities calculations and study (Iglesias et

al. 1990, Iglesias and Rogers 1992, Rogers and Iglesias 1992, 1995, 1999, Seaton 1993, Mostovych et al. 1995), atmospheres and winds of hot stars investigations (Butler 1995), investigation of Ga II lines in the spectrum of Ap stars (Lanz et al. 1993). Stark broadening data calculated within the modified semiempirical method entered in a critical overview of atomic data for stellar abundance analysis (Lanz and Artru 1988), and a catalogue of atomic data for low-density astrophysical plasma (Golovatyj et al. (1997), Stark broadening parameter regularities and systematic trends research (Glenzer et al. 1992, 1994, Wrubel et al. 1998, Purić et al. 1987, 1988a-d, Purić 1996)... The modified semiempirical method entered also in computer codes, as e. g. OPAL opacity code (Rogers and Iglesias 1995), handbooks (Peach 1996, Vogt 1996) and monographs (Gray 1992, Griem 1997, Konjević 1999).

In order to make the application and usage of our Stark broadening data obtained within the semiclassical and modified semiempirical approaches more easier, we are organizing them now in a database BELDATA.

7. REGULARITIES AND SYSTEMATIC TRENDS

When reliable data do not exist, the knowledge on regularities and systematic trends of line broadening parameters can be used for quick acquisition of new data especially when high accuracy of each particular value is not needed.

Regularities and systemic trends for the widths of isolated non−hydrogenic spectral lines in plasmas have been studied in a number of papers (see for example Purić et al. 1980, 1987, 1988a-d, 1991, Konjević and Dimitrijević, 1981, Dimitrijević 1982, Wiese and Konjević 1982, 1992, Lakićević and Purić 1983, Dimitrijević 1985, Vitel et al. 1988, Dimitrijević and Popović 1989, Dimitrijević and Peach 1990, Djeniže et al. 1990, Glenzer et al. 1992, 1994, Purić 1996, Wrubel et al. 1998, Purić and Šćepanović 1999). The aim of such studies is to find out if regularities and systematic trends can be used to predict line widths and to critically evaluate experimental data. With the suitable use of the knowledge of regularities and systematic trends, we might use the existing experimental and theoretical values for the interpolation of new data needed in stellar spectroscopy. One must take into account however, that the validity of systematic trends and line broadening data is limited to the plasma conditions for which they are derrived and extrapolations are of low accuracy.

At the end, it is interesting to emphasize that the Stark broadening research is a developed research field in Yugoslavia, which has a critical mass of scientists. In Dimitrijević (1990b, 1991, 1994, 1997, 2001) reviewing spectral line shapes investigations in Yugoslavia and Serbia within 1962 - 2000 periode, it is shown that during this periode 1427 (1222 by serbian authors) bibliographic items have been published by 179 Yugoslav authors (152 from Serbia, 26 from Croatia and 1 living in France). Majority of these articles concern Stark broadening.

References

Ackermann, A., Finken, K. H., Musielok, J.: 1985, *Phys. Rev. A* **31**, 2597.
Alecian, G., Michaud, G., Tully, J.: 1993, *Astrophys. J.* **411**, 882.
Benett S. M. and Griem H. R.: 1971 *Calculated Stark Broadening Parameters for Isolated Spectral Lines from the Atom Helium through Calcium and Cesium*, Univ. Maryland, Techn.Rep. No 71−097, College Park, Maryland.

Blagojević, B., Popović, M. V., Konjević, N.: 1999, *Physica Scripta* **59**, 374.
Blagojević, B., Popović, M. V., Konjević, N., Dimitrijević, M. S.: 1996, *Phys. Rev. E* **54**, 743.
Bolcal, C., Kocer, D., Adelman, S. J.: 1992, *Month. Not. Roy. Astron. Soc.* **258**, 270.
Böttcher, F., Breger, P., Hey, J. D., Kunze, H. -J.: 1988, *Phys. Rev. A* **38**, 2690.
Brandt, J. C., Heap, S. R., Beaver, E. A., Boggess, A., Carpenter, K. G., Ebberts, D. C., Hutchings, J. B., Jura, M., Leckrone, D. S., Linsky, J. L., Haran, S. P., Savage, B. D., Smith, A. M., Trafton, L. M., Walter, F. M., Weymann, R. J., Proffitt, C. R., Wahlgren, G. M., Johansson, S. G., Nilsson, H., Brage, T., Snow, M., Ake, T. B.: 1999, *Astron. J.* **117**, 1505.
Butler, K.: 1995, in *Astrophysical Applications of Powerful New Databases*, eds. S. J. Adelman, W. L. Wiese, *ASP Conf. Series* **78**, 509.
Charo, E., López-Ayuso, J. L., Martin, I.: 1999, *J. Phys B* **32**, 4555.
Chayer, P., Fontaine, G., Wesemael, F.: 1995a, *Astrophys. J. Suppl. Series* **99**, 189.
Chayer, P., Vennes, S., Pradhan, A. K., Thejll, P., Beauchamp, A., Fontaine, G., Wesemael, F.: 1995b, *Astrophys. J.* **454**, 429.
Cowley, C. R., Aikman, G. C. L.: 1975, *Astrophys. J.* **196**, 521.
Dimitrijević, M. S.: 1982, *Astron. Astrophys.* **112**, 251.
Dimitrijević, M. S.: 1983, *Astron. Astrophys.* **127**, 68.
Dimitrijević, M. S.: 1985, *Astron. Astrophys.* **145**, 439.
Dimitrijević, M. S.: 1990a, in *Accuracy of Element Abundances from Stellar Atmospheres*, ed. R. Wehrse, Lecture Notes in Physics **356**, Springer, Berlin-Heidelberg, 31.
Dimitrijević, M. S.: 1990b, *Line Shapes Investigations in Yugoslavia 1962-1985 (Bibliography and citation index), Publ. Obs. Astron. Belgrade* **39**.
Dimitrijević, M. S.: 1991, *Line Shapes Investigations in Yugoslavia II. 1985-1989 (Bibliography and citation index), Publ. Obs. Astron. Belgrade* **41**.
Dimitrijević, M. S.: 1994, *Line Shapes Investigations in Yugoslavia and Serbia III. 1989-1993 (Bibliography and citation index), Publ. Obs. Astron. Belgrade* **47**.
Dimitrijević, M. S.: 1996, *Zh. Prikl. Spektrosk.* **63**, 810.
Dimitrijević, M. S.: 1997, *Line Shapes Investigations in Yugoslavia and Serbia IV. 1993-1997 (Bibliography and citation index), Publ. Obs. Astron. Belgrade* **58**.
Dimitrijević, M. S.: 2001, *Line Shapes Investigations in Yugoslavia and Serbia V. 1997-2000 (Bibliography and citation index), Publ. Obs. Astron. Belgrade* **70**.
Dimitrijević, M. S., Feautrier N., Sahal–Bréchot S.: 1981, *J. Phys. B* **14**, 2559.
Dimitrijević, M. S., Konjević, N.: 1980, *J. Quant. Spectrosc. Radiat. Transfer* **24**, 451.
Dimitrijević, M. S., Konjević, N.: 1981, in *Spectral Line Shapes*, ed. B.Wende, W. de Gruyter, Berlin, New York , 211.
Dimitrijević, M.S., Konjević, N.: 1987, *Astron. Astrophys.* **172**, 345.
Dimitrijević, M. S., Kršljanin, V.: 1986, *Astron. Astrophys.* **165**, 269.
Dimitrijević, M. S., Peach, G.: 1990, *Astron. Astrophys.* **236**, 261.
Dimitrijević, M. S., Popović, M. M.: 1989, *Astron. Astrophys.* **217**, 201.
Dimitrijević, M. S., Popović, L. Č.: 1993, *Astron. Astrophys. Suppl. Series* **101**, 583.
Dimitrijević, M. S., Popović, L. Č.: 2001, *Zh. Prikl. Spektrosk.* **68**, 685.
Djeniže, S., Srećković, A., Platiša, M., Konjević, R., Labat, J., Purić, J.: 1990, *Phys. Rev. A* **42**, 2379.
Gies, D. R., Lambert, D. L.: 1992, *Astrophys. J.* **387**, 673.
Glenzer, S., Hey, J. D., Kunze, H. -J.: 1994, *J. Phys. B: At. Mol. Opt. Phys.* **27**, 413.
Glenzer, S., Uzelac, N. I., Kunze, H. -J.: 1992, *Phys. Rev. A* **45**, 8795.
Golovatyj, V. V. Sapar, A., Feklistova, T., Kholtygin, A. F.: 1997, *Astron. Astrophys. Transactions* **12**, 85.
Gonzales, J. F., Artru, M. -C., Michaud, G.: 1995a, *Astron. Astrophys.* **302**, 788.
Gonzales, J. F., LeBlanc, F., Artru, M. -C., Michaud, G.: 1995b, *Astron. Astrophys.* **297**, 223.
Gonzales - Delgado, R. M., Leitherer, C., Heckman, T. M.: 1999, *Astrophys. J. Suppl. Series* **125**, 489.

Gray, D. F.: 1992, *The Observation and Analysis of Stellar Photospheres*, Cambridge University Press, Cambridge.
Griem, H. R.: 1968, *Phys. Rev.* **165**, 258.
Griem, H. R.: 1974 *Spectral Line Broadening by Plasmas*, Academic Press, New York and London.
Griem, H. R.: 1997, *Principles of Plasma Spectroscopy*, Cambridge Monographs of Plasma Physics 2, Cambridge University Press.
Hauschildt, P. H., Baron, E.: 1999, *J. Comp. Applied Math.* 109, 41.
Heacox, W. D.: 1979, *Astrophys. J. Suppl.* **41**, 675.
Heading, D. J., Wark, J. S., Lee, R. W., Stamm, R., Talin, B.: 1997, *Phys. Rev. E* **56**, 936.
Iglesias, C. A., Rogers, F. J., Wilson, B. G.: 1990, *Astrophys. J.* **360**, 221.
Iglesias, C. A., Rogers, F. J.: 1992, *Revista Mexicana de Astronomia y Astrofisica* **23**, 161.
Jones, W. W. Benett, S. M. and Griem, H. R.: 1971 *Calculated Electron Impact Broadening Parameters for Isolated Spectral Lines from Singly Charged Ions Lithium through Calcium*, Univ. Maryland , Techn.Rep. No 71−128, College Park, Maryland.
Kobilarov, R., Konjević, N.: 1990, *Phys. Rev. A* **41**, 6023.
Konjević, N.: 1999, *Physics Reports* **316**, 339.
Konjević, R.: 1995, *Publ. Obs. Astron. Belgrade* **50**, 87.
Konjević, N. and Dimitrijević, M. S.: 1981 in *Spectral Line Shapes I* ed. B.Wende, W.de Gruyter, Berlin, New York. p. 211.
Konjević, N., Pittman, T. L.: 1987, *J. Quant. Spectrosc. Radiat. Transfer* **37**, 311.
Kudritzki, R., Hummer, D. G.: 1990, *Ann. Rev. Astron. Astrophys.* **28**, 303.
Kurucz, R. L.: 1993. Model atmosphere program ATLAS9 published on CDROM13
Lakićević, I. S. and Purić, J.: 1983 in *Spectral Line Shapes II*, ed. K. Burnett, W. de Gruyter, Berlin, New York, p 147.
Lanz, T., Artru, M. -C.: 1988, in *Elemental abundance analysis*, eds. S.J.Adelman, T.Lanz, Institut d Astronomie de l Universite de Lausane, 156.
Lanz, T., Artru, M. -C., Didelon, P., Mathys, G.: 1993, *Astron. Astrophys.* **272**, 465.
LeBlanc, F., Michaud, G.: 1995, *Astron. Astrophys.* **303**, 166.
Leckrone, D. S., Proffitt, C. R., Wahlgren, G. M., Johansson, S. G., Brage, T.: 1999, *Astron. J.* **117**, 1454L
Leckrone, D. S., Wahlgren, G. M., Johansson, S. G., Adelman, S. J.: 1993, in *Peculiar Versus Normal Phenomena in A-Type and Related Stars*, ASP Conference Series, Vol. 44 (eds. M. M. Dworetsky, F. Castelli and R. Faraggiana), p.42
Lennon, D. J., Lynas-Gray, A. E., Brown, J. F., Dufton, P. L.: 1986, *Mon. Not. Roy. Astron. Soc.* **222**, 719.
Michaud, G., Richer, J.: 1992, in *Spectral Line Shapes*, **9**, eds. M. Zoppi, L. Ulivi, *AIP Conf. Proc.* **386**, 397.
Milosavljević, V., Konjević, R., Djeniže, S.: 1999, *Astron. Astrophys. Suppl. Series* **135**, 565.
Mostovych, A. N., Chan, L. Y., Kearney, K. J., Garren, D., Iglesias, C. A., Klapisch, M., Rogers, F. J.: 1995, *Phys. Rev. Lett.* **75**, 1530.
Peach, G.: 1996, *Collisional broadening of spectral lines*, in *Atomic, Molecular, & Optical Physics Handbook*, ed. G. W. F. Drake, AIP Press, Woodbury, New York, 669.
Piskunov, N. E.: 1992, in *Stellar magnetism*, eds. Yu. V. Glagolevskij, I. I. Romanyuk, Nauka, St. Petersburg, p. 92
Popović, L. Č., Dimitrijević, M. S.: 1996a, *Phys. Scripta* **53**, 325.
Popović, L. Č., Dimitrijević, M. S.: 1996b, *Astron. Astrophys. Suppl. Series* **116**, 359.
Popović, L. Č., Dimitrijević, M. S.: 1998, *Astron. Astrophys. Suppl. Series* **127**, 259.
Popović, L.Č,. Dimitrijević, M.S., Ryabchikova, T.: 1999, *Astron. Astrophys.* **350**, 719.
Popović, L. Č., Milovanović, N., Dimitrijević, M. S.: 2001a, *Astron. Astrophys.* **365**, 656.
Popović, L. Č., Simić, S., Milovanović, N., Dimitrijević, M. S.: 2001b, *Astrophys. J. Suppl. Series* **135**, 109.
Purić, J.: 1996, Zh. Prikl. Spektrosk. **63**, 816.
Purić, J., Ćuk, M., Dimitrijević, M. S. and Lesage, A.: 1991, *Astrophys. J.* **382**, 353.

Purić, J., Djeniže, S., Labat, J., Platiša, M., Srećković, A., Ćuk, M.: 1988a, *Z. Phys. D* **10**, 431.
Purić, J., Djeniže, S., Srećković, A., Ćuk, M., Labat, J., Platiša, M.: 1988b, *Z. Phys. D.* **8**, 343.
Purić, J., Djeniže, S., Srećković, A., Platiša, M., Labat, J.: 1988c, *Phys. Rev. A.* **37**, 498.
Purić, J. Lakićević, I. and Glavonjić, V.: 1980, Phys. Lett. **76a**, 128.
Purić, J., Šćepanović, M.: 1999, *Astrophys. J. Suppl.* **521**, 490.
Purić, J., Srećković, A., Djeniže, S., Platiša, M.: 1987, *Phys. Rev. A* **36**, 3957.
Purić, J., Srećković, A., Djeniže, S., Platiša, M.: 1988d, *Phys. Rev. A* **37**, 4380.
Reader, J., Acquista, N.: 1997, *Phys. Scr.* **55**, 310.
Rogers, F. J., Iglesias, C. A.: 1992, *Astrophys. J. Suppl. Series* **79**, 507.
Rogers, F. J., Iglesias, C. A.: 1995, in *Astrophysical Applications of Powerful Databases* eds. S.J. Adelman, W.L. Wiese, *ASP Conf. Series* **78**, 31.
Rogers, F. J., Iglesias, C. A.: 1999, *Space Sci. Rev.*, **85**, 61.
Sahal-Bréchot, S.: 1969a, *Astron. Astrophys.* **1**, 91.
Sahal-Bréchot, S.: 1969b, *Astron. Astrophys.* **2**, 322.
Seaton, M. J.: 1993, *IAU Colloquium 137*, eds. W. W. Weiss, A. Baglin, *Publ. Astron. Soc. Pacific Conf. Series* **40**, 222.
Seaton, M. J.: 1997, *Month. Not. Roy. Astron. Soc.* **289**, 700.
Sikström, C. M., Lundberg, H., Wahlgren, G. M., Li, Z. S., Lyngå, C., Johansson, S., Lecrone, D. S., 1999, *Astron. Astrophys.* **343**, 297.
Smith, K. C.: 1993, *Astron. Astrophys.* **276**, 393.
Vitel, Y., Skowronek, M., Dimitrijević, M. S. and Popović, M. M.: 1988, *Astron. Astrophys.* **200**, 285.
Vogt, H. H. ed.: 1996, *Stellar atmospheres: Atomic and molecular data, Astronomy and Astrophysics*, Extension and Suppl. to Vol. 2, Subvol. B, *Stars and Star Clusters*, Landolt-Boernstein, Group VI: *Astron. Astrophys.* Vol. 3, Sp ringer, 57.
Wiese, W. L. and Konjević, N.: 1982, *JQSRT* **28**, 185.
Wiese, W. L. and Konjević, N.: 1992, *JQSRT* **47**, 185.
Wrubel, T., Ahmad, I., Buscher, S., Kunze, H. -J.: 1998, *Phys. Rev. E*, **57**, 5972.
Wrubel, Th., Glenzer, S., Büscher, S., Kunze, H. -J., Alexiou, S.: 1996, *Astron. Astrophys.* **306**, 1023.

Publ. Astron. Obs. Belgrade No. 73 (2002), 27 - 36 *Invited lecture*

HOT DUST IN GALAXIES

E. KRÜGEL[1] and R. SIEBENMORGEN[2]
[1]*MPIfR, Auf dem Hügel 69, D-53121 Bonn, Germany*
E-mail p309ekr@mpifr-bonn.mpg.de

[2]*ESO, Karl-Schwarzschild-Str. 2, D-85748, Germany*
E-mail rsiebenm@eso.org.

Abstract. We present an approximate method for calculating the infrared emission from a galactic nucleus that has recently undergone a starburst and is powered mainly by massive stars of spectral type O and B. Such nuclei are usually heavily obscured by dust and we outline the radiative transfer in a dusty medium with scattered sources. We include in the model transiently heated small dust particles and illustrate their dominating influcence on the near and mid infrared spectrum.

1. Galactic nuclei

Galactic nuclei are a most interesting class of objects as they are the site of diverse kinds of activity often accompanied by large infrared luminosities. The origin of the activity may be either rapid star formation or accretion onto a massive black hole. In both cases, the hard primary radiation, from the star or the black hole, is converted into infrared photons by dust. We here consider stars as the source of energy. As galactic nuclei, like the center of the Milky Way, usually possess a fair degree of spherical symmetry, one may try to model their infrared spectral energy distribution.

2. Hot spots in a spherical stellar cluster

To model the infrared emission of a dusty galactic nucleus, one has to specify the properties and space density of the stars, the distribution of the dust grains and then solve in some approximate way the radiative transfer in the dusty medium. The radiative transfer in a star cluster is, however, complicated by the fact that the geometrical configuration is intrinsically three–dimensional because the dust temperature varies not only on a large scale with galactic radius r, which is the distance to the center of the stellar cluster, but also locally with the separation to the nearest star. This circumstance must be taken into account [Krü78]. Loosely speaking, the temperature of a grain located in the immediate vicinity of a star is determined by the distance to and the properties of that star, whereas a grain at the same galactic distance, but not very close to any star, absorbs only the mean interstellar radiation field $J_\nu^{\rm isrf}(r)$ and will thus be cooler. The spherical symmetry is broken on a small scale because

the surroundings of a star constitute a hot spot (abbreviated HS) in the interstellar medium. Their presence significantly changes the spectral appearance of a galactic nucleus.

Let us assume that the hot spots are homogeneous dusty spheres, each with a star of monochromatic luminosity L_ν at the center. It will turn out that their total volume fraction is small, so they are distributed over the galactic nucleus like raisins in a cake. The radius $R^{\rm HS}$ of a hot spot is determined by the condition that outside, a dust grain is mainly heated by the interstellar radiation field, whereas inside, heating by the star dominates. If τ_ν is the optical depth from the star to the boundary of the hot spot and Q_ν the absorption efficiency of a dust grain, $R^{\rm HS}$ follows from

$$\int Q_\nu J_\nu^{\rm isrf}\, d\nu \;=\; \frac{1}{(4\pi R^{\rm HS})^2} \int Q_\nu L_\nu\, e^{-\tau_\nu}\, d\nu \;. \qquad (1)$$

$R^{\rm HS}$ is a function of r. Furthermore, $R^{\rm HS}$ depends on the strength and spectral shape of the interstellar radiation field, the monochromatic stellar luminosity L_ν, the dust distribution or density within the hot spot, and on the grain properties via the absorption efficiency Q_ν. Equation (1) can readily be formulated for a dust mixture. Then all hot spots at any given galactic distance r have the same radius $R^{\rm HS}(r)$.

3. Low and high luminosity stars

It is useful to divide the stars in a galactic nucleus into two categories, each containg identical objects. Stars of the first class have small or moderate luminosity, a space density $n^*(r)$ and a monochromatic and bolometric luminosity L_ν^* and L^*, respectively, where

$$L^* \;=\; \int L_\nu^*\, d\nu \;.$$

They represent the population of old stars. The second class consists of young and luminous OB stars that were formed in a starburst; the corresponding values are denoted $n^{\rm OB}(r)$, $L_\nu^{\rm OB}$ and $L^{\rm OB}$.

- The low luminosity stars are very numerous, altogether there are typically 10^9 in a nulceus, and the contribution of their hot spots to the overall spectrum may be neglected. To see why consider a nucleus of integrated luminosiy $L_{\rm nuc}$ containing N identical stars of luminosity L^*. When we fix $L_{\rm nuc} = NL^*$, but increase N and thus lower L^*, the intensity of the interstellar radiation field in the galactic nucleus is to first order independent of N. In view of the definition for $R^{\rm HS}$ in (1), one finds

  $$R^{\rm HS} \;\propto\; \sqrt{L^*} \;\propto\; N^{-1/2} \;.$$

  Therefore, the total volume $N \cdot (R^{\rm HS})^3$ of all hot spots decreases as $N^{-1/2}$. A large population of low luminosity stars may be smeared out smoothly over the galactic nucleus and the structure of their hot spots need not be evaluated. To account for the radiation of these stars, one only has to introduce in the numerator of the source function (see equation (2)) the volume emission coefficient

  $$\Gamma_\nu^*(r) \;=\; n^*(r) \cdot L_\nu^* \;.$$

If the stellar atmospheres are black bodies of temperature T^*, one may put $L_\nu^* \propto B_\nu(T^*)$. Note that L_ν^* need not be specified, only the product $\Gamma_\nu^*(r) = n^*(r) \cdot L_\nu^*$.

- The OB stars, on the other hand, are very bright and not so numerous. There are rarely more than 10^6 in a galactic nucleus and their space density $n^{\rm OB}(r)$ is moderate, typically one star per pc^3 or less in the starburst region. The emission of their hot spots is not negligible and has to be evaluated explicitly. Before solving the radiative transfer on a large scale in the galactic nucleus, one has to determine the luminosity $L_\nu^{\rm HS}(r)$ emerging from a hot spot. The frequency integral $\int L_\nu^{\rm HS} d\nu$ is, of course, equal to the luminosity $L^{\rm OB} = \int L_\nu^{\rm OB} d\nu$ of a single OB star, but $L_\nu^{\rm OB}$ and $L_\nu^{\rm HS}$ are different because much of the hard stellar UV flux is converted by dust into infrared radiation.

To obtain $L_\nu^{\rm HS}(r)$, we calculate for each galactic radial grid point the radiative transfer of a spherical cloud centrally heated by an OB star. This is a standard task of radiative transfer. The cloud radius $R^{\rm HS}$ is determined from (1). The hot spot is illuminated at its edge by an interstellar radiation field (isrf), which fixes the outer boundary condition for the intensity. Because the volume emission coefficient due to the hot spots is

$$\Gamma_\nu^{\rm HS}(r) = n^{\rm OB}(r) \cdot L_\nu^{\rm HS} \ ,$$

the source function in a spherical galactic nucleus becomes

$$S_\nu \ = \ \frac{\Gamma_\nu^{\rm HS}(r) + \Gamma_\nu^*(r) + K_\nu^{\rm abs} B_\nu(T_{\rm d}) + K_\nu^{\rm sca} J_\nu^{\rm isrf}}{K_\nu^{\rm ext}} \ . \qquad (2)$$

$K_\nu^{\rm abs}$ and $K_\nu^{\rm sca}$ are the absorption and scattering coefficient of a grain, $K_\nu^{\rm abs} B_\nu(T_{\rm d})$ is the emissivity of dust at temperature $T_{\rm d}$, and the expression $K_\nu^{\rm sca} J_\nu^{\rm isrf}$ is due to isotropic scattering. With this source function, one then solves the integral equation (we now drop the frequency index ν)

$$I(\tau) \ = \ I(0) \cdot e^{-\tau} + \int_0^\tau S(x) \cdot e^{-(\tau - x)} dx \qquad (3)$$

for the intensity in positive and negative direction, I^+ and I^-, along lines of constant impact parameter. From I^+ and I^- one can readily deduce the mean intensity $J_\nu(r)$. As the galactic nucleus in this model consists of two phases, a dusty medium interspersed with hot spots, equation (3) is not strictly correct. It gives, however, a good approximation as long as the volume fraction γ of the hot spots,

$$\gamma(r) \ = \ \frac{4\pi}{3} \cdot n^{\rm OB}(r) \cdot \left[R^{\rm HS}(r) \right]^3$$

is small; $\gamma(r)$ shrinks when $n^{\rm OB}(r)$ becomes large. For typical space densities of OB stars in starburst nuclei, γ is of order 10^{-3}.

4. Small grains with temperature fluctuations

Because of the copious UV radiation field in a galactic nucleus, we also consider in our model the presence of small grains (radii $a \sim 10$Å) and polycyclic aromatic hydrocarbons (PAHs). Such particles have heat capacity of the same order as the energy of an UV photon and therefore undergo temperature fluctuations which strongly influence the near and mid IR part of the spectrum. Such fluctuations require a special numerical treatment ([Guh89], [Li01]).

The top panel of Fig. 1 displays for illustration the temperature variation $T(t)$ of a silicate grain as a function of time over an interval of 1400 s. The grain has a radius of 10Å and is at a distance $r = 10^{17}$ cm from a B1V star ($L = 10^4\, L_\odot$, $T_* = 2 \cdot 10^4$). The probability density $P(T)$ in the lower left panel of Fig. 1 gives the chance $P(T)$ of finding the grain within a temperature interval of 1 K width centered on T; the area under the curves equals one.

When looking at the temperature evolution $T(t)$, one hesitates to assign an average temperature to the grain at all, although mathematically this can, of course, be done. There are two disparate regimes: Most of the time the grain has a temperature of about 40 K, but occasionally the grain is excited to a high temperature from which it rapidly cools radiatively. The probability density $P(T)$ is asymmetric and has its maximum is at $T_{\max} = 51.9$ K, so this is the most likely temperature. On the other hand, the equilibrium temperature $T_{\rm eq}$, which one would obtain if one disregards the stochastic character of photon absorption, is 116.2 K and thus much larger. $T_{\rm eq}$ follows from the energy balance between heating and cooling,

$$\int Q_\nu J_\nu \, d\nu \;=\; \int Q_\nu B_\nu(T_{\rm eq}) \, d\nu \;,$$

where J_ν is the mean intensity of the radiation field. By comparing the dotted and solid line in the lower left box of Fig. 1, we see that to evaluate the grain emission without taking into account its hot excursions would underestimate the near and mid infrared flux by orders of magnitude; this explains the immense influence which small particles have on the spectral energy distribution in this wavelength range. Nevertheless, the frequency integrated emission for both curves is the same and equal to the absorbed flux. Note also the strong 10μm silicate feature.

As a further illustration, we show in Fig. 2 the (optically thin) emission from a dust mixture in a reflection nebula. The dust includes the standard three major components:

- big grains with a size range between 300Å and 3000Å consisting either of silicate material or amorphous carbon. Their temperatures are not time–variable.
- Very small grains (vsg) with temperature fluctuations consisting of silicate material or graphite (a form of crystalline carbon).
- polycyclic aromatic hydrocarbons (PAHs). These are planar molecules, made of a number of benzene rings, usually with hydrogen atoms bound to the edges. The smallest consist of barely more than a dozen atoms, so they are intermediate between molecules and grains. They account for a number of well studied near and mid infrared resonances. Their temperatures strongly fluctuate.

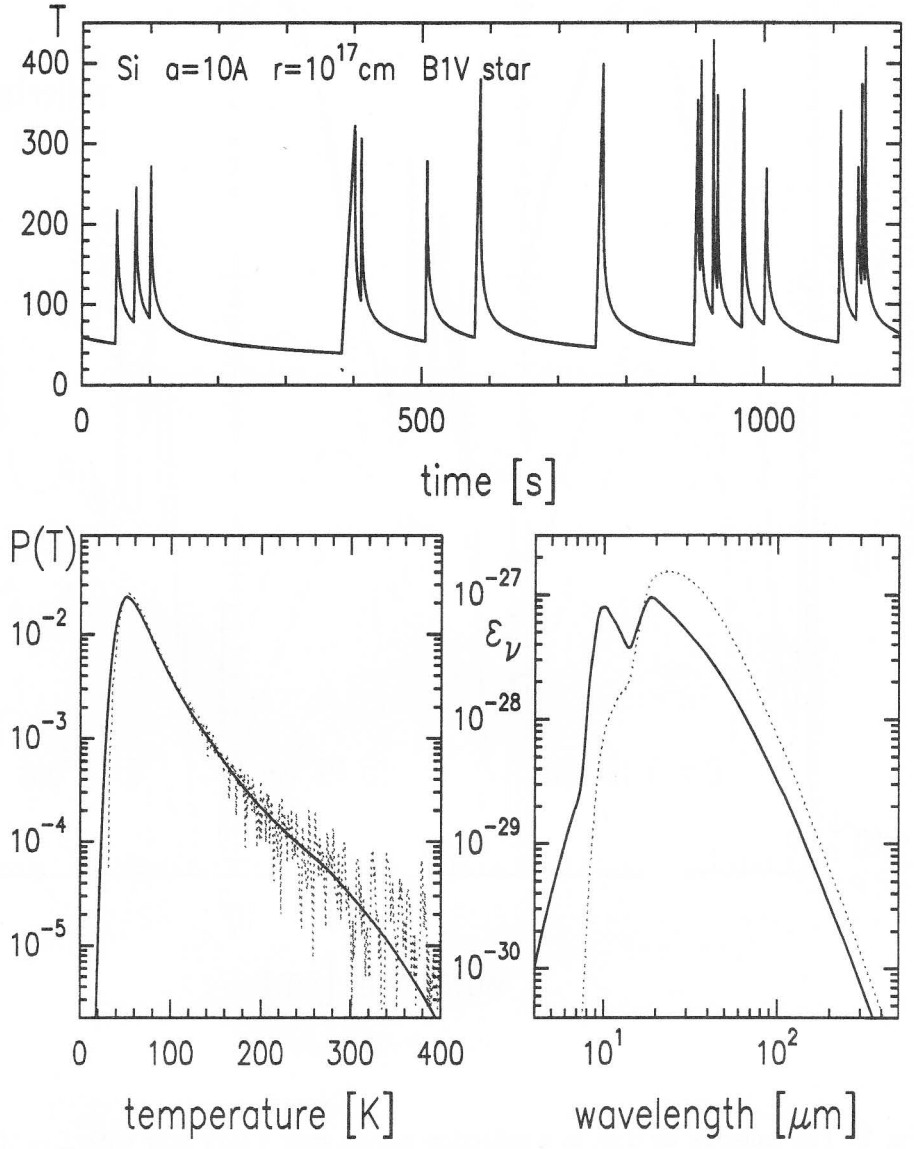

Fig. 1: Temperature fluctuations of a small silicate grain (radius $a = 10$Å) at a distance of 10^{17} cm from a B1V star. *Top:* Stochastic temporal evolution of the temperature. *Lower left:* The solid line shows the probability density $P(T)$ of the temperature; the jittery dotted curve is ignored. *Lower right:* Emissivity ϵ_ν of the grain in erg/s Hz ster. Dots show the emission under the wrong assumption that the temperature is constant; the solid line correctly includes temperature fluctuations.

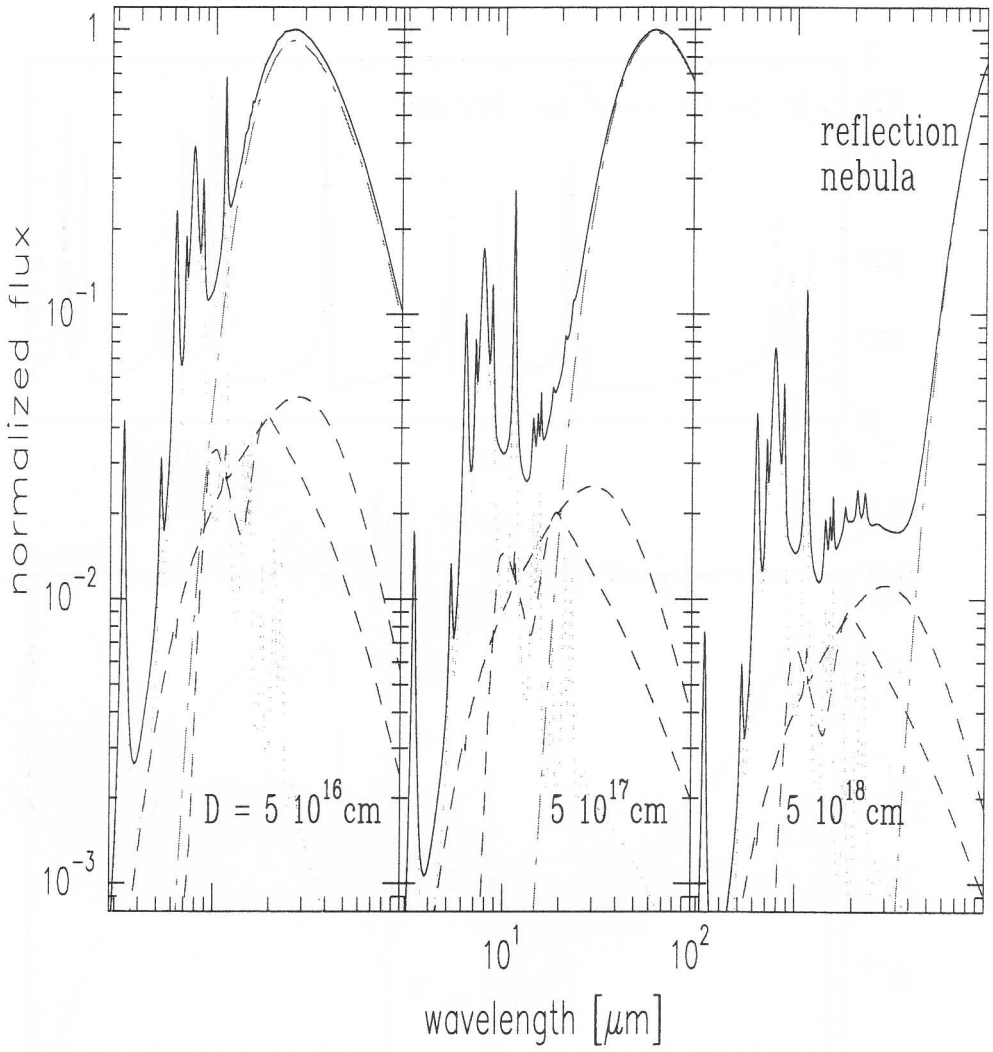

Fig. 2: The emission by dust in a reflection nebula near a B3V star with $L = 10^3\,L_\odot$ and $T_{\rm eff} = 18000\,K$ at various distances D to the star. The spectra are normalized at their maxima. The maximum occurs at $\sim 25\mu$m in the left box where the dust is at a distance $D = 5 \cdot 10^{16}$ cm, and is shifted beyond 100μm for $D = 5 \cdot 10^{18}$ cm. *Solid:* total spectrum of all three dust components. *dash–dot:* big grains only. *dashed:* very small graphite and silicate grains (vsg) of 10Å radius; the silicates have a hump at 10μm. *dots:* PAHs.

5. The influence of hot spots and PAHs on the spectrum

The nucleus of a galaxy is usually deeply embedded in dust and can therefore only be probed by infrared observations. One way to derive the structure of the nucleus, to find out how dust and stars are geometrically arranged, what the total extinction and the gas mass are, or to which spectral type the stars belong, is to model the dust emission spectrum.

Following the procedure discussed above (for details, see [Krü94]), we compute the radiative transfer and the resulting emission spectrum from a dusty starburst nucleus. First, we convince ourselves that it is indeed necessary to properly include the surroundings of the OB stars (we call them hot spots). If one does not separately treat the emission from the hot spots, where the dust is much warmer than elsewhere, but takes averages of the dust emission over larger volumes, one grossly underrates the mid–infrared flux. This can be seen from Fig. 3, where spectra are displayed that have been calculated with and without hot spots. Their presence also reduces the depth of the 10μm silicate absorption feature (except for the highest hot spot density of $n(\mathrm{H}) = 10^5$ H atoms per cm^3).

None of the spectra in Fig. 3 includes PAHs or very small grains (except for the point source model, see below). An improved model that is closer to reality has, of course, to incorporate these dust components. Their importance arises mainly from the fact that they undergo temperature fluctuations. In this way, their emission becomes prominent at much shorther wavelengths than if they were at an equilibrium temperature. We see from Fig. 4 that PAHs and very small grains appreciably further enhance the mid infrared flux compared to the models of Fig. 3 and radically change its spectral appearance. As a consequence, it is now not obvious at all how to derive from the 10μm silicate feature, which lies between PAH bands, an absorption optical depth. We add that in view of the strong and hard radiation field prevalent in a galactic nucleus, the radiative transfer code must allow for the possibility of photo–destruction of PAHs.

Of interest is also a point source model of the same luminosity and spectral appearance as the exciting stars, but where the stars are squeezed into a tiny volume at the center of the galactic nucleus. It is shown by the upper dotted curve in Fig. 4. It too yields a very strong mid–infrared flux, but differs from the models with extended emission out of a stellar cluster by its small angular size. Mid–infrared cross cuts of high spatial resolution over the galactic nucleus allow to discriminate between the two alternatives.

A massive black hole with an accretion disk appears to an observer also as a point source, but it is one with a considerably harder emission spectrum than OB stars. Usually one assumes for the black hole a power law $S_\nu \propto \nu^\alpha$ with $\alpha \simeq -0.5$. If the dust is exposed to the flux from such an object, PAHs will evaporate in its vicinity (they can only survive farther out) and the ratio of mid infrared over total luminosity is reduced. This can be checked observationally. However, spectral lines from multiply ionized atoms, which require for their excitation more energetic photons than are found in HII regions, are generally a better diagnostic for the presence of a powerful non–thermal source.

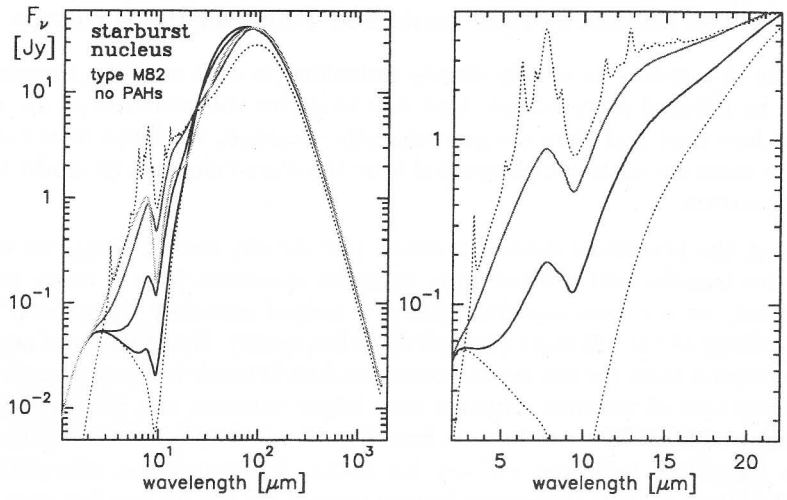

Fig. 3: Radiative transfer models of a starburst nucleus similar to M82. Source distance $D = 20\,\mathrm{Mpc}$, further parameters in Table 1. *Left:* The two dotted curves are benchmarks for comparison with the right box and with Fig. 4. The lower dotted curve shows the case without hot spots. The upper one depicts a point source model, and this is the only curve in the figure where PAHs and very small grains are included. The remaining solid lines are computed with hot spots. The density in the hot spots ranges from $n(\mathrm{H}) = 10^2\,\mathrm{cm}^{-3}$ to $n(\mathrm{H}) = 10^5\,\mathrm{cm}^{-3}$ in steps of a factor 10. *Right:* Enlargement of left box showing only the intermediate and probably more realistic hot spot densities 10^3 (lower solid line) and $10^4\,\mathrm{cm}^{-3}$ (upper solid line).

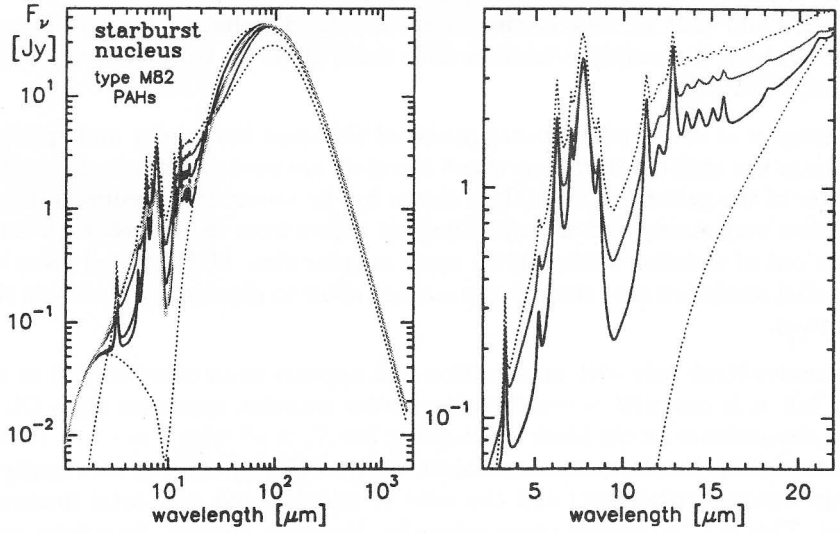

Fig. 4: *Left:* As Fig. 3 and with the same benchmark models (upper and lower dotted curves), but now with hots spots *and* PAHs and very small grains. *Right:* Enlargement of left box, but only for hot spot densities 10^3 and $10^4\,\mathrm{cm}^{-3}$.

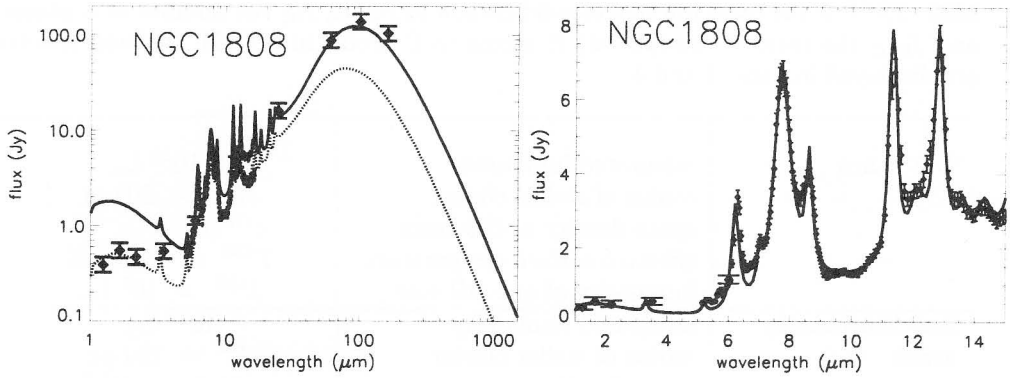

Fig. 5: *Left:* Dust emission from the nucleus of the galaxy NGC 1808. The dotted (solid) line shows the model flux received in a 25″ (100″) aperture. The galaxy is at a distance of 11 Mpc where 1″ corresponds to 53 pc. Circles represent observational data [Sie00]. *Right:* Blowup of the near and mid infrared data and of the 25″ aperture model. The model fit is very good.

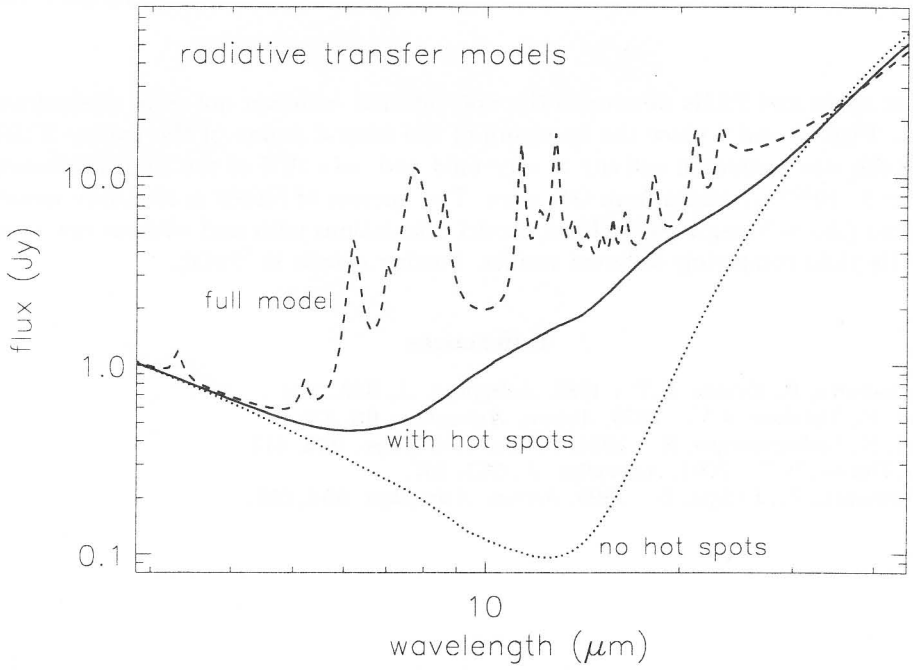

Fig. 6: The influence of the hot spots and the PAHs on the spectrum of the galaxy N1808. The line labeled full model includes PAHs and hot spots.

Table 1: Typical parameters for a galactic nucleus with a starburst, like the archetype M82. Y_C^{PAH} is the mass fraction of solid carbon in PAHs, N_C the number or C atoms, and $f_{H/C}$ the ratio of (peripheral) H atoms to C atoms in a PAH. Infrared spectra are displayed in Figs. 3 and 4.

OB stars	integrated luminosity	$3 \cdot 10^{10}\ L_\odot$
	radius of stellar cluster	$R^{OB} = 200$ pc
	space density of OB stars	$n^{OB}(r) \propto r^{-1/2}$
	effective surface temperature	$T^{OB} = 25\,000$ K
	luminosity of one OB star	$L^{OB} = 10^5\ L_\odot$
low luminosity stars	integrated luminosity	$10^{10}\ L_\odot$
	radius of stellar cluster	$R^* = 700$ pc
	space density	$n^*(r) \propto r^{-1.8}$
	effective surface temperature	$T^* = 4000$ K
dust	radius of dust cloud	$R_{dust} = 800$ pc
	density $\rho_{dust}(r)$	= const for $r \leq 230$ pc
	$\propto r^{-1/2}$ for $r > 230$ pc	
	A_V from cloud edge to center	29 mag
	A_V from $r = 0$ to $r = 230$ pc	10 mag
PAHs	small ones ($N_C = 50$)	$Y_C^{PAH} = 0.05$, $f_{H/C} = 0.4$
	big ones ($N_C = 300$)	$Y_C^{PAH} = 0.05$, $f_{H/C} = 0.16$
very small grains	radius $a = 10$Å	graphites: $Y_C^{vsg} = 0.05$

Hot spots and PAHs determine the mid infrared emission not only of starburst nuclei. Figs. 5 and 6 show the spectrum of the central region of the galaxy N1808 where the star formation activity is very mild and only 10% of the total luminosity ($L_{tot} \simeq 5 \cdot 10^{10}\ L_\odot$) comes from OB stars. The nucleus of N1808 is also only weakly obscured ($A_V \sim 5$ mag). Neverthless, model calculations with and without hot spots or PAHs yield completely different results. Further details in [Sie00].

References

Guhathakurta, P., Draine, B.T. : 1989, *Astrophys. J.*, **345**, 230.
Krügel, E., Tutukov, A.V. : 1978, *Astron. Astrophys.*, **63**, 375.
Krügel, E., Siebenmorgen, R. : 1994, *Astron. Astrophys.*, **282**, 417.
Li, A., Draine, B.T. : 2001, *Astrophys. J.*, **551**, 807.
Siebenmorgen, R., Krügel, E. : 2000, *Astron. Astrophys.* **364**, 625.

Publ. Astron. Obs. Belgrade No. 73 (2002), 37 - 48 *Invited lecture*

EUROPEAN COLLABORATION TOWARDS THE ASTRONOMICAL DATAGRID

iAstro - A Collaboration in Astronomy in the Framework of COST 283 Action "Computational and Information Infrastructure in the Astronomical DataGrid"

ST 283 Team: V. GOLEV[1], M. TSVETKOV[2], F. MURTAGH[3], D. EGRET[4], G. LONGO[5], V. DI GESU[6], LLEN[7], A. HOLL[8], A. SHEARER[9], A. GOLDEN[9], L. SASTRY[10], D. BOYD[10], J. NUNẼZ[11], R. MOLINA[12], . VAZQUEZ[13], I. M. LLORENTE[14], PH. JETZER[15], A. CSILLAGHY[16], and P. WINTLEV-JENSEN[17]

[1] *Astronomical Observatory of the St. Kliment Okhridski University of Sofia, Bulgaria*
E-mail : valgol@phys.uni-sofia.bg

[2] *Institute of Astronomy of the Bulgarian Academy of Sciences, Sofia, Bulgaria*
E-mail : tsvetkov@skyarchive.org

[3] *The Queen's University of Belfast, United Kingdom (Action Chear)*

[4] *Strasbourg Astronomical Observatory, France (Action ViceChair)*

[5] *Osservatorio Astronomico di Capodimonte, Napoli, Italy*

[6] *Dipartimento di Matematica ed Applicazioni Universita degli Studi di Palermo, Italy*

[7] *Albert Einstein Institute, Potsdam, Germany*

[8] *Konkoly Astronomical Observatory, Hungary*

[9] *Department of Information Technology, NUI Galway, Ireland*

[10] *Rutherford Appleton Laboratory, United Kingdom*

[11] *Universidad Barcelona, Espanã*

[12] *Universidad Granada, Espanã*

[13] *Centro de Astrobiologia & Universidad Complutense, Madrid, Espanã*

[14] *Departamento de Arquitectura de Computadores y Automatica, Universidad Complutense, Madrid, Espanã*

[15] *Institut für Theoretische Physik, Zurich, Switzerland*

[16] *University of Applied Sciences, Windisch, Switzerland*

[17] *COST - Coordination in the field of Scientific and Technical Research, European Commission, Brussels, Belgium*

Abstract. The implementation of a European Concerted Research Action designated as COST Action 283 "Computational and Information Infrastructure in the Astronomical DataGrid" is described. The main objective of the Action is to develop innovative and well focused approaches to data and information handling, in the context of astronomy and astrophysics. This includes processing and interpretation of data and, more generally, information, at the time of data capture or later ("archival research", "data mining" and "virtual observatories" and so forth), and including aspects of the collaborative work and man-machine environments needed for this.

1. INTRODUCTION

"The brain does not have a single CPU that processes each command in sequence. Rather, it has millions of processors working together at the same time. Such massively parallel processing will be the future for the electronic intelligence as well."

S. Hawking 'The Universe in a Nutshell'

Exponential improvements in telescope, detector and computer technologies mean that the amount of high-quality observational data available is roughly doubling every year. These extra data are coming mainly from new extremely powerful sky surveys like the Sloan Digital Sky Survey (SDSS) for example. The desire to make the best use of such huge data volumes has led both astronomers and computer scientists to propose the creation of Virtual Observatories (VO).

The idea of VO is to store all observations in digital archives that would be accessed by the whole-world astronomical community over a fast computer network similar to the "classical" Internet using the so-called AstroGrid technology. Such VO projects need to overcome a significant technical challenge – how to provide access to the huge databases and archives of **each (and every)** modern astronomical instrument through a **single** interface. Each database is stored separately and it is not practical to move all the data to one "'central"' location. In many cases such movement would take several years over a good Internet connection.

Other main idea taking to heart in Astronomical DataGrid concept is to provide access to the separate databases and archives using the technology of distributed computing which shares out processing and storage tasks between the various computers involved in the DataGrid network. This would allow astronomers to summon up data to their own computers from any of the external databases and archives sharing in the Astronomical DataGrid. The software to do this doesn't exist yet.

It is obvious that the various VO and Astronomical DataGrid initiatives over the world (like the Astrogrid Consortium in the UK which is one of the Europe-pioneering Astronomical DataGrid projects) should work closely together in order to solve globally all arising problems. For these reasons the European COST Action 283 called "Computational and Information Infrastructure in the Astronomical DataGrid" or simply ***iAstro*** emerged at the end of 2001. The ***iAstro*** initiative brings cross-disciplinary perspectives to bear on above-mentioned areas, in which European scientists currently excel. This Action is centred on the potential related to the Grid, taking astronomy as a leading case. Below the details of ***iAstro*** are described.

2. ACTION OBJECTIVES

The COST 283 Action mission statement is as follows.

The Grid is the infrastructure of the virtual organization of the future, providing high performance and high added value services relating to computational, data, information and knowledge processing requirements. Those involved in ***iAstro*** aim at ensuring best application of new theory and tools in the astronomy application domain, and simultaneously Grid-enabling the most appropriate areas of the application domain. The means applied by ***iAstro*** to achieve these ends are, respectively, further developing and bridging the many ongoing projects (i.e., disseminating exciting theories and good practice aimed at astronomers), and through selection and bringing Grid-appropriate areas of the application into focus (i.e., expressing and focusing application requirements aimed at computer scientists, and data and information analysts). An additional objective is the spreading of new national and international projects, where appropriate and needed.

3. PARTICIPATION AND COORDINATION

3. 1. MANAGEMENT COMMITTEE

Chairperson and Secretary:

Prof. Fionn Murtagh
School of Computer Science, Queen's University
Belfast, Belfast BT7 1NN, UK,
tel +44 28 9027-4620, fax +44 28 9068-3890,
f.murtagh@qub.ac.uk

Vice-Chairperson:

Prof. Daniel Egret
Observatoire Astronomique de Strasbourg,
11, rue de l'Universite, 67000 Strasbourg, France,
tel +33-3 88 15 07 11, fax +33-3 88 15 07 60,
egret@astro.u-strasbg.fr

COST – Coordination in the field of Scientific and Technical Research European Commission:

Mr Peter Wintlev-Jensen
200, Rue de la Loi
1049 Brussels, Belgium
Peter.Wintlev-Jensen@cec.eu.int

3. 2. PARTICIPATING INSTITUTES

St. Kliment Okhridski University of Sofia, BG
Institute of Astronomy, Sofia, BG

Konkoly Observatory, Budapest, H
Albert-Einstein-Institute, Golm, D
National University of Ireland, IRL
Rutherford Appleton Laboratory, GB
Queen's University Belfast, GB
Astronomical Observatory, Strasbourg, F
Universita Federico II, Naples, I
Universita di Palermo, I
University of Barcelona, E
University of Granada, E
Universidad Complutense, Madrid, E
ETH Zurich, CH
University of Applied Sciences, Windisch, CH

3. 3. WEB SITE

The Action's web area is at `http://www.iAstro.org`. This domain name was purchased, and the site is hosted at Queen's University Belfast. The site contains reports on Management Committee meetings, information on how to subscribe to email distribution lists associated with the Action, and entry points to a long list of national and interantional projects and consortia working on closely related themes.

4. THE STRUCTURE

The Action is structured in the following Working Groups:

- Working Group 1
  - ⋆ Interoperability, data correlation and federation;
  - ⋆ Data quality/correlation/fusion.
- Working Group 2
  - ⋆ Visualization;
  - ⋆ Advanced visual user interfaces for data mining.
- Working Group 3
  - ⋆ Heterogeneous, multimedia data;
  - ⋆ Image/signal restoration;
  - ⋆ Data mining.
- Working Group 4
  - ⋆ Surveys;
  - ⋆ Wide-field imaging;
  - ⋆ Robotic observatories.

5. EXERPTS FROM THE MEMORANDUM OF UNDERSTANDING

Memorandum of Understanding For the implementation of a European Concerted Action Research Action designated as
COST Action 283
"Computational and Information Infrastructure in the Astronomical DataGrid"

The signatories of this Memorandum of Understanding, declaring their common intention to participate in the concerned Action referred to above and described in the Technical Annex of the Memorandum have reached the following understanding

1. The Action will be carried out in accordance with the provisions of the document COST400/94 Rules and Procedures for Implementing COST Actions, the contents of which are fully known to the Signatories.

2. The main objective of the Action is to develop innovative and well focused approaches to data and information handling, in the context of astronomy and astrophysics. This includes processing and interpretation of data and, more generally, information, at the time of data capture or later ("archival research"), and including aspects of the collaborative work and man-machine environments needed for this.

3. The overall cost of the activities carried out under the Action has been estimated, on the basis of information available during the planning of the Action, at 6 Million EUR in 2001 prices.

4. The Memorandum of Understanding will take effect of being signed by at least five Signatories.

5. The Memorandum of Understanding will remain in force for a period of 4 years, unless the duration of the Action is modified according to the provisions of the document referred to in Point 1 above.

Technical Annex of the Memorandum

A. Background

Many areas of science, engineering, commerce and the arts are facing continual evolution in needs related to data, information and knowledge. COST Action 283 brings cross-disciplinary perspectives to bear on these areas, in which European scientists currently excel. This Action is centred on the potential related to the Grid, taking astronomy as a leading case. The Action includes representatives of other disciplines among its supporters, and aims at dissemination towards, and collaboration with, newly developing areas of the Grid.

The scientific and public resonance of the astronomy application domain is far-reaching. The application of new data extraction and information understanding technologies to, among many other examples, the Sloan Digital Sky Survey, and to Hubble Space Telescope data stores, have been profiled in the communications media

and in outreach work (articles in The Economist, Liberation, and elsewhere). The computer science of relevance to astronomy includes high performance computing (e.g. for theoretical modelling), distributed computing, and dealing with massive databases - very often image databases. The interface areas with telecommunications and software engineering are now so close that they cannot be separated. Information retrieval and cognitive science are strongly represented. There is a continuing perception, however, of a gap between the computer sciences and astronomy. Those who are pioneering new approaches in data mining, distributed computing, Bayesian and spatial modelling, multiresolution vision modelling, new information delivery technologies, and who are active in other fields of computer science, statistics and other disciplines, are very rarely doing such work with astronomy in mind. Both astronomy and the computational sciences have much to gain from collegial linkage.

A selection of important computational issues on the agenda today includes the following.

- What is to be understood by data mining in astronomy, and why is this radically different from commercial and business data mining?
- What are the challenges of semantic description of scientific data and information? Such challenges go far beyond writing a few DTDs.
- Bayesian modelling can help with the all-important problem of model selection. What are the leading scientific decisions requiring such model-based decision making?
- Data and information storage and processing are integrally linked to delivery. What are the new paradigms emerging on the human-machine interface, and what are the implications for image and catalog archives?
- How is science going to change given availability of broadband networks? What are the implications of 3G wireless communication, in conjunction with very high bandwidth backbone links? What are the implications - and the potential - of wide availability of inexpensive, very high quality display devices?

In the recent past (1995-1997), the European Science Foundation supported a Scientific Network on "Converging Computing Methodologies in Astronomy" (CCMA, see http://astro.u-strasbg.fr/ ccma). Out of this consortium grew a number of initiatives - standardization in practices in electronic publishing in astronomy; the development of methods and techniques for wavelets and multiscale transforms, with many publications; and recently a rapidly increasing number of meetings and initiatives related to XML for resource discovery. Links exist in other directions too - the origin of the CCMA network owed a lot to Technical Committee 13 ("Astronomy and Astrophysics") of the International Association for Pattern Recognition, and IAU (International Astronomical Union) committees and working groups. Astronomy has benefited from French Ministry of Education support under the Cognitive Science theme, and 4th and 5th Framework projects (e.g. the 5th Framework IRAIA project on smart information and agent technologies) are relevant to the themes described above and are a spin-off of work in astronomy.

There are a number of other initiatives of direct relevance to this Action. A "thematic network" called OPTICON (Optical-Infrared Coordinated Network for Astronomy) is funded by 5FP. A Fifth Framework proposal on the Virtual Observatory was launched from a consortium linked with the Action in February 2001. In December 2000, a large National Virtual Observatory proposal was submitted to the National Science Foundation ("ITR/IM - Building the Framework for the National Virtual Observatory"). In January 2001, the EC DataGrid initiative was launched. In the UK, a consortium of leading institutes is submitting an AstroGrid proposal to the PPARC research council with a start date of April/May 2001. The First AstroGrid Workshop (http://strule.cs.qub.ac.uk/ fmurtagh/astro-grid) was hosted by Prof Murtagh on January 29-30, 2001. Linkage with the international EC DataGrid project is assured through organisational collaborations on every level - institutional, funded, conference organisational, joint scientific work, and so on. Among other developments which principal participants of this Action are leading is an SPIE conference in San Diego in July/August 2001 on Astronomical Data Analysis, and a conference at Penn State University in July 2001 on Statistical Challenges in Modern Astronomy. Relative to this rich interlocking set of initiatives, the goal of this COST Action is (i) to begin with computer science and engineering perspectives, with a trajectory towards the pressing applications in astronomy, rather than starting with the "science drivers", and (ii) to carry out this work on the European level.

The evolution of broadband networks to IP backbones is (cf. the joint statement by Academia Europaea and European Science Foundation, February 2000, entitled "The need for high bandwidth computer-based networking in Europe") an ongoing area of technology evolution which will greatly benefit the Action. In wireless communication, the advent of much greater bandwidth 3G UMTS technology will motivate the carrying out of scientific work in qualitatively new ways. This Action will contribute actively to such an evolution.

The very diverse set of different initiatives at national and international level clearly justify an Action in which coordination can be undertaken to create higher critical mass and in order to promote convergence towards common solutions, standards and resulting systems and services.

That COST is a particularly appropriate mechanism is due to the collaborative nature of many of these issues - for example, semantic description of scientific data and information cannot be undertaken in isolation; nor can data mining in astronomy take place without close linkages between computer scientists and astronomy. Traditionally, in this area of science, ESA and ESO in Europe have devoted their attention more or less exclusively to the pursuit of scientific installations - ground-based or space-borne observatories. EU research programs have sought commercial drivers. Yet it is precisely the possibility of the linking up with commercial drivers (e.g. in the area of innovative data mining) in the framework of information technology and telecommunications which implies that COST is more appropriate than a less application- driven ESF scientific programme.

Theme area 1 of Action 283: Data centres and data curation for the DataGrid.

Unlike in Earth observation or meteorology, astronomers do not want to interpret data and, having done so, delete it. Variable objects (supernovae, comets, etc.) bear

witness to the need for astronomical data to be available indefinitely. The unavoidable problem is the sheer overwhelming quantity of data which is now collected. The only basis for selective choice for what must be kept long-term is to associate more closely the data capture with the information extraction and knowledge discovery processes. It is necessary to understand the current scientific knowledge discovery mechanisms better in order to make the correct selection of data to keep long-term, including the appropriate resolution and refinement levels.

Data ingest to archives and long-term databases therefore requires knowledge discovery (KDD), computational intelligence and cognitive science, with scientific drivers rather than commercial drivers. The small number of custodians and curators of society's (astronomy) memory can also be supported by more and better use of results from the best of Europe's (computer science, software engineering and telecoms) labs and departments.

Theme area 2 of Action 283: Visualization.

The vast quantities of visual data collected now and in the future present us with new problems and opportunities. Critical needs in the associated software systems include compression and progressive transmission, support for differential detail and user navigation in data spaces, and "thinwire" transmission and visualization. The technological infrastructure is one side of the picture.

Another side of this same picture, however, is that the human ability to interpret vast quantities of data is limited. A study by D. Williams, CERN, has quantified the maximum possible volume of data which can conceivably be interpreted at CERN. This points to another more fundamental justification for addressing the critical technical needs indicated above. This is that selective and prioritized transmission, which has been termed intelligent streaming, is increasingly becoming a key factor in human understanding of the real world, as mediated through the computing and networking base. It is necessary to receive condensed, summarized data first, and the understanding of the data can be aided by having more detail added progressively. A hyperlinked and networked world makes this need for summarization more and more acute. The resolution scale needs to be taken into account in the information and knowledge spaces. This is a key aspect of an intelligent streaming system.

A further area of importance for scientific data interpretation is that of storage and display. Long-term storage of astronomical data, as already noted, is part and parcel of society's memory. With the rapid obsolescence of storage devices, considerable efforts must be undertaken to combat social amnesia. Exciting opportunities are opening up, especially in the area of new Internet-delivery platforms, sales of which are forecast to overtake personal computers by about 2004. Can astronomy benefit from these developments? Videogame consoles are a case in point. Sony's earlier PlayStation, offering outstanding graphics and storage based on DVD disks, sold 60 million units. It and other vendors are ensuring Internet- capability of their machines. This is one example of new, thus far unexploited, opportunities, not least in regard to educational spinoffs and public outreach.

Theme area 3 of Action 283: Multimedia data handling.

Astronomy's data centres and image and catalogue archives play an important role in society's collective memory. For example, the SIMBAD database of astronomical objects at Strasbourg Observatory contains data on nearly 3 million objects, based on 7.5 million object identifiers. Constant updating of SIMBAD is a collective cross-institutional effort. The MegaCam camera the Canada-France-Hawaii Telescope (CFHT), Hawaii, will produce images of dimensions 16000 x 16000, 32-bits per pixel. The European Southern Observatory's VLT (Very Large Telescope) is beginning to produce vast quantities of very large images. There are many examples of images of size 1 GB or greater, for a single image. CCD detectors on other telescopes, or automatic plate scanning machines digitizing photographic sky surveys, produce lots more data. Resolution and scale are of key importance, and so also is region of interest. In multiwavelength astronomy, the fusion of information and data is aimed at, and this can be helped by the use of resolution similar to human cognitive processes. Processing (calibration, storage and transmission formats and approaches) and access are not coupled as closely as they could be. Knowledge discovery is the ultimate driver, and it is this which the Action seeks to closely couple to the processing of data, and thereby to data ingest.

B. Objectives and benefits

The objective of the Action is to develop innovative and well focused approaches to data and information handling, in the context of astronomy and astrophysics. This includes processing and interpretation of data and, more generally, information, at the time of data capture or later ("archival research"), and including aspects of the collaborative work and man-machine environments needed for this. To achieve this very broad goal, this Action will address a range of problems on the interface between astronomy and astrophysics, and the computational sciences. Serendipitously this Action will seek to tie together the work of astronomers and computer scientists, to mutual benefit.

The first problem this Action addresses is particularly relevant in the context of the astronomical DataGrid, i.e. the work of data centres, and their critical need for smart tools, especially for data ingest. Data centres require better ways to ingest their databasases and archives, since their current operations are simply not scalable. The individual astronomer has an analogous requirement, to master the heterogeneous and distributed sources of data and information.

Associated with this problem activity, the Action will concentrate efforts on a third-generation search interface for integrated access to distributed information services. This will include user profiling and support of metadata, characteristic of a second-generation system like ISAIA (details below in Section C), and will also include more general (structured and unstructured) online resources, visualization agents, and a natural language interface.

A second problem cluster this Action will address is that of visualization of scientific data, often across the network, and often too involving both virtual (i.e. simulated) data - of the heavens or of the instruments used for observing - and real data. Closely-related are technology trends in ultra high performance display capability (cf. large wall displays; or advances in mobile displays).

A third problem cluster this Action will address is related to very large image storage, transmission and processing. The Action will develop what may be termed

high performance data streaming. As an example consider how wavelet and other multiresolution transforms allow for progressive transfer. Consider too how large image delivery based on foveation makes use of the limited region of interest in the image data. Such paradigms, used for storage and transmission of images and video, have implications ultimately for scientific interpretation itself. How can the fusion of information and data, required by multiwavelength astronomy, be built seamlessly into these technologies (including resolution scale, compression, and region of interest)?

Keywords describing the principal areas of activity, targeted at astronomy and astrophysics, include: Cognitive science, collaborative work, knowledge discovery, data mining, computational intelligence, streaming interfaces, multiwavelength astronomy, data and information fusion, Bayesian modelling, display and storage device technology, distributed computing, distributed and heterogeneous databases.

C. Scientific programme

In order to fulfil these objectives, the scientific programme of the Action will be developed according to the following structure:

Data centres and data curation for the DataGrid.

This theme is concerned with the critical need for smart tools especially for data ingest.

A particular focus of the activities is to enhance data and information handling initiatives where participants in this Action have played a leading role, and develop new generation query agents to distributed heterogeneous astronomical databases and catalogues. One such project, involving major astronomical data providers in Europe, the US and Canada, was Astrobrowse. A new initiative is now building on this basis - ISAIA, a query and response agent, which is XML-based and embodies user profiling.

- Sub-themes:
  - distributed data,
  - information summarization,
  - information fusion,
  - metadata.
- Immediate tasks:
  - further development of metadata interoperability standards and of object-oriented databases in astronomy,
  - textual summarization tools,
  - first initiatives in user profiling in astronomy.

Visualization.

This theme is concerned with convergence between display technology and scientific interpretation.

The handling and scientific understanding of data will benefit from new developments in display technology, but not by simply (and crudely) scaling up traditional

procedures. Instead, qualitatively new and better ways of navigating information spaces, extracting knowledge from information, etc., have to be developed. It is only by defining and then addressing the specific scientific needs that it will be possible to provide spin-offs back into the commercial and industrial arena (and not the contrary, e.g. by taking, "undigested", currently-practiced data mining approaches from the commercial world).

Through a synergy between computer science and other closely-related methodological disciplines (e.g. statistics), with astronomers and astrophysicists, this Action seeks to have scientists collectively driving new developments in technology and methodology.

- Sub-themes:
  - display of information,
  - fusion of model and observed data,
  - knowledge discovery and data mining.
- Immediate tasks:
  - visualization for knowledge discovery and data mining,
  - further development of visual user interfaces to information spaces (currently in operational use for bibliographical and some catalogue databases).

Multimedia data handling.

This theme is concerned with the particular multimedia information which astronomy deals with: very large images, data of great accuracy and precision (and noise!), fusion of image and non-image information, and the links between observed data and (cosmological, instrument) model data.

- Sub-themes:
  - delivery platforms,
  - networks, wireless,
  - distributed computing,
  - multiband and hyperspectral image data.
- Immediate tasks:
  - display-optimized delivery of large images,
  - distributed image processing across the major image databases.

The three Theme Areas and corresponding Working Groups described in this Action clearly have areas of overlap with each other. Some of the data centres in WG1 are primarily concerned with image data (a major concern of WG3). The handling of image and other multimedia data (in WG2) is close to the priorities of WG3. The results of numerical simulations (cosmological, solar/planetary) in WG2

themselves comprise a data repository, of relevance for WG1, etc. All WGs are related to the DataGrid which is now being developed in Europe and further afield.

The Action web area will contain results of all meetings (programmes, presentations, and - where this proves feasible - a streaming video record on the web of all presentations).

Working visits of between a number of days to a week in duration will be arranged between partners, particularly for the PhD students and research assistants taking part in this work. Each such visit will have a particular theme, and specified targets (optimally part of a scientific paper, or to contribute to a software and/or hardware system).

Coordination visits between partners will also take place, especially to plan workshop themes which are relevant to more than one WG, and to focus aspects of the Action's activities in the broader scope of DataGrid and Virtual Observatory projects.

Interaction with other Grid initiatives.

The UK AstroGrid consortium came together during 2000 to propose a programme of DataGrid developments for UK astronomy to the PPARC research council. The anticipated spend by AstroGrid is around 5M £. The consortium represents a very wide range of data types, skills, and experience, with Edinburgh (sky survey data), Leicester (x-ray mission data), Rutherford Appleton Laboratories (space astronomy, solar and solar/terrestrial physics databases, and Starlink software project), Mullard Space Science Laboratory (solar databases), Cambridge (UK observatory archives), and Belfast (Computer Science). In addition there are formal links to the Edinburgh Parallel Computing Centre and the UK particle physics Grid coordination at Rutherford Appleton Laboratories. The year-1 workpackages focus on

(a) development of a science requirements document, and

(b) testing, assessment, and deployment of datamining hardware and Grid middleware toolkits.

The Working Groups described above in this COST Action match closely the data mining, visualization and information discovery workpackages planned in the AstroGrid work. Key participants in this Action are also core members of the AstroGrid consortium.

The UK AstroGrid is participating in the Fifth Framework AVO (Astrophysical Virtual Observatory) submission in February 2001. AstroGrid is represented as a group, through AstroGrid lead investigator Prof. Andy Lawrence, Royal Observatory Edinburgh. AVO lead investigators are Dr. Peter Quinn (ESO), Prof. Francoise Genova (Strasbourg) - cf. Steering Committee and supporters of this Action - and Dr. Piero Benvenuti (Space Telescope - European Coordinating Facility, located at ESO).

Liaison with relevant US activities will be facilitated through participation in NSF funded activities by a number of the participants in this Action, by possible participation of US experts in the Actions and by regular scientific contributions to conferences and workshops in North America, etc.

It is clear that this COST Action is well integrated with major current developments (just a few of which have been listed in this section). The COST Action coordinates and focuses unique computer and related information science perspectives in a way which is not done directly by the other projects.

Publ. Astron. Obs. Belgrade No. 73 (2002), 49 - 65 *Invited lecture*

GRAVITATIONAL MICROLENSES IN ACTIVE GALACTIC NUCLEI

L. Č. POPOVIĆ, P. JOVANOVIĆ, E. BON and M. S. DIMITRIJEVIĆ

Astronomical Observatory, Volgina 7, 11160 Belgrade, Serbia
E-mail lpopovic@aob.bg.ac.yu

Abstract. A short review of the gravitational microlensing phenomenology is given. The microlensing influence on radiation of QSOs is discussed. Taking into account recent determination of the Broad Line Region (BLR) size of AGN, we present our investigation of the importance of microlensing effect for spectral line shapes of AGN.

1. INTRODUCTION

The phenomenology of gravitational lenses effect, and introduction to this field has been given in several review papers and books (Schneider et al. 1992, Rafsdal and Surdej 1994, Fort and Mellier 1994, Zakharov 1996, Narayan and Bartelmann 1999, Paczyński 1996, Wambsganss 1999, Bartelmann and Schneider 1999, Mellier 1999, Claeskens and Surdej 2002). Consequently, we will no discuss here all aspects of the gravitational lenses in the universe, but we are going to present shortly the nature of the gravitational lensing effect in order to give the basic relations. The special attention we will pay to influence of gravitational microlensing on spectral line shapes.

The influence of microlensing effects on multiply imaged QSOs has been widely discussed (Ostriker and Vietri 1985; Kayser et al. 1986; Schneider and Weiss 1987; Nemiroff 1988; Irwin et al. 1989; Schneider and Wambsganss 1990; Yonehara et al. 1999; Mineshige and Yonehara 1999; Agol and Krolik 1999; Kraus et al. 1999; Belle and Lewis 2000; Popović et al. 2001ab, Abajas et al. 2002). It has been routinely assumed that only the continuum-emitting region of Active Galactic Nuclei (AGNs) is sufficiently compact to be affected by microlensing. However, recent results (e.g. Wandel et al. 1999, Kaspi et al. 2000) indicate that, also, Broad Line Regions (BLRs) of AGNs are smaller than was supposed before. Consequently, gravitational microlensing by stars in the lens galaxy can affect not only the continuum but also the broad emission lines of multiply imaged AGN (Popović et al. 2001ab, Abajas et al. 2002).

The aim of this paper is to give a short review of microlensing effect in AGNs, especially of the influence of microlensing effect on broad emission line shapes of AGN. In Section 2 we discus the gravitational lensing effect in general. In Section 3 we include microlensing effect in the case of different dynamics of emitting gas of

AGN and give the results of our investigation. In Section 4 conclusion is given. Some of the useful relations are given in Appendix (Section 5)

2. GRAVITATIONAL LENSING – PHENOMENOLOGY

Phenomelogy of multi-imaged celestial objects, well known as gravitational lens can be explained simply comparing this effect with atmospheric mirages. Since the light speed in a material medium is $v = c/n$ (where c is the light speed in vacuum, n is the refractive index), the light rays are bent when they travel into an inhomogeneous medium. Consequently in the lower atmospheric air layers with strong temperature or density gradients, the atmospheric mirages may be formed. On the other side, as a consequences of general relativity theory, space-time is curved by the gravitational potential ϕ, which depends on object mass, and in weak gravitational field approximation ($\phi/c << 1$) the equation of metric is (see e.g. Weinberg 1972)

$$ds^2 = -(1 + \frac{2\phi}{c^2})c^2dt^2 + (1 - \frac{2\phi}{c^2})(dx^2 + dy^2 + dz^2). \quad (1)$$

In the vicinity of the massive object, the light path is defined by null geodesic ($ds^2 = 0$). Moreover, taking into account that ($\phi/c << 1$), we can obtain for speed of light

$$v' \approx \frac{c}{1 - \frac{2\phi}{c^2}}, \quad (2)$$

and we can see that ϕ acts on the light speed as a medium with an effective refractive index n_ϕ as

$$n_\phi \approx 1 - \frac{2\phi}{c^2}. \quad (3)$$

Taking into account that a gradient in the Newtonian gravitational field exist in the vicinity of a massive object, the angular deflection of light trajectories $\vec{\alpha}$ will appear. Such deflected rays cause that an observer see the gravitational mirage of the source. The face of the mirage depends of mass of deflector, and the distances between the observer-source (D_{OS}), observer-lens (D_{OL}) and lens-source (D_{LS}).

Let us consider mass (M), so called deflector, at a distance D_{OD} from the observer and a point source S at a distance D_{OD} from the observer (see Fig. 1). The lens equation connects the source position, ($\vec{\theta_s}$) and the positions of the images ($\vec{\theta}$) seen by an observer (O), given the deflection angle $\vec{\alpha}$ produced by the gravitational lens (Fig 1). The lens equation can be written (see e.g. Zakharov 1996, Claeskens and Surdej 2002)

$$\vec{\theta_s} = \vec{\theta} - \frac{(D_{OS} - D_{OD})}{D_{OS}}\vec{\alpha}(D_{OD}\,\vec{\theta}). \quad (4)$$

To obtain the basic equations, let us consider two planes perpendicular to the line of sight, at the deflector and at the source distances, respectively. As seen by the observer (O), the deflector has angular coordinates (x_m, y_m) in the sky. Its projections in these two planes are in points A and A_s, with the corresponding linear coordinates

$$X_A = x_m D_{OD}, \qquad Y_A = y_m D_{OD}, \quad (5)$$

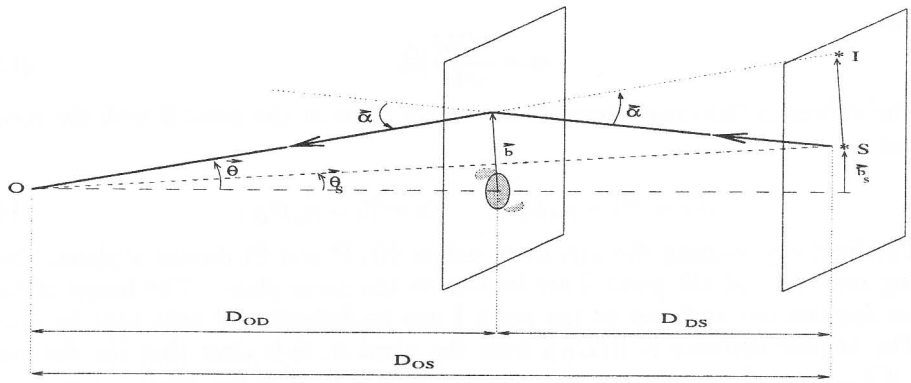

Fig. 1: The geometry of gravitational lensing: The observer, the lensing mass, and the source are located at the points O, M, and S, respectively. Light rays are deflected near the lensing mass by the angle α, and the image of the source appears to be located at the point I, not at S. The distances from the observer to the lens (deflector) and to the source are indicated as D_{OD} and D_{OS}, respectively.

$$X_{A_s} = x_m D_{OS}, \qquad Y_{A_s} = y_m D_{OS}. \tag{6}$$

Let the observer (O) look at the sky in the direction with angular coordinates (x, y). The line of sight intersects the deflector plane at point B which is defined by $\vec{b}$ and have coordinate

$$X_B = x D_{OD}, \qquad Y_B = y D_{OD}. \tag{7}$$

If there was no deflection of light by the massive object, the line of sight would intersect the source plane at point I with coordinates

$$X_I = x D_{OS}, \qquad Y_I = y D_{OS}. \tag{8}$$

The light ray passes the deflector at a distance

$$R = |\vec{b}| = \sqrt{(X_B - X_A)^2 + (Y_B - Y_A)^2}. \tag{9}$$

The light ray is deflected by the angle

$$\vec{\alpha} = \frac{4GM}{c^2}\vec{b}, \tag{10}$$

i.e. the angle has two components

$$\alpha_x = \alpha \frac{X_B - X_A}{R}, \tag{11}$$

$$\alpha_y = \alpha \frac{Y_B - Y_A}{R}, \tag{12}$$

where

$$\alpha = \frac{4GM}{c^2 b^2}|\vec{b}|. \tag{13}$$

The deflection light ray intersects the source plane at the point S with the coordinates

$$X_S = X_I - \alpha_x D_{DS}, \quad Y_S = Y_I - \alpha_y D_{DS}. \tag{14}$$

The light ray, passing through three points (O, B and S) defines a plane. The lensing mass M and the point I are located in the same plane. The image of the source appears not at S but at the point I due to deflection of light rays by mass M. The angular distance is R/D_{OD} from the point A. It is clear that the distance $|\vec{b}| + |\vec{b_s}| = (R + R_s)$ in the deflector plane is proportional to the distance between I and S in the source plane, and the latter can be calculated with Eq. (14). Including the Eqs. (11) and (12) in Eq (14) we obtain

$$R + R_s = \sqrt{(X_S - X_I)^2 + (Y_S - Y_I)^2}\frac{D_{OD}}{D_{OS}}, \tag{15}$$

$$R + R_s = \frac{4GM}{c^2 R^2}\frac{D_{DS}D_{OD}}{D_{OS}}, \tag{16}$$

This equation can be written as

$$R + R_s = \frac{R_E^2}{R},$$

where

$$R_E^2 = \frac{4GM}{c^2}\frac{D_{DS}D_{OD}}{D_{OS}} \tag{17}$$

is the Einstein Ring Radius (ERR). Eq. (16) has two solutions:

$$R_\pm = \frac{R_s^2 \pm \sqrt{R_s^2 + 4R_E^2}}{2}$$

This solution indicate two images of the source, located on the opposite side of the point A, at the angular distances R_+/D_{OD} and R_-/D_{OD}, respectively. Any of the lensing conserves surface brightness. The ratio of the image to source intensity, called amplification (A^m), is given by the ratio of their areas. This ratio can be calculated as (Pacyński 1996)

$$A_\pm^m = |\frac{R_\pm dR_\pm}{R_s dR_s}| = \frac{u^2+2}{2u\sqrt{u^2+4}} \pm \frac{1}{2}, \tag{18}$$

where distance between projected lens and source, expressed in ERR in source plane is

$$u = \frac{|\vec{b_s}|}{R_E}.$$

In the case of microlensing, it is not possible to see images of the source, but microlensing effect cause amplification of the source brightness. In this case the source amplification will be

$$A_+^m + A_-^m = \frac{u^2+2}{2u\sqrt{u^2+4}}. \tag{19}$$

On the other side, the chance of seeing a MLE is usually expressed in terms of the optical depth τ, which is probability that at any instant of time the source is covered by a deflector. The optical depth can be estimated computing the number of lenses within one ERR in line-of-sight. Let all lensing objects have identical mass $M_{\rm ml}$. We will divide the space between observer and source in a thin slabs, where one slab has thickness ΔD_{OD}. There is, on average one lens per surface area $\pi R^2 = \frac{M_{\rm ml}}{\rho \Delta D_{OD}}$, where ρ is the average mass density due to lenses in the volume $\pi\xi^2 \Delta D_{OS}$. The cross section of each lens is πR_E^2, where R_E is determined from Eq. (17).

The slab contribution to the optical depth is given as (Paczyński 1996)

$$\Delta\tau = \frac{\pi R_E^2}{\pi R^2} = [\frac{4\pi G\rho}{c^2}\frac{D_{DS}D_{OD}}{D_{OS}}]\Delta D_{OD}. \tag{20}$$

Taking that $\Delta D \to 0$, the total optical depth due to all lenses located in the part of spherical envelop can be calculated as

$$\tau = \frac{4\pi G}{c^2}\int_0^{D_s} \rho(D_{OD})\frac{D_{DS}D_{OD}}{D_{OS}} dD_{OD} \tag{21}$$

The solution of the integral in Eq. (21) depends on mass distribution of the deflectors, and several solution were performed (see e.g. Paczyński 1991, Kiraga and Paczyński 1994, Zakharov 1996).

As one can see from Eq. (21) the optical depth depends on the total mass in all lenses, but it is independent of the masses of individual lens. If the density of lenses is constant, we obtain

$$\tau = \frac{2\pi}{3}\frac{G\rho_{Av}}{c^2} D_{OS}^2$$

where ρ_{Av} is the averaged mass density of deflectors.

2. 1. CAUSTIC CROSSING

In most of cases we can not simply consider that microlensing is caused by an isolated compact object but we must take into account that the micro-deflector is located in an extended object (typically, the lens galaxy). In this case, when the size of the ERR of the microlens is larger than the size of the accretion disc, we can describe the microlensing in terms of the crossing of the disc by a straight fold caustic (Schneider et al. 1992). The amplification at a point close to the caustic is given by (Chang and Refsdal 1984),

$$A^m(X,Y) = A_0^m + \frac{K}{\sqrt{\kappa(\xi-\xi_c)}}\cdot H(\kappa(\xi-\xi_c)), \tag{22}$$

where A_0^m is the amplification outside the caustic, $K = A_0^m\beta\sqrt{\eta_0}$ is the caustic amplification factor, where β is constant of the order of unity (e.g. Witt et al. 1993). ξ is the distance perpendicular to the caustic and ξ_c is the minimum distance from the

source center to the caustic. The more complex function of caustic can be found in Shalyapin et al. (2002).

Some other useful relations are given in the Appendix.

3. MICROLENSING INFLUENCE ON AGN RADIATION

3. 1. STANDARD MODEL OF AGN

The investigation of influence of microlensing on AGN radiation (in first order on QSO radiation) is important for our knowledge about structure of AGN emission region. To simplify the task, the papers devoted to this theme usually take in consideration two cases: a) the source is a point and lens has complex structure (see e.g. Shalyapin 2002); b) the source is complex and lens is point-like (see e.g. Yonehara et al. 1999, Agol and Krolik 1999). Very rarely consideration of complex structure of source and complex structure of lens is given (Popović et al. 2002a, 2003).

The geometry of emission line region in AGN is very complex. Narrow Line Region (NLR) is too large that microlensing can affect the light from this region, but Broad Line Region and continuum source is enough compact that this effect may play a role. As a standard model of AGN we can adopt that in the central part of emission line region a Black Hole exist. The innermost part radiate in the X-ray range (including the X-ray continuum and lines, e.g. Fe Kα line). The continuum emitting source of AGN is also compact (several light days), while the BLR lay between several light days and several tens of light days (Wandel et al. 1999, Kaspi et al. 2000). Taking into account the dimensions of the emitting region we will consider only microlensing of radiation coming from X-ray and optical part in continuum and in lines.

The geometry of emission region of AGN can be very complex, usually three geometries may be considered: spherical, biconical and cylindrical (Robinson 1995). It is interesting that one part of radiation coming from accretion disc (especially in X-ray, and also in some cases in UV and optical wavelength region, see e.g Eracleous and Halpern 1994, Popović 2001b), or from the region which has more complex structure (accretion disc + one more emission region, see e.g. Popović et al. 2001c)

3. 2. MICROLENSING OF AGN

Quasars are the first objects observed as gravitational lenses. The importance of gravitational microlensing by individual stars in a 'lensing galaxy' was first pointed out by Chang and Refsdal (1979). Till now, the investigation of this type of the microlensing has been performed by a number of authors (see e.g. Schneider et al. 1992, Zakharov 1996). When a QSO is lensed by a galaxy into multiple images, the probability that one of the stars belonging to the lens transit just in front of one of the microlensed QSO images is much higher. The microlensing can be used to analyze the structure of the emitting region in AGN. It was the accepted opinion that the microlensing preferentially amplifies the continuum emission region, coming from the central part ($\sim 10^{-4} - 10^{-3}$ pc), while the broad emission line (BEL) flux remains unchanged, because the dimension of BEL assumed to be around 1pc (e.g. Rees 1984, Claeskens and Surdej 2002).

The change in the continuum flux of quasars by stars or compact objects in intervening galaxies is now a well-established observational phenomenon. Several studies have attempted to resolve the structure of the region generating the optical and UV

continuum by using the microlensing effect as a gravitational telescope (see Yonehara 1999).

Only extended objects of sizes comparable to or smaller than the Einstein radius associated with the gravitational lens will experience appreciable amplifications (e.g., Schneider et al. 1992). Thus, in the framework of the AGN standard model, in which the BLR is supposed to have a radius in the 0.1 – 1 pc range, only massive deflectors could give rise to significant amplifications. However, recent results from the MACHO project indicate that the most likely microdeflector masses in the Galactic halo are within the range 0.15 – 0.9 $M_{\odot}$ (Alcock et al. 2000a). In the Galactic bulge the microdeflector masses are in good agreement with normal-mass stars (Alcock et al. 2000b). Estimates from the light curve of Q2237+0305 (Wyithe et al. 2000) are also in reasonable agreement with these values. Consequently, significant amplifications of the BEL would not be expected according to the standard model. This result has been pointed out by other authors (Nemiroff 1988, Schneider and Wambsganss 1990), even if they were somewhat optimistic concerning the distribution of the microlens mass adopted. However, recent studies indicate that the BLR size is smaller (from several light days to several tens of light days) than supposed in the standard model (Wandel et al. 1999, Kaspi et al. 2000). On the other side, analyzing the spectral line shape of Akn 120 and NGC 3516 Popović et al. (2001c, 2002b) found that the broad line shape can be fitted with two-component model, where significant contribution has emission of disc or disc-like region. They found that the radius of disc region is of the order of 1000 R_g. Taking into account that the mass of black hole in AGNs is somewhere about $10^8 M_{\odot}$, the dimension of this region is $\sim 10^{-3} - 10^{-2}$ pc. These investigations showed that the influence of microlensing on the broad emission lines should be revised, and consequently, recently in several papers this influence have been presented (Popović et al. 2001ab, Abajas et al. 2002, Popović et al. 2002a).

Moreover, the X-Rays of AGNs are generated in the innermost region of an accretion disc around a central super-massive Black Hole (BH). An emission line from iron Kα (Fe Kα) has been observed at 6-7 KeV in the vast majority of AGNs (see e.g. Nandra et al. 1997, Fabian et al. 2000). This line is probably produced in the very compact region near the BH of an AGN (Iwashawa et al. 1999, Nandra et al. 1999, Fabian et al. 2000) and can bring essential information about the plasma conditions and the space geometry around the BH. Thus it seems clear that the Fe Kα line can be strongly affected by microlensing and recent observations of two lens systems seem to support this idea (Oshima et al. 2002, Chartas et al. 2002). In following part of this paper we will present the investigation devoted to microlensing of broad line region and X-ray emitting region.

3. 3. THE MICROLENSING INFLUENCE ON THE BLR OF QSOS

In order to calculate the influence of microlensing to the broad emission lines of AGN, we started from the relation

$$F_{\lambda} = \int_{V} \varepsilon(x,y) I(x,y,\lambda) A^{m}(x,y) dV \tag{23}$$

where F_{λ} is the line flux, $\varepsilon(x,y)$ is the emissivity, $I(x,y,\lambda,\lambda_0)$ is the function of line intensity which also depends on geometry of line emitting region and velocity of emission gas. $A^m(x,y)$ is the amplification defined by Eq. (19) for point-like deflector

and Eq. (22) for straight fold caustic. In this case the integration is in the plane of source, where $u = |\vec{b_s}(x,y)|/R_E$. The function of emissivity for BLR can be taken as

$$\varepsilon(r) = \varepsilon_0 \cdot r^q,$$

where q is the index of emissivity (e.g. in the case of disc emission $q = -3$, see e.g. Eracleous and Halpern 1994). The geometry and kinematics of emission gas determine the line intensity distribution through emission region. Very often the velocity of emission gas is assumed to be only function of distance from the central source (Robinson 1995)

$$v(r) = v_0 r^p$$

where p is the velocity index.

3. 4. MICROLENSING INFLUENCE ON X-RAY EMISSION

The influence of microlensing on X-ray radiation in continuum were considered in the papers of Yonehara et al. (1999). The influence on spectral line shape of Fe Kα line has been discussed in Chartas et al. (2002) and Popović et al. (2001b, 2002a).

In the standard configuration, microlensing affects one of the images of a lensed QSO and is produced by a star-sized object in the lens galaxy. An event of this type affecting the Fe Kα line has been reported in the quadruple imaged QSO J0414+0534 by Chartas et al. (2002). These authors observed a sudden increase in the iron line equivalent width from $\sim$ 190 eV to 900 eV only on image B of J0414+0534 proposing that it has been caused by a microlensing event. We can try to reproduce this enhancement with our models under the assumption of amplification by a straight fold caustic crossing. However the problem is highly unconstrained because both sets of variables, the one related to the microlensing (relative amplification, β, orientation of the caustic with respect to the rotation axis, direction of the caustic crossing, microlens mass) and the other related to the relativistic disc model (outer radius, emissivity, metric) should be considered to fit a unique number. Thus, we can do only an exploration of scenarios compatible with the result. In the first place we can fix the disc parameters adopted until now to study which values of the parameter β can reproduce the observed amplification in both metrics, Schwarzschild and Kerr. We have computed the maximum amplification for a caustic crossing along the accretion disc. The resulting amplifications indicate that there is a range of β values and microlens masses that can give rise to the observed amplification (see Table 1 and 2 in Popović et al. 2002a). For instance, for the value $\beta = 0.2$ (Chartas et al. 2002), a microlens of a solar mass can produce the observed enhancement. For $\beta = 1$, a low mass lens ($\sim 0.001\ M_\odot$) can also produce the required amplification.

Oshima et al. (2001) have also reported the presence of a strong (EW$\sim 960eV$) emission Fe Kα line in the integrated spectra of the lensed QSO H 1413+117. Oshima et al. (2001) interpreted this results as produced by iron K_α emission arising from X-Ray re-processing in the broad absorption line region flow. Alternatively, we can assume that the individual spectra of the components (not available) are different, and that the excess emission in the iron line arises only from one of the components, like in the case of J0414+0534.

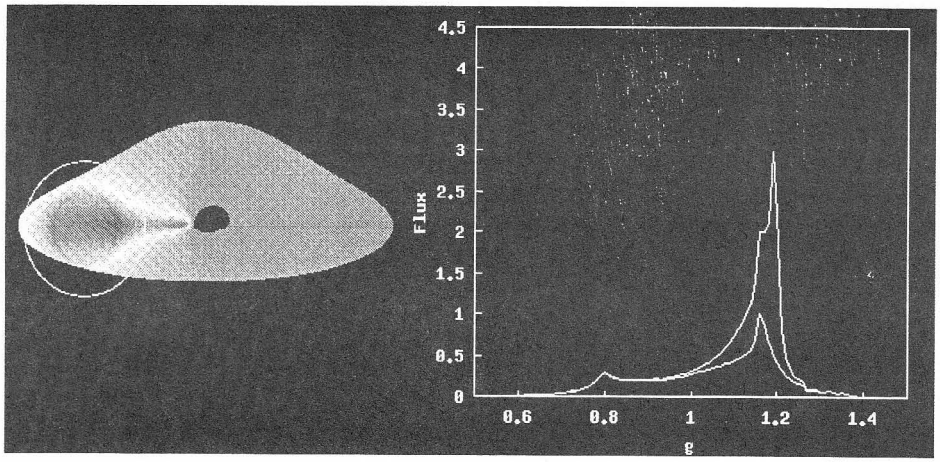

Fig. 2: *Left:* The point-like deflector crossing an accretion X-ray disc in Kerr metrics (illustration). *Right:* Corresponding amplification of Fe Kα line, bottom is unperturbed line (Popović et al. 2003)

Regardless of the true nature of the two events reported in J0414+0534 and H 1413+117, our analysis show that objects in a foreground galaxy with even relatively small masses can bring strong changes in the line flux. This fact indicates that changes in the Fe Kα line flux will be higher than in the UV and optical lines. Thus, the observation of the iron line in multi-imaged AGNs opens new possibilities to study the unresolved structure in QSOs and also the nature and distribution of compact objects in lens galaxies.

From this investigation one can conclude (see Popović et al. 2002a, 2003)

– Microlenses of very small projected Einstein radii ($\sim$ 10 R_g) can give rise to significant changes in the iron line profiles. The effects are two or three order of magnitude larger than the ones inferred for the UV and optical lines (Popović et al. 2001a). Off-centered microlenses would induce strong asymmetries in the observed line profiles.

– The effects of microlensing show differences in the Kerr and Schwarzschild metrics, the amplitude of the magnification being larger in the Kerr metric. The transit of a microlens along the rotation axis of the accretion disc would induce a strong amplification of the blue peak in the Schwarzschild metric when the microlens was centered in the approaching part. In the Kerr metric the amplification will be larger but will not affect so preferentially the blue part of the line. This difference could be interesting to probe the rotation of an accretion disc.

– Even objects of very small masses could produce observable microlensing in the iron Kα line of multiple imaged QSOs. We obtain that microlenses of 1 solar mass can explain the measured Fe Kα line excess in the J0414+0534 and H 1413+117 lens systems.

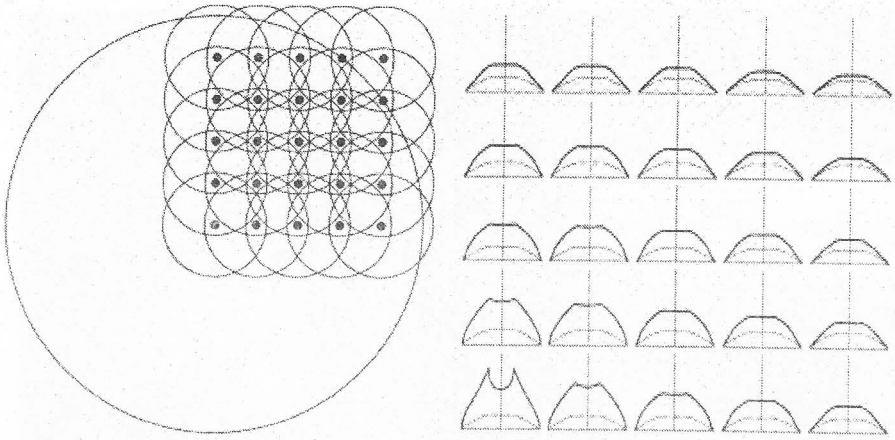

Fig. 3: *Left:* Grid of relative displacements between the microlens and the BLR. The large disc represents the BLR. The small discs correspond to the Einstein circle associated with the microlens, represented by a point. For each point (corresponding to a displacement of the microlens in the positive quadrant we compute an emission-line profile. *Right:* Spherical model with p=0.5, q=-1.5, and ERR is equivalent to dimension of BLR. On the x-axis we represent $x = v_{max}(\lambda - \lambda_0)/(c \cdot \lambda_0)$, which varies between -1 and 1. On the y-axis we represent the flux. The heavy solid line is the amplified line profile, and the lighter solid line is the unamplified line profile (Abajas et al. 2002).

3. 5. MICROLENS OF BLR; UV AND OPTICAL LINES

Here we will present some of the results concerning the microlensing influence on broad spectral line shapes. First, for different geometries the influence is given in Abajas et al. (2002), where the spherical, cylindric and biconical geometries of BLR were considered. Also, the influence in the case of Keplerian accretion disc was considered (Popović et al. 2001a)

From the investigation of the influence of microlensing on spectral line shapes of broad line from Broad Line Region we can conclude (see Abajas et al. 2002):

– The global amplification of the BEL induced by microlensing events could be relevant. It was identified a group of 10 gravitational lens systems (about 30% of the total sample) for which the microlensing effect could be observable, especially in high-ionization lines. In other gravitational lenses the microlensing amplifications would be much more modest.

– Even for relatively small microlenses corresponding to high values of the BLR radius/Einstein radius quotient, (BLR dimension are around 4 times larger than ERR), the effects produced by the differential amplification of the line profile (relative enhancement of different parts of the line profile, line asymmetries, displacement of the peak of the line, etc.) would be easily detectable except for highly symmetric velocity fields. The displacement of the peak of the line profile caused by microlensing is especially interesting, since it could otherwise induce inexplicable redshift differences between the different images in a gravitational lens system.

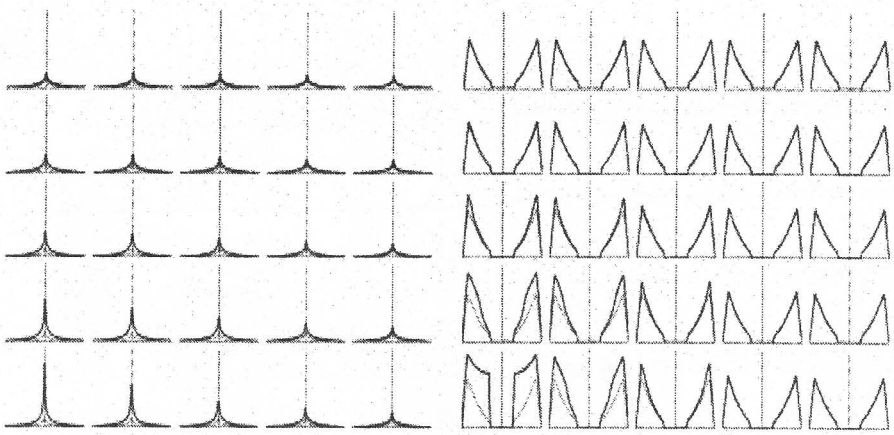

Fig. 4: *Left:* The same as in Fig. 3 (left), but for p=2, q=-1.5 *Right:* The same as at left, but for biconical model with i= 0, p=0.5, q=-1.5, and ERR is 1/4 of BLR dimension.

– The study of the changes between the BEL profiles corresponding to microlensed and non-microlensed images, or among the BEL profiles of lines with different ionization in a microlensed image, could be useful for probing current ideas about BLR size and stratification.

The influence of gravitational microlensing on the spectral line profiles originating from a relativistic accretion disc was considered in Popović et al. (2001a). Using the Chen et al. (1989) model for the disc, we show the noticeable changes that microlensing can induce in the line shape when the Einstein radius associated with the microlens is of a size comparable to that of the accretion disc. Of special interest is the relative enhancement between the blue and red peaks of the line when an off-center microlens affects the approaching and receding parts of the accretion disc asymmetrically (Popović et al. 2001a).

In an AGN formed by a super-massive binary in which the accretion disc is located around one of the super-massive companions (the primary), we discuss the possibility of microlensing by the secondary. In this case the ratio between the blue and red peaks of the line profile would depend on the orbital phase. We have also considered the more standard configuration of microlensing by a star-sized object in an intervening galaxy and find that microlensing may also be detected in the broad emission lines of multiply imaged QSOs. The changes observed in the line profile of Arp 102 B are taken as a reference for exploring both scenarios.

From this investigation one can conclude (Popović et al. 2001a):

– Gravitational microlensing can induce significant changes in the spectral line profiles generated by an accretion disc, even for relatively small values of the Einstein ring radius associated with the microlens (ERR$\simeq$ 40 R_g). Off-centered microlenses can induce relative enhancements of the blue and red peaks of the line profile, or even give rise to a central peak. These effects could be very strong when ERR is comparable to the disc dimension, $R_{out} - R_{in}$.

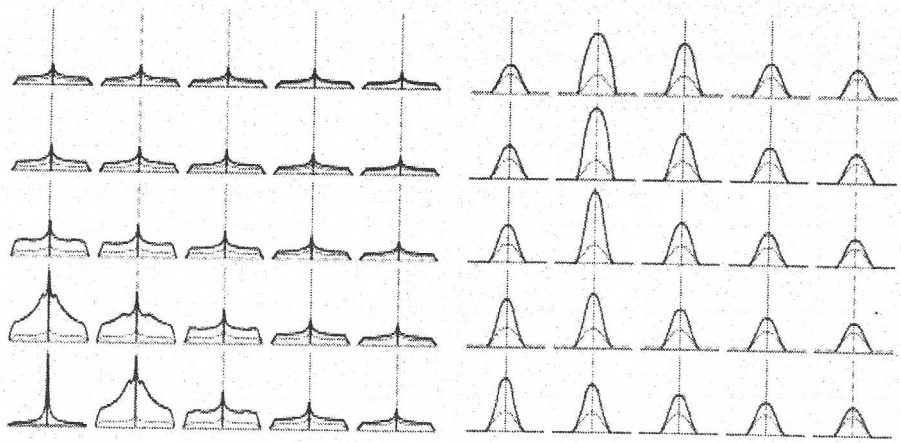

Fig. 5: *Left:* The same as in Fig. 4(right), but for i=0, p=2, q=-1.5, and REE is the same as BLR dimension. *Right:* The same as left, but for i=90, p=0.5, q=-1.5 (Abajas et al. 2002).

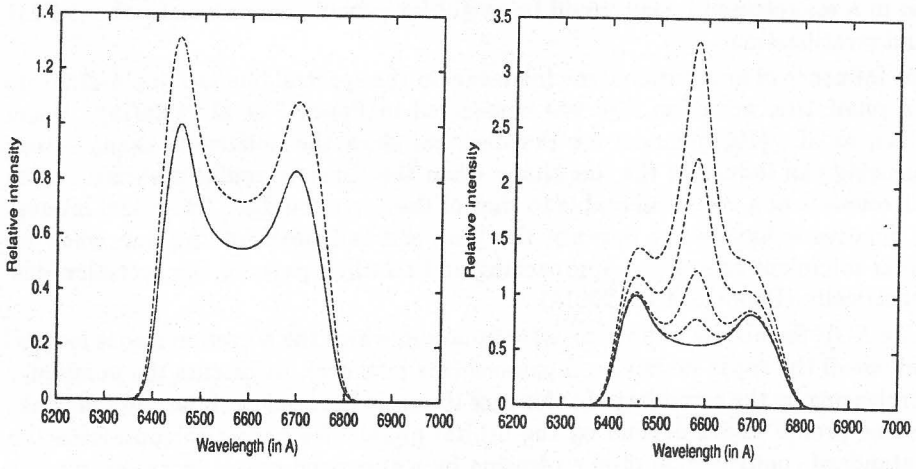

Fig. 6: *Left:* The H_α line profile calculated for a relativistic disc with parameters $i = 32°$, $R_{\rm in} = 350\ R_{\rm g}$, $R_{\rm out} = 1000\ R_{\rm g}$ and $\sigma/\lambda_0 = 850$ km s^{-1}. The profile deformed by gravitational microlensing is represented by the dashed line. The parameters of the gravitational microlens are: $\xi_0 = 0\ R_{\rm g}$, ERR= $500\ R_{\rm g}$ and $\phi_0 = 90°$. The unperturbed profile is represented by the solid line. *Right:* The line profiles for different Einstein ring radii of the lenses ERR= $100\ R_{\rm g}$, $200\ R_{\rm g}$, $400\ R_{\rm g}$ and $600\ R_{\rm g}$, respectively. The intensity of the central part is higher for higher ERR. The calculations were performed for $\xi_0 = 500\ R_{\rm g}$ and $\phi_0 = 0°$ (Popović et al. 2001a).

– We found that a compact object of $\sim 1\ M_\odot$ in an intervening galaxy could give rise to effects easily detectable in the emission line profiles. That implies that, contrary to what has been assumed, not only the continuum but also the emission lines may be susceptible to microlensing in multiply imaged QSOs (in so far as the accretion disc model for Arp 102 B applies to a typical BLR).

– The transit of a microlens along the accretion disc can qualitatively reproduce the quasi-periodical variability of the ratio of red-to-blue peak intensities observed in the case of Arp 102 B in the 1990–1995 period.

In Popović et al. (2001a) two different physical scenarios that could reproduce the observed variability in Arp 102 B: i) microlensing by a super-massive companion ($M \approx 10^7\ M_\odot$) located at a distance of around 0.3 pc, and ii) microlensing by a compact object of a mass $\sim 1\ M_\odot$ in an intervening galaxy. The sinusoidal-like variation induced by microlensing does not extend beyond one period. It can be reproduced again after a long lapse of time (in the case of the super-massive companion) or randomly (in the case of the microdeflector in a intervening galaxy). This could be useful in distinguishing between microlensing and other different options that are strictly periodical, such as the model of an accretion disc with a hot spot.

4. Concluding remarks

The microlensing effect is widely investigated. Using this effect in the case of AGN we can investigate the structure of continuum source, as well as structure of line emitting region from X-ray to optical wavelength region. Recent investigation showed that this effect can be useful for mapping of very compact and kinematically complex continuum and line region in AGN.

5. Appendix

5. 1. SOME RELATION WHERE $D_{OD} \approx D_{OS}$

The size of the ERR projected on the source, R_E increases with the distance between the source and the microlens. For this reason, appreciable amplifications of the optical and UV Broad Emission Lines (i.e. R_E comparable or larger than the dimensions of the accretion disc) induced by a star-sized object are only possible if the microlens is far away from the source, in an intervening galaxy (typically the lens galaxy). In the optical and UV case, appreciable amplifications of the BELs from an object in the host galaxy of the AGN are possible only by a very massive object (Popović et al. 2001a). However, due to the comparatively tiny dimensions of the X-Ray line emission region, microlensing of a star-sized object in the host galaxy becomes a possibility.

In the case $D_{OD} \approx D_{OS}$ the distance, $D = D_{OL} = D_{OS} - D_{OL}$, between the microlens and the accretion disc is negligible with respect to the distance between the observer and the microlens, the expression for R_E (Eq. 17) can be approximated as

$$R_E \approx \sqrt{\frac{4GM_s}{c^2} \cdot D}, \qquad (A1).$$

From Eq. (A1) the mass of the microlens can be estimated as

$$M_s \approx \frac{R_E^2}{D} \cdot \frac{c^2}{4G} = 5.23 \cdot 10^{12} \cdot \frac{R_E^2}{D}\ M_\odot, \qquad (A2)$$

where R_E and D, are given in parsecs.

It is sometimes convinient to express Eq. (A1) in gravitational radii:

$$R'_E \approx \sqrt{\frac{4GM_{ml}}{c^2} \cdot D}, \tag{A3}$$

where $R'_E = R_E \cdot R_g$, and from Eq. (A3) the mass of the microlens can be estimated as

$$M_{ml}[M_\odot] \approx \frac{R_E^2}{D} \cdot \frac{G}{4c^2} M_{BH}^2 = 1.19 \cdot 10^{-14} \cdot \frac{R_0^2}{D} M_{BH}^2, \tag{A4}$$

where R_E is given in gravitational radii, D is given in parsecs and M_{BH} is given in solar masses.

5. 2. OPTICAL DEPTH FOR MICROLENSING OF HOST BULGE AND HALO STARS

The probability of seeing a MLE is usually expressed in terms of the optical depth τ. As far as the potential microdeflectors have an Einstein radius similar or larger than the radius of the disc, τ can be estimated as the fraction of the area in the source plane covered by the projected Einstein radii of the microlenses. Taking also into account that the distance between the accretion disc and the microlenses are negligible as compared with the distance between the observer and the microlenses

$$\tau \sim \frac{4\pi G}{c^2} \int_0^R \rho(r) r dr \tag{A5},$$

where R is the radius of the bulge or halo.

To estimate the order of magnitude of τ we assume a constant mass density, thus

$$\tau \approx \frac{2\pi G}{c^2} \rho_o R^2. \tag{A6}$$

Czerny et al. (2001) estimated that the total mass of the AGN bulges can reach values of $10^{12} M_{sun}$ and Schade et al. (2000) found typical values for the radius of the AGN bulges within the range 1–10 Kpc. Both results yield to a maximum optical depth from the bulge $\tau_b \sim 10^{-4}$. Using also favorable numbers for the galactic halo ($\rho \sim 0.01 M_{\rm sun}$ pc^{-3}, $R \sim 150$ Kpc) the optical depth could reach values of $\tau_h \sim 10^{-4}$. Adding both contributions a maximum optical depth of $\tau \sim 0.001$ would be expected in a favorable situation. A detailed computation of τ, in addition to include accurate density profiles, should include a cut in the lower limit of integration (r_{min}) to exclude from the integral the microdeflectors with Einstein radii smaller than the radius of the disc (although the approximation $r_{min} \sim 0$ used does not change significantly the order of magnitudes estimated for τ especially in the case of the halo).

5. 3. RELATION MASS OF DEFLECTOR *vs.* *CORRESPONDING REE*

Very often it is needed to calculate the masses of deflectors able to produce the visible amplification of the line. In this case it is convenient to express the REE in gravitational radii. As a rule, if the REE is with size of the order of emitting region, than we can expect that microlensing is present.

In a Friedmann universe for an observer at redshift z_i and a source at redshift z_j, the angular diameter distance is given by (Grogin and Narayan 1996)

$$D(z_i, z_j) = \frac{2c}{H_0} \frac{(1 - \Omega_0 - G_i G_j)(G_i - G_j)}{\Omega_0^2 (1 + z_i)(1 + z_j)^2}, \qquad (A7)$$

where H_0 is the Hubble constant, and we suppose that $H_0 = 50$ km s^{-1} Mpc^{-1}, $\Omega_0 = 1$. The factors G_{ij} are

$$G_{ij} = \sqrt{1 + \Omega_0 \cdot z_{ij}}. \qquad (A8)$$

As an example we will calculate this relation for MG J0414+0534, taking into account that $Z_{QSO} = 2.64$ and $Z_{lens} = 0.96$, we obtain $D_{0,0.96} = 1749$, $D_{0,2.64} = 1574$, and $D_{0.96,2.64} = 630$. Using the Eq. (17) for ERR we can calculate the ERR in deflector plane

$$r_E = \frac{R_E}{D_{OD}},$$

or

$$r_E = \sqrt{\frac{4GM_{ml}}{c^2} \cdot D'}$$

where

$$D' = \frac{D_{OS} D_{DS}}{D_{OD}}.$$

In our case $D' = 567$ Mpc and if we put the constants, we obtain

$$r_E = \frac{9.2 \cdot 10^{-2}}{M_8^{BH}} \sqrt{M_{ml} \cdot D'}$$

where mass of black hole is given in 10^8 solar masses, M_{ml} is given in solar mass, D in parsecs and r_E in gravitational radii. For the case MG J0414+0534 the relation between ERR and mass of lens is

$$r_E = 2.19 \cdot 10^3 \sqrt{M_{ml}},$$

and as we can see the object of mass of only 0.0001 $M_\odot$, has an ERR of about 50 R_g, and can produce significant amplification of Fe Kα line if we assume that the dimension of the region of formation of Fe Kα line is around 100 R_g (Nandra et al. 1997).

References

Abajas, C., Mediavilla, E. G., Muñoz, J. A., Popović, L. Č., Oscoz, A.: 2002, *Astrophys. J.*, **576**, 640.

Agol, E., Krolik, J.: 1999, *Astrophys. J.*, **524**, 49.

Alcock, C.: 2000a, *Astrophys. J.*, **541**, 734.

Alcock, C.: 2000b, *Astrophys. J.*, **542**, 281.

Bartelmann, M., Schneider, P.: 1999, *Astron. Astrophys.*, **345**, 17.

Belle, K.E., Lewis, G.F.: 2000, *Publ. Astron. Soc. Pacific*, **112**, 320.

Chang, K, Refsdal, S.: 1979, *Nature*, **282**, 561.

Chang, K, Refsdal, S.: 1984, *Astron. Astrophys.*, **132**, 168.

Chartas, G., Agol, E., Eracleous, M., Garmire, G., Bautz, M. W., Morgan, N. D.: 2002, *Astrophys. J.*, **568**, 509.

Chen, K., Halpern, J. P., Filippenko, A. V.: 1989, *Astrophys. J.*, **339**, 742.

Claeskens, J.-F., Surdej, J.: 2002, *Astron. Astrophys. Rev.*, **10**, 263.
Czerny, B., Nikolajuk, M., Piasecki, M., Kuraszkiewicz, J.: 2001, *Mon. Not. Roy. Ast. Soc.*, **325**, 865.
Fabian, A.,C., Iwashawa, K., Reynolds, C.,S., Young, A.,J.: 2000, *Publ. Astron. Soc. Pacific*, **112**, 1145.
Fort, B., Mellier, Y.: 1994, *Astron. Astrophys. Rev.*, **5**, 239.
Grogin, N. A., Narayan, R.: 1996, *Astrophys. J.*, **464**, 92.
Eracleous, M., Halpern, J. P.: 1994, *Astrophys. J.*, **549**, 205.
Irwin, M. J., Webser, R. L., Hewett, P. C., et al.: 1989, *Astron. J.*, **98**, 1989.
Iwashawa, K., Fabian, A. C., Young, A. J., Inoue, H., Matsumoto, C.: 1999, *Mon. Roy. Astr. Soc.*, **306**, L19.
Kaspi, S., Smith, P. S., Netzer, H., Maoz, D., Jannuzi, B. T., Giveon, U.: 2000, *Astron. Astrophys.*, **533**, 631.
Kayser, R., Refsdal, S., Stabell, R.: 1986, *Astron. Astrophys.*, **166**, 36.
Kiraga, M., Paczyński, B.: 1994, *Astrophys. J.*, **430**, L101.
Kraus, A., Witzel, A., Krichbaum, T. P., Lobanov, A. P., Peng, B., Ros, E.: 1999, *Astron. Astrophys.*, **352**, 107.
Mellier, Y.: 1999, *Ann. Rev. Astron. Astrophys.*, **37**, 127.
Mineshige, S., Yonehara, A.: 1999, *Publ. Astron. Soc. Japan*, **51**, 497.
Nandra, K., George, I. M., Mushotzky, R. F., Turner, T. J. and Yaqoob, T.: 1997, *Astrophys. J.*, **477**, 602.
Nandra, K., George, I. M., Mushotzky, R. F., Turner, T. J. and Yaqoob, T.: 1999, *Astrophys. J.*, **523**, L17
Narayan, R., Bartelmann, M.: 1999, in: *Formation of Structure in the Universe* (Eds. A. Dekler, J.P. Ostriker) Cambridge University Press, p. 360.
Nemiroff, R. J.: 1988, *Astrophys. J.*, **335**, 593.
Oshima, T., Mitsuda, K., Fujimoto, R., Iyomoto, N., Futamoto, K., et al.: 2002, *Astrophys. J.*, **563**, L103.
Ostriker, J. P., Vietri, M.: 1985, *Nature*, **318**, 446.
Paczyński, B.: 1991, *Astrophys. J.*, **371**, L63.
Paczyński, B.: 1996, *Annu. Rev. Astron. Astrophys.*, **34**, 419.
Popović, L. Č., Mediavilla, E. G., Muñoz, J.: 2001a, *Astron. Astrophys.*, **378**, 295.
Popović, L. Č., Mediavilla, E. G., Muñoz, J., Dimitrijević, M. S., Jovanović, P.: 2001b, *Serb. Astron. J.*, **164**, 73 (Also, presented on GLITP Workshop on Gravitational Lens Monitoring, 4-6 June 2001, La Laguna, Tenerife, Spain).
Popović, L. Č., Stanić, N., Kubičela, A., Bon, E.: 2001c, *Astron. Astrophys.*, **367**, 780.
Popović, L. Č., Mediavilla, E. G., Jovanović, P. Muñoz, J.: 2002a, *Astron. Astrophys.*, accepted.
Popović, L. Č., Mediavilla, E. G., Kubičela, A., Jovanović, P.: 2002b, *Astron. Astrophys.*, **390**, 473.
Popović, L. Č., Jovanović, P., Mediavilla, E. G., Muñoz, J.: 2003, *Astron. Astrophys. Trans.*, accepted.
Rafsdal, S., Surdej, J.: 1994, *Rep. Progr. Phys.*, **57**, 117.
Rees, M.J.: 1984, *Ann. Rev. Astron. Astrophys.*, **22**, 471.
Robinson, A.: 1995, *Mon. Not. Roy. Ast. Soc.*, **272**, 647.
Schade, D. J., Boyle, B. J., Letawsky, M.: 2000, *Mon. Not. Roy. Ast. Soc.*, **315**, 498.
Schneider, P., Wambsganss, J.: 1990, *Astron. Astrophys.*, **237**, 42.
Schneider, P., Weiss, A.: 1987, *Astron. Astrophys.*, **171**, 49.
Schneider, P., Ehlers, J., Falco, E. E.: 1992, *Gravitational Lenses*, Springer-Verlag, Berlin Heidelberg, New York.
Shalyapin, V. N., Goicoechea, L.J., Alcalde, D., Mediavilla, E. Muñoz, J.A., Gil-Merino, R.: 2002, *Astrophys J.*, **579**, 127.
Wambsganss, J.: 1999, *Reviews in Modern Astronomy* , **12**, 142.
Wandel, A., Peterson, B. M., Malkan, M. A.: 1999, *Astrophys. J.*, **526**, 579.
Weinberg, S.: 1972, *Gravitation and Cosmology*, John Wiley and Sons Inc., New York – London – Sydney – Toronto.
Witt, H. J., Kayser, R., Refsdal, S.: 1993, *Astron. Astrophys.*, **268**, 501.

Wyithe, J. S. B., Webster, R. L., Turner, E. L.: 2000, *Mon. Not. Roy. Astron. Soc.*, **315**, 51.
Yonehara, A., Mineshige, S., Fukue, J., Umemura, M., Turner, E. L.: 1999, *Astron. Astrophys.*, **343**, 41.
Захаров, А. Ф.: 1996, *Гравитационные линзы и микролинзы*, Наука, Москва.

Publ. Astron. Obs. Belgrade No. 73 (2002), 67 - 71 *Poster*

TURING FORMATIONS IN ACCRETION DISC - AS A REACTION-DIFFUSION SYSTEM

ANDREEVA D. V., FILIPOV L. G., DIMITROVA M. M.
Space Research Institute, BAS
E-mail danvasan@space.bas.bg

Abstract. The necessary conditions which have to be realized for structures formation are presented. We have given the description of Turing formations and their corresponding equations, related to the reaction-diffusion processes. As a result, we have shown that in accretion discs the solutions for appearing of these structures exist.

1. Introduction

We present the following statements and results on the base of the theory of regular spatial structures and new tendency in nonlinear sciences in some hydrodynamical flows.

Below are shown the principles and necessary conditions for arizing of such structures (Stratonovich 1985, Ebeling 1979):

- Dissipative structures can be formed in open systems only, where the energy exchange is possible, which provide the existence of order states.
- Dissipative structures may arize in macroscopic systems. Necessary are states far from equilibrium.
- The evolution laws must operate in these systems.
- Dissipative structures can be formed in systems, described only by nonlinear equations for macroscopic functions.

When given conditions for thermodynamical equilibrium exist, then this corresponds to the largest rate of disorder. Due to this, higher organized states must be in nonequilibrium.

The states, obtained from equilibrium by continuous disturbance, Prigozin (Glensdorf & Prigozin 1973) terms thermodynamical branching. If the deviation from equilibrium exceeds the critical value, these states would become unstable. After that the system turns into new regime and establishes as a dissipative structure.

This qualitative reconstruction of the system, when the parameter crosses the critical value, is known as bifurcation.

To make this clear, we show one process (Nicolis & Prigozin 1979), which causes systematical deviations from equilibrium by increasing some parameters, describing states or outer influence - λ .

According to the minimum entropy theorem - the closest equilibrium stationary states are asymptotically stable /Fig. 1/ (a).

When the parameter of the system reaches the critical value $\lambda_{\tilde{n}}$, it is very possible that the thermodynamical branching becomes unstable (b).

In this case the smallest perturbation is sufficient to change the system. The new stability regime in the system probably corresponds to the orderly state (c). So, with $\lambda = \lambda_{\tilde{n}}$ the bifurcation acts and as a result the new branching of solution has occurred.

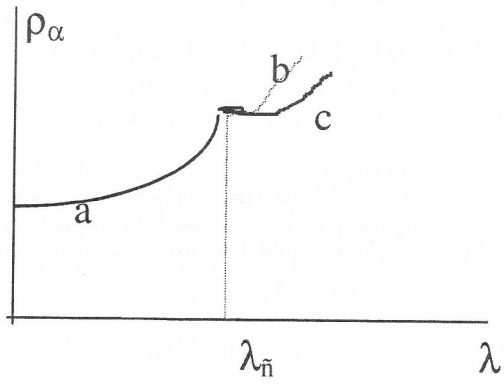

Fig. 1:

In our discussion of accretion disc, there is a similar transition. The arising of some hydrodynamical instability transfers the system from one state to another and therefore the structures are formed in disc. We have shown in the previous work, that the accretion discs are typical dissipative structures. Our aim here is to consider in particular their mode.

2. Reaction - diffusion equations and Turing instability

The reaction - diffusion systems are the exibition of spatial or temporal patterns if they are far from equilibrium (Engelhardt 1994), which is one important condition for formation of the dissipative structures.

First we apply one standard equation of reaction - diffusion (Engelhardt 1994):

$$\frac{\partial c}{\partial t} = F(C) + D\nabla^2 C \qquad (1)$$

where the first term on the right side is the reaction and the second is the diffusion. D is the diffusion coefficient (or matrix of the transport coefficient), C- concentration of matter.

In some systems the coupling between two transport procceses provides the engine of instability. Then the growth of this instability is defined by the difference of the diffusion coefficients in the different direction of the transport acting there (Borckmans et all. 2001).

Then the reaction - difusion equation could be written as:

$$\frac{\partial C}{\partial t} = F(C) + D_x \frac{\partial^2 C}{\partial x^2} + D_y \frac{\partial^2 C}{\partial y^2} \tag{2}$$

That difference between two components of diffusion coefficients is the necessary restriction for the Turing instability to appear (Engelhardt 1994).

3. The accretion disc equations and the appearing of Turing structures

The accretion disc is considered as a hydrodynamical systems and it is described by the hydrodynamical equations (Frank et all. 1991).

In the first place this is the continuity equation, which expresses the mass conservation:

$$\frac{\partial \rho}{\partial t} + \nabla.(\rho v) = 0 \tag{3}$$

The conservation of momentum for each gas element gives with Euler equation:

$$\rho \frac{\partial v}{\partial t} + \rho v.\nabla v = -\nabla P + F \tag{4}$$

where for both equations the quantities ρ, v, P, F are respectively: the density, the velocity, the pressure and the selected force.

We present the equation of motion for viscous fluid (Navier Stokes eq.) in cylindrical coordinates. Due to averaging in z-direction we express all derivatives in terms of the coordinates (r, φ):

$$\frac{\partial V_r}{\partial t} + V_r \frac{\partial V_r}{\partial r} + \frac{V_\varphi}{r} \frac{\partial V_r}{\partial \varphi} - \frac{V_\varphi^2}{r} =$$

$$-\frac{1}{\rho}\frac{\partial P}{\partial r} + \frac{1}{\rho} F_r + \nu \left(\frac{\partial^2 V_r}{\partial r^2} + \frac{1}{r^2}\frac{\partial^2 V_r}{\partial \varphi^2} + \frac{1}{r}\frac{\partial V_r}{\partial r} - \frac{2}{r^2}\frac{\partial V_\varphi}{\partial \varphi} - \frac{V_r}{r^2} \right) \tag{5}$$

$$\frac{\partial V_\varphi}{\partial t} + V_r \frac{\partial V_\varphi}{\partial r} + \frac{V_\varphi}{r} \frac{\partial V_\varphi}{\partial \varphi} - \frac{V_r V_\varphi}{r} =$$

$$-\frac{1}{\rho r}\frac{\partial P}{\partial \varphi} + \frac{1}{\rho} F_\varphi + \nu \left(\frac{\partial^2 V_\varphi}{\partial r^2} + \frac{1}{r^2}\frac{\partial^2 V_\varphi}{\partial \varphi^2} + \frac{1}{r}\frac{\partial V_\varphi}{\partial r} - \frac{2}{r^2}\frac{\partial V_r}{\partial \varphi} - \frac{V_\varphi}{r^2} \right) \tag{6}$$

Here ν is the kinematic viscousity, V_r and V_φ are the two component of the velocity.

The equation of energy transfer could be presented as follows:

$$\frac{\partial}{\partial t}\left(\frac{1}{2}\rho v^2 + \rho\varepsilon \right) + \left[\left(\frac{1}{2}\rho v^2 + \rho\varepsilon + P \right) v \right] = f.v - \nabla.F_{rad} \tag{7}$$

where $\frac{1}{2}\rho v^2$ - the kinetic energy per unit volume, $\rho\varepsilon$ – internal or thermal energy per unit volume. The last term in the square brackets represents the so-called pressure work. On the righ hand side:

F_{rad} – the radiative flux vector;

$-\nabla.F_{rad}$ – gives the rate at which radiant energy is being lost by emission, or increased by absorbtion.

In accretion disc we consider the transport of "vortical" function or vorticity, which we may imply with Ψ. This term we take from the vortical equation (Nauta 2000):

$$\left(\frac{\partial}{\partial t} + \vec{v}.\nabla\right) \frac{\nabla \times \vec{v}}{\rho} = 0 \tag{8}$$

which is obtained, combining the rotation of momentum equation and the continuity equation. So, $\Psi = \nabla \times \vec{v}$ and for eq. (8) yelds:

$$\left[\frac{\partial \Psi}{\partial t} + \nabla.(\Psi \vec{v})\right] = f \tag{9}$$

We express that equation in cylindrical coordinates in terms of r, φ again:

$$[\frac{\partial \Psi_r}{\partial t} + V_r \frac{\partial \Psi_r}{\partial r} + \frac{\Psi_\varphi}{r}\frac{\partial V_r}{\partial \varphi} - \frac{\Psi_\varphi^2}{r}] = f \tag{10}$$

$$[\frac{\partial \Psi_\varphi}{\partial t} + V_r \frac{\partial \Psi_\varphi}{\partial r} + \frac{\Psi_\varphi}{r}\frac{\partial V_\varphi}{\partial \varphi} - \frac{\Psi_r \Psi_\varphi}{r}] = f \tag{11}$$

Here with f we express the transport engine of the vortex or the diffusion from Eq. (1) and for our consideration the f is in the form: $D\nabla^2\Psi$.

Taking into account the vortical equation (9) and the expressions (10) and (11), the reaction - diffusion equation (1) becomes:

$$\frac{\partial \Psi_r}{\partial t} = h(r, \varphi) + D_r \nabla^2 \Psi_r \tag{12}$$

$$\frac{\partial \Psi_\varphi}{\partial t} = g(r, \varphi) + D_\varphi \nabla^2 \Psi_\varphi \tag{13}$$

h and g are the source functions and they take the form: $(\Psi.\nabla)v$

Thereby we obtained two equations with different diffusion coefficients, which is expanded in two components.

The evidence that in accretion discs the necessary condition is that the ratio between D_r and D_φ is not equal to unity and zero exists. This gives us the confirmation of possibility for the appearance of Turing instability in this reaction - diffusion system.

4. Conclusion

These instabilities being the expression of spatial pattern of the biffurcation area, the structures may arise in the disc, particularly: vortical structures and so called the Rossby solitons.

The essence in the accretion discs investigations is the finding out of connection between the kind of instability and the arising of the engine of structure formation, when all required above conditions are present.

The theory of Turing structures is one of the many of such modeling pattern formations and here we showed that it works in the reaction - diffusion system of the accretion disc, too.

References

Borckmans, P., Dewel, G., de Wit, A., Walgraef, D. : 2001, *Turing bifurcations and Pattern selection*, submitted to Chemical Waves and Patterns.

Ebeling, V. : 1979, *The structure formations in non-reversal processes* (in Russian), Mir, Moskva.

Engelhardt, R. : 1994, *Modeling Pattern Formation in Reaction-Diffusion Systems*, Univ. of Copenhagen.

Frank, J., King, A. R., Raive, D. J. : 1991, *Accretion power in astrophysics*, Cambridge University press.

Glensdorf, P., Prigozin, I. : 1973, *Thermodynamical theory of structure, instability and fluctuations* in Russian), Mir.

Nauta, M. D. : 2000, *Two-dimensional vortices and accretion disks*, University Utrecht.

Nicolis, G., Prigozin, I. : 1979, *Self - organization in nonequilibrium systems* (in Russian), Mir, Moskva.

Stratonovich, R. L. : 1985, *Nonlinear nonequilibrium thermodynamic* (in Russian), Nauka, Moskva.

Publ. Astron. Obs. Belgrade No. 73 (2002), 73 - 80 *Poster*

H_2O^+ IONS IN THE PLASMA TAIL OF COMET IKEYA-ZHANG

T. BONEV[1], G. BORISOV[1,2] and A. IVANOVA[1]

[1] *Institute of Astronomy, Bulgarian Academy of Sciences, 1784 Sofia, Bulgaria*
E-mail tbonev@astro.bas.bg

[2] *Astronomy Department, University of Sofia, P.O.Box 36, BG-1504, Sofia, Bulgaria*
E-mail gborisov@astro.bas.bg.bg

Abstract. We present observations of Comet Ikeya-Zhang, obtained on May 4, 2002 with the Focal Reducer Rozhen (FoReRo), attached to the 2-m telescope of the National Astronomical Observatory, Rozhen, Bulgaria. A narrow-band interference filter was used to isolate the emission line of H_2O^+ at 6158.86 Å. Several structures have been identified in the plasma tail of this comet. The gradual tailward displacement of these structures has been used to determine the velocity of the ions in the plasma tail of comet Ikeya-Zhang. The derived velocity has been used to estimate the water production rate of comet Ikeya-Zhang by using the similarity laws of magnetohydrodynamics.

1. INTRODUCTION

The most abundant molecule in comets is water. When a comet approaches the Sun the frozen water ice sublimates and the neutral gas molecules flow radially outward with a thermal speed of about 1 km s^{-1}. Different neutral coma gases have different lifetimes in the radiation field of the Sun. Typical photoionization rates are 10^{-6} s^{-1}. The photoionization rate is inversely proportional to the lifetime of the neutrals, i.e. the neutral coma extends to about 10^6 km. But photoionization is not the only mechanism which destroys the neutral gases. Water has a photodissociation rate greater than 10^{-5} s^{-1}, and therefore the neutral water coma extends to distances less than 10^5 km. Thus, the water ions are born closer to the nucleus in comparison to the most of the other ions in a cometary plasma tail. Because H_2O is faster destroyed by photodissociation a relatively small amount of the neutral water is converted into H_2O^+.

In order to obtain this amount from observations we have to derive the ion flux into the tail and to compare it with measurements of the water production rate acquired at the same time. To calculate the flux of ions we need a sequence of well calibrated images and the tailward velocity of the ions. The ion velocities can be measured by two methods. First, by the Doppler shift, measured in a spectrum of the comet, and second, by tracing stable structures in the plasma tail.

In this paper we present observations of water ions in the plasma tail of comet Ikeya-Zhang. We have found several structures in the tail of this comet and traced

one of them to determine the plasma velocity. We first describe the image processing applied to the data for enhancement of the observed structures. Then we measure the locations of these structures in our sequence of images. Finally, we derive the velocity and use it to estimate the water production rate of comet Ikeya-Zhang by applying the similarity laws of magnetohydrodynamics.

2. THE OBSERVATIONS AND THEIR REDUCTION

The images analyzed in this paper are presented in Fig. 1. Here they are shown after bias subtraction, flat-fielding, and conversion to one-second-exposures. The numbers above the images are the Start-times of the exposures (UT). The plasma tail consists of several streamers, well distinguished at greater cometocentric distances. Close to the nucleus the plasma structures are hidden in the strong continuum contribution coming from solar radiation scattered by the cometary dust particles, and from the denser cloud of ions at smaller cometocentric distances. We applied several image

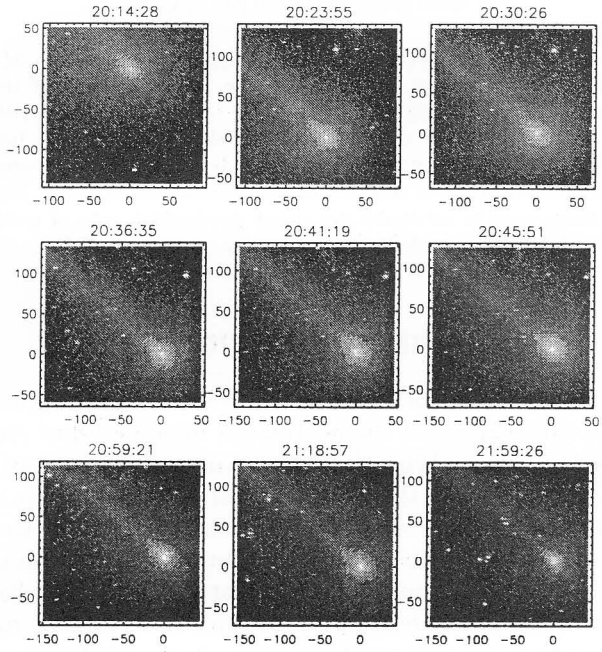

Fig. 1: The images of H_2O^+ ions in comet Ikeya-Zhang, obtained on May 4, 2002. The UT-start times of the exposures are given on top of each particular image. The spatial scale is in 10^3 km.

processing steps in order to reveal the plasma structures close to the nucleus. The most important of these steps are described below:

2. 1. TRANSFORMATION TO POLAR COORDINATES

We have measured the extent of the plasma tail in azimuthal direction and have transformed to polar coordinates only that sector of the image which contains the

tail. The result of this procedure is shown in Fig. 2.

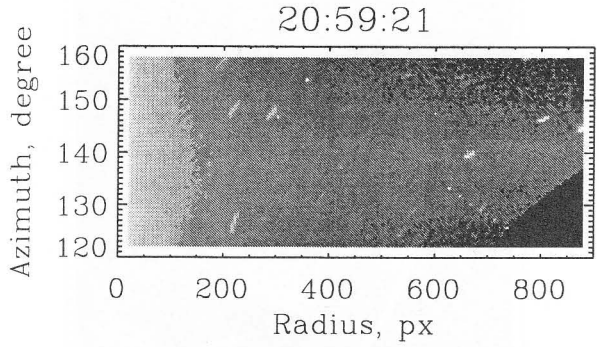

Fig. 2: Example of an image transformed to polar coordinates.

2. 2. ENHANCING THE STRUCTURES

In this subsection we show the result of a procedure which was conceived to enhance the structures in a cometary tail. The structures should extend predominantly in radial direction.

The described procedure is similar to the rotational shift-differencing method used by Larson and Sekanina (1984), and later by Hoban et al. (1989). The difference consists in the usage of an image which is averaged in azimuthal direction instead of taking simply an image rotated by a given angle. The azimuthal averaging has been done by taking a mean vector of the image in polar coordinates along the second dimension, and by expanding this mean vector back to a 2-dimensional array with the dimensions of the original image in polar coordinates. In the next step the difference between the original and the averaged image is calculated. As the plasma structures are extended in radial direction, this step enhances their contrast.

2. 3. BACK TO CARTESIAN COORDINATES

Here, the result of the previous subsection is transformed back to Cartesian coordinates. One example of an image from our sequence after this step is shown in Fig. 3. It is well seen that the bright smooth contribution close to the nucleus has disappeared and only the discrete structures have remained.

2. 4. TRACING OF THE STRUCTURES

The images have been rotated at the position angle of the extended radius- vector. The aim of this transformation is to bring the Sun-Comet radius-vector in direction of the positive X-axis. We have extracted only that portion from the rotated image which contains the tail. The result is shown in Figs. 4, 5, and 6.

The axes are transformed to the projected linear scale calculated at the comet's geocentric distance. Several structures in the plasma tail can be distinguished but only one is particularly stable. It can be identified in all 9 images and its tail-ward motion can be traced. We have marked this structure with an arrow.

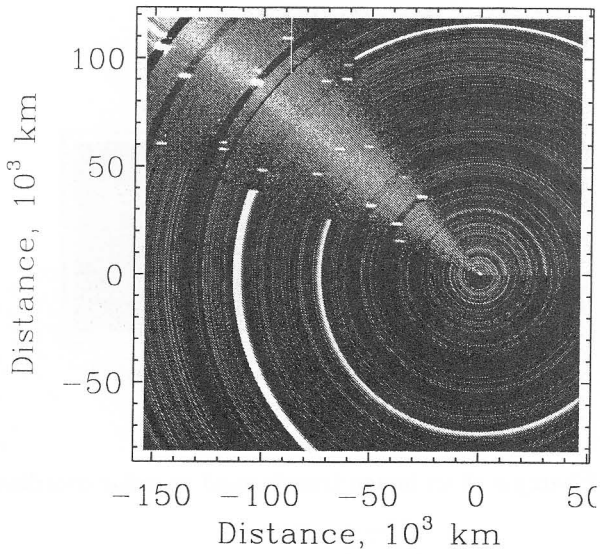

Fig. 3: This image is transformed back to Cartesian coordinates after the image processing described in the previous sections

3. DISCUSSION

In Fig. 7 the cometocentric distance of the marked structure is plotted against the time elapsed from UT 0.0 on May 4, 2002. The full line represents a linear fit to the data. The slope of the fitted line gives a mean velocity of the ions in the plasma tail of comet Ikeya-Zhang of 17.6 km s^{-1}. During the observations the phase angle was 64°. After correcting with this angle for the aspect of the observations we obtain a velocity of 19.4 km s^{-1}. for the tailward plasma flow. Wegmann et al. (1987) modeled the plasma tail of comet Halley for the time of the Giotto encounter. According to their model comet Halley should have a velocity of 20 km s^{-1} at a distance of about 5 10^4 km tailward of the nucleus. A comparison between our measured velocity and the models by Wegmann et al. (1987) can be used to estimate the water production rate of comet Ikeya-Zhang. This comparison can be made by utilizing the similarity law of the magnetohydrodynamic description of the solar wind – comet interaction (Wegmann (1995), Jockers et al., (1999)). If all other conditions have been equal, the water production rate of comet Ikeya-Zhang during our observations has been about 2 times smaller in comparison to comet Halley during the Giotto encounter.

4. CONCLUSION

We have presented narrow-band images of H_2O^+ ions in the plasma tail of comet Ikeya-Zhang The images reveal structures in the tail and close to the nucleus. We have enhanced the structures by subtracting an azimuthal average from the original image. By tracing one of these structures we derived a mean velocity of 17.6 km s^{-1} at a cometocentric distance 10^5 km in tailward direction. The derived velocity of the plasma structures suggests that at the time of our observations the H_2O production

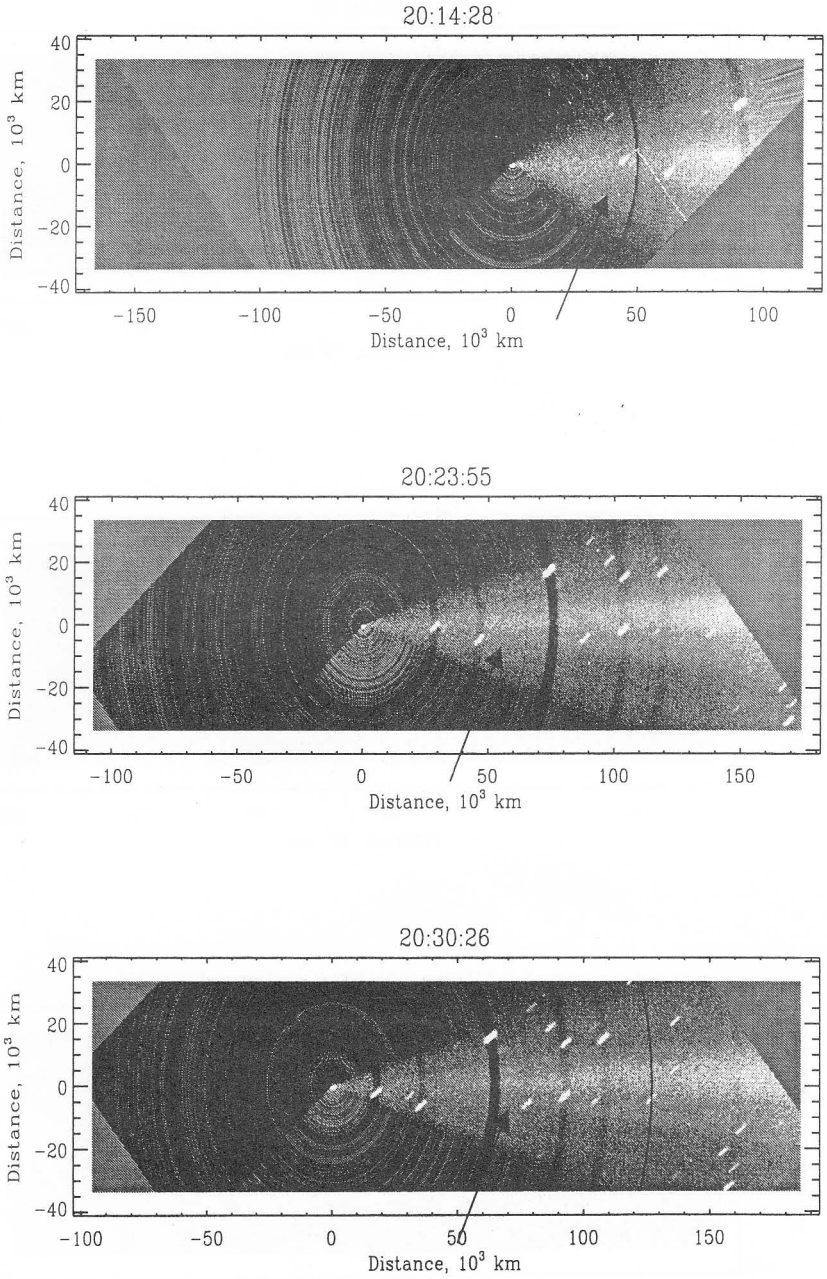

Fig. 4:

rate of comet Ikeya-Zhang has been about 2 times lower in comparison to that of comet Halley during the Giotto encounter.

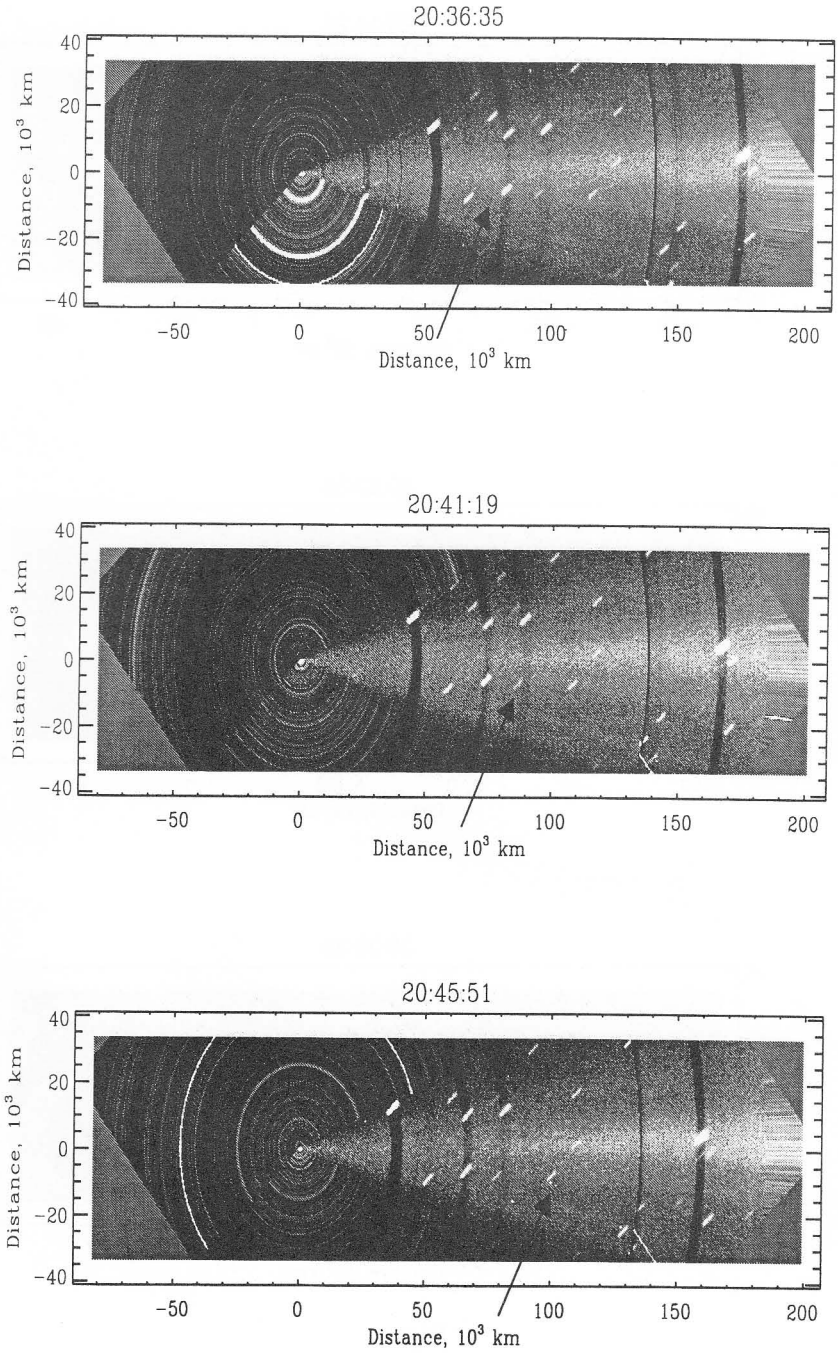
20:36:35
20:41:19
20:45:51
Distance, 10^3 km
40
20
0
−20
−40
−50
0
50
100
150
200

Fig. 5:

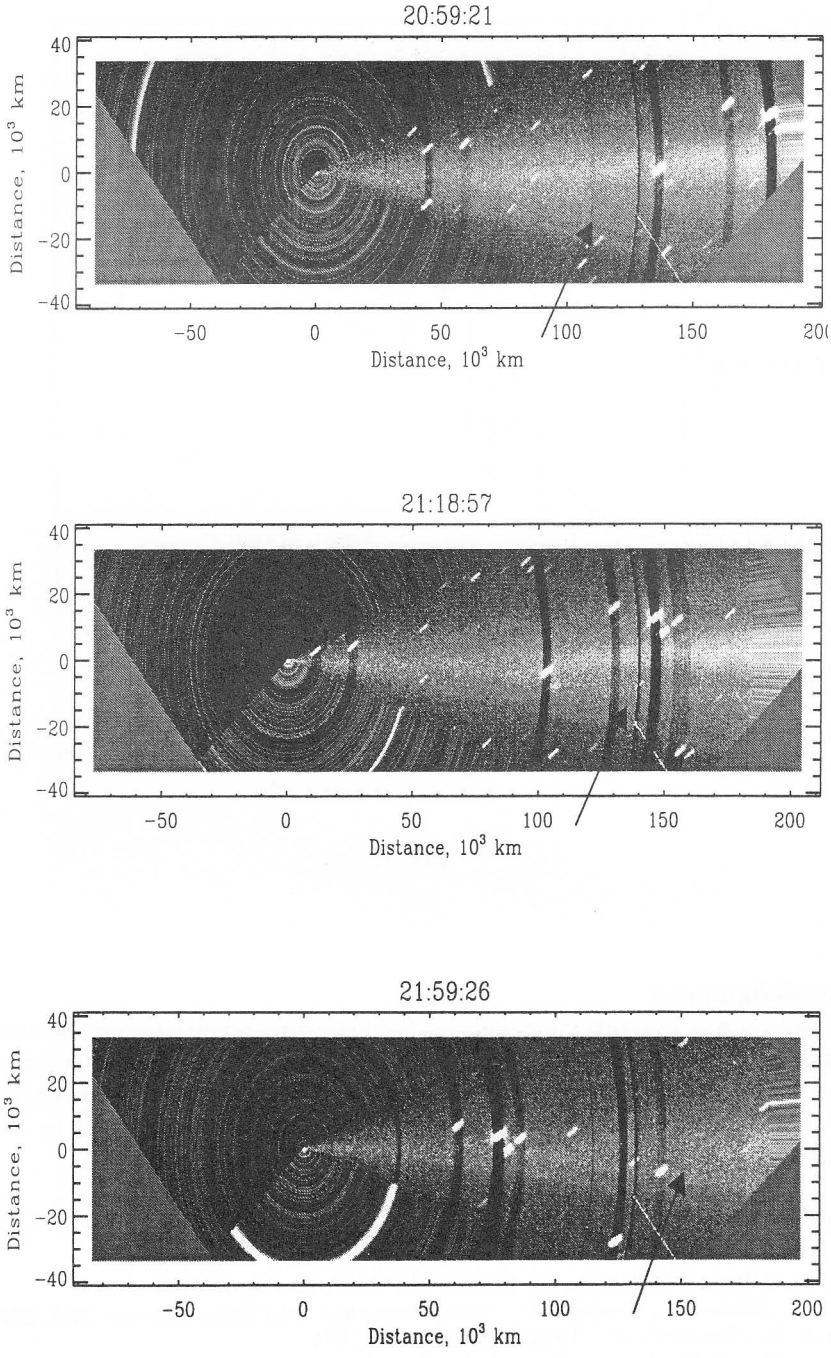
20:59:21
21:18:57
21:59:26
Distance, 10^3 km
Distance, 10^3 km
40
20
0
-20
-40
-50
0
50
100
150
200

Fig. 6:

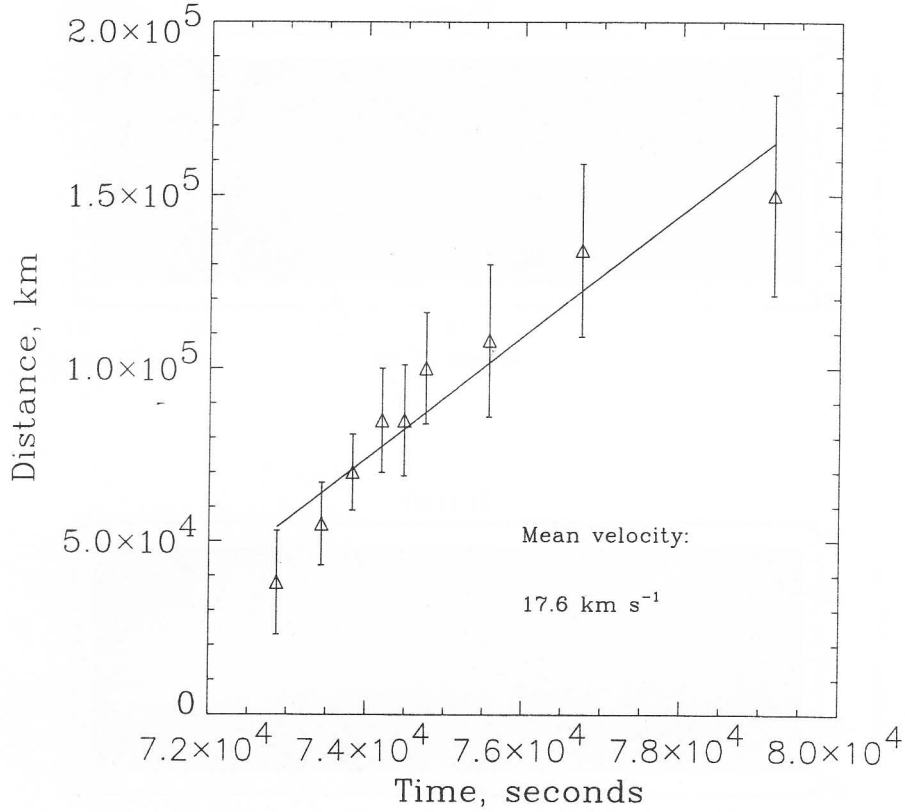

Fig. 7:

Acknowledgments:
This research was supported by contract F-1009/00 with the National Science Fund, Ministry of Education and Science, Bulgaria. The narrow-band filter used in the observations was available in the framework of the collaboration between the Max-Planck Institut für Aeronomie, Germany and the Institute of Astronomy, Bulgarian Academy of Sciences.

References

Hoban, S., A'Hearn, M., Birch, P., Martin, R. : 1989, *Icarus*, **79**, 145.
Jockers, K., Bonev, T., Credner, T. : 1999, *Astrophys. and Space Science*, **264**, 227.
Larson, S. M., Sekanina, Z. : 1984, *Astron. J.*, **89**, 571.
Wegmann, R. : 1995, *Astron. Astrophys.*, **294**, 601.
Wegmann, R., Schmidt, H. U., Huebner, W. F., Boice, D. C. : 1987, *Astron. Astrophys.*, **187**, 339.

Publ. Astron. Obs. Belgrade No. 73 (2002), 81 - 90 *Poster*

SEARCH FOR LONG-TERM PERIODICITY IN THE PLEIADES ACTIVE DWARF STARS FROM PHOTOGRAPHIC SKY SURVEYS

A. P. BORISOVA [1] , M. K. TSVETKOV [1] , K. P. TSVETKOVA [1], N. HAMBLY [2], and D. G. KALAGLARSKY [3]

[1] *Institute of Astronomy, Bulgarian Academy of Sciencies, 72 Tsarigradsko Shosse Blvd., 1784 Sofia, Bulgaria*
E-mail ana@skyarchive.org
E-mail tsvetkov@skyarchive.org
E-mail katya@skyarchive.org

[2] *Institute for Astronomy, The University of Edinburgh, Royal Observatory, Blackford Hill, Edinburgh EH9 3H, U.K.*
E-mail nch@roe.ac.uk

[3] *Sofia University "St. Kliment Ohridsky, Faculty of Mathematics and Informatics, 5 James Bourchier Blvd., 1164 Sofia, Bulgaria*
E-mail damyan@skyarchive.org

Abstract. A program for searching for long-term periodicity of the Pleiades active dwarf stars is presented. As a basis the Pleiades flare stars (or UV Cet type stars) from the Flare Stars Database, which are identified in the USNO A2.0 catalogue are used. The investigation for long-term variability will be made by the usage of European astronomical plate archives, included in the Wide-Field Plate Database (http://www.skyarchive.org), whose time distribution covers more than 100 years. Among these plate archives are those of Rozhen Observatory (Bulgaria), Konkoly Observatory (Hungary), Byurakan (Armenia), Potsdam (Germany), Royal Observatory of Edinburgh (UK), Bamberg (Germany), etc. Limited number of the existing plates in the Pleiades region are already digitized with different scaning machines as PDS 1010 (Sofia), PDS 2020 (Muenster), SUPER COSMOS (Edinburgh) and some flatbed scanners.

1. INTRODUCTION

The long-term brightness variations in the active dwarf stars are subject of special interest in the contemporary stellar astrophysics because of the detection of the long-term solar like activity cycles in these stars. Because there is no theoretical understanding of the solar activity cycle, it is very important to detect such cycles in other dwarf stars in order to constrain the theoretical models. Mirzoyan (1977) first indicated to a cyclic recurrence of the flare activity from two groups of the Pleiades flare stars with duration about two decades. The analysis of the behaviour of several red dwarfs in the solar vicinity shows that their changes in photographic magnitudes range

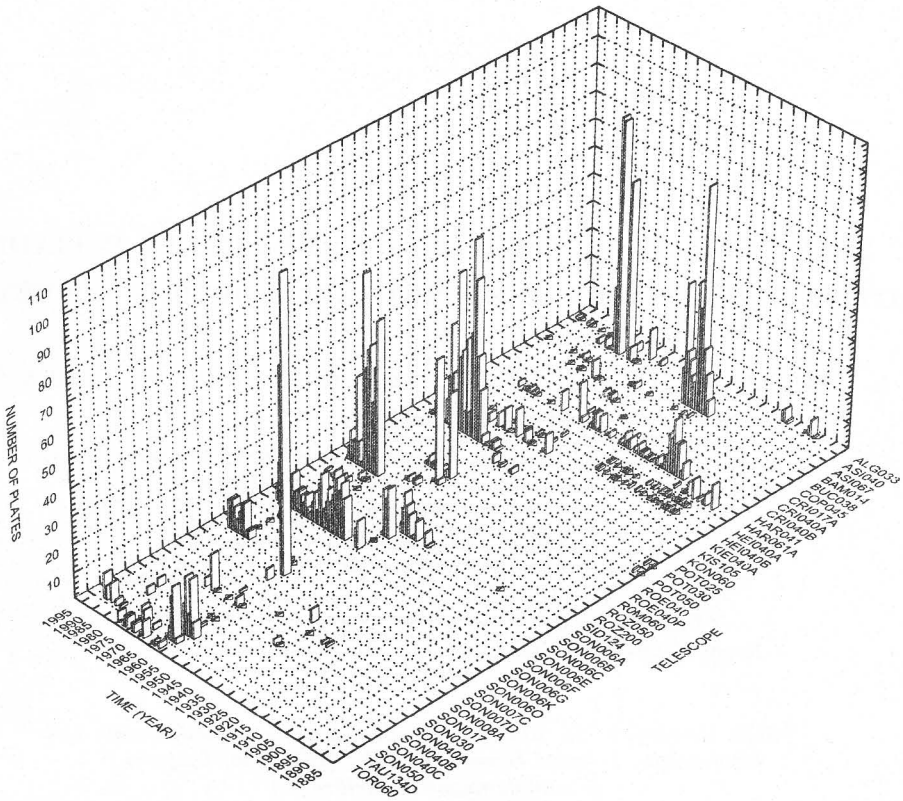

Fig. 1: Distribution of the Pleiades plates for the archives included into the Wide-Field Plate Database (http://www.skyarchive.org)

from 0.2 to 1.0 with typical time scale of variability from 10-60 years (see Pettersen et al. 1992, Mavridis and Avgolupis 1993, Bondar 1995). Cutispoto (1990) executed another dedicated program for long-term photoelectric monitoring of selected southern active dwarf stars in the European Southern Observatory. Recently Gershberg (1998) also appealed to the owners of the plate archives to study the flare stars long term behaviour on the basis of photographic monitoring since the 60's of the last century. There is no systematic monitoring before 1963. Therefore the plate archives are very important.

2. RESEARCH PROGRAMME

The Pleiades open cluster (M45) in Taurus is one of the most studied stellar clusters in the Galaxy according to the existing data in CDS (http://simbad.u-strasbg.fr/Simbad) and WEBDA (http://obswww.unige.ch/webda/). This young open cluster ($7x10^7$ years) is a constant target for study of the stellar evolution stages in comparison with the comparatively old stellar cluster Praesepe (M44) and very young aggregate in

Table 1: List of known astronomical archives containing the Pleiades plates.

WFPDB Telescope Identifier	Location of the Archive	Telescope Type	Years of Operation
ALG033	Floirac, France	Ast	1891-1975
ASI040	Asiago, Italy	Sch	1958-1992
ASI067	Asiago, Italy	Sch	1965-1992
BAM014A	Bamberg, Germany	Cam	1928-1938
BUC038	Bucharest, Romania	Rfr	1930-
COP045	Brorfelde, Denmark	Sch	1966-
CRI017A	Crimea, Ukraine	Cam	1948-1965
CRI040A	Crimea, Ukraine	Ast	1947-1950
CRI040B	Crimea, Ukraine	Ast	1951-1984
HAR041	Cambridge, USA MA	Rfr	1909-1932
HAR061A	Cambridge, USA MA	Rfr	1893-1895
HEI040A	Heidelberg, Germany	Ast	1900-1981
HEI040B	Heidelberg, Germany	Ast	1900-1981
KIE040A	Kiev, Ukraine	Ast	1950-1996
KIS105	Kiso, Japan	Sch	1977-
KON060	Budapest, Hungary	Sch	1962-
POT025	Potsdam, Germany	Sch	1948-1956
POT030	Potsdam, Germany	Rfr	1879-1930
POT050	Potsdam, Germany	Sch	1952-1970
ROE040	Edinburgh, UK	Sch	1962-1974
ROE040P	Edinburgh, UK	Sch	1962-1974
ROM060	Edinburgh, UK	Sch	1967-
ROZ050	Sofia, Bulgaria	Sch	1979-
ROZ200	Rozhen, Bulgaria	RCr	1979-
SID124	Edinburgh, UK	Sch	1973-
SON006A	Sonneberg, Germany	Cam	1941-1953
SON006B	Sonneberg, Germany	Cam	1953-1962
SON006C	Sonneberg, Germany	Cam	1956-1962
SON006E	Sonneberg, Germany	Cam	1956-
SON006F	Sonneberg, Germany	Cam	1956-
SON006G	Sonneberg, Germany	Cam	1957-
SON006K	Sonneberg, Germany	Cam	1958-
SON006O	Sonneberg, Germany	Cam	1958-
SON007C	Sonneberg, Germany	Cam	1963-1965
SON007D	Sonneberg, Germany	Cam	1963-1965
SON008A	Sonneberg, Germany	Cam	1925-1939
SON017	Sonneberg, Germany	Cam	1923-1971
SON030	Sonneberg, Germany	Sch	1960-1976
SON040A	Sonneberg, Germany	Ast	1938-1945
SON040B	Sonneberg, Germany	Ast	1960-
SON040C	Sonneberg, Germany	Ast	1961-
SON050	Sonneberg, Germany	Sch	1952-
TAU134	Tautenburg, Germany	Sch	1960-
TOR060	Torun, Poland	Sch	1962-

Table 2: List of already scanned plates.

WFPDB Plate Identifier	Date of Observation	Scanning Machine
CLU020 000003	19 02 1952	UMAX 3000
CLU020 000007	26 10 1953	UMAX 3000
CLU020 000008	27 10 1953	UMAX 3000
CLU020 000078	25 09 1955	UMAX 3000
CLU020 000448	missing date	UMAX 3000
CLU020 000473	27 07 1956	UMAX 3000
CLU020 000474	18 07 1956	UMAX 3000
CLU020 000475	27 07 1956	UMAX 3000
CLU020 000476	28 07 1956	UMAX 3000
KON060 000833	25 11 1965	UMAX 3000
KON060 002767	29 10 1968	UMAX 3000
KON060 002878	12 01 1969	UMAX 3000
KON060 002877	11 01 1969	UMAX 3000
KON060 003868	26 12 1970	UMAX 3000
KON060 003898	01 02 1971	UMAX 3000
KON060 003928	27 02 1971	UMAX 3000
KON060 003929	24 05 1971	UMAX 3000
KON060 004180	22 09 1971	UMAX 3000
POT030 000153	04 12 1885	PDS 2020, EPSON
POT030 000154	18 03 1886	PDS 2020, EPSON
POT030 000155	23 03 1886	PDS 2020, EPSON
POT030 000206	04 12 1888	PDS 2020, EPSON
POT030 000209	05 12 1888	PDS 2020, EPSON
POT050 000041	05 09 1953	PDS 2020, UMAX 3000
POT050 000039	05 09 1953	PDS 2020, UMAX 3000
POT050 000040	05 09 1953	PDS 2020, UMAX 3000
POT050 000045	05 09 1953	PDS 2020, UMAX 3000
POT050 000048	22 02 1954	PDS 2020, UMAX 3000
POT050 000077	04 02 1954	PDS 2020, UMAX 3000
POT050 000121	15 11 1955	PDS 2020, UMAX 3000
POT050 000447	07 11 1964	PDS 2020, UMAX 3000
POT050 000465	18 02 1966	PDS 2020, UMAX 3000
ROE040 000134	26 11 1962	UMAX 3000
ROE040 000537	28 12 1965	UMAX 3000
ROE040 000538	28 12 1965	UMAX 3000
ROE040 000540	17 01 1966	UMAX 3000
ROE040 000541	17 01 1966	UMAX 3000
ROE040 000547	14 02 1966	UMAX 3000
ROE040 001012	17 10 1969	UMAX 3000
ROE040 001013	17 10 1969	UMAX 3000
ROE040 001026	04 11 1969	UMAX 3000
ROE040 001182	19 01 1969	UMAX 3000
ROE040 001262	26 10 1971	UMAX 3000
ROE040 001279	16 11 1971	UMAX 3000
ROE040 001363	07 12 1972	UMAX 3000
ROE040 001587	14 12 1973	UMAX 3000
ROE040 001588	14 12 1973	UMAX 3000
ROE040 001869	29 03 1972	UMAX 3000
SID124 008935	08 12 1983	SUPER COSMOS
SID124 008960	23 12 1983	SUPER COSMOS

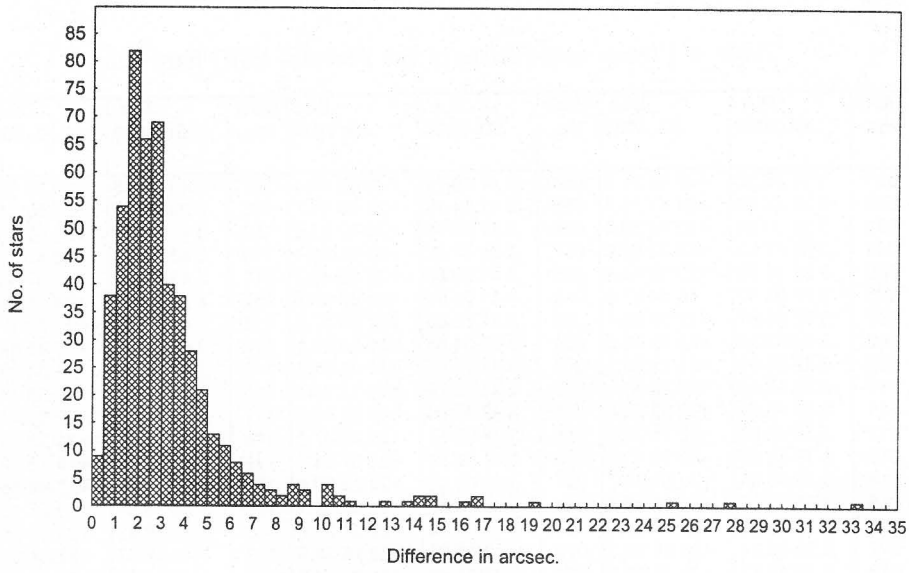

Fig. 2: Differences in the star location between Kazarovets (1993) and our estimations.

Orion (M42/43). The major population of the Pleiades consists of red dwarfs, which have important role in the identification of faint cluster members for deriving of the complete luminosity function. The total number of the known Pleiades flare stars according to the Flare Stars Database (Tsvetkova et al. 1995) is 547, having in view that for some stars published as flare stars better observations are needed to confirm their membership to the flare star class of variables according to Tsvetkova and Tsvetkov (1989). The statistical evaluation of the total number of all flare stars in the Pleiades (registered and not registered up to now) is about 1000 (Hambaryan et al. 1990). Taking this in consideration we think that the Pleiades is a good and accessible sample for studying of long-term brightness variations in the red dwarf stars.

Having access to different Pleiades wide-field photographic plates (from the archives in Bamberg, Sonneberg, Potsdam, Rozhen, Edinburgh, Byurakan, Konkoly) we are going to investigate G-K-M dwarf type stars for long term variability over unprecedently large time-scale since 1885. A detailed information on the Pleiades plate selection can be provided by the Wide-Field Plate Database (WFPDB), created in Bulgaria (http://vizier.u-strasbg.fr/viz-bin/VizieR?-source=VI/90) or (http://www.skyarchive.org) which compiles the information for more than 2 000 000 astronomical plates, stored in 337 archives. Using the search resources (http://www.skyarchive.org/) (Table 1) we found 3 890 Pleiades plates, made in the period 1885–1998 (their distribution is presented in Fig. 1) and it gives the opportunity to obtain almost continuous photometric data set for the red dwarf stars in the cluster.

In the frames of our cooperation with Konkoly and Potsdam observatories we scanned 49 plates, given in Table 2 with PDS 2020 (Muenster), SUPER COSMOS (Edinburgh), PDS 1010 (Sofia), UMAX 3000 (Konkoly) and Epson scanners. We

Table 3: Precise coordinates of the Pleiades HCG flare stars

HCG No.	R.A. JD. 2000	Dec. JD. 2000	HCG No.	R.A. JD. 2000	Dec JD. 2000	HCG No.	R.A. JD. 2000	Dec. JD. 2000
001	3 36 25.30	+24 53 39.8	054	3 41 50.75	+25 05 19.4	107	3 43 18.48	+23 34 10.0
002	3 36 27.30	+24 41 19.8	055	3 41 54.13	+25 43 49.7	108	3 43 26.55	+24 59 41.8
003	3 36 30.99	+22 46 59.4	056	3 41 58.78	+26 12 23.8	109	3 43 28.13	+24 53 33.2
004	3 36 37.60	+23 27 55.5	057	3 41 47.00	+22 51 27.4	110	3 43 18.93	+22 47 12.9
005	3 36 38.50	+23 08 44.5	058	3 41 58.86	+25 19 46.7	111	3 43 22.50	+23 07 48.8
006	3 37 03.42	+24 44 37.9	059	3 41 53.94	+23 32 41.1	112	3 43 34.07	+25 35 28.5
007	3 37 45.57	+22 00 30.7	060	3 41 50.66	+22 55 17.2	113	3 43 36.35	+25 21 37.7
008	3 37 52.26	+22 42 26.2	061	3 42 04.63	+25 53 11.5	114	3 43 26.39	+22 42 44.7
009	3 38 23.93	+23 11 55.1	062	3 42 08.77	+25 45 25.4	115	3 43 37.23	+25 24 34.8
010	3 38 33.45	+23 23 43.8	063	3 42 02.79	+24 12 38.6	116	3 43 27.37	+22 37 44.0
011	3 38 43.24	+25 22 29.8	064	3 42 02.84	+23 55 56.2	117	3 43 32.11	+22 52 49.3
012	3 38 48.62	+25 11 21.9	065	3 42 03.77	+24 42 47.3	118	3 43 36.85	+24 23 40.5
013	3 38 52.83	+25 14 13.6	066	3 41 58.59	+22 57 04.2	119	3 43 36.58	+24 13 58.6
014	3 38 49.51	+23 51 51.7	067	3 42 01.60	+22 23 29.0	120	3 43 44.73	+25 59 43.3
015	3 38 53.84	+24 25 09.5	068	3 42 10.85	+24 05 11.1	121	3 43 36.53	+23 27 16.3
016	3 39 08.06	+24 46 17.1	069	3 42 09.73	+22 31 38.8	122	3 43 36.48	+23 12 36.7
017	3 39 06.74	+23 59 58.3	070	3 42 10.63	+22 15 38.5	123	3 43 42.07	+24 34 25.7
018	3 39 12.12	+25 14 50.9	071	3 42 21.46	+24 39 54.9	124	3 43 38.99	+23 44 08.0
019	3 39 29.60	+24 58 00.3	072	3 42 28.00	+25 11 33.0	125	3 43 48.37	+25 02 39.3
020	3 39 29.14	+23 30 00.0	073	3 42 26.22	+24 14 10.1	126	3 43 53.80	+25 28 32.6
021	3 39 32.25	+24 16 04.0	074	3 42 31.17	+24 49 23.9	127	3 43 52.08	+24 50 32.0
022	3 39 42.66	+23 54 30.2	075	3 42 26.22	+22 53 43.0	128	3 43 51.69	+24 14 18.3
023	3 39 46.95	+25 25 43.7	076	3 42 27.25	+22 34 27.0	129	3 43 56.63	+24 59 39.0
024	3 40 01.81	+24 46 28.5	077	3 42 29.36	+22 47 28.3	130	3 43 55.62	+24 25 37.3
025	3 39 56.68	+22 28 24.9	078	3 42 38.03	+24 41 20.7	131	3 44 02.76	+25 39 25.1
026	3 40 00.13	+23 26 08.4	079	3 42 36.20	+23 22 07.1	132	3 44 04.42	+25 51 25.1
027	3 40 03.62	+24 30 04.2	080	3 42 40.16	+23 59 24.0	133	3 43 57.20	+24 13 22.9
028	3 40 10.85	+26 06 43.3	081	3 42 48.08	+25 54 59.5	134	3 44 02.21	+25 03 56.0
029	3 40 06.71	+24 25 08.6	082	3 42 41.11	+24 01 45.0	135	3 43 56.93	+23 57 08.4
030	3 40 06.74	+23 21 57.5	083	3 42 47.56	+25 17 51.9	136	3 43 54.43	+23 21 16.5
031	3 40 09.61	+23 10 35.0	084	3 42 35.56	+21 50 32.4	137	3 43 57.39	+23 34 42.8
032	3 40 12.68	+23 09 37.9	085	3 42 42.32	+23 30 12.8	138	3 44 13.89	+25 32 17.7
033	3 40 22.98	+25 29 50.2	086	3 42 42.33	+23 20 24.2	139	3 43 59.22	+22 34 21.6
034	3 40 24.12	+24 35 06.4	087	3 42 46.20	+23 27 12.0	140	3 44 09.85	+24 16 06.2
035	3 40 26.80	+23 50 17.7	088	3 42 56.60	+25 58 52.8	141	3 44 08.74	+23 04 49.9
036	3 40 31.10	+25 08 55.5	089	3 43 00.28	+25 50 26.6	142	3 44 26.31	+26 02 33.2
037	3 40 31.06	+24 21 43.2	090	3 42 53.24	+23 31 09.4	143	3 44 23.32	+25 21 32.5
038	3 40 31.63	+24 32 36.3	091	3 42 53.10	+23 26 52.2	144	3 44 16.38	+23 37 06.4
039	3 40 42.50	+25 42 22.0	092	3 42 56.67	+24 13 45.9	145	3 44 17.69	+24 26 49.0
040	3 40 39.91	+24 44 11.6	093	3 42 56.49	+24 05 00.5	146	3 44 19.01	+24 35 20.8
041	3 40 43.57	+22 15 07.2	094	3 43 05.05	+25 44 38.5	147	3 44 21.83	+24 46 08.7
042	3 40 57.36	+25 50 58.6	095	3 43 03.92	+25 20 18.9	148	3 44 24.62	+24 51 55.9
043	3 40 51.75	+23 13 52.8	096	3 43 07.50	+25 34 31.5	149	3 44 24.76	+24 46 08.5
044	3 40 54.97	+22 21 01.1	097	3 43 05.46	+24 49 30.9	150	3 44 25.52	+24 40 55.3
045	3 41 02.93	+23 43 23.9	098	3 43 10.99	+25 25 03.5	151	3 44 28.22	+25 15 38.9
046	3 41 06.05	+22 53 21.0	099	3 43 05.84	+23 52 51.7	152	3 44 30.07	+25 35 48.1
047	3 41 08.05	+23 12 56.7	100	3 43 09.67	+24 41 35.3	153	3 44 22.99	+24 04 08.3
048	3 41 19.28	+23 51 44.1	101	3 43 04.12	+22 48 05.7	154	3 44 27.24	+24 50 40.6
049	3 41 22.82	+23 55 50.6	102	3 43 12.06	+24 44 47.5	155	3 44 20.81	+23 33 42.4
050	3 41 33.65	+25 06 51.0	103	3 43 13.00	+24 39 21.7	156	3 44 26.81	+24 24 34.0
051	3 41 25.25	+22 32 58.4	104	3 43 13.49	+24 23 11.0	157	3 44 33.01	+25 45 12.1
052	3 41 37.49	+22 16 41.4	105	3 43 26.13	+26 02 33.3	158	3 44 27.95	+24 10 19.8
053	3 41 39.37	+22 20 57.3	106	3 43 20.64	+24 26 34.6	159	3 44 36.71	+24 36 03.5

Table 3: continued

HCG No.	R.A. JD. 2000	Dec. JD. 2000	HCG No.	R.A. JD. 2000	Dec JD. 2000	HCG No.	R.A. JD. 2000	Dec. JD. 2000
160	3 44 39.54	+24 31 46.8	213	3 45 59.39	+22 26 15.4	266	3 47 22.63	+23 44 09.0
161	3 44 36.21	+23 30 13.2	214	3 46 05.17	+22 58 56.3	267	3 47 15.64	+22 21 19.8
162	3 44 47.49	+25 54 58.1	215	3 46 08.33	+23 20 53.1	268	3 47 37.29	+25 20 04.8
163	3 44 48.28	+25 47 37.1	216	3 46 10.84	+23 37 18.5	269	3 47 26.68	+23 38 04.8
164	3 44 37.84	+22 55 19.1	217	3 46 09.51	+22 42 39.8	270	3 47 23.77	+23 08 59.4
165	3 44 44.44	+24 10 30.5	218	3 46 23.56	+24 01 49.5	271	3 47 17.33	+22 12 58.4
166	3 44 47.69	+24 12 54.5	219	3 46 25.32	+24 09 39.3	272	3 47 21.58	+22 22 12.3
167	3 44 47.26	+24 00 40.5	220	3 46 18.03	+22 42 36.2	273	3 47 30.55	+24 22 16.4
168	3 44 50.11	+24 54 42.3	221	3 46 24.09	+23 02 19.2	274	3 47 23.15	+22 14 42.6
169	3 44 55.08	+25 21 41.8	222	3 46 28.56	+24 45 34.8	275	3 47 25.61	+22 21 02.2
170	3 44 58.55	+24 23 28.2	223	3 46 27.72	+23 35 36.0	276	3 47 28.72	+22 22 38.2
171	3 44 55.93	+23 55 55.7	224	3 46 31.13	+24 07 04.8	277	3 47 33.40	+23 41 35.2
172	3 45 01.05	+24 46 43.7	225	3 46 32.24	+23 58 58.3	278	3 47 33.60	+24 41 05.3
173	3 44 57.22	+23 59 31.5	226	3 46 49.39	+26 18 47.7	279	3 47 35.80	+24 52 28.9
174	3 45 14.48	+25 05 19.6	227	3 46 36.02	+23 58 02.4	280	3 47 38.01	+24 53 32.7
175	3 45 19.97	+26 03 31.3	228	3 46 37.22	+24 20 38.8	281	3 47 38.36	+24 44 04.3
176	3 45 06.73	+23 36 53.4	229	3 46 35.27	+23 24 44.3	282	3 47 39.28	+24 27 34.1
177	3 45 12.23	+24 30 19.7	230	3 46 53.00	+26 21 36.6	283	3 47 40.30	+24 18 09.3
178	3 45 16.92	+25 15 50.1	231	3 46 40.18	+24 55 54.0	284	3 47 34.69	+22 48 07.0
179	3 45 18.07	+25 06 00.6	232	3 46 39.96	+23 59 17.5	285	3 47 41.37	+23 58 21.2
180	3 45 12.21	+24 15 24.5	233	3 46 45.71	+25 27 32.7	286	3 47 41.11	+23 44 27.2
181	3 45 16.59	+24 34 34.7	234	3 46 39.95	+23 47 00.2	287	3 47 45.83	+24 38 03.9
182	3 45 06.18	+22 38 35.4	235	3 46 34.77	+22 56 10.4	288	3 47 44.99	+24 48 10.2
183	3 45 16.11	+24 07 17.3	236	3 46 48.36	+24 18 06.6	289	3 47 50.06	+24 47 09.3
184	3 45 13.35	+23 31 03.3	237	3 46 49.15	+24 36 02.3	290	3 47 40.91	+22 55 50.5
185	3 45 12.07	+23 21 55.5	238	3 46 54.59	+24 59 10.6	291	3 47 45.02	+23 52 20.0
186	3 45 10.76	+23 03 00.6	239	3 46 47.16	+23 17 35.6	292	3 47 49.71	+24 25 45.2
187	3 45 11.89	+23 06 55.3	240	3 46 50.02	+23 31 58.5	293	3 47 51.18	+25 59 58.9
188	3 45 23.42	+24 51 05.0	241	3 46 53.96	+25 14 47.1	294	3 47 49.71	+24 28 16.0
189	3 45 24.50	+25 02 42.1	242	3 46 55.66	+25 12 37.0	295	3 47 50.90	+24 30 21.0
190	3 45 29.52	+23 45 40.0	243	3 46 57.07	+25 04 15.5	296	3 47 51.86	+24 05 47.7
191	3 45 28.46	+22 59 06.5	244	3 46 53.55	+24 17 17.4	297	3 47 59.21	+24 30 24.2
192	3 45 32.88	+24 18 14.2	245	3 46 48.70	+23 04 09.8	298	3 47 47.84	+22 33 22.6
193	3 45 33.34	+23 35 34.6	246	3 46 58.47	+24 27 42.5	299	3 47 44.60	+22 23 55.8
194	3 45 36.64	+24 39 09.0	247	3 46 57.02	+23 15 04.6	300	3 47 59.67	+24 43 55.0
195	3 45 41.61	+25 41 14.7	248	3 47 04.66	+25 22 52.7	301	3 47 52.06	+22 52 48.8
196	3 45 38.96	+25 13 30.4	249	3 47 03.52	+24 09 37.0	302	3 47 55.20	+23 19 08.1
197	3 45 40.28	+24 50 39.2	250	3 47 10.37	+24 57 19.0	303	3 47 58.92	+23 29 05.9
198	3 45 41.59	+24 04 32.5	251	3 47 03.71	+23 37 01.1	304	3 48 12.37	+26 35 04.0
199	3 45 52.58	+25 51 44.5	252	3 47 06.22	+24 18 13.2	305	3 48 16.29	+26 20 07.5
200	3 45 44.01	+24 04 29.0	253	3 47 08.09	+24 18 27.0	306	3 48 08.89	+24 29 39.6
201	3 45 48.87	+23 51 12.7	254	3 47 10.98	+24 13 51.6	307	3 48 07.90	+23 44 26.0
202	3 45 52.67	+23 27 56.4	255	3 47 07.27	+23 13 37.2	308	3 48 21.60	+25 43 43.4
203	3 45 46.40	+22 06 47.7	256	3 47 08.48	+23 42 41.1	309	3 48 05.76	+23 02 05.4
204	3 46 06.62	+25 14 46.9	257	3 47 09.38	+23 44 33.9	310	3 48 11.17	+23 39 45.3
205	3 45 56.89	+23 01 31.5	258	3 47 13.60	+23 49 55.5	311	3 48 13.27	+23 58 49.3
206	3 46 03.48	+24 20 58.3	259	3 47 17.07	+25 56 39.4	312	3 48 17.23	+24 30 18.3
207	3 46 01.59	+23 43 17.6	260	3 47 30.51	+26 16 47.3	313	3 48 20.24	+24 54 57.2
208	3 46 06.83	+24 33 48.4	261	3 47 22.90	+24 50 58.6	314	3 48 05.63	+22 38 11.9
209	3 46 08.65	+24 40 35.7	262	3 47 18.28	+24 02 11.7	315	3 48 13.70	+23 38 01.8
210	3 46 07.45	+24 22 30.0	263	3 47 25.71	+25 08 35.8	316	3 48 26.04	+25 13 07.9
211	3 46 09.83	+24 40 27.5	264	3 47 09.00	+22 17 32.8	317	3 48 25.97	+25 14 43.3
212	3 45 58.56	+22 19 56.5	265	3 47 32.96	+25 38 20.2	318	3 48 16.35	+22 32 42.6

Table 3: continued

HCG No.	R.A. JD. 2000	Dec. JD. 2000	HCG No.	R.A. JD. 2000	Dec JD. 2000	HCG No.	R.A. JD. 2000	Dec. JD. 2000
319	3 48 22.71	+23 58 23.3	372	3 49 32.95	+24 32 05.2	425	3 51 14.00	+25 23 11.5
320	3 48 26.70	+25 03 30.7	373	3 49 36.04	+23 56 25.7	426	3 51 17.76	+25 02 28.5
321	3 48 20.48	+23 31 00.9	374	3 49 34.85	+23 27 19.3	427	3 51 24.09	+26 03 14.0
322	3 48 25.20	+24 14 28.3	375	3 49 36.44	+24 18 16.7	428	3 51 25.80	+24 47 41.4
323	3 48 22.56	+22 52 24.1	376	3 49 35.84	+22 09 07.6	429	3 51 24.36	+24 05 16.9
324	3 48 30.99	+24 16 55.6	377	3 49 42.58	+24 19 07.3	430	3 51 25.30	+23 53 24.2
325	3 48 24.73	+22 24 28.5	378	3 49 51.72	+21 18 28.4	431	3 51 29.89	+23 53 59.7
326	3 48 31.82	+24 04 46.6	379	3 49 49.40	+25 06 42.4	432	3 51 39.07	+24 35 31.3
327	3 48 31.80	+24 02 01.3	380	3 49 55.72	+24 44 33.9	433	3 51 35.51	+25 29 59.2
328	3 48 29.68	+23 58 08.3	381	3 49 57.03	+25 05 14.8	434	3 51 36.52	+26 26 02.3
329	3 48 25.42	+22 12 43.9	382	3 50 02.09	+23 51 47.0	435	3 51 37.98	+23 11 02.2
330	3 48 29.64	+23 00 03.3	383	3 50 01.55	+24 36 49.1	436	3 51 47.18	+24 13 20.8
331	3 48 27.96	+23 18 05.1	384	3 50 00.58	+25 23 57.8	437	3 51 50.54	+22 53 46.7
332	3 48 26.48	+23 11 32.1	385	3 50 01.77	+25 12 43.6	438	3 51 50.88	+23 17 41.1
333	3 48 40.37	+24 36 36.4	386	3 50 08.32	+25 32 58.2	439	3 51 54.45	+23 33 34.0
334	3 48 32.17	+23 26 43.1	387	3 50 12.36	+24 32 01.1	440	3 51 54.99	+23 57 44.8
335	3 48 35.57	+24 12 02.2	388	3 50 11.89	+24 17 46.9	441	3 51 53.87	+24 02 54.0
336	3 48 35.48	+23 46 05.9	389	3 50 11.10	+23 55 42.6	442	3 51 57.15	+23 59 48.7
337	3 48 39.88	+24 12 45.3	390	3 50 12.84	+24 21 09.2	443	3 51 56.71	+24 14 41.6
338	3 48 41.85	+25 01 21.5	391	3 50 12.20	+23 59 47.6	444	3 51 53.34	+24 23 15.3
339	3 48 42.08	+25 00 30.7	392	3 50 13.38	+23 25 39.4	445	3 51 59.25	+24 40 01.4
340	3 48 35.22	+22 53 43.2	393	3 50 15.03	+22 40 24.8	446	3 51 57.44	+25 48 33.9
341	3 48 37.57	+22 46 11.8	394	3 50 15.18	+24 13 38.6	447	3 52 01.57	+25 01 31.6
342	3 48 45.77	+25 56 50.1	395	3 50 20.92	+23 19 25.8	448	3 52 02.19	+24 39 49.7
343	3 48 40.90	+23 14 20.2	396	3 50 25.08	+23 55 44.0	449	3 52 07.91	+25 27 57.3
344	3 48 45.35	+23 20 22.5	397	3 50 23.89	+24 28 43.4	450	3 52 07.29	+25 39 01.1
345	3 48 37.57	+22 15 24.8	398	3 50 22.86	+22 11 20.6	451	3 52 13.27	+26 08 39.4
346	3 48 45.32	+24 37 27.8	399	3 50 21.97	+22 37 34.9	452	3 52 12.14	+26 22 11.6
347	3 48 46.10	+25 07 44.6	400	3 50 24.32	+22 27 10.9	453	3 52 18.98	+25 35 28.0
348	3 48 49.26	+23 58 40.0	401	3 50 31.90	+22 08 49.7	454	3 52 20.62	+24 33 58.1
349	3 48 57.30	+24 19 46.0	402	3 50 28.11	+24 23 00.6	455	3 52 21.85	+24 39 51.0
350	3 48 51.83	+22 53 39.2	403	3 50 29.89	+25 03 09.2	456	3 52 30.86	+24 32 42.1
351	3 49 00.91	+24 54 12.4	404	3 50 37.34	+22 28 10.6	457	3 52 37.47	+24 44 57.3
352	3 49 00.60	+23 57 30.3	405	3 50 39.77	+23 01 04.6	458	3 52 34.42	+22 30 09.9
353	3 49 00.94	+22 58 52.2	406	3 50 43.58	+22 17 38.7	459	3 52 31.13	+25 29 40.2
354	3 49 05.81	+23 44 25.3	407	3 50 34.01	+24 52 31.6	460	3 52 48.64	+21 42 30.7
355	3 49 10.94	+24 20 54.1	408	3 50 46.04	+21 52 38.3	461	3 52 38.83	+25 50 27.7
356	3 49 03.54	+22 51 12.2	409	3 50 48.91	+22 40 14.5	462	3 52 51.67	+22 31 35.3
357	3 49 05.89	+23 06 24.7	410	3 50 43.11	+25 19 41.8	463	3 52 56.91	+22 26 03.7
358	3 49 11.23	+23 33 21.2	411	3 50 53.97	+24 45 55.1	464	3 52 54.21	+25 17 45.5
359	3 49 15.32	+24 34 05.0	412	3 50 56.55	+25 35 08.8	465	3 53 05.35	+24 46 04.3
360	3 49 11.15	+22 10 38.7	413	3 50 53.74	+23 43 01.3	466	3 53 09.55	+26 00 06.8
361	3 49 11.41	+22 16 23.2	414	3 50 58.09	+23 55 45.1	467	3 53 15.64	+22 52 16.8
362	3 49 16.29	+24 03 48.3	415	3 50 57.35	+24 06 33.3	468	3 53 18.34	+25 55 17.7
363	3 49 21.46	+23 39 08.5	416	3 50 57.02	+24 24 49.8	469	3 53 25.50	+23 37 59.7
364	3 49 17.17	+24 20 50.2	417	3 51 02.26	+25 03 21.5	470	3 53 21.82	+25 38 35.1
365	3 49 12.55	+25 42 09.8	418	3 51 05.52	+24 44 14.7	471	3 53 24.43	+25 02 09.4
366	3 49 20.19	+25 25 44.9	419	3 51 07.24	+24 28 53.9	472	3 53 26.57	+25 31 22.0
367	3 49 20.48	+25 49 07.2	420	3 51 23.83	+22 06 50.8	473	3 53 40.91	+24 25 11.9
368	3 49 19.50	+24 48 28.1	421	3 51 10.28	+24 24 08.4	474	3 53 47.52	+23 44 33.5
369	3 49 20.54	+24 46 38.6	422	3 51 11.47	+24 23 15.8	475	3 53 45.28	+25 55 34.0
370	3 49 27.56	+24 31 56.7	423	3 51 15.76	+23 16 58.5	476	3 53 48.93	+25 21 14.4
371	3 49 32.45	+23 55 44.9	424	3 51 18.99	+24 10 15.8	477	3 53 57.22	+23 20 45.5

Table 3: continued

HCG No.	R.A. JD. 2000	Dec. JD. 2000	HCG No.	R.A. JD. 2000	Dec JD. 2000	HCG No.	R.A. JD. 2000	Dec. JD. 2000
478	3 54 00.59	+22 46 11.5	492	3 54 39.56	+22 36 36.5	506	3 56 15.57	+25 29 23.7
479	3 54 02.15	+24 19 10.7	493	3 54 50.02	+24 45 35.9	507	3 56 19.05	+23 55 52.5
480	3 54 07.06	+22 53 49.1	494	3 54 54.53	+23 02 49.4	508	3 56 23.44	+24 49 58.7
481	3 54 10.35	+23 05 36.5	495	3 54 52.52	+24 34 36.6	509	3 56 30.32	+24 17 20.9
482	3 54 12.95	+23 20 53.1	496	3 55 00.99	+24 27 30.3	510	3 56 25.07	+26 08 11.2
483	3 54 20.70	+22 06 44.6	497	3 55 02.46	+25 19 32.5	511	3 56 57.02	+24 48 36.6
484	3 54 11.42	+25 18 45.2	498	3 55 28.90	+23 46 24.4	512	3 57 09.10	+22 01 54.0
485	3 54 13.30	+25 28 28.9	499	3 55 33.80	+22 48 34.3	513	3 57 18.95	+22 05 24.3
486	3 54 23.17	+25 59 34.8	500	3 55 45.26	+26 15 56.9	514	3 57 37.00	+25 24 20.3
487	3 54 25.22	+24 42 43.5	501	3 55 50.92	+24 12 03.2	515	3 57 40.62	+25 16 06.4
488	3 54 34.74	+21 53 04.3	502	3 55 48.68	+23 55 38.2	516	3 57 42.90	+25 23 09.4
489	3 54 27.91	+23 50 09.9	503	3 55 51.74	+23 04 30.3	517	3 57 50.80	+24 52 05.3
490	3 54 30.48	+24 29 05.0	504	3 55 56.37	+25 18 01.9	518	3 57 59.56	+24 29 16.0
491	3 54 33.56	+25 40 46.0	505	3 56 08.55	+21 45 49.6	519	3 58 56.98	+23 42 33.6

intend to collect as much as possible plates in the Pleiades obtained in different observatories in order to cover the period of more than 100 years on the way of long term brightness variations investigation of selected UV Cet type stars.

3. COORDINATES OF THE PLEIADES FLARE STARS

The results of the joint flare stars optical monitoring programme since 1963 in which 8 observatories (Tonantzintla, Asiago, Byurakan, Konkoly, Sonneberg, Abastumani, Rozhen, Palomar) took part up to 1981 have been presented in the Catalog and Identification Charts of the Pleiades Flare Stars of Haro et al. (1982, HCG stars) for 519 flare stars with very rough coordinates and magnitudes. More precise coordinates of the Pleiades flare stars have been provided in the Catalogue of Kazarovets (1993), available via VizieR (http://vizier.u-strasbg.fr/cgi-bin/VizieR?-source=J/other/PZ/23.141), but because of the problems in the star identification in such crowded field as the Pleiades the coordinates are not enough correct for automated photometric measurements. This is one of the reasons for recalculating the coordinates for all UV Cet type stars found in the Pleiades for which the finding charts have been published.

As a result of cooperation with the Royal Observatory of Edinburgh we obtained a Super COSMOS scan of the UKST plate No. R 8935. We estimated the exact coordinates of the UV Cet stars from the Catalog of Haro et al. (1982) and of 13 stars included in the Flare Stars Database (Tsvetkova at al. 1995), using the USNO A2.0 Catalogue of Astrometric Standards (Monet at al. 1998, http://www.nofs.navy.mil). The results are presented in Tables 3 and 4. The differences between the estimated coordinates and those from the Catalogue of Kazarovetz (http://vizier.u-strasbg.fr/cgi-bin/VizieR?-source=J/other/PZ/23.141) are presented in Fig.2.

Acknowledgements. We are very thankful to Prof. U. Heber and Prof. I. Bues for the help and hospitality, and to the Alexander von Humboldt Foundation for the support. This work is done in the frames of the joint research project 436 BUL/113 with Deutsche Forschung Gemeinschaft.

Table 4: Coordinates of the additional Pleiades flare stars with published finding charts from the Flare Stars Database, not included in the Catalog of Haro et al. (1982). The Hertzsprung (1947) HII numbers are given.

GCVS No.	HII No.	R.A. JD 2000	DEC JD 2000
V1041TAU	738	03 45 39.33	+23 45 17.5
	1332	03 47 13.47	+23 42 53.7
V1048TAU	2381	03 49 36.64	+23 29 08.4
	2870	03 50 51.40	+23 19 47.0
V1051TAU	2984	03 51 16.81	+23 49 38.1
V1054TAU	3096	03 51 39.24	+24 32 58.6
V0877TAU		03 49 48.38	+22 10 50.9
V0851TAU		03 45 10.25	+24 23 31.0
V0854TAU		03 45 27.45	+23 37 59.5
V0859TAU		03 45 12.36	+22 41 53.5
V0853TAU		03 46 31.25	+22 18 22.4
	378	03 44 33.65	+23 41 24.4
	1451	03 47 32.55	+24 36 17.4

References

Bondar, N.I. : 1995, *Astron. Astrophys. Suppl. Ser.*, **111**, 259.

Cutispoto, G. : 1990, *Astron. Astrophys. Suppl. Ser.*, **84**, 397.

Gershberg, R.E. : 1998, *IBVS*, **4589**.

Hambaryan, V.V., Garibjanian, A.T., Mirzoyan, L.V., Mirzoyan, A.L. : 1990, *Flare Stars in Star Clusters, Associations, and the Solar Vicinity*, Proc. 137 IAU Symposium, 1989, eds. L.V. Mirzoyan, B.R. Pettersen, M.K. Tsvetkov, p. 121.

Haro, G., Chavira, E., Gonzales, G. : 1982, *Bull. Inst. Tonontzintla*, **3**, 1.

Hertzsprung, E. : 1947, *Ann. Leiden Obs.*, **19**, No. 1A.

Kazarovetz, E. V. : 1993, *Variable Stars*, **23**, No. 3, 141 (or http://vizier.u-strasbg.fr/cgi-bin/VizieR?-source=J/other/PZ/23.141).

Mavridis, L.N., Avgolupis, S. : 1993, *Astron. Astrophys.*, **280**, L5.

Mirzoyan, L.V. : 1977, *Proc. IAU Colloquium 42 "The Interaction of Variable Stars and their Enviroment"*, p. 106.

Monet, D., Bird, A., Canzian, B., Dahn, C., Guetter, H., Harris, H., Henden, A., Levine, S., Luginbuhl, C., Monet, A.K.B., Rhodes, A., Riepe, B., Sell, S., Stone, R., Vrba, F., Walker, R. : 1998, *VizieR On-line Data Catalog: I/252.*

Pettersen, B.R, Olah, K., and Sandman, W.H. : 1992, *Astron. Astrophys. Suppl. Ser.*, **96**, 497.

Tsvetkova, K.P., Tsvetkov, M.K. : 1989, *IBVS*, **3366**.

Tsvetkova, K.P., Tsvetkov, M.K., Stavrev, K.Y. : 1995, *Proceedings of the IAU Symp. 164 "Stellar Populations"*, eds. P.C. van der Kruit and G. Gilmore, Kluwer, p. 360.

Publ. Astron. Obs. Belgrade No. 73 (2002), 91 - 95 *Poster*

AN ANALYTICAL MODEL FOR DIFFERENTIAL SPECTRUM OF COSMIC RAYS

M. B. BUCHVAROVA

Space Research Institute, Bulgarian Academy of Sciences, 1000 Sofia, Bulgaria
E-mail marusjab@yahoo.com

Abstract. Galactic cosmic rays (GCRs) are the highest energy particle radiation to reach Earth. When GCRs enter our Solar System, they must overcome the outward – flowing solar wind. This wind impedes and slows the incoming GCRs, reducing their energy and preventing the lowest energy ones from reaching Earth. This effect is known as solar modulation. The Sun has an 11-year activity cycle which is reflected in the characteristics of the solar wind to modulate GCRs. As a result, the GCR intensity at Earth is anti – correlated with the level of solar activity, i. e., when solar activity is high - the GCR intensity at Earth is low.

Expression for differential cosmic ray spectrum $D(E)$ with smoothing function f containing tanh (*Tangens hyperbolicus*) is determined in this paper. The seven unknown coefficients in spectrum $D(E)$ are determined by means of Newton method. Results for different levels of solar activity are obtained.

Our analyses show that: 1. The ionization effect of the GCRs is inverse to the level of the solar activity (expressed by sunspot number, or Wolf number W) because of the solar wind modulation of the high energetic particles. 2. The GCRs have important influence on the solar-terrestrial relations during the solar minimum.

1. Introduction

Our atmosphere is continuously bombarded by a flux of high-energy primary Cosmic Rays (CRs). The cosmic rays radiation arriving at the orbit the Earth is composed of ≈98% nucleons stripped of all their orbital electrons, and ≈2 % electrons and positrons. The nuclear component consists ≈87% hydrogen, ≈12% helium and ≈1% of all the heavier nuclei from lithium to the actinides (Simpson, 1992).

The CRs spectrum spans a large range, from some MeV to 10^{21} eV. Toward low energies CR intensity is modulated by Solar Activity (Simpson, 1983). In the present paper will be modeled the differential spectrum (1.8 MeV – 100 GeV) of galactic cosmic ray with smoothing function tanh (*Tangens hyperbolicus*) (Velinov 2002, Buchvarova 2001, Velinov et al. 2001). In spectrum $D(E)$ are introduced eight coefficients. Using these coefficients we receive better correspondence between observed and experimental data (Hillas, 1972).

2. Cosmic ray spectrum

Here we use the following expression for the differential spectrum (energy range E from about 30 MeV to 100 GeV) of the galactic cosmic rays with account of the anomalous cosmic rays (energy range E from 1 MeV to about 30 MeV)(Velinov 2002, Buchvarova 2001):

$$D(E) = K\left(1+\frac{\alpha}{E}\right)^{-\beta}(1+E)^{-\gamma}\left(\frac{\tanh[s(E-\varepsilon)]}{2}+0.5\right)+ \\ +\lambda\left(1+\frac{\mu}{E^{\nu}}\right)\left(-\frac{\tanh[s(E-\varepsilon)]}{2}+0.5\right) \tag{1}$$

This formula can be presented by exponential function also, using the relations between functions tanh and exponential function:

$$D(E) = K\left(1+\frac{\alpha}{E}\right)^{-\beta}\frac{(1+E)^{-\gamma}}{1+e^{-2X}}+\frac{\lambda}{1+e^{2X}}\left(1+\frac{\mu}{E^{\nu}}\right) \tag{2}$$

The new variable

$$X = (\tanh[s\,(E-\varepsilon)]) \tag{3}$$

is involved here. The coefficient s has value s = 40 (Velinov et al. 2001). The coefficients K, α, β, γ, λ, μ, ν and ε are solutions of the interpolation problem of this function through the points with the seven energy values 0.0018 GeV, 0.01 GeV, 0.023 GeV, 0.1 GeV, 0.39 GeV, 10 GeV and 100 GeV. These points are related also with the normalization conditions of spectrum (Velinov 1991). The value for γ was taken as constant, equal to 2.6 (Hillas 1972, Ginzburg and Syrovatskiy 1963). The calculation of the other parameters is treated by algorithm that combines the rapid local convergence of Newton's method with a globally convergent method for nonlinear systems of equations (Press et al. 1991). By inserting seven experimental measured points(E_i, D_i),one will get seven unknowns K, α, β, λ, μ, ν and ε

$$f_i[D_i(E_i), E_i, K, \alpha, \beta, \lambda, \mu, \nu, \varepsilon] = 0, i = 1, ...7.$$

Such nonlinear systems are treated by Newton - Raphson method in combination with line searches and backtracking. This algorithm is closely related to the quasi – Newton method of minimization. The strategy is quite simple: we always first try the full Newton step. However, we check at each iteration that the proposed step reduces f. If not, we *backtrack* along the Newton direction until we have an acceptable step. Because the Newton step is a descent direction for f, we are guaranteed to find an acceptable step by backtracking. The backtracking algorithm is discussed in more detail in (Press et al. 1991). The described program is realized in algorithmic language C.

3. Results

Table 1 contains a summary of the experimental data (E_i, D_i) for seven different levels of the energy E (Hillas 1972). For the energies $E < 390$ MeV a strong solar wind modulation of the cosmic rays intensity is observed. For each energy $E_i$in the interval between the energies 1.8 MeV $\div$ 100 GeV eleven values of the solar activity level are given. Computation values of the coefficients K, α, β, λ, μ, ν and ε for eleven

Table 1: Data for protons/(m2.sec.str.MeV/nucleon) on seven energy (GeV) levels

	18E-4	10E-3	23E-2	10E-2	39E-2	10E+0	10E1
1	1.2645E+0	5.5217E-2	3.8924E-2	2.1553E-1	8.7000E-1	1.2300E-2	8E-5
2	1.4050E+0	6.0267E-2	4.1700E-2	2.2343E-1	9.0000E-1	1.2700E-2	8E-5
3	2.8100E+0	1.0100E-1	5.5600E-2	2.6294E-1	1.0000E+0	1.3900E-2	8E-5
4	4.2150E+0	1.5150E-1	8.3400E-2	3.4196E-1	1.1000E+0	1.5100E-2	8E-5
5	5.6200E+0	2.0200E-1	1.1120E-1	4.2098E-1	1.2000E+0	1.6300E-2	8E-5
6	7.0250E+0	2.5250E-1	1.3900E-1	5.0000E-1	1.3000E+0	1.7500E-2	8E-5
7	8.4300E+0	3.0300E-1	1.6680E-1	6.0000E-1	1.4000E+0	1.8700E-2	8E-5
8	9.8350E+0	3.5350E-1	1.9460E-1	7.0000E-1	1.5000E+0	1.9900E-2	8E-5
9	1.1240E+1	4.0400E-1	2.2240E-1	8.0000E-1	1.6000E+0	2.1100E-2	8E-5
10	1.2645E+1	4.5450E-1	2.5020E-1	9.0000E-1	1.7000E+0	2.2300E-2	8E-5
11	1.4040E+1	5.0500E-1	2.7800E-1	1.000E+0	1.8000E+0	2.3500E-2	8E-5

Table 2: Table 2. Coefficients K, α, β, λ, μ, ν and ε for curves 1 – 11 in the Figures 1 and 2

	K	α	β	λ	μ	ν	ε
1	22.553150	386.46588	0.347691	0.036069	0.000007	2.429358	0.118382
2	20.044742	245.44085	0.348596	0.038453	0.000008	2.4152250	0.118404
3	16.835422	109.29264	0.348861	0.047304	0.000029	2.2991270	0.117610
4	15.416599	62.021542	0.351491	0.071056	0.000028	2.2996740	0.115203
5	14.619727	38.608494	0.356963	0.094805	0.000028	2.2999020	0.113239
6	14.118236	24.972239	0.366218	0.118554	0.000028	2.3000380	0.111523
7	18.780476	16.264205	0.374302	0.142232	0.000028	2.2999110	0.109040
8	13.542305	10.374169	0.405133	0.165912	0.000028	2.2997980	0.106623
9	13.368533	6.2441400	0.446995	0.189606	0.000028	2.2997020	0.103899
10	13.238158	3.2969230	0.532534	0.213349	0.000028	2.2996190	0.099913
11	13.137741	1.2151520	0.799753	0.237266	0.000028	2.2992360	0.088612

values of the experimental data are shown in Table 2. They are obtained by means of the above mentioned Newton - Raphson method with line searches and backtracking (Press et al. 1991).

In the Figs. 1 and 2 are presented the results from the computation for the differential energy spectrum $D(E)$ of primary protons – the predominant component in the composition of the galactic cosmic rays and anomalous cosmic rays. Actually these curves are constituted on the basis of the results in Table 2.

The first four years of 11 - year solar cycle are characterized by increase of solar activity (SA) and the next seven years by its slow decrease (Velinov et al. 1974). In Fig. 1 are shown $D(E)$ during high and comparative medium SA levels, while Fig. 2 represents $D(E)$ during low and comparatively medium SA levels; curve 11 is for solar minimum. The other curves from the Figures give the spectrums $D(E)$ by different SA levels: curve 5 (Fig. 1) and curve 6 (Fig. 2) show a comparatively medium levels of the solar activity and curve 1 – the solar maximum.

4. Analysis of the results

The coefficients K and γ form the spectrum of the galactic cosmic rays. The

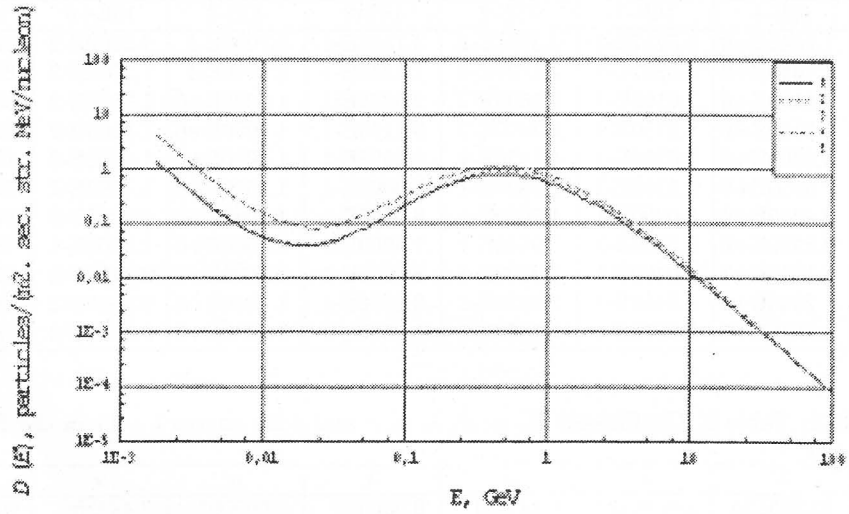

Fig. 1: The modeled differential spectrum D(E) of galactic CR protons and ACR for high and comparatively medium SA levels

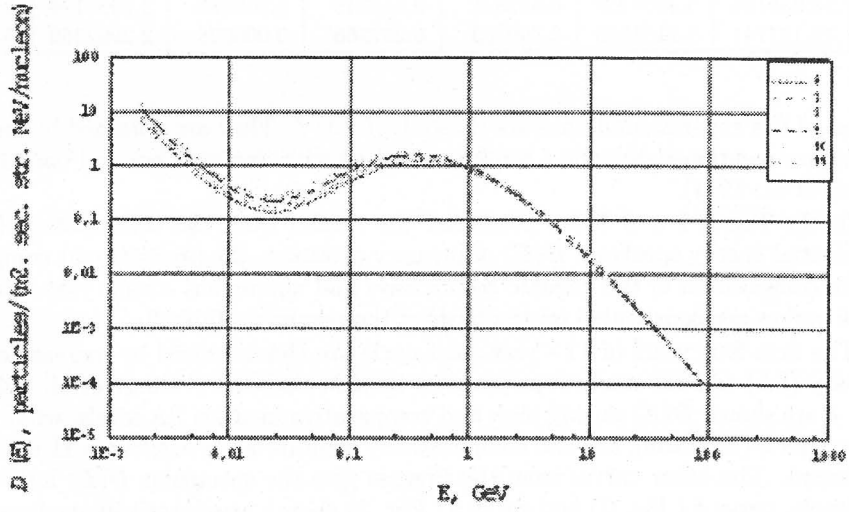

Fig. 2: The modeled differential spectrum D(E) of galactic CR protons and ACR for low and comparatively medium SA levels

parameters α and β show the influence of solar wind modulation on the primary cosmic ray spectrum. The coefficients λ, μ and ν relate to the anomalous cosmic rays.

The values of K, α and β remain constant in solar maximum (curve 1) and by average solar activity (curve 6). At the same time the coefficients λ and μ increase 3 – 4 times, while ν and ε are almost constant.

From the medium (curve 7) to minimum (curve 11) solar activity the values of $K$and α begin to decrease, while β remains almost constant. β increases twice only for solar minimum – curve 11. The coefficients λ, μ, ν and ε change very slowly in the transition from the medium to minimum solar activity.

$(1+E)^{-\gamma}$ In the interval $E \geq 1$GeV the main contribution gives the term:

In the interval between the energies 30 MeV $\div$ 1GeV the first addend of the spectrum $D(E)$ gives the main contribution.

$\frac{\lambda}{1+e^{-2X}}\left(1+\frac{\mu}{E^{\nu}}\right)$ The energy range 1.8 MeV $\div$ 30 MeV is determined predominantly by the second addend

The term with tanh is smoothing function f, which is introduced in (Velinov 2002).

5. Conclusion

In this way, the modeled improved spectrum $D(E)$ presents well the 11-year variations of galactic cosmic rays which are one of the most important sources for ionization and dissociation in the Near Earth environment. We can determine the cosmic ray spectrum in the interval between the energies 1.8 MeV $\div$ 100 GeV for any level of the solar activity. The differential spectrum $D(E)$ can by used for computation of the electron production rate profiles and chemical balance in the ionospheric CR – layer (in the lower ionosphere 50 – 90 km) both for middle and high latitudes (Velinov et al. 1974). The present investigations are important also for the modeling of the ozone distribution in the middle atmosphere during different phases of solar activity (Tassev 1992ab).

References

Buchvarova, M. : 2001, *Compt. Rend. Acad. Bulg. Sci.*, **54**, No. 3, 43.

Ginzburg, V. L., Syrovatskiy, S. I. : 1963, *Origin of the Cosmic Rays*, Moskow, Publ. House of USSR Acad. Sci.

Hillas, A. M. : 1972, *Cosmic Ray*, Oxford, Pergamon Press.

Press, W. H., Flannery, B. P., Teukolsky, S. A., Vetterling, W. T. : 1991, *Numerical Recipes in C- The Art of Scientific Computing*, Cambridge, Cambridge University Press.

Simpson, J.A. : 1983, *Ann Rev. Nucl. Part.Sci.*, **33**, 330.

Simpson, J.A. : 1992, in: *Frontiers in Cosmic Physics. Annals of N.Y.Acad. Sci.*, **655**, 95.

Tassev, Y.K. : 1992, *Compt. Rend. Acad. Bulg. Sci.*, **45**, No. 3, 17.

Tassev, Y. K. : 1992, *Compt. Rend. Acad. Bulg. Sci.*, **45**, No. 12, 37.

Velinov, P. I. Y., Nestorov, G., Dorman, L. I. : 1974, *Effect of Cosmic Rays on the Ionosphere and Radiowave Propagation*, Sofia, Publ. House of BAS.

Velinov, P. I. Y. : 1991, *Compt. Rend. Acad. Bulg. Sci.*, **44**, No. 2, 33.

Velinov, P. I. Y., Buchvarova, M., Mateev, L., Ruder, H. : 2001, *Adv. Space Res.*, **27**, No. 11, 1901.

Velinov, P. I. Y. : 2002, *Compt. Rend. Acad. Bulg. Sci.*, **55**, No. 1.

Publ. Astron. Obs. Belgrade No. 73 (2002), 97 - 104 *Poster*

CLASSICAL DENSE MATTER PHYSICS: SOME BASIC METHODS AND RESULTS

VLADAN ČELEBONOVIĆ[1]
[1]*Institute of Physics, Pregrevica* 118, 11080 *Zemun – Beograd, Yugoslavia*
E-mail vladan@phy.bg.ac.yu

Abstract. This is an introduction to the basic notions, some methods and open problems of dense matter physics and their applications in astrophysics. Experimental topics cover the range from the work of P. W. Bridgman to the discovery and basic results of use of the diamond anvil cell. On the theoretical side, the semiclassical method of P. Savić and R. Kašanin is described. The choice of these topics is conditioned by their applicability in astrophysics and the author's research experience. At the end of the paper is presented a list of some unsolved problems in dense matter physics and astrophysics, some (or all) of which could form a basis of future collaborations.

1. Introduction

The aim of this paper is to review some of the basic methods and results of classical dense matter physics. The term "classical" here has a loose meaning of " not so dense to require taking into account general relativistic effects". In practical terms, this corresponds to densities in the range $10^3 - 10^5 kg/m^3$. The text is divided into several sections. The first one is devoted to the main instrument of modern static high pressure experiments-the diamond anvil cell (DAC). In the follow-up, a short review is given of the theoretical method developed by P. Savić and R. Kašanin in Belgrade, and the paper ends with a list of selected open problems in dense matter physics and astrophysics.

This paper has been written with the astronomically oriented readers in mind. That is, people who are "at ease" in physics, but whose main interest is the application of dense matter physics to different kinds of celestial objects and not various technical details of pure physics.

In mentioning astronomy as a science, one is inclined to think about vast regions of nearly empty interstellar or interplanetary space, scarcely populated by stars and other celestial objects. Apart from this aspect of astronomy, there exists another "side of the story". Namely, in the interiors of stars, planets, and various other kinds of astronomical objects, materials are subdued to extremely high values of temperature and pressure. Although this has been known "in principle" for centuries, experimental studies of materials under high pressure have became possible only in the last 5-6 decades.

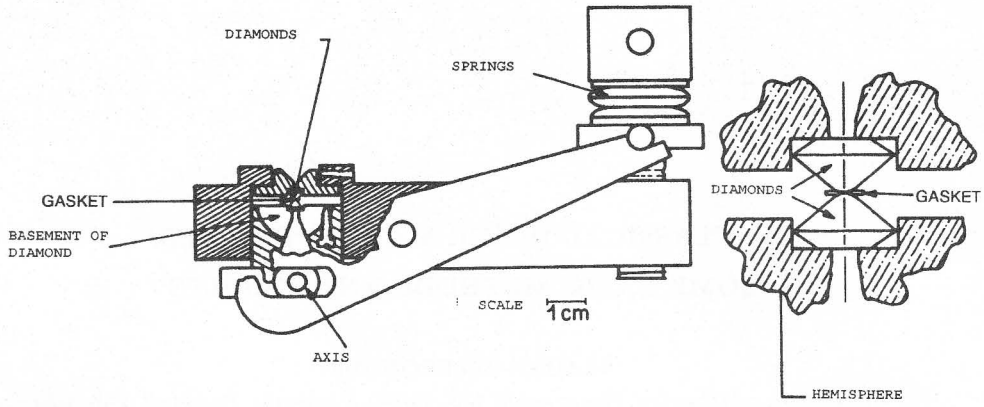

Fig. 1: the DAC of the NBS type

2. Static experiments

First attempts at studies of the behaviour of materials under high pressure have been made in the $XVIII$ century (Block et. al., 1980). It has been noted at the time that a wealthy English "gentleman" named Mr. Canton, compressed water at room temperature to a pressure of about $0.1GPa$. To his astonishment, as a result of this compression, water was transformed into ice. This was an isolated attempt of experiments under high pressure. The start of systematic work had to wait for more than a century. For comparison, note a recent example of a modern study of ice in Putrino and Parinello (2002).

Systematic high pressure experiments were initiated by P. W. Bridgman at Harvard (Bridgman, 1964). For his monumental achievements Bridgman was awarded the Nobel prize for physics in 1946.

Bridgman used large volume presses which had the advantage that the they contained large samples, and that the $P-T$ gradients in them were small. At the same time, they had the drawback that the accessible region of $P-T$ space was limited, and (which was perhaps worse) were expensive to build and maintain in operational conditions.

A real breakthrough in high pressure experimental work occurred around the middle of the XX century, with the invention of the DAC. Details about this instrument are already available in the literature, and some have been discussed by the present author (Čelebonović, 1993 and references given there).

A cross section of a DAC (of the so-called NBS type) is shown in the following figure, taken from (Jayaraman, 1983).

The term DAC comes from the fact that the most important part of this instrument is a couple of diamonds and a thin metal plate (called the gasket) between them.Diamonds are important because they are hard and transparent;this implies that a specimen can be compressed to high pressure and remain visible. The optical accessibility of a specimen is a big advantage compared to Bridgman's experimental

cells.A hole is drilled in the gasket, and in this way one gets a "working volume" in which the experiment is performed. Experiments in DACs are complicated by the miniaturized scale of the xpecimen and the working volume. The gasket is thin (usually, around 250 μm), and the diameter of the hole in it is about 200 μm. The typical size of the specimen is around 40μm. Note, as an additional difficulty, that the "working" volume contains the pressure sensor and the pressure transmitting medium. In the working volume pressure is transmitted hydrostatically. The chemical composition of the hydrostatic fluid depends on the pressure and temperature at which the experiment is preformed. For example, for $P \leq 11GPa$ a mixture of methyl and ethyl alcohol in the ratio 4 : 1 is universally used (Jayaraman, 1983).

The pressure is measured in the so-called "'ruby scale". It has been shown several decades ago (for example Jayaraman, 1983 and references given there) that the spectrum of ruby ($Al_2O_3 : Cr^{3+}$) excited with a laser beam or spectral lamp consists of two spectral lines with pressure dependent wavelengths. The physical process in which these two lines are created is the transition ${}^4A_2 \rightarrow {}^2E$ in the ion Cr^{3+} (Eggert et al., 1989). The pressure dependence is linear up to at least $30GPa$, while in its no-linear form the ruby scale can be applied up to $250GPa$.The intensity of the ruby lines diminishes with increasing pressure, and this scale becomes inapplicable for pressure higher than $250GPa$. Above that treshold, measurements can be performed only by using X-ray techniques.The final expression for the pressure dependence of the RI line (the stronger of the two) is (Mao et al., 1978):

$$P[GPa] = 380.8(1 + \frac{\Delta\lambda}{694.2})^5 - 1) \tag{1}$$

The measurement of pressure is in fact indirect:the measured quantity is the change of wavelength of the RI line, and the pressure is calculated from Eq. (1).

The region of phase space accessible to experiments in DACs is limited by $4 \leq T[K] \leq 7000$ and $P \leq 450GPa$ (Čelebonović). Note that the upper limit is of the order of magnitude of the pressure in the center of the Earth.

The applicability of DACs in space science is virtually unlimited. It is well known that the interiors of planets and satellites are inaccessible to direct observation. Some of their observable parameters (for example the magnetic moment or the content of water(Mallin and Edgett, 2000)) critically depend on the conditions in their interiors.The only reliable experimental method for investigating materials under such conditions is the DAC.

In every high pressure experiment one encounters the existence of two "interfering" complex characteristics of this branch of physics. One is the often complicated physical nature of phenomena occurring under high pressure, and the other is the complicated nature of the preparation and actual performing of the experiments. A perfect illustration of this statement, spanning more than 50 years of research and still unsolved, is offered by the behaviour of hydrogen under high pressure.

It has been predicted many times since the mid-thirties of the last century that hydrogen undergoes a phase transition and becomes metallic at a pressure of the order of 250-300 GPa. These predictions have been made so many times, by various authors using different methods of calculation, that the result of all these calculations was taken almost as an experimental value. For a long time so high values of pressure were experimentally unfeasible, but everybody in the researchers community was

certain that once they become measurable, they were just going to confirm theoretical predictions.

Results of real experiments came as a complete surprise to the high pressure researchers. It was first shown (Narayana et. al., 1998) that metallization of hydrogen **does not** occur for $P \leq 342GPa$. As a further set-back, came a result from the Lawrence Livermore National Laboratory, that the transition semiconductor $\rightarrow$ metal in fluid hydrogen occurs at the point $P = 140GPa; T = 3000K$ (Weir et. al., 1996; Nellis et. al., 1997). One possible explanation in "circulating" at the time of writing this paper (summer 2002) invokes effects of disorder (Nellis, 2002).

What can be concluded from this example? Hydrogen is a well known chemical element. It would be logical to expect that everything is known about it, and that the position of a point on its phase diagram can be predicted with arbitrary certainity. It appears that this is not the case, in spite of nearly 60 years of research on the problem.

No definite explanation has been found, but in the oppinion of the present author it should be sought in one of the following directions:

- Some of our theoretical methods and ideas are probably wrong and/or not applicable to hydrogen.
- Perhaps everything is all right with the methodology, but we are making errors in predicting the experimentally measurable consequences of the metallisation transition.

The settling of this "dispute" would have useful consequences for pure astronomy. For example, hydrogen is a constituent of the giant planets of our planetary system. Improvement of its phase diagram under high pressure would enable expanding our knowledge of their interiors.

Experiments in DACs are capable of giving information about the behaviour of various materials in a large region of the $P - T$ plane. A much wider region is accessible theoretically. The remainder of this paper is devoted to a brief review of the main ideas of a semiclassical theory of dense matter, proposed years ago by P. Savić and R. Kašanin. It has been previously discussed (for example Čelebonović, 2000 and references given there), so we shall not go into detailed considerations.

3. Semiclassical studies of dense matter:a particular theory

A specimen of a solid, although it may appear macroscopically small, is actually a typical example of a many-body system. It is a standard practice in statistical physics to describe the state of such a system by a Hamiltonian, which has the following general form:

$$H = \sum_{i=1}^{N}(-\frac{\hbar^2}{2m})\nabla_i^2 + \sum_{i=1}^{N} V(\vec{x_i}) + \sum_{i,j=1}^{N} v(\vec{x_i} - \vec{x_j}) \qquad (2)$$

The first term in this expression denotes the kinetic energy, the second is the interaction of the system with a possible external field, and the third denotes the pair-wise interaction of the particles. According to the rules of statistical mechanics, proceeding from a Hamiltonian of the general form given by Eq. (2), one should

calculate the free energy and all the other thermodynamic potentials. Singularities in these potentials would be identified with the phase transition points of the system under consideration.

This algorithm may seem clear and straightforward, but scientific reality is exactly the opposite. Sums in Eq. (2) go over all the particles of the system, and this number is usually of the order of Avogadro's number $N_A \approx 10^{23}$. It follows that these sums can not be performed for systems containing realistic numbers of particles, and that various approximate methods have to be found. One of such approximate methods is the semi-classical approach proposed by Pavle Savić and Radivoje Kašanin (Savić and Kašanin 1962/65).

At the beginning of the sixties they have started developing a semiclassical theory of dense matter. The starting point was astronomical one: they have shown that the mean volumetric planetary densities can be related to the mean solar density by a simple relationship:

$$\rho = \rho_0 2^{\varphi} \tag{3}$$

where $\rho = \frac{4}{3}$ is the mean solar density, and φ an integer. By choosing suitable values of this integer, it becomes possible to reproduce the measured values of the densities. Using this result, and a fact known from geophysics and high pressure experiments that at certain values of pressure abrupt changes of the mass density occur, they came to the conclusion that the atomic structure changes under the influence of high external pressure.

Proceeding from these ideas, they proposed a set of 6 postulates which govern the behaviour of materials under high pressure. Each of them is based on known experimental results. Developing further these postulates, they have set up a computing scheme, which gives the possibility of theoretical studies of dense matter physics. Full details about their postulates and the ensuing algorithm for calculation were recently discussed by Čelebonović (2000). In the remainder of this section we shall describe the applicability of their theory in astronomy.

Input data needed for modelling the internal structure of a planet, satellite or asteroid are the mass and the radius of the object. Starting from this pair of values, it is possible to determine the following characteristics of the body:

- the number of zones in the interior and their thickness ;
- the distribution of P, ρ, T within each of the zones ;
- the magnetic moment of the object ;
- the mean atomic mass of the chemical mixture which the object is made of ;
- the allowed interval in which the speed of axial rotation of the object must be.

Numerous examples of astronomical applications of this theory exist in the literature ([11] and references given there) and the reader interested in details is advised to consult these publications.

All the planets except Saturn and Pluto, as well as the satellites of the Earth, Jupiter and Uranus, and the asteroids 1 Ceres and 10 Hygiea have been modelled so far. Assembling the values of the mean atomic masses of all these objects one gets the following tables - which in fact show the spatial distribution of the chemical

Table 1: The chemical composition of the Solar System

object	A
Sun	1.4
Mercury	113
Venus	28.12
Earth	26.56
Mars	69
1 Ceres	96
Jupiter	1.55
Saturn	/
Uranus	6.5
Neptune	7.26
Pluto	/

elements in the planetary system and within the Jovian and Uranian satellite systems (Čelebonović, 2000).

Although Table 1. is incomplete, several physically interesting conclusions can be drawn from it. It shows, for example, that the planetary system is chemically inhomogeneous. The well known qualitative difference between the terrestrial and Jovian planets is reflected in their mean atomic masses. Striking similarities are visible in Table 1; they can be interpreted as consequences of violent events in the early history of the Solar system. It turns out that Ceres and Mercury and Triton and Mars have similar values of the mean atomic mass. As they are at present in widely different regions of the solar system, it is almost certain that they have moved out of regions in which they have been formed. The physical causes of such migrations are at present an open subject of research (for example Kuchner and Lecar, 2002).

Values of gradients of A found in the Jovian and Uranian satellite systems (see Table 2) have been interpreted as a consequence of various transport processes in the respective circumplanetary accretion disks. The values of A found for the Earth and Mars suggest that the Moon is a result of a "deep impact" into the Earth of a body which originated somewhere near the present orbit of Mars. A completely open question is the physical mechanism which provoked this impact. Judging by pure physical "'intuition"' it must have been some sort of a close encounter or direct collision of two bodies in the asteroid belt.

4. What now?

The aim of this lecture was to describe some results in two field of dense matter which have direct applications in astronomy. The choice of the material included was of course subjective - it was conditioned by the author's research experience and by work being performed in the author's laboratory in the Institute of Physics (IoP) in Belgrade.

On of the topics covered is the ruby scale for measurements of pressure in DACs. Although it is widely used, research work is going on with the aim of finding new

Table 2: The chemical composition of some satellites

satellite	A
Moon	71
J1	70
J2	71
J3	18
J4	19
U1	38
U2	43
U3	44
U4	32
U5	32
Triton	67

materials which could be used as pressure sensors. Some work along these lines is going on in IoP ((Jovanić et. al, 1996 and later work). Experiments along these lines could be performed jointly with colleagues from Bulgaria.

At the time of writing of this text (April 2002 in draft form) new results have emerged concerning the behaviour of hydrogen under high pressure (Amer. Inst. of Physics, 2002). They were obtained in the United States, in two big national laboratories:Sandia and Livermore, and concern the compressibility of hydrogen under high pressure. As it could have been expected (by experience with previous research on this topic), the preliminary results are contradictory. These results show once more that the problem of the behaviour of hydrogen under high pressure is far from being solved, in spite of some 60 years of research on the subject. As such, it could be a possible subject for collaboration of physicist and astronomers from Serbia and Bulgaria. Taking into account the experimental facilities needed, it would have to be theoretically oriented.

Another interesting line of research, actively pursued in Belgrade, concerns high pressure metrology. Basically, the problem is to find a replacement for the ruby scale. In view of the experimental equipment which exists both in Serbia (IoP) and Bulgaria (Institute of Solid State Physics), it seems that a fruitful experimental collaboration could be initiated.

Concerning astronomy as such, it would be very interesting to measure optical reflection spectra and the behaviour under high pressure of various materials which enter in the composition of asteroids and planets.

The theory proposed four decades ago by Savić and Kašanin needs a major "modernization". Ongoing work shows that according to modern data Eq. (3) can be replaced by

$$\rho = \frac{7}{5}\exp[\theta] \tag{4}$$

where the exponent θ is non-integer. Details are currently being elaborated, and will be discussed elsewhere.

The list of problems presented here is certainly not exhaustive, which anyhow was

not the aim of this contribution. Much simpler, the aim of this lecture was to describe to some extent two basic notions and indicate some open problems, which could form the basis for further collaboration.

5. Acknowledgement

The purchase of one of the references (High Pressure Research)was made possible by a donation of the Royal Dutch Embassy in Yugoslavia.

References

Amer. Inst. of Physics: 2002, *Phys. News Update*, **587**.
Block, S., Piermarini, G. J. and Munro, R.: 1980, *La Recherche*, **11**, 806.
Bridgman, P. W. : 1964, *Collected Experimental Papers*, **I-VIII**, Harvard Univ. Press, Cambridge, Mass.
Čelebonović, V.: 1993, *Publ. Obs. Astron. Belgrade*, **44**, 103.
Čelebonović, V.: 2000, *Publ. Obs. Astron. Belgrade*, **67**, 19.
Eggert, J. H. , Goettel, K. A. and Silveira, I. F. : 1989, *Phys. Rev.*, **B40**, 5724.
Jayaraman, A. : 1983, *Rev. Mod. Phys.*, **55**, 65.
Jovanić, B. R., Radenković, B. and Zeković, Lj.: 1996, *J. Phys.: Condens. Matt.*, **8**, 4107.
Kuchner, J. and Lecar, M.: 2002, preprint astro-ph/0206232.
Mao, H. K., Bell, P. M., Shaner, J. W. and Steinberg, D. J.: 1978, *J. Appl. Phys.*, **49**, 3276.
Mallin, M. C. and Edgett, K. S.: 2000, *Science*, **288**, 2330.
Narayana, C., Luo, H., Orloff, J. and Ruoff, A. L.: 1998, *Nature*, **393**, 46.
Nellis, W. J., Louis, A. A. and Ashcroft, N. W.: 1997, preprint cond-mat/9708144.
Nellis, W. J.: 2002, *High Pressure Research*, **22**, 1.
Putrino, A. and Parinello, M.: 2002, *Phys. Rev. Lett.*, **88**, 176401.
Ruoff, A. L., Luo, H., Xia, H. and Vandenborgh, C.: 1993, *Mat. Sci. Ctr. Cornell University*, MSC Report 7659.
Ruoff, A. L., Xia, H. and Xia, Q.: 1992, *Rev. Sci. Instr.*, **73**, 4342.
Weir, S. T., Mitchell, A. C., and Nellis, W. J.: 1996, *Phys. Rev. Lett.*, **76**, 1860.

Publ. Astron. Obs. Belgrade No. 73 (2002), 105 - 108 *Poster*

INFLUENCE OF REFERENCE FRAMES ON THE DETERMINATION OF LONGITUDES AND LONGITUDE DIFFERENCES

Z. CVETKOVIĆ[1] and G. PEROVIĆ[2]

[1] *Astronomical Observatory, Volgina 7, 11160-Belgrade 74, Yugoslavia*
E-mail zcvetkovic@aob.aob.bg.ac.yu

[2] *Faculty of Civil Engineering, Kralja Aleksandra 73/I, 11000 Belgrade, Yugoslavia*
E-mail perg@grf.bg.ac.yu

Abstract. Within the framework of establishing the European longitude network in 1988, the longitude differences Munich-Vienna-Graz were determined by zenith distance observations with Danjon astrolabe. Two reference frames were used in the reduction of observations: *one dynamical*, specified by the FK5 catalogue and *the other kinematical*, specified by HIPPARCOS catalogue, the mathematical model serving for smoothing the measurements in both cases being the same. By comparing the longitudes obtained for Munich, Vienna and Graz from two reference frames a systematic difference was revealed of 3 msec, which is cancelled in the longitude difference determination.

1. INTRODUCTION

The establishing of the new European Longitude Network (ELN), involved several campaigns of precise determination of longitude differences between the national reference stations. One of the more recent campaigns was carried out in 1988 between Munich, Vienna and Graz stations. The observations were made by W. Wende according to equal zenith distances method with Danjon astrolabe (*Wende 1992*). Observed were FK5 stars with magnitudes between $m_v = 2$ and $m_v = 6$. This observational material was kindly ceded to these authors by Prof. Dr Rudolf Zigl and Dipl. Ing. Werner Wende.

In the course of 23 nights in 1988 at all three stations were observed 52 series. There were altogether 1604 star transits, comprising 19248 measurements. Some of the results of treatment and analysis of these measurements were published earlier *Perović & Cvetković 1998, Cvetković & Perović 1999, Cvetković & Perović 2000*).

The first author made comprehensive researches (*Cvetković 2002*) of the mathematical models of smoothing, alike of functional and stochasting ones, aimed at reducing the effects of the random and systematic errors. Out of 12 studied mathematical models the third functional one ($FM3$) was adopted, with the stochastic model (weight model P_{KD3}) since it manifested the best accordance with the obser-

vations. Besides, with this mathematical model the star positions from two reference frames were used in the reduction of observations, the dynamical one as given by FK5 catalogue, and the kinematical one - given by HIPPARCOS catalogue. The aim was to put under scrutiny the accordance of the obtained longitudes and longitude differences.

2. LONGITUDES AND LONGITUDE DIFFERENCES OBTAINED BY USING THE HIPPARCOS CATALOGUE

After smoothing the measurements using the best adopted mathematical model (i.e. $FM3 + P_{KD3}$) the longitudes were determined of three stations participators in the campaign: Munich, Vienna and Graz and, subsequently, their longitude differences.

The results of longitude determinations are given in Table 1 and those of the longitude differences in Table 2.

Table 1: Longitudes λ of three stations; σ_λ are the errors of their determination

Stations	λ [h m s]	σ_λ [s]
Munich	0 46 16.8747	0.00064
Vienna	1 05 20.9012	0.00076
Graz	1 01 58.5779	0.00080

Table 2: Longitude differences $\Delta\lambda$; $\sigma_{\Delta\lambda}$ – errors of their determination

From – To	$\Delta\lambda$ [h m s]	$\sigma_{\Delta\lambda}$ [s]
Munich – Graz	−0 15 41.7032	0.00090
Graz – Vienna	−0 03 22.3233	0.00104
Vienna – Munich	0 19 04.0265	0.00096

3. LONGITUDES AND LONGITUDE DIFFERENCES OBTAINED BY USING FK5 CATALOGUE

Research was made as to how much the star positions affect the longitudes and longitude differences determination. For this reason the measurements of the entire campaign were smoothed, including the star positions taken from FK5. The same mathematical smoothing model was used ($FM3 + P_{KD3}$).

The results of longitude determination, obtained by using the FK5 star positions are listed in Table 3, and those pertaining to longitude differences in Table 4. Given in these Tables are also the differences with respect to the values obtained using the HIPPARCOS catalogue.

Table 3: Longitudes λ of three stations; σ_λ are the errors of longitudes; $\lambda_{FK5} - \lambda_{Hipp}$ are the longitude differences resulting from using the star positions from FK5 and HIPPARCOS catalogues

Stations	λ [h m s]	σ_λ [s]	$\lambda_{FK5} - \lambda_{HIPP}$ [s]	$\sigma_{\lambda_{FK5}-\lambda_{HIPP}}$ [s]
Munich	0 46 16.8778	0.00065	0.0031	0.00091
Vienna	1 05 20.9041	0.00077	0.0029	0.00108
Graz	1 01 58.5809	0.00079	0.0030	0.00112

Table 4: Longitude differences $\Delta\lambda$; $\sigma_{\Delta\lambda}$ are errors of the longitude differences; $\Delta\lambda_{FK5} - \Delta\lambda_{HIPP}$ are the differences between longitude differences obtained by using star positions from FK5 and HIPPARCOS catalogues.

From – To	$\Delta\lambda$ [h m s]	$\sigma_{\Delta\lambda}$ [s]	$\Delta\lambda_{FK5} - \Delta\lambda_{HIPP}$ [s]
Munich – Graz	−0 15 41.7031	0.00091	0.0001
Graz – Vienna	−0 03 22.3232	0.00104	0.0001
Vienna – Munich	0 19 04.0263	0.00096	0.0002

4. DISCUSSION OF THE RESULTS

From Table 3 it is seen that the longitude differences $\lambda_{FK5} - \lambda_{Hipp}$ for all three stations are equal – ***0.0030 seconds of time***, originating from the difference of the two celestial reference frames.

The existence of the systematic difference between the FK5 reference frame and that of the HIPPARCOS has been investigated applying the F-test. The test statistics reads:

$$F = \frac{(\lambda_{FK5} - \lambda_{HIPP})^2}{(\sigma_{\lambda_{FK5}-\lambda_{HIPP}})^2} \,. \tag{1}$$

By comparing the test of the quantity F with the quantil F-distribution:

$$1^o \qquad F_M = \left(\frac{0.003138}{0.0009109}\right)^2 = 11.868 > 3.85 \approx F_{0.95;1;1280} \tag{2}$$

$$2^o \qquad F_B = \left(\frac{0.002929}{0.0010808}\right)^2 = 7.344 > 3.85 \approx F_{0.95;1;1280} \tag{3}$$

$$3^o \qquad F_G = \left(\frac{0.003049}{0.0011243}\right)^2 = 7.354 > 3.85 \approx F_{0.95;1;1280} \tag{4}$$

we conclude that ***there exists a systematic difference between the two reference frames.***

The FK5 catalogue frame is obtained by optical observations of the fundamental stars, being linked to the mean equator and dynamic equinox for J2000.0. The HIPPARCOS frame is kinematic one, linked to the direction toward the observed extragalactic radio sources through VLBI. The two frames involve a slight residual rotation that can be investigated by way of a comparison of positions and proper

motions of fundamental stars in both catalogues. From the position differences one is able to determine the vector representing the difference of the orientation between the two reference frames. From the difference of the proper motions one might derive the vector representing the difference of rotation of the two frames. The preliminary results obtained from catalogue differences for all 1535 FK5 stars, referred to the epoch J1991.25 are given in the Preface to the HIPPARCOS catalogue.

The rigidly rotation (non-coincidence of the celestial coordinate directions) i.e. the difference of the star positions in FK5 and HIPPARCOS catalogues affect the longitude determination, but not the determination of longitude differences, as seen in Table 4. ***The differences*** $\Delta\lambda_{FK5} - \Delta\lambda_{HIPP}$ ***practically equal zero.***

5. CONCLUSION

One ought to state that in this campaign only one segment of the reference frame has been used. The observation programme contains only 121 FK5 stars (out of 1535), which is below 10% of the total number. Moreover, these stars are located in one part of the celestial sphere. Their declinations range from $+20^o$ to $+70^o$ and their right ascensions for the western transits are between 14^h and 20^h5 and for the eastern transits between 20^h and 25^h5. Nevertheless, *a constant longitude difference* $\lambda_{FK5} - \lambda_{Hipp}$ *has been obtained for all the three stations.* This, on one hand, is *a proof of the firm rotation between the two reference frames* and, on another, *a proof of the adequacy of the functional smoothing model and of the model of determining the observation weights.*

References

Cvetković, Z., Perović, G. : 1999, *Publ. Astron. Obs. Belgrade*, **65**, 131.
Cvetković, Z., Perović, G. : 2000, *Publ. Astron. Obs. Belgrade*, **67**, 9.
Cvetković, Z. : 2002, *PhD thesis*, Faculty of Civil Engineering of Belgrade University.
Perović, G., Cvetković, Z. : 1998, *Serb. Astron. J.*, **157**, 1.
Wende, W. : 1992, *Weröff. Bayer. Komm. f.d. Int. Erdmessung*, Astronom.-Geod. Arbeiten, München, **50**, 7.

Publ. Astron. Obs. Belgrade No. 73 (2002), 109 - 112 *Poster*

STARK SHIFT IN THE Si IV SPECTRUM

M.S. DIMITRIJEVIĆ[1], S. DJENIŽE[2], A. SREĆKOVIĆ[2] and S. BUKVIĆ[2]
[1] *Astronomical Observatory, 11160 Belgrade, Volgina 7, Serbia, Yugoslavia*

[2] *Faculty of Physics, University of Belgrade, 11001 Belgrade, P.O.B. 368, Serbia, Yugoslavia*

Abstract. Stark shifts measurements and semiclassical calculations of six Si IV spectral lines belonging to four transitions have been presented for elctron temperature 10^4 K and 10^{23} m^{-3} electron density.

1. INTRODUCTION

Atomic data such as Stark widths (W) and shifts (d) play an important role in the diagnostics and modelling of various cosmic and laboratory plasmas (Griem 1974; Lesage& Fuhr 1999; NIST 2002). The basic plasma parameters such as electron temperature (T) and density (N) may be obtained on the basis of the known d and W values. However, various optical depths of the emitting plasma may result in self-absorption influencing the line width value (screening the Stark contribution). Thus, Stark shifts independent of self-absorption are more reliable and consequently more interesting for diagnostic purposes. Silicon ions are among the most abundant emitters or absorbers in many kinds of the cosmic plasmas. As impurities they are present also in many, high current, laboratory plasma sources. The knowledge of the triply (Si IV) ionized silicon spectral lines Stark shifts is necessary in various astrophysical calculations. According to available bibliographies (Lesage & Fuhr 1999) no experimental Stark shift data exist for Si IV and only one work (Dimitrijević et al 1991) is devoted to the Si IV Stark shift calculation.

In this work we wish to present the first Stark shifts measurements of six Si IV spectral lines belonging to four transitions. Our measured shift values have been compared to the existing data taken from recent available data sources.

2. EXPERIMENT

The linear pulsed arc (Djeniže & Bukvić 2001; Djeniže et al 2002a,b; Srećković et al 2001a) has been used as a plasma source. A pulsed discharge was driven in a Pyrex discharge tube of 5 mm inner diameter and effective plasma length of 7.7 cm.

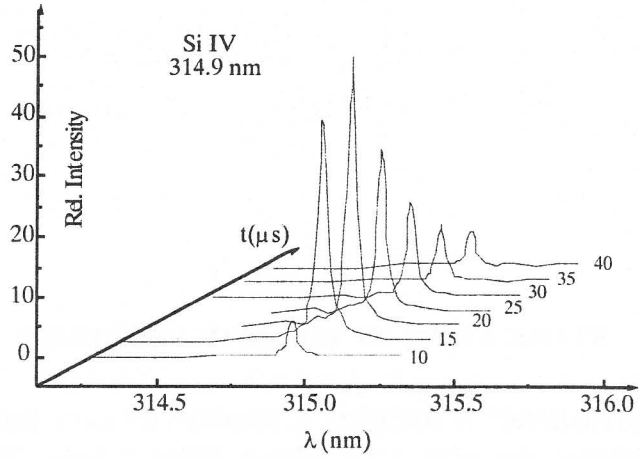

Fig. 1: Temporal evolution of the 314.9 nm Si IV spectral line profiles in oxygen plasma.

Spectroscopic observations of isolated spectral lines were made along the axis of the discharge tube. Atoms of silicon were obtained as impurities by sputtering from a Pyrex discharge tube. As a driving gas oxygen and SF_6 have been used at filling pressures of 130 Pa and 70 Pa, respectively. Highly ionized oxygen, sulfur and fluorine ions facilitate erosion of the glass walls of linear part of discharge tube. Furthermore, O_2 and SF_6, as working gases, left the observed lines of Si IV isolated. Discharge of the condenser of 8 μF capacity charged to 4 kV was selected for maximum efficiency in releasing silicon atoms. The reproducibility of the investigated silicon spectral line radiation intensities was 90%, which can be taken as acceptable considering the method by which the impurity atoms were introduced.

The line profiles were recorded using a step-by-step technique described in Refs. [5-7]. The averaged photomultiplier signal (five shots at the same spectral range) was digitized using an oscilloscope, interfaced to a computer. A sample output, is shown in Fig. 1.

Plasma reproducibility was monitored by the O III and S III lines radiation and by the discharge current (it was found to be within $\pm 5\%$). The discharge characteristics were determined by analyzing the Rogowski coil signal. The values found were: discharge current = 6.7 kA, discharge period = 28 μs, thermal resistance = 0.29 Ω, and decrement = 2.4.

The plasma parameters were determined using standard diagnostic methods (Griem 1974; Rompe& Steenbeck 1967). Thus, in the case of the oxygen plasma the electron temperature was determined from the Boltzmann plot of the relative intensities of nine O III spectral lines, with an estimated error of $\pm 13\%$, assuming the existence of local thermodynamic equilibrium (LTE). All necessary atomic data were taken from NIST (2002). In the case of the SF_6 plasma, electron temperature was determined from the ratio of the relative intensities (Saha equation) of the 334.6 nm S III to the 481.6 nm S II spectral lines supposing the existence of LTE with an estimated error of $\pm 11\%$.

Electron density, in the case of the oxygen plasma, was measured using the well-known single laser interferometry technique for the 632.8 nm He-Ne laser wavelength with an estimated error of ±6%. In the case of the SF_6 plasma the electron density decay was observed by monitoring the Stark width values of the convenient 375.9 nm O III spectral line within an estimated error of ±8%. Namely, oxygen ions produced as impurities in SF_6 discharge, due to their small concentration give convenient Stark width values due to the absence of the self-absorption. Corresponding N values, predicted by semiclassical theory (Griem 1974), were taken from Srećković et al. (2001b).

The Stark shifts were measured relative to the unshifted spectral lines emitted by the same plasma (Djeniže et al 2002a,b and references therein). Stark shift data are determined with ±0.8 pm error at a given N and T. Our measured (d_{exp}) Stark shifts are presented in Table. I. and in Djeniže et al (2002b).

3. METHOD OF CALCULATION

The semiclassical perturbation formalism (SCPF), as well as the corresponding computer code have been updated and optimized several times. The calculation procedure, with the discussion of updatings and validity criteria, has been briefly reviewed (Dimitrijević et al 1991). The calculated S IV d values are presented in Dimitrijević et al. (1991) and in Table 1. at our plasma parameters.

4. RESULTS AND CONCLUSION

The results of the measured Stark shift (d_{exp}) values are shown in Table.1. Our calculated Stark shift values (d_{Th}) are presented also in Table.1.

Table 1. Our measured (d_{exp} in pm) and calculated (d_{Th} in pm) electron Stark shift values at a given electron temperature (T in 10^4 K) and at 10^{23} m^{-3} electron density. Atomic data are taken from NIST (2002). Positive shifts is toward the red.

Transition	λ (nm)	E_u	T	d_{exp}	d_{Th}
Si IV					
4s $^2S_{1/2}$– 4p $^2P^o_{3/2}$	408.886	27.08	3.3	−1.2 ± 0.8	−0.86*
4p $^2P^o_{1/2}$– 4d $^2D_{3/2}$	314.956	30.99	5.2	2.0 ± 0.8	1.15*
4p $^2P^o_{3/2}$– 4d $^2D_{5/2}$	316.569	30.99	3.1	1.7 ± 0.8	1.08*
4d $^2D_{5/2}$– 5p $^2P^o_{3/2}$	376.245	34.29	3.2	1.5 ± 0.8	−0.18*
4d $^2D_{3/2}$– 5p $^2P^o_{1/2}$	377.315	34.28	3.2	0.3 ± 0.8	−0.18*
5p $^2P^0_{3/2}$– 5d $^2D_{5/2}$	670.121	36.14	5.2	7.5 ± 0.8	22.3*

Our measured Stark shifts and calculated ones presented in Dimitrijević et al (1991) are very small and agree very well mutually within the experimental accuracy and uncertainties of the calculations. The only exception is the d value of the higher lying $5p^2P^o - 5d^2D$ (670.121 nm) transition where the d_{Th} overvalues measured ones about 3 times.

Generally, we have found satisfying agreement between measured and theoretical Stark shift values calculated on the basis of the semiclassical perturbation formalism (SCPF).

Acknowledgment

This work is a part of projects "Determination of the atomic parameters on the basis of the spectral line profiles" and "Influence of collision processes on astrophysical plasma lineshapes" supported by the Ministry of Science, Technologies and Development of the Republic of Serbia. The research was supported also by the Fonds zur Förderung der wissenschaftlichen Forschung (Project S7303-AST). S.Djeniže is grateful to the Foundation " Arany János Közalapitvány" Budapest, Hungary.

References

Dimitrijević, M. S., Sahal-Bréchot, S. and Bommier, V.: 1991, *Astron. Astrophys. Suppl. Series* **89**, 591.

Djeniže, S. and Bukvić, S.: 2001, *Astron. Astrophys.* **365**, 252.

Djeniže, S., Milosavljević, V. and Dimitrijević, M. S.: 2002a, *Astron. Astrophys.* **282**, 359.

Djeniže, S., Dimitrijević, M. S., Srećković, A. and Bukvić, S.: 2002b, *Astron. Astrophys.*, (submitted).

Griem, H. R.: 1974, *Spectral Line Broadening by Plasmas*, (Acad.Press, New York).

Lesage, A. and Fuhr, J. R.: 1999, *Bibliography on Atomic Line Shapes and Shifts (April 1992 through June 1999)*, Observatoire de Paris.

NIST: 2002, Atomic Spectra Data Base Lines http://physics.nist.gov.

Rompe, R. and Steenbeck, M.: 1967, *Ergebnisse der Plasmaphysik und der Gaselektronik,*, Band 1 (Akademie Verlag, Berlin).

Srećković, A., Drinčić, V., Bukvić, S. and Djeniže, S.: 2001a, *Phys. Scr.* **63**, 306. .

Srećković, A., Dimitrijević, M. S. and Djeniže, S.: 2001b, *Astron. Astrophys.* **371**, 354.

Publ. Astron. Obs. Belgrade No. 73 (2002), 113 - 119 *Poster*

STARK SHIFT IN THE Ne II SPECTRUM

M. S. DIMITRIJEVIĆ[1], V. MILOSAVLJEVIĆ[2] and S. DJENIŽE[2]

[1] *Astronomical Observatory, Volgina 7, 11160 Belgrade, Serbia, Yugoslavia*
E-mail mdimitrijevic@aob.bg.ac.yu

[2] *Faculty of Physics, University of Belgrade, 11001 Belgrade, P.O.B. 368, Serbia, Yugoslavia*

Abstract. Experimental Stark shifts for 38 Ne II spectral lines at electron temperature 35 300 K and electron density of 1.83 10^{23} m^{-3}, as well as calculated Stark shift values for 22 multiplets for electron density of 10^{23} m^{-3} and for electron temperatures from 5 000 K up to 100 000 K, are presented.

1. INTRODUCTION

After earlier investigations of Ne II Stark shifts (d) the first measurements of d at convenient plasma parameters, T and N, have been carried out in only one experiment (Purić et al. 1987) where d-values of 18 Ne II spectral lines from 13 multiplets have been measured at T=35 000 K and N=1.42 10^{23} m^{-3}.

Theoretical semiclassical calculations have been made up to T = 40 000 K for only seven Ne II multiplets (Griem 1974).

We have measured Stark shift values of 38 Ne II spectral lines that belong to 22 multiplets and we have calculated Stark shift values for 22 multiplets, 30 from them are new determinations. Our plasma parameters were T=35 300 K and N=1.83 10^{23} m^{-3}. Our value of N is about 30% higher than those in the experiment of Purić et al. (1987) providing higher accuracy. For the calculations of the d-values we used the updated version of the semiclassical perturbation formalism (SCPF).

2. EXPERIMENT

The modified version of the linear low pressure pulsed arc (Djeniže et al. 1992, 2002, Milosavljević 2001) has been used as an optically thin plasma source. The working gas was pure neon at 133 Pa filling pressure in the flowing regime. Spectroscopic observations of isolated spectral lines were made along the axis of the discharge tube. The line profiles were recorded using a step-by-step technique with a photomultiplier (EMI 9789 QB) and a grating spectrograph (Zeiss PGS-2, reciprocal linear dispersion 0.73 nm/mm in the first order) system.

The measured profiles were of the Voigt type due to the convolutions of the Lorentzian, Stark and the Gaussian profiles from Doppler and instrumental broadening. For

the electron density and temperature of our experiments the Lorentzian fraction in the Voigt profile was dominant (over 88%). Van der Waals and resonance broadening were estimated to be smaller by more than one order of magnitude in comparison to Stark, Doppler and instrumental broadening. The standard deconvolution procedure (Davies & Vaughan 1963, Milosavljević & Poparić 2001) was applied using the least squares algorithm.

The plasma parameters were determined using standard diagnostic methods (Rompe & Steenbeck 1967). Thus, the electron temperature (T) was determined from the Boltzmann plot of the relative intensities of Ne II spectral lines.

The electron temperature decay is presented in Fig. 3 in Djeniže et al. (2002), together with the electron density (N) decay. The latter was measured using a well-known single laser interferometry technique (Ashby et al. 1965) for the 632.8 nm He-Ne laser wavelength with an estimated error of ±4%.

3. STARK SHIFT MEASUREMENTS

The Stark shifts were measured relatively to the unshifted spectral lines emitted by the same plasma (Milosavljević et al. 2000) and references therein. The Stark shift of spectral line can be measured experimentally by evaluating the position of the spectral line center recorded at two different electron density values during the plasma decay. In principle, the method requires recording of the spectral line profile at the high electron density that causes an appreciable shift and then later when the electron concentration has dropped to the value lower by at least an order of magnitude. The Stark shift data were corrected for the electron temperature decay (Popović et al. 1992). Stark shift data are determined with ± 0.8 pm error at a given N and T.

4. METHOD OF CALCULATION

The semiclassical perturbation formalism, as well as the corresponding computer code (Dimitrijević & Sahal-Bréchot 1996ab), have been updated and optimized several times (see Djeniže et al. (2002) and references therein). The calculation procedure, with the discussion of updating and validity criteria, has been briefly reviewed (e.g. in Dimitrijević & Sahal-Bréchot (1996ab)).

Atomic energy levels not existing (or revised) from Moore (1971; Bashkin & Stoner 1978) have been taken in Quinet (1994). One should mention that the Ne II spectrum is not well determined experimentally so that the set of experimental perturbing atomic energy levels needed for a semiclassical perturbation method calculation with the usual average accuracy of ±30%, is not complete.

5. RESULTS

The results of the measured Stark shift (d_m) values at T=35 300 K electron temperature and 1.83 10^{23} m^{-3} electron density are shown in Table 1.

Our calculated Stark shift values are presented in Table 2.

Table 1: Our measured Stark shift (d_m) values for the Ne II spectral lines at 35 300 K electron temperature and 1.83 10^{23} m^{-3} electron density. Positive shift is toward the red.

Transition	*Multiplet*	$\lambda(nm)$	$d_{exp}(pm)$
3s-3p	^4P-$^4P^0$	369.419	-0.7
	(1)	366.411	-0.2
	^4P-$^4D^0$	333.487	-0.6
	(2)	336.063	0.0
		332.716	-0.8
	^4P-$^4S^0$	300.166	-0.8
	(4)	302.886	0.0
	^2P-$^2D^0$	372.708	-2.5
	(5)		
	^2P-$^2P^0$	332.375	0.0
	(7)	337.828	0.0
3s'-3p'	^2D-$^2F^0$	356.853	-0.6
	(9)		
	^2D-$^2P^0$	331.975	-1.0
	(10)		
3p-3d	$^4P^0$-^4D	303.448	0.0
	(8)	302.704	0.4
		303.773	0.2
	$^4D^0$-^4D	332.920	0.8
	(12)	335.790	1.4
		337.410	3.1
		336.289	0.9
		337.939	2.5
	$^2D^0$-^2F	341.771	2.4
	(20)	341.482	3.1
	$^2D^0$-^2D	341.682	4.2
	(21)		
	$^2D^0$-^4P	337.187	0.7
	(22)		
	$^2S^0$-^2P	350.361	0.0
	(28)		
	$^2P^0$-^2P	362.806	3.5
	(41)		
	$^4S^0$-^2D	365.993	4.0
	(33)	363.275	6.9
	$^4S^0$-^4F	357.126	2.9
	(31)		
	$^4S^0$-^4P	356.584	2.2
	(34)		
3p'-3d'	$^2P^0$-^2D	333.612	1.3

Table 1: (continued)

Transition	*Multiplet*	$\lambda(nm)$	$d_{exp}(pm)$
3p-4s	$^2P^0$-^2P	337.728	5.4
	$^4D^0$-^4P	303.965	6.4
		303.598	2.0
3d-4f	^4F-$^4F^0$	439.194	-7.2
	(56)	440.930	-5.5
	^4F-$^4G^0$	429.040	-3.3
	(57)	441.320	-14.9

6. CONCLUSION AND DISCUSSION

In order to make easier the comparison between measured and calculated Stark shift values, the theoretical Stark shift dependence on the electron temperature together with the values of other authors and our experimental results at electron density 10^{23} m^{-3} are presented graphically in Fig. 1.

Generally, we have obtained very small shift values. Both experimental and measured d values are below one pm, within our experimental accuracy (±0.8 pm). Our measured and calculated d values have the same sign (see Fig. 1, Tables 1 and 2).

Stark shifts, corresponding to the 3p-3d and 3p-4s transition arrays have finite and positive values. Measured shift values, corresponding to the 3d-4f transition are negative and confirm the earlier obtained sign in Purić et al. (1987). Our calculated (SCPF) d values are smaller than those from Griem (1974), by up to a factor 6.

Satisfactory agreement exists between our measured and calculated d values in the case of the lines that belong to the 3p-3d transition. Earlier measured 3p-3d shift values (Purić et al. 1987) agree also with our calculated values.

It should be pointed out that we have not performed calculations of d values belonging to lines in 3d-4f transition because of the incompleteness of the set of the experimentally determined perturbing energy levels.

The large theoretical d values for 3p $^2P^0$-4s ^2P, 3p $^4D^0$-4s ^4P and 3p $^4P^0$-4s ^4P multiplets are due to close 4p $^2P^0$ and 4p $^4P^0$ perturbing levels contributing positively to the shift. The reason for strong disagreement with our measurements might indicate that 4p $^2P^0$ and 4p $^4P^0$ levels are in fact a combination of different contributions which results in decrease of their influence.

We have presented in this work experimental Stark shifts for 38 Ne II spectral lines at electron temperature 35 300 K and electron density 1.83 10^{23} m^{-3}, as well as calculated Stark shift values for 22 multiplets for electron density 10^{23} m^{-3} and for electron temperatures from 5 000 K up to 100 000 K. The shift values found are, generally, small. In the case of the 3s-3p and 3s′-3p′ transitions they are practically equal to zero. The common characteristics of these d values is the weak dependence on the electron temperature up to 100 000 K. Thus, these can be used for diagnostics purposes as data independent of self-absorption in the optically thick astrophysical plasmas.

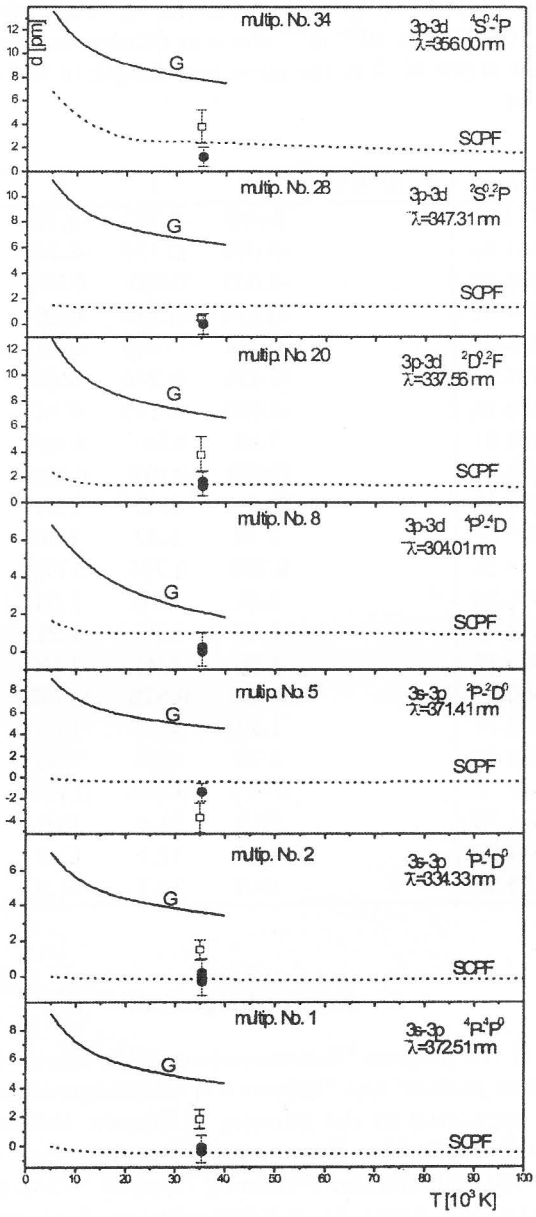

Fig. 1: Stark shift (d in pm) dependence on the electron temperature for various transitions at 10^{23} m^{-3} electron density. ● our experimental data and □, from Purić et al. (1987). G, theoretical calculations taken form Griem (1974) and our calculated (SCPF) Stark shift values taken from Table 2. The error bars of ±0.8 pm represent the uncertainties of the shift measurements. Positive shift is toward the red.

Table 2: Electron Stark shift (d in pm) calculated by using the semiclassical perturbation formalism (SCPF) at 10^{23} m^{-3} electron density for electron temperatures from 5 000 K up to 100 000 K. $\bar{\lambda}$ is the mean wavelength in the multiplet. Positive shift is toward the red.

Transition	$\lambda(nm)$	$T(10^4K)$:	0.5	1	2	3	5	10
3s ^{4}P-3p ^{4}P^0	372.51		0.003	-0.365	-0.480	-0.432	-0.543	-0.455
3s ^{4}P-3p ^{4}D^0	334.33		-0.035	-0.136	-0.187	-0.178	-0.216	-0.189
3s ^{4}P-3p ^{4}S^0	298.83		-0.039	0.021	0.052	0.049	0.065	0.037
3s ^{2}P-3p ^{2}D^0	371.41		-0.113	-0.287	-0.394	-0.379	-0.455	-0.381
3s ^{2}P-3p ^{2}P^0	334.27		-0.107	-0.058	-0.047	-0.032	-0.036	-0.060
3s$'$ ^{2}D-3p$'$ ^{2}F^0	357.21		-0.128	-0.246	-0.332	-0.308	-0.377	-0.321
3s$'$ ^{2}D-3p$'$ ^{2}P^0	333.78		-0.056	-0.113	-0.141	-0.131	-0.158	-0.150
3p ^{4}P^0-3d ^{4}D	304.01		1.66	0.987	0.937	0.968	1.04	0.869
3p ^{4}D^0-3d ^{4}D	335.26		0.820	0.879	0.860	0.964	1.01	0.864
3p ^{2}D^0-3d ^{4}F	342.15		2.51	1.45	1.34	1.43	1.49	1.27
3p ^{2}D^0-3d ^{2}F	337.56		2.45	1.42	1.30	1.38	1.45	1.24
3p ^{2}D^0-3d ^{2}D	343.23		0.760	0.797	0.782	0.892	0.975	0.828
3p ^{2}D^0-3d ^{4}P	335.26		2.81	1.70	1.53	1.57	1.63	1.40
3p ^{2}S^0-3d ^{2}P	347.31		1.47	1.36	1.22	1.36	1.42	1.26
3p ^{2}P^0-3d ^{2}P	365.18		1.30	1.24	1.12	1.30	1.35	1.23
3p ^{4}S^0-3d ^{2}D	365.00		0.526	0.573	0.507	0.674	0.709	0.644
3p ^{4}S^0-3d ^{4}F	363.78		1.12	1.13	1.05	1.23	1.25	1.13
3p ^{4}S^0-3d ^{4}P	356.00		6.79	4.40	2.46	2.61	2.17	1.58
3p$'$ ^{2}P^0-3d$'$ ^{2}P	342.27		0.871	0.883	0.826	0.966	1.01	0.850
3p ^{2}P^0-4s ^{2}P	341.23		27.3	21.0	15.7	14.4	11.9	9.32
3p ^{4}D^0-4s ^{4}P	304.53		22.2	17.1	12.9	11.7	9.68	7.61
3p ^{4}P^0-4s ^{4}P	278.52		19.0	14.7	11.3	10.1	8.46	6.58

7. Acknowledgment

This work is a part of the projects "Determination of the atomic parameters on the basis of the spectral line profiles" and "Influence of collision processes on astrophysical plasma line shapes" supported by the Ministry of Science, Technologies and Development of the Republic of Serbia. The research was supported also by the Fonds zur Förderung der wissenschaftlichen Forschung (Project S7303-AST). S.Djeniže is grateful to the Foundation " Arany János Közalapitvány" Budapest, Hungary.

References

Ashby, D. E. T. F., Jephcott, D. F., Malein, A., Raynor, F. A. : 1965, *Appl. Phys.*, **36**, 29.

Bashkin, S., Stoner, J. O. Jr. : 1978, *Atomic Energy Levels and Grotrian Diagrams Vol. I*, North Holland. Amsterdam.

Davies, J. T., Vaughan, J. M. : 1963 *Astrophys. J.*, **137**, 1302.

Djeniže, S., Milosavljević, V., Dimitrijević, M. S. : 2002, *Astron. Astrophys.*, **382**, 359.

Djeniže, S., Srećković, A., Labat, J., Konjević, R., Popović, L. Č. : 1992, *Phys. Rev. A*, **44**, 410.

Dimitrijević, M. S., Sahal-Bréchot, S. : 1996a, *Physica Scripta*, **54**, 50.

Dimitrijević, M. S., Sahal-Bréchot, S. : 1996b, *Astron. Astrophys. Suppl. Series*, **119**, 369.

Griem, H. R. : 1974 *Spectral Line Broadening by Plasmas*, Acad. Press, New York.

Milosavljević, V. : 2001 *PhD Thesis (unpublished)* University of Belgrade, Faculty of Physics, Belgrade.

Milosavljević, V., Djeniže, S., Dimitrijević, M. S., Popović, L. Č. : 2000, *Phys. Rev. E*, **62**, 4137.

Milosavljević, V., Poparić, G. : 2001 *Phys. Rev. E*, **63**, 036404.

Moore, C. E. : 1971, *Atomic Energy Levels Vol I*, NS RDS-NBS 35, (US Department of Commerce, National Bureau of Standards, Washington D. C.).

Popović, L. Č., Srećković, A., Djeniže, S. : 1992, *Proc. 11^{th} ICSLS*, **A25**, Carry le Rouet, France, edited by N. Feautrier et al. (Universite de Provence en Marseille, Marseille).

Purić, J., Djeniže, S., Srećković, A., Labat, J., Ćirković, Lj. : 1987, *Phys. Rev. A*, **35**, 2111.

Quinet, P., Palmeri, P., Biémont, E. : 1994, *Physica Scripta*, **49**, 436.

Rompe, R., Steenbeck, M. : 1967 *Ergebnisse der Plasmaphysik und der Gaselektronik*, Band 1, Akademie Verlag, Berlin.

Publ. Astron. Obs. Belgrade No. 73 (2002), 121 - 124 *Poster*

Si 6142 AND 6155 Å LINES IN STELLAR ATMOSPHERES: STARK BROADENING EFFECT

M. S. DIMITRIJEVIĆ[1], L. Č. POPOVIĆ[1], T. RYABCHIKOVA[2]

[1] *Astronomical Observatory, Volgina 7, 11160 Belgrade, Yugoslavia*
E-mail mdimitrijevic@aob.bg.ac.yu

[2] *Institute for Astronomy of Russian Academy of Science*

Abstract. We study the influence of Stark broadening effect on Si I lines in the ro Ap 10 Aql star, where the lines are asymmetrical and shifted. First we have calculated Stark broadening parameters using by the semi-clasical method for two Si I lines: 6142.48 Å and 6155.13 Å. We have adopted SYNTH code to include into account both Stark width and shift for these lines. From comparison of our calculation data with observations we found that Stark broadening plus stratification effect can explain the width and the asymmetry of the Si I lines in the atmosphere of ro Ap 10 Aql star.

1. Introduction

The Stark broadening mechanism is very important for A and B type of stellar atmospheres, and one has to take into account this effect for investigations, analysis and modeling of such stellar atmospheres. In one of our previous work (Popović et al. 2001) we obtained that by neglecting this mechanism, we introduced an error between 10% and 45% in the equivalent width determination, and corresponding errors in the abundance determination. On the other hand, in A and B stars some of the lines have blue or red asymmetry. Especially this is the case for Cp stars, where e.g. Si I 6155.134 Å line has red asymmetry, which is not the case in the Solar as well as in other non-Cp star spectra. Moreover, in spectra of Ap 10 Aql star the lines of Si I 6142.483 Å and 6155.134 Å are shifted to the blue side with respect to the other Si I lines.

The aims of the paper are: a) to calculate the Stark broadening for Si I lines (6142.483 Å and 6155.134 Å); b) to test the contribution of Stark and stratification effect to asymmetry and shift of Si I 6142.483Å and 6155.134 Å.

2. The Stark broadening parameters calculation

Calculations have been performed within the semi-classical perturbation formalism, developed and discussed in detail in Sahal-Bréchot (1969ab). This formalism, as

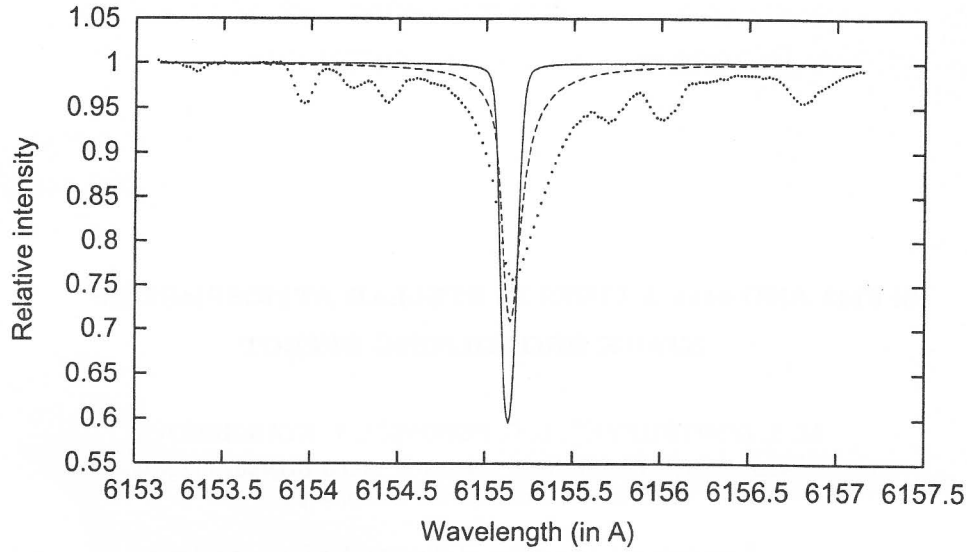

Fig. 1: The observed profile (dots) compared with the modeled one whereby we included calculated Stark parameters (dashed line). The solid line is the profile whereby Stark parameters are approximatively given in the code.

well as the corresponding computer code, have been optimized and updated (Sahal-Bréchot, 1974; Dimitrijević and Sahal- Bréchot, 1984a, Dimitrijević, 1996).

The atomic energy levels needed for calculations were taken from Martin and Zalubas (1983), but LS determination of $6s^1P^o$ and $7s^1P^o$ terms has been adopted according to Moore (1971). Oscillator strengths have been calculated by using the method of Bates and Damgaard (1949) and tables of Oertel and Shomo (1968). For higher levels, the method described in van Regemorter, Binh Dy and Prud'homme (1979) has been used. Our results for electron-, proton-, and ionized helium-impact line widths and shifts for three Si I spectral lines, for perturber density of 10^{14} cm^{-3} and temperatures T = 2,500 − 50,000 K, are shown in Table I. For perturber densities lower than those tabulated here, Stark broadening parameters vary linearly with perturber density. Nonlinear behavior of Stark broadening parameters at higher densities is the consequence of the influence of Debye shielding and has been analyzed in detail in Dimitrijević and Sahal- Bréchot (1984b).

3. Results

The results of our Stark broadening calculation are given in Table I. The calculated Stark broadening data were used to explain the asymmetry of Si I 6142.483 Å and 6155.134 Å. We have modeled the Si I 6142.48 Å and 6155.13 Å lines including calculated Stark broadening parameters. The corresponding parameters were included in each layers of stellar atmosphere. In Fig. 1 one can see the line profile without

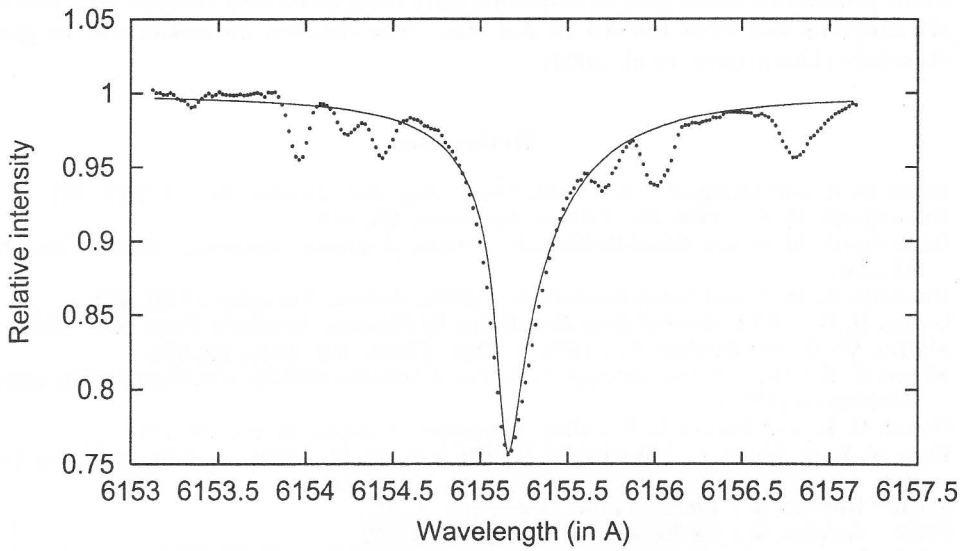

Fig. 2: The observed profile (dots) compared with the modeled one, whereby we have included Stark broadening and stratification.

Table 1: Stark Broadening Parameters for Si I Spectral Lines. This Table shows electron-, proton-, and ionized helium-impact broadening parameters for Si I for perturber density of 10^{14} cm^{-3} and temperatures from 2,500 to 50,000 K. The quantity C (given in Å cm^{-3}), when divided by the corresponding full width at half maximum, gives an estimate for the maximum perturber density for which tabulated data may be used. For higher densities, the isolated line approximation used in calculations breaks down. WIDTH(A) denotes Full line width at half maximum in Å, while SHIFT denotes Line Shift in Å. A positive shift is toward red.

		ELECTRONS		PROTONS		HELIUM IONS	
TRANSITION	T(K)	FWHM(A)	SHIFT(A)	FWHM(A)	SHIFT(A)	FWHM(A)	SHIFT(A)
SiI 4S - 5P	2500.	0.509E-02	0.333E-02	0.160E-02	0.701E-03		
2.0 1.0	5000.	0.581E-02	0.409E-02	0.172E-02	0.898E-03		
5950.2 A	10000.	0.652E-02	0.381E-02	0.183E-02	0.109E-02	0.167E-02	0.851E-03
C= 0.36E+19	20000.	0.740E-02	0.328E-02	0.194E-02	0.127E-02	0.175E-02	0.101E-02
	30000.	0.811E-02	0.271E-02	0.202E-02	0.139E-02	0.181E-02	0.111E-02
	50000.	0.903E-02	0.212E-02	0.213E-02	0.153E-02	0.188E-02	0.123E-02
SiI 3p3-5f	2500.	0.971E-01	-0.585E-01	0.176E-01	-0.145E-01	*0.145E-01	-0.115E-01
3D3-3D3	5000.	0.109	-0.624E-01	0.196E-01	-0.168E-01	0.161E-01	-0.134E-01
6142.48A	10000.	0.120	-0.597E-01	0.220E-01	-0.193E-01	0.178E-01	-0.155E-01
	20000.	0.132	-0.447E-01	0.248E-01	-0.219E-01	0.198E-01	-0.176E-01
	30000.	0.140	-0.368E-01	0.267E-01	-0.236E-01	0.211E-01	-0.190E-01
	50000.	0.146	-0.286E-01	0.295E-01	-0.258E-01	0.229E-01	-0.208E-01
SiI 3p3-5f	2500.	0.831E-01	-0.591E-01	0.176E-01	-0.146E-01	0.146E-01	-0.115E-01
3D3-3G4	5000.	0.916E-01	-0.644E-01	0.196E-01	-0.169E-01	0.161E-01	-0.135E-01
6155.13A	10000.	0.102	-0.616E-01	0.219E-01	-0.194E-01	0.179E-01	-0.155E-01
	20000.	0.110	-0.446E-01	0.245E-01	-0.220E-01	0.199E-01	-0.177E-01
	30000.	0.118	-0.360E-01	0.261E-01	-0.237E-01	0.212E-01	-0.191E-01
	50000.	0.125	-0.281E-01	0.285E-01	-0.260E-01	0.230E-01	-0.209E-01

Stark broadening (solid line) and with Stark broadening (dashed) line in comparison with observations (dots)

As one can see from Fig. 1, Stark broadening effect alone cannot explain the line shape. Next step was to take into account the stratification effect which is characteristic for atmospheres of Ap stars. As one can see in Fig. 2, the modeled line whereby

Stark broadening effect plus stratification have been taken into account very well fits the observed line from the Ap 10 Aql star. The detailed discussion will be given elsewhere (Dimitrijević et al. 2002)

References

Bates, D. R. and Damgaard, A. : 1949, *Trans. Roy. Soc. London, Ser. A*, **242**, 101.
Dimitrijević, M. S. : 1996, *Zh. Priklad. Spektrosk.*, **63**, 810.
Dimitrijević, M. S. and Sahal-Bréchot, S. : 1984a, *J. Quant. Spectrosc. Radiat. Transfer*, **31**, 301.
Dimitrijević, M. S. and Sahal-Bréchot, S. : 1984b, *Astron. Astrophys.*, **136**, 289.
Griem, H. R. : 1974, *Spectral Line Broadening by Plasmas*, Academic Press, New York.
Martin, W. C. and Zalubas, R. : 1983, *J. Phys. Chem. Ref. Data*, **12**, 323.
Moore, C. E. : 1971, *Atomic Energy Levels Vol. I*, NSRDS-NBS 35, U.S. Govt. Print. Office, Washington (1971).
Oertel, G. K. and Shomo, L. P. : 1968, *Astrophys. J. Suppl. Series*, **16**, 175.
Popović, L. Č., Simić, S., Milovanović, N., Dimitrijević, M. : 2001, *ApJ Suppl. Series*, **135**, 109.
Sahal – Bréchot, S. : 1969a, *Astron. Astrophys.*, **1**, 91.
Sahal – Bréchot, S. : 1969b, *Astron. Astrophys.*, **2**, 322.
Sahal – Bréchot, S. : 1974, *Astron. Astrophys.*, **35**, 321.
van Regemorter, H., Hoang Binh Dy and Prud'homme, M. : 1979, *J. Phys. B*, **12**, 1073.

Publ. Astron. Obs. Belgrade No. 73 (2002), 125 - 129 *Poster*

STARK BROADENING OF Cd III LINES

M. S. DIMITRIJEVIĆ[1], Z. SIMIĆ[1], N. MILOVANOVIĆ[1], L. Č. POPOVIĆ[1]
[1] *Astronomical Observatory, Volgina 7, 11000 Belgrade, Yugoslavia*
E-mail mdimitrijevic@aob.aob.bg.ac.yu
E-mail zsimic@aob.aob.bg.ac.yu
E-mail nmilovanovic@aob.aob.bg.ac.yu
E-mail lpopovic@aob.aob.bg.ac.yu

Abstract. Using a modified semiempirical approach, we have calculated Stark line widths for 10 Cd III transitions for an electron density of 10^{23}m^{-3} and temperatures from 10 000 K to 300 000 K.

1. INTRODUCTION

Investigation of Stark broadening parameters of Cd III spectral lines is of interest for a number of problems as e.g. for the laboratory plasmas, fusion plasmas and laser produced plasmas research as well as for testing and developping of the Stark broadening theory for multicharged ion lines. Moreover, such data are of interest also for the consideration of stellar plasma, since with the development of space born spectroscopic techniques, even trace elements become more and more of interest. The electron-impact broadening mechanism is the main pressure broadening mechanism in hot star atmospheres (having effective temperature $T_{eff} \gtrsim 10000$ K), and it is of interest especially for A type stars and white dwarfs. Cd III Stark broadening data are also of importance for the investigations of regularities and systematic trends particularly along isoelectronic sequences.

The sophisticated strong coupling quantum mechanical (see e.g. Griem, 1974) or semiclassical-perturbation (Sahal-Bréchot, 1969ab) formalism for Stark broadening parameter calculations are not applicable in an adequate way, for a large number of interesting spectral lines of various emitters. In such a case one can apply the modified semiempirical method (Dimitrijević and Konjević, 1980, Dimirijević and Kršljanin, 1986) which needs a considerably smaller number of atomic data. The spectrum of Cd III is poorly known, so the modified semiepirical approach is the only applicable for Stark broadening parameter calculations.

This contribution is the continuation of our efforts to provide needed data for the analysis of laboratory and astrophysical plasmas (see for example Dimitrijević 1996, Dimitrijević and Popović, 2001 and references therein).

2. THEORETICAL REMARKS

According to the modified semiempirical (MSE) approach (Dimitrijević and Konjević, 1980; Dimitrijević and Kršlajnin, 1986) the electron impact full width (FHWM) of an isolated ion line is given as (Popović and Dimitrijević, 1996)

$$W_{MSE} = N\frac{8\pi}{3}\frac{\hbar^2}{m^2}\left(\frac{2m}{\pi kT}\right)^{1/2}\frac{\pi}{\sqrt{3}}\frac{\lambda^2}{2\pi c}\cdot\{\sum_{\ell_i\pm1}\sum_{A_{i'}J_{i'}}\vec{\Re}^2[n_i\ell_iA_iJ_i,n_i(\ell_i\pm1)A_{i'}J_{i'}]\tilde{g}(x_{\ell_i,\ell_i\pm1})+$$

$$+\sum_{\ell_f\pm1}\sum_{A_{f'}J_{f'}}\vec{\Re}^2[n_f\ell_fA_fJ_f,n_f(\ell_f\pm1)A_{f'}J_{f'}]\tilde{g}(x_{\ell_f,\ell_f\pm1})+\left(\sum_{i'}\vec{\Re}^2_{ii'}\right)_{\Delta n\neq0}g(x_{n_i,n_i+1})+ \tag{1}$$

$$+\left(\sum_{f'}\vec{\Re}^2_{ff'}\right)_{\Delta n\neq0}g(x_{n_f,n_f+1})\},$$

and the corresponding Stark shift as

$$d_{MSE} = N\frac{4\pi}{3}\frac{\hbar^2}{m^2}\left(\frac{2m}{\pi kT}\right)^{1/2}\frac{\pi}{\sqrt{3}}\frac{\lambda^2}{2\pi c}\cdot\{\sum_{A_{i'}J_{i'}}\sigma_{J_iJ_{i'}}\vec{\Re}^2[n_i\ell_iA_iJ_i,n_i(\ell_i+1)A_{i'}J_{i'}]\tilde{g}_{sh}(x_{\ell_i,\ell_i+1})-$$

$$-\sum_{A_{i'}J_{i'}}\sigma_{J_iJ_{i'}}\vec{\Re}^2[n_i\ell_iA_iJ_i,n_i(\ell_i-1)A_{i'}J_{i'}]\tilde{g}_{sh}(x_{\ell_i,\ell_i-1})$$

$$-\sum_{A_{f'}J_{f'}}\sigma_{J_fJ_{f'}}\vec{\Re}^2[n_f\ell_fA_fJ_f,n_f(\ell_f+1)A_{f'}J_{f'}]\tilde{g}_{sh}(x_{\ell_f,\ell_f+1})+$$

$$+\sum_{A_{f'}J_{f'}}\sigma_{J_fJ_{f'}}\vec{\Re}^2[n_f\ell_fA_fJ_f,n_f(\ell_f-1)A_{f'}J_{f'}]\tilde{g}_{sh}(x_{\ell_f,\ell_f-1})+\left(\sum_{i'}\vec{\Re}^2_{ii'}\right)_{\Delta n\neq0}g_{sh}(x_{n_i,n_i+1})-$$

$$-2\sum_{i'(\Delta E_{ii'}<0)}\sum_{A_{i'}J_{i'}}\vec{\Re}^2(n_i\ell_iA_iJ_i,n_i\ell_{i'}A_{i'}J_{i'})g_{sh}(x_{\ell_i,\ell_{i'}})-\left(\sum_{f'}\vec{\Re}^2_{ff'}\right)_{\Delta n\neq0}g_{sh}(x_{n_f,n_f+1})+ \tag{2}$$

$$+2\sum_{f'(\Delta E_{ff'}<0)}\sum_{A_{f'}J_{f'}}\vec{\Re}^2(n_f\ell_fA_fJ_f,n_f\ell_{f'}A_{f'}J_{f'})g_{sh}(x_{\ell_f,\ell_{f'}})+\sum_k\delta_k\}$$

where the initial level is denoted as i and the final one as f and the square of the matrix element $\{\vec{\Re}^2[n_k\ell_k A_k J_k, (\ell_k \pm 1)A_{k'}J_{k'}], \quad k = i, f\}$ is

$$\vec{\Re}^2[n_k\ell_k A_k J_k, n_k(\ell_k \pm 1)A'_k J'_k] = \frac{\ell_>}{2J_k+1} Q[\ell_k A_k, (\ell_k \pm 1)A'_k] Q(J_k, J'_k)[R^{n^*_k(\ell_k\pm1)}_{n^*_k\ell_k}]^2 \tag{3}$$

Also, $\ell_> = \max(\ell_k, \ell_k \pm 1)$ and

$$\left(\sum_{k'} \vec{\Re}^2_{kk'}\right)_{\Delta n\neq 0} = \left(\frac{3n^*_k}{2Z}\right)^2 \frac{1}{9}(n^{*2}_k + 3\ell^2_k + 3\ell_k + 11) \tag{4}$$

In Eqs. (1) and (2)

$$x_{\ell_k,\ell_{k'}} = \frac{E}{\Delta E_{\ell_k,\ell_{k'}}}, \quad k = i, f$$

and $E = \frac{3}{2}kT$ is the electron kinetic energy and $\Delta E_{\ell_k,\ell_{k'}} = |E_{\ell_k} - E_{\ell_{k'}}|$ is the energy difference between levels ℓ_k and $\ell_k \pm 1$ $(k = i, f)$,

$$x_{n_k,n_k+1} \approx \frac{E}{\Delta E_{n_k,n_k+1}},$$

where for $\Delta n \neq 0$, the energy difference between energy levels with n_k and n_k+1, $\Delta E_{n_k,n_k+1}$ is estimated as $\Delta E_{n_k,n_k+1} \approx 2Z^2 E_H/n^{*3}_k$, $n^*_k = [E_H Z^2/(E_{ion} - E_k)]^{1/2}$ is the effective principal quantum number, Z is the residual ionic charge (for example Z=1 for neutrals) and E_{ion} is the appropriate spectral series limit.

If we have an oscillator strength, e.g. from literature, the corresponding matrix element may be calculated as

$$\vec{\Re}^2_{k,k'} \approx 3\frac{E_H}{E_{k'} - E_k} \cdot f_{k'k} \qquad (E_{k'} > E_k), \quad k = i, f$$

or

$$\vec{\Re}^2_{k,k'} \approx 3\frac{E_H}{E_k - E_{k'}} \frac{2k'+1}{2k+1} \cdot f_{kk'} \qquad (E_{k'} < E_k), \quad k = i, f \tag{5}$$

where $f_{k'k}$ (for $E_{k'} > E_k$) and $f_{kk'}$ (for $E_{k'} < E_k$) are oscillator strengths and E_H is the hydrogen ionization energy.

In Eqs. (1 – 4) N and T are electron density and temperature, respectively, while $Q(\ell A, \ell' A')$ and $Q(J, J')$ are multiplet and line factors. The value of A depends on the coupling approximation (see e.g. Sobel'man, 1979). In the case of the LS coupling approximation, applied here, $A = L$, for the jK approximation $A = K$ and for the jj approximation $A = j$. The $[R^{n^*_k\ell_k\pm1}_{n^*_k\ell_k}]$ is the radial integral, and with $g(x)$ (Griem, 1974), $\tilde{g}(x)$ (Dimitrijević and Konjević, 1980) and $g_{sh}(x)$ (Griem, 1974), $\tilde{g}_{sh}(x)$ (Dimitrijević and Kršljanin, 1986) are denoted the corresponding Gaunt factors for width and shift, respectively. The factor $\sigma_{kk'} = (E_{k'} - E_k)/|E_{k'} - E_k|$, where E_k and $E_{k'}$ are the energy of the considered and its perturbing level. The sum $\sum_k \delta_k$ is different from zero only if perturbing levels with $\Delta n \neq 0$ strongly violating the assumed approximations exist, so that they should be taken into account separately, and may be evaluated as

$$\delta_i = \pm\vec{\Re}^2_{ii'}[g_{sh}(\frac{E}{\Delta E_{i,i'}}) \mp g_{sh}(x_{n_i,n_i+1})], \quad (7)$$

for the upper level, and

$$\delta_f = \mp\vec{\Re}^2_{ff'}[g_{sh}(\frac{E}{\Delta E_{f,f'}}) \mp g_{sh}(x_{n_f,n_f+1})], \quad (8)$$

for the lower level. In eqs. (7) and (8) the lower signs correspond to $\Delta E_{kk'} < 0$, $k = i, f$.

3. RESULTS AND DISCUSSION

Energy levels for Cd III lines have been taken from Bashkin and Stoner (1975). Oscillator strengths have been calculated by using the method of Bates and Damgaard (1949) and the tables of Oertel and Shomo (1968). Our results for ten Cd III transitions, for perturber density of 10^{23}m^{-3} and temperatures T = 10 000 - 300 000K will be published in Milovanović et al (2002).

Table 1
This Table shows Stark broadening full half-widths (FWHM) for Cd III for the electron density of 10^{23} m^{-3} and temperatures from 10 000 up to 300 000 K.

TRANSITION	$T(K)$	WIDTH(Å)
CdIII	10000	0.6119E-01
	20000	0.4327E-01
	50000	0.2736E-01
5s $^3D_3$-5p $^3P^0_2$	100000	0.1939E-01
λ =1874.095Å	150000	0.1661E-01
	300000	0.1419E-01
CdIII	10000	0.4184E-01
	20000	0.2959E-01
	50000	0.1871E-01
5s $^3D_3$-5p $^3D^0_3$	100000	0.1323E-01
λ =1601.579Å	150000	0.1118E-01
	300000	0.9388E-02

For the first time we have provided the Stark broadening parameters for ten Cd III transitions. We hope that the present results will be of interest in the the stellar, laboratory, fusion and laser produced plasma investigation and modeling.

References

Bates, D. R. and Damgaard, A.: 1949, *Trans.Roy.Soc. London, Ser. A* **242**, 101.
Bashkin, S., Stoner Jr. J. O.: 1975, Atomic Energy Levels and Grotrian Diagrams, Vols. I-II, Amsterdam.
Dimitrijević, M. S., 1996, *Zh. Prikl. Spektrosk.* **63**, 810.
Dimitrijević M. S. and Konjević N.: 1980, *J. Quant. Spectrosc. Radiat. Transfer* **24**, 454.
Dimitrijević, M. S. and Kršljanin, V.: 1986, *Astron. Astophys.*, **165**, 269.

Dimitrijević, M. S. and Popović, L. Č.: 2001, *Zh. Prikl. Spektrosk.* **68**, 685.
Griem, H. R.: 1974, Spectral Line Broadening by Plasmas, Academic Press, New York.
Milovanović, N., Simić, Z., Dimitrijević, M. S. and Popović, L. Č.: 2002, *Astron. Astrophys.*, to be submited.
Oertel,G.K. and Shomo,L.P.: 1968, *Astrophys.J. Suppl. Series* **16**, 175.
Popović, L. Č., Dimitrijević, M. S.: 1966, Phys. Scr, 53, 325.
Sahal – Bréchot S.: 1969a, *Astron. Astrophys.* **1**, 91.
Sahal – Bréchot S.: 1969b, *Astron. Astrophys.* **2**, 322.
Sobel'man, I. I.: 1979, Atomic Spectra and Radiative Transitions, Springer-Verlag, Berlin.

Publ. Astron. Obs. Belgrade No. 73 (2002), 131 - 136 *Poster*

PATTERN FORMATION AND ANGULAR MOMENTUM TRANSPORT IN ACCRETION FLOWS

M. M. DIMITROVA, L. G. FILIPOV and D. V. ANDREEVA
Space Research Instirute, 6 Moskovska str., 1000 Sofia, Bulgaria
E-mail maria@space.bas.bg
E-mail lfilipov@space.bas.bg
E-mail danvasan@space.bas.bg

Abstract. The presence of accretion disks around active galactic nuclei and quasars as well as in close binaries and protoplanetary objects made of the investigation of the accretion flows a question not only for astrophysics but also for theoretical hydrodynamics and magnetohydrodynamics. In close binaries a possibility exists for one of the stars to be a compact object and the second at the same time to be a giant, losing mass and originating in this way accretion flow toward the compact one, but this gas has a big angular momentum which must vanish before reaching compact object surface. Physical mechanisms for angular momentum transfer in accretion flows in close binaries are the theme of this work. One of the possibilities is the presence of some structures and shock fronts in the flow, where energy exchange is very effective. Here we present the results of two kinds of numerical simulations, showing the spiral structure formation and the vortices production separately.

1. INTRODUCTION

The accretion onto a compact stellar object is one of the most effective energy transfer mechanisms in the Universe. Because of that the physical behavior of accretion flows is of great interest for the astrophysicists. The availability of accretion disks around active galactic nuclei and quasars as well as in close binaries and protoplanetary objects made the investigation of the accretion mechanisms a more common question not only for astrophysics but also for theoretical hydrodynamics and magnetohydrodynamics. In close binaries with different stellar masses the evolution of both stars runs in different time scales. This gives the possibility for one of the stars to be in a compact object state and the second at the same time to be a giant, losing mass and thus originating accretion flow toward the compact one. The flow can take place through a wind or through the inner Lagrangian point. The presence of gas around the compact object is not the unique condition for accretion. In close binaries this gas has a big angular momentum which must vanish before reaching compact object surface (Papaloizou et. al. 1995). Physical mechanisms for angular momentum transfer in accretion flows in close binaries are the theme of this work. There is not yet common point of view about the most important operator in that. Some of the authors regard the flow as an axis-symmetric one and angular momentum transfer as a result

of viscous forces. They try to include all physical processes in the alpha parameter. Others assume that these processes are not sufficiently effective and they search for possibilities for turbulisation of the flow. Some regard as good possibility to remove the angular momentum with the help of hydrodynamical instabilities (Dubrule et. al. 1992). Moreover, for some of them magnetohydrodynamical instabilities are the unique possibility for that (Balbus et. al. 1991, Caroline et. al. 2001). An alternative possibility is the availability of some structures and shock fronts in the flow, where energy exchange is very likely to occur. Our point of view is that spiral shock fronts are present in the flow and there are areas with outflow, which carried away the angular momentum. Spiral shock fronts are formed as a result of tidal forces. During the last years there are observational evidences for that (Marales-Rueda et.al., 2002, Streeght et.al. 1997, 1998). The vortices are other structures but more probable in the active galactic nucleus and quasars. The origin of Rossby solitons are small perturbations in axis-symmetric flows. But because of the large gradient of density and different speed directions along the shocks the conditions for these vortices to occur are present (Filipov 2000, 2001, Dimitrova et. Al. 2002). In this work we present the results of two kinds of numerical simulations, showing the spiral structure formation and the vortices production separately.

2. NUMERICAL MODELS

The models are built under the assumption that the flow may be considered as two-dimensional. For investigation of the structure and dynamics of the flow we use our own large particle method (Dimitrova et.al 1991, Dimitrova 1997b). In thermodynamical equation of the flow we include gravitational forces from both stars as well as both gaseous and radiative pressures. We also include the viscous forces and use full energy exchange equation. This gives the possibility to exchange the binary system parameters, inflow gas parameters, viscous and energy exchange coefficients. The reason for that is to be able to investigate the influence of each of them over total dynamics and structure of the flow. The model is built for the flow through the inner Lagrangian point, but there are no principal restrictions to adapt them for wind flow or protoplanetary system. To find the verticals we use axis-symmetric steady state flow and follow the evolution of small perturbations placed in.

3. SIMULATIONS AND RESULTS

The typical view of steady state accretion flow in close binary through the inner Lagrangian point is presented in Figs. 1 and 2.

In the first we are showing the density distribution and in the second - the velocity is placed at point (-1, 0) in the Figures. The calculations begin with no gas in the area and the field in steady state reached in a system. The calculations are made for a close binary, including a neutron star and a red giant. We have shown the area around the compact star, placed in the point (0, 0) in the Figures. The first Lagrangian point stopped when the stream reached a steady state (no change in parameters). Using different binary parameters we obtained steady states with different maximal density, but the full picture has the same general pattern.

As it is seen from the above pictures, in the accretion flow there are two spirals with high density, whereby the velocity changes its direction. In areas around the

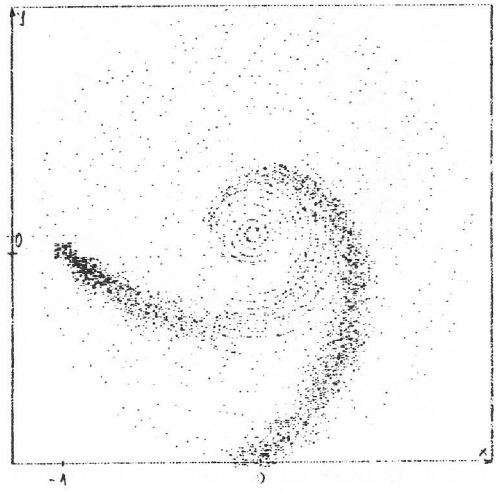

Fig. 1: Density distribution around the compact steady state object.

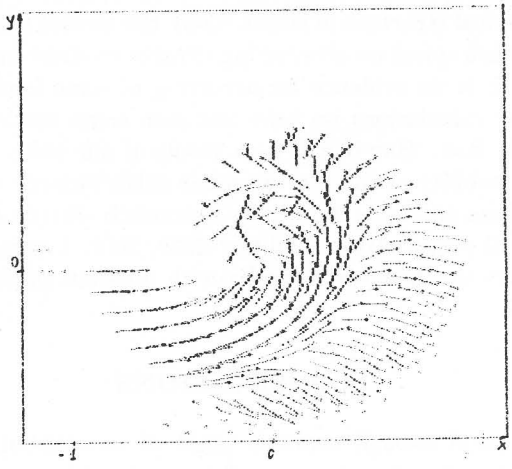

Fig. 2: Velocity field around the compact steady state object.

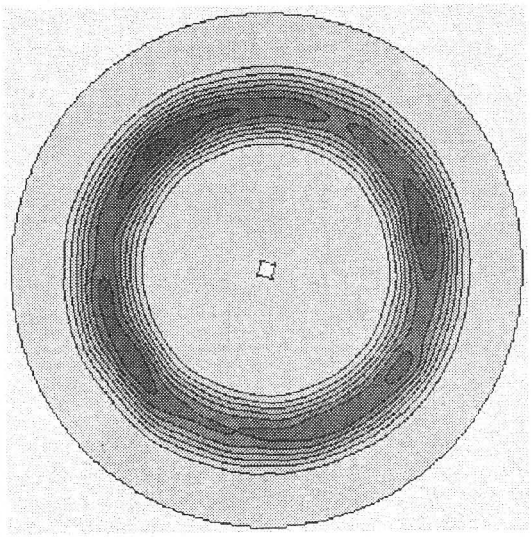

Fig. 3: Density distribution for perturbed flow.

points (-1, 0) and (1, 0) some amount of the gas leaves the system. This outflow takes away some angular momentum. This is in our view the true mechanism for angular momentum transporting away. In our previous investigations we show that the spiral structure does not strongly depend on viscous mechanisms and inner energy transfer processes (Dimitrova 1998), but the boundary conditions act on it very strongly (Dimitrova 1999). In all cases, wherever the spirals exist, they ensure the angular momentum transporting away. In the cases with nonstationar inflow stream (Dimitrova, 1997a) the spiral structure is stable. Only the second front becomes larger. In the places beyond each spiral we observe big density gradient and an exchange of the velocity direction. It is an evidence for occurring of some kinds of hydrodynamical instabilities. In our calculations we have not seen some vertical or other patterns, typical of nonstable flow. But it can be a result of our not sufficiently small cells. To investigate the stability of the flow we made other numerical model, using FEMLAB. We started from steady state axially symmetric distribution and searched for a solution with small perturbations (Filipov 2000, 2001, Lavelace, et. Al., 1999)) In the following Figures we show some results with different perturbation number and initial distributions.

4. DISCUSSIONS

There is not a good enough common point of view about mechanisms, ensuring angular momentum transport away and energy transfer mechanisms in accretion flows as a whole. Most of the authors are looking for some turbulisation processes (Papaloisou et. Al. 1995). But, if we accept the spiral shock structure of the flow, we have no need of any kind of additional turbulisation actions. The shocks themselves are the place for all energy exchanges and at the same time - the condition for occurring of instabilities. Many scientists assume that if the gravitational force from

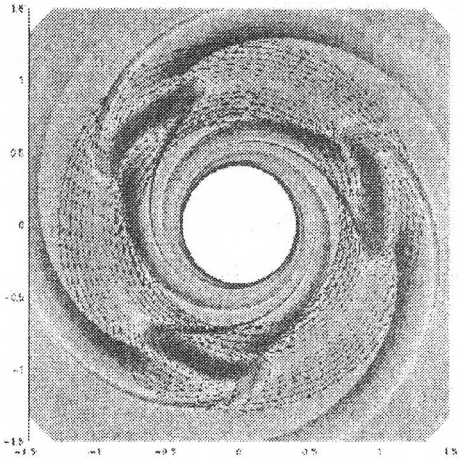

Fig. 4: Density and velocity distribution for m=3.

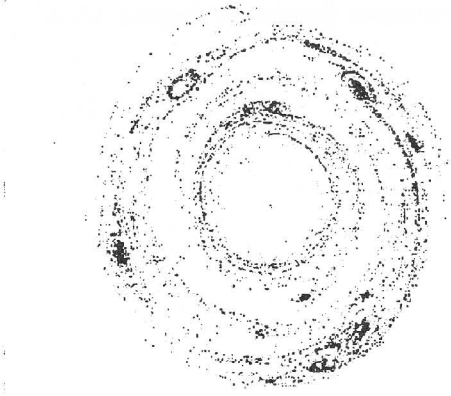

Fig. 5: Density distribution for m=4.

the second star is not strong, the spiral does not exist. The latest observational data (Streeght 1998, 1999) show the presence of such spiral flows in close binaries. There are evidences for presence of such structures in many cataclysmic variables (Murales-Rueda et. al. 2002). In our investigations of systems with second star of smaller mass, the second spiral is not so clearly seen, but still exists and the velocity fields have the same distribution (Dimitrova 1998). More than this, in some protoplanetary disk models we see the same kind of spiral structure (Burkert et. al. 1997). Planets or secondary stars are formed along these formats. The structure is stable in non-stationar flows. All this means in our opinion, that the spiral structure is something deeply intrinsic for rotating in gravitational field gas flows. It allows energy transfer as well as conditions for instability occurrence.

References

Balbus, S.S., Hawley, J. F. : 1991, *Astrophys. J.*, **376**, 214.

Burkert, A., Bate, R., Bodenheimer, P.: 1997, *Mon. Not. Roy. Astron. Soc.* **289**, 497.

Caroline, E.J.M., Terquet, L.J. : 2001, *arXiv:astro-ph/0107408.*

Dimitrova, M.M., Filipov, L.G. : 1990, *ESA SP-311*, 255.

Dimitrova, M.M. : 1997a, *Aerospace Research in Bulgaria*, **13**, 27.

Dimitrova, M.M. : 1997b, *Aerospace Research in Bulgaria*, **13**, 19.

Dubrule, B., Valdettarao, L. : 1992, *Astron. Astrophys.*, **263**, 387.

Dimitrova, M.M., Filipov, L.G., Andreeva, D.V., *The behavior of non-linear accretion disc structures under effects of MHD instabilities*, 2002, Cospar coloquium "Interball and beyond", 4-8 February, Sofia, Bulgaria (in press).

Lavelace, R.V.E., Li, H., Colgate, S.A., Nelson, A.F. : 1999, *Astrophys. J.*, **513**, 805.

Filipov; L.G. : 2001, *Mon. Not. Roy. Astron. Soc.* (in press).

Filipov, L.G. : 2000, *The Accretion disk- a Typical Reaction-Diffusion system*, Physics of Accretion and Associated Outflows, 5-8 January 2000, Cophenhagen, Denmark.

Marales-Rueda, L., Marsh, T.R. : 2002, *axXiv-astro-ph/0201368.*

Papaloizou, J.C.B., Lin, D.N.C. : 1995, *Annu. Rev. Astron. Astrophys.*, **33**, 505.

Streeght, D., Harlaftis, E., Horne, K. : 1997, *Mon. Not. Roy. Astron. Soc.*, **290**, L28.

Streeght, D., Harlaftis, E., Horne, K. : 1998, *Mon. Not. Roy. Astron. Soc.*, **296**, 463.

Dimitrova, M.M. : 1998, *Aerospace Research in Bulgaria*, **14**, 11.

Dimitrova, M.M. : 1999, *Aerospace Research in Bulgaria*, **15**, 3.

Publ. Astron. Obs. Belgrade No. 73 (2002), 137 - 141 *Poster*

EFFECTS OF WIND INTERACTIONS ON DOUBLE WR+O STARS SPECTRA

B. EFREMOVA[1] and L. GEORGIEV[2]

[1] *Astronomy Department, Sofia University "St. Cl. Ohridski", 5 James Bourcheir Blvd., 1164 Sofia, Bulgaria*
E-mail befremova@albireo.phys.uni-sofia.bg

[2] *Instituto de Astronomia, UNAM, CD Univercitaria, Apartado Postal 70-264, 04510 Mexico D.F., Mexico*
E-mail georgiev@astroscu.unam.mx

Abstract. The phase dependent spectral variability of three WR + O binary system is discussed (WR79, WR155 and WR48). Three main effects are suggested to cause UV line profile variations. The line variability is found to be due mainly to the wind eclipse effect while the effects of the presence of wind – wind interaction region are less prominent but the absorbing O star wind is clearly detectable. It is suggested that in WR79 and WR155 the stagnation point is located so close to the O star surface that the front part of the O star wind does not reach its V_∞. In WR48 there are no wind interaction effects detectable.

1. INTRODUCTION

The determination of the properties of binary systems containing Wolf–Rayet (WR) star and a young massive companion is complicated by the presence of WR stars massive, radiation driven stellar winds. We can observe only the broad emission lines with violet shifted absorption components, originating in the wind. It's difficult to obtain a reliable radial velocity (RV) curve because of the asymmetries in the WR emission lines caused by the presence of the companion. So that the determination of the orbital parameters and the physical characteristics of the stars is uncertain. There is also a problem with the determination of the wind structure of WR stars. The observations show that the WR winds have more momentum than can be introduced by a single photon scattering. If we could observationally constrain the wind structure this could help our understanding of the WR wind acceleration mechanism. There is interaction between the winds of the two stars and a structure of two shock waves and a contact discontinuity (CD) is formed (Luo et al. 1990). The resulting cone–shaped structure can be regarded as a "hole" in the WR wind, filled with the O–star wind. The line profiles in the WR spectra are affected by the presence of the wind – wind interaction region (WWIR). The purpose of this paper is to find out if WWIR presence has the predicted effects on the spectrum of three WR+O binary systems (WR79, WR155 and WR48). The model predicted line profile variations are discussed

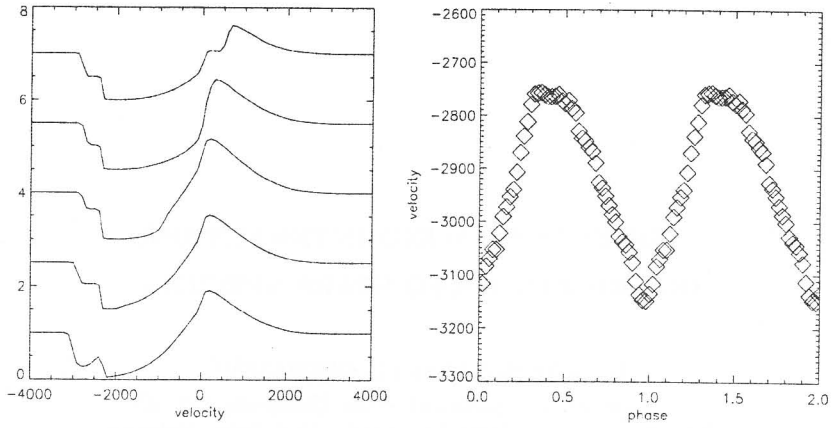

Fig. 1: Left: Line profile variations due to the wind eclipse effect for $i = 40^o$. Bottom - phase 0.0 next + 0.12 to top 0.48. Right: The expected behavior of the blue wing of the absorption component at level 0.8 of the continuum.

in section 2. The results and discussion are given in section 3.

2. PREDICTED LINE PROFILE VARIATIONS

2. 1. ABOUT THE MODEL

The calculation of the source functions is made under the assumption that the two winds are spherically symmetric and independent. The formal solution accounts for the deformation of the winds by the presence of the WWIR and the radiative interaction. The velocity fields of both winds are assumed to obey the standard β-law. The continuum opacity is grey and proportional to the electron density. The radiation field is calculated using local approximated Λ operator (Olson et al. 1986). The line source function is calculated in Sobolev approximation. The CD surface is calculated following Stevens at al. (1992). The flux is obtained using Monte Carlo integration of the emergent intensity along the system in direction to the observer. There are three main effects that cause line profile variations in WR + O binary systems.

2. 2. MAIN EFFECTS

1. Wind eclipse: This effect is due to the presence of the WR stars wind only! Let us assume for a moment that the O star has no wind. During its orbital motion the disk of the O star is eclipsed by different parts of the WR star wind. The WR wind absorbs the O star continuum much more intensively in its line frequencies than in its continuum. So a in a line originating in the WR wind appears additional absorption that widens with the O star motion to the back side of the WR star because of the larger velocity range of the WR wind projected on its disk. (See Fig. 1 left pannel)

2. "Hole" in the WR wind: Let the O star wind be transparent in the line frequencies. Then there is a hole in the WR wind surrounding the O star and changing its position towards the observer in the orbital motion. Hence at phase 0 (O star in

Table 1: Orbital elements

Star	*SpClass*	*P(days)*	$i(^o)$	Reff.
WR79	WC7+O5-8V	8.8908	44	Seggewiss (1974)
WR155	WN6+O9II-Ib	1.6412	65	Walker et al. (1983)
WR48	WC6+O9.5/B0Ia)	18.341	–	Moffat & Seggewiss (1977)

front) the hole "cuts off" the maximal negative velocities of the PCyg absorption. Passing at back it cuts parts of the WR wind with greater velocities but there the effect is hardly detected.

3. Absorbing O star wind: This effect is due to the O star wind opaque in the considered line. The cone shaped volume around the O star absorbs at the line frequencies and if its terminal velocity is greater than that of the WR wind, an additional violet absorption should occur at velocities equal to the O star V_∞. If the O star wind is evacuated from the front part of the WWIR the additional high velocity absorption occurs at phase 0, and then the blue wing of the absorption decreases its velocity. (Fig.1 right)

3. RESULTS AND DISCUSSION

The orbital parameters of the regarded systems are given in Table 1.

The phases are calculated so that $ph = 0.0$ is the passage of the O star in front of the WR star. Our study of the systems is based on the 21 (WR79), 13 (WR155), 17 (WR48) IUE high dispersion spectra in the wavelength region 1200, 1990 Å. The spectra where processed using IDL package. The spectra were rebinned to have uniform dispersion, and the normalization to the continuum was made in the regarded spectral lines. Our measurements of the WR radial velocity confirm the 8.8908d period obtained by the other authors for WR79, but the semi-amplitude of our RV curve is significantly lower. This could be a result of the different method of determination of RV. Seggewiss at al. and Lurs at all. (1997) make measurements of the radial velocity using the center of broad emission lines in the optical wavelengths. Our measurements are of the center of the blue shifted PCyg absorption of the *CIII*] λ1909Å line. The effect of wind eclipse introduces great asymmetries in the line profiles of optically thick lines, which could make emission line center deviations from the laboratory wavelength inappropriate for measuring the radial velocities of the star. The *CIII*] λ1909Å line used for our measurements is optically thin so the wind eclipse should not affect its form. For WR155 we obtain an RV curve in good agreement with the published period. For WR48 there has not been obtained a reliable RV curve.

We use the 3 emission lines of the WR star spectrum to compare the predicted line profile variations with the observations.

1. The resonance doublets *SiIV* $\lambda\lambda$1393, 1402Å and *CIV* $\lambda\lambda$1548, 1550Å should show the wind eclipse. Also the absorbing O star wind effect should be seen if present, because the doublets originate in both winds. The wind eclipse effect is clearly observable in our data for WR79 and WR155. In Fig. 2 (left) there are shown the blue wing velocities of the considered emission lines for WR79. The behavior of *SiIV* doublet in WR155 is similar. The line shows phase dependent variations predicted to

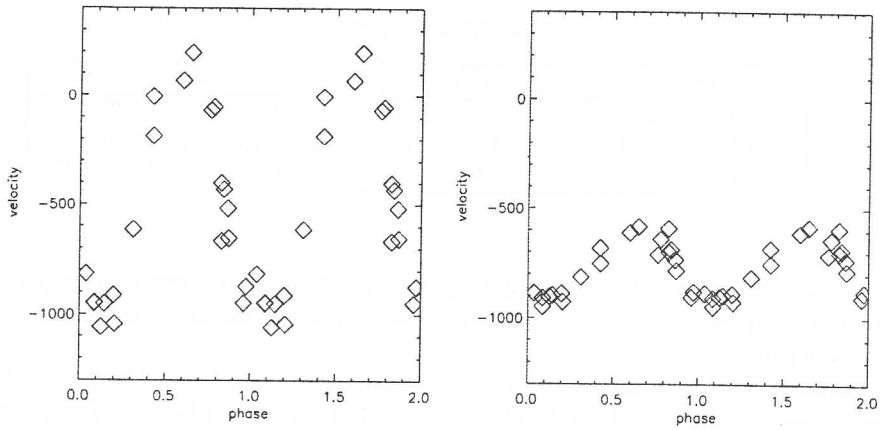

Fig. 2: WR79 blue wing of the *SiIV* $\lambda\lambda$1393, 1402Å (left), and *CIV* $\lambda\lambda$1548, 1550Å (right) emission line

occur if the wind eclipse effect is present. The maximally affected by the wind eclipse velocities in WR79 are about 1600 km/s which if we assume $V_\infty = 2270 km/s$ gives 45° for the inclination angle. This is in good agreement with the value obtained by St. Louis in pollarimetric study. In the spectra of WR48 there is no phase dependent variability of the blue wing of the emission lines, so there is no wind eclipse effect observable in this system. The lack of this effect is supporting the suggestion of St. Louis et al. (1987), that the O star companion of WR48 does not participate in the orbit.

In Fig. 3 is shown the behavior of the blue wing of the absorption component of *SiIV* λ1393Å measured at level 0.8 of the continuum.

The phase dependent variability is clearly visible for both WR79 and WR155. Such a behavior could be expected if the absorption line in the O star wind is formed in a region deformed by the CD surface so that the absorption in the O wind occurs only at phases close to 0.0 when the unperturbated O wind is directed towards the observer. In the front part of the WWIR the line does not originate so the high velocity blue wing gradually disappears towards phase 0.5. In the WR48 spectra such effect is not detectable.

2. The line *CIII*] λ1909Å is chosen because it is assumed not to occur in the O star wind, so we can test if the presence of non absorbing "hole" in the WR wind could be seen in this system. (For WC stars only). The line is collisionally existing so the wind eclipse effect should not be present. The emission line profile does not show significant variations. Thus it is not affected by the wind eclipse effect and could be used for radial velocity determination. The other effect expected to contribute to the CIII] variability – "hole" in the WR wind – is not present or not detectable in WR79. The blue wing of the absorption component remains at constant velocities with 40 km/s dispersion which is within the error limits.

If the "hole" effect is absent, it means that at phase 0 (O star in front) the cone shaped WWIR does not disturb the minimal radial velocities. Hence, knowing the

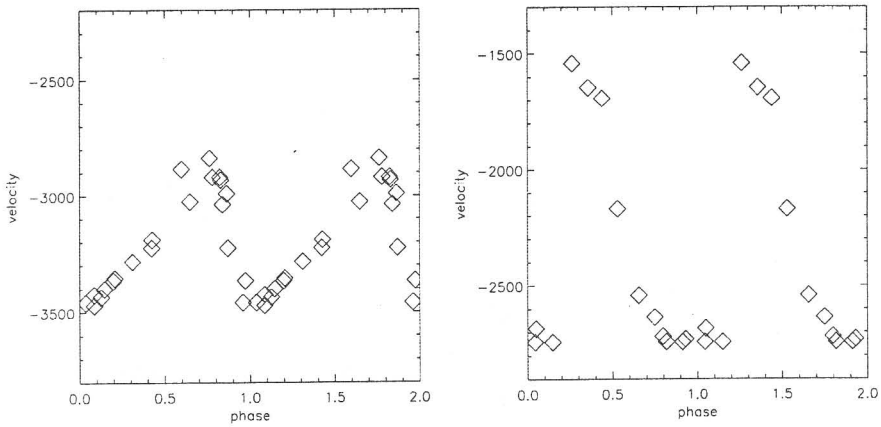

Fig. 3: WR79 blue wing of the *SiIV* λ1393Å absorption line at level 0.8. Left: WR79. Right: WR155

inclination of the system to be $i = 45°$, we can conclude that the half opening angle of the cone should be less than 45°.

We can conclude that the main effect which causes phase dependent line profile variations of WR79 and WR155 spectral lines is the wind eclipse. The contribution of the presence of a "hole" in the case of transparent O star wind is not detectable in this binary systems. In both systems the absorption from the O star wind is clearly detected, which allows us to use this effect for determination of O star wind properties. In the WR48 spectra there are not any of discussed effects detectable. It confirms the suggestion that the WR and the O star do not orbit around each other.

References

Auer, L., Koenigsberger, G. : 1994, *Astrophys. J.*, **436**, 859.
Luo, D., McCray, R., Mac Low, M. : 1990, *Astrophys. J.*, **362**, 267.
Lurs, S. : 1997, *Publ. Astron. Soc. Pacific*, **109**, 504.
Moffat, A. F. J., and Seggewoss, W. : 1977, *Astron. Astrophys.*, **54**, 607.
Olson, G. : 1982, *Astrophys. J.*, **255**, 267.
Prinja, R., Barlow, M., Howarth, I. : 1990, *Astron. J.*, **361**, 607.
Seggewiss, W. : 1974, *Astron. Astrophys.*, **31**, 211.
St-Louis, H., Drissen, L., Moffat, A.F.J., Bastien, P. : 1987, *Astrophys. J.*, **322**, 870M.
Steavens, I., Blondin, J., Pollock, A. : 1992, *Astrophys. J.*, **386**, 265.
Walker, E. N., Lloyd, C., Pike, C. D., Stickland, D. J., and Zuiderwijk, E. J. : 1983, *Astron. Astrophys.*, **128**, 394.

Publ. Astron. Obs. Belgrade No. 73 (2002), 143 - 148 *Poster*

EXTINCTION ESTIMATION FROM THE COLOUR-MAGNITUDE DIAGRAMS OF RESOLVED DWARF GALAXIES

Ts. B. GEORGIEV

Institute of Astronomy, Bulgarian Academy of Sciences
72 Tsarigradsko Shosse, 1784 Sofia, Bulgaria
E-mail tsgeorg@astro.bas.bg

Abstract. Differential color functions are established for revealing the apparent color indexes of the sequences of OB stars, blue He burning stars and red He burning stars as raw extinction estimators. The standard error of the extinction estimation seems to be 0.2 mag and this method may be useful for galaxies observed through the Milky Way. Examples of the estimation of the total extinction of the resolved stellar populations of the galaxies NGC 3109, NGC 2366, NGC 4449 and Ho IX are shown.

1. INTRODUCTION

The color-magnitude diagram (CMD) of the resolved stars in a late type galaxy contains a mix of stellar populations. Usually the top part of the CMD consists of blue and red plume stars (BPS, RPS), containing the brightest blue and red supergiants (BBS, BRS). These stars, with absolute magnitudes from –7 to –9 and –6 to –8, respectively, are used as distance indicators so far. However, usually the apparent BBS are not single stars and the apparent BRS may be Milky Way dwarfs, which could cause misleading results in the distance estimations. Moreover, the number of the used BBS and BRS is usually only 3 and the mean color indexes of these stars are poorly defined.

More information about extinction, metallicity and star formation may be obtained from statistical study of the bright blue and red stars, e.g. by means of the color and luminosity functions of the blue and red plume of the CMD, blue-to-red supergiant ratio, etc. This approach seems to be efficient in the case of dwarf starforming galaxies rather than of giant ones. The reason for this is that the dwarf irregular galaxies usually have young stellar population with uniform metallicity, which is a result of one episode of global star formation.

In principle, the majority of the BPS and RPS belong to the nearby part of the studied galaxy and therefore they are weakly influenced by the internal extinction. The mean color indexes of BPS are practically metallicity independent and they may be used as raw extinction indicator. The color indexes of the RPS are metallicity dependent - when the metallicity grows the color indexes become more red. So, if the extinction is already estimated, the RPS may be used as metallicity indicator. In

principle, if the metallicity is known, the RPS may be used as extinction indicator, too. However, the mean color indexes of the BPS and RPS are poorly defined.

There are three interesting sequences of stars with absolute magnitudes from –4 to –6 on the CMD: (i) the main sequence OB stars (OBS), (ii) the blue He burning stars (BHS, blue loop stars) and (iii) the red He burning stars (RHS, red loop stars). The brightest parts of the first two of these sequences have blue colors. Such colors are rare for the foreground Milky Way stars and the contamination from the Milky Way may be considered negligible.

The OBS and BHS have almost vertical displacement on the CMDs, with narrow intervals of color indexes ($\sim$ 0.2) and they may be used for extinction estimation. The color indexes of the RHS are intermediate, worse defined and metallicity dependent. These color indexes correspond to the most typical Milky Way stars - red dwarfs. In principle, when the Milky Way contamination may be concidered negligible, RHS may be used, too. Moreover, when the Milky Way extinction is high (e.g. $>$ 1 mag), the color indexes of the RHS become more red. Then the apparent RHS occur in the zone of the very red dwarfs, which are more rare objects and the bump of the RHS seems to be detectable.

The spike of the red giant stars (RGS, red giant branch stars) is another important formation on the CMD, which is used more efficiently as distance and metallicity indicator in the last ten years. However, the absolute magnitudes of the RGS are $<$ – 2.5 mag ($<$ –4 mag in I band) and their use needs significantly deeper observations.

In the present paper we discuss the mean colors and the revealing of the reddening of the OBS, BHS and RHS on the CMDs for their use as extinction indicators.

2. THE MEAN COLOR INDEXES OF THE CHOSEN STELLAR SEQUENCES

The main sequence of the OBS forms a well pronounced vertical strip with higher concentrations of stars on the blue part of the CMD. Comparing data from many sources (Schmidt-Kaler 1965; Flower 1977; Humphryes 1978; Straizys 1977, 1987; Drilling and Landolt 2000) we adopt the mean true color index for these stars to be $(B-V)_0 = (V-I)_0 = -0.3$, within estimated uncertainty of 0.05.

Detailed CMDs from HST and model investigations show that in the case when continuous star formation process had taken place from 10–15 Gyr ago, the stellar content is prominent also by well-pronounced blue loop, containing BHS. We analyzed the CMDs given in numerous papers, mainly based on HST observations, e.g. Dohm-Palmer et al. (1997) for Sextans A, Gallagher et al. (1998) for Pegasus, Dohm-Palmer et al. (1998) for GR 8, Lynds et al. (1998) for UGC 6456, Tolstoy et al. (1998) for Leo A, etc., as well as the simulated CMDs of Aparicio et al. (1997) and Tolstoy et al. (1998). For the brightest of the BHS we adopt all mean color indexes to be $(B-V)_0 = (V-I)_0 = 0.0$ with estimated uncertainty of 0.05.

In the mentioned papers we see also prominent branches of the RHS, consisting of G5–K5 supergiants, with absolute magnitudes up to about –6 mag. The RHS form on the CMDs a vertical column, like the columns of the BHS. The color indexes of these stars are metallicity dependent and thay may be used for extinction estimation if the metallicity is known. Here we adopt raw mean color indexes for the RHS, in the case of low metallicity, to be $(B-V)_0 = 1$ and $(V-I)_0 = 1.2$, within estimated

Table 1: Adopted mean color indexes for the discussed supergiant stars

Stars	$(B-V)_0$	$(V-R)_0$	$(B-R)_0$	$(V-I)_0$	uncert-ainty
Main sequence OB stars	-0.3	-0.1	-0.4	-0.3	0.05
Blue He burning stars	0	0	0	0	0.05
Red He burning stars	1.0	0.5	1.5	1.2	0.1
Plume of BSS	-0.1	-0.05	-0.15	-0.1	0.1
Plume of RSS	1.5	0.7	2.2	1.7	0.2

uncertainty about 0.1. After respective callibration, the RHS may be raw metallicity indicators.

The color indexes of OBS stars and BHS are similar and they could hardly be distinguished from ground observations, when they merge together. The same problem appears in the HST observations of more distant galaxies. For such cases we must adopt also mean color indexes for the BPS for very raw extinction estimations. This is a more complicated task. Let us compare the luminosities of the components of the BPP. In galaxies with continuous long star forming process the BHS stars may be more than the OBS. We must account also for the possible presence of rare BBS. These stars are observed more frequently in cases of star formation of massive stars. The concentrations of the different components in the BSP are previously not known and we can not recognize them. So, we may adopt an arbitrary mean value for the color index. Here we adopt mean values for OBS and BHS stars, giving to the BHS twice greater weight. Then the mean color indexes for the brightest part of the BPS, containing the BSB, are $(B-V)_0 = (V-I)_0 = -0.1$, within estimated uncertainty of about 0.1.

In rare cases, if the population of the BRSs is sufficiently rich, the CMD shows prominant RPS. The mean color indexes of these stars are the most poorly defined among the considered types of stars and they are metallicity dependent. Looking at the CMDs in the mentioned papers, we can see some BRS, but they do not form significant concentration. These rare stars are situated arbitrarily above and to the right from the spike of the RGS. For the cases of well-pronounced RPS, in conditions of low metallicity, we adopt the main color indexes $(B-V)_0 = 1.5$ and $(V-I)_0 = 1.7$, within possible uncertainty of about 0.2. Probably, the brightest RPS may be used also as very raw metallicity indicator.

The adopted mean color indexes for the discussed bright stars, useful for reddening estimations, are given in Table 1.

For calculating the extinctions and the color excesses in different bands of the $BVRI$ system we use relations, adopted from the paper of Fitzpatrick (1999):

$$A_V = 0.76A_B, \quad A_R = 0.57A_B, \quad A_I = 0.38A_B,$$
$$E_{B-V} = 0.24A_B, \quad E_{V-R} = 0.19A_B,$$
$$E_{B-R} = 0.43A_B, \quad E_{V-I} = 0.38A_B.$$

Using the estimated uncertainities of the mean color indexes in Table 1, we may estimate the errors of the extinction derivations. In the case of excess error of 0.05

Table 2: Data on the galaxies and extinction estimations

Galaxy	A_B(PGC)	V-intervals	R- or I-intervals	A_B(T)	$\sigma_{A_B(T)}$	N
NGC 3109	0.41	17.7 - 20.0 - 21.5	19.6 - 21.0 - 22.0	0.83	0.11	3
NGC 2366	0.41	18.2 - 21.0 - 23.0	19.6 - 21.0 - 22.0	0.95	0.25	4
NGC 4449	0.26	17.0 - 20.4 - 23.0	17.0 - 20.6 - 22.5	0.48	0.10	4
Ho IX	0.32	19.0 - 21.8 - 23.4	19.6 - 21.4 - 22.8	0.55	0.32	3

and 0.1 mag the extinction errors belong to the intervals from 0.12 mag (for $B-R$) up to 0.26 mag (for $V-R$) as well as from 0.23 (for $B-R$) up to 0.52 mag (for $V-R$). We consider the mean estimated error of the method as 0.2.

3. RESULTS

The OBS, HBS and RBS sequences appear as vertical strips of higher concentrations stars on the CMDs. Therefore, they may be recognized as local maximums in the differential distributions of the stars along the color index range. We call such kind of stellar distributions color functions (CFs). Our experience shows that two magnitude intervals, including the brightest resolved objects and the interemediate ones, are enough for revealing the local maximums of the CFs, which may be used as detectors of the mean colors of OB, HBC and RBC stars.

We set up smoothed CFs using published CMDs from ground based observations for four star forming dwarf galaxies: NGC 3109 (Greggio et al. 1993), NGC 2366 (Aparicio et al. 1995), NGC 449 (Karachentsev & Drozdovski 1998) and Ho IX (Georgiev & Bomans 2002). The data for three of these galaxies are obtained in the BVR system and in the case of NGC 4449 the system is BVI. The CFs are presented in Fig.1. Interpreting the local maximums of the CFs as regions of higher concentration of OBS, BHS or RHS, we derive the extinction estimations and their errors from 3–5 individual estimations of the color excesses, using the color data for OB, BH and (sometimes) RHS.

The data are listed in Table 2, where A_B(PGC) is the estimation of the Milky Way extinction in the B band, adopted from the catalog PGC. The magnitude intervals of two CFs (plotted in Fig.1) are given in V and R (or I) bands by means of three magnitudes: the top limit of the first interval, the intermediate magnitude (that is bottom limit of the first interval and the top limit of the second interval) and the bottom limit of the second interval. Further A_B(T), $\sigma_{A_B(T)}$ and N are the estimations of the mean total extinctions (foreground and internal) toward the resolved stellar population, its standard error and the number of the individual estimations.

Table 2 shows that our total extinction estimations are significantly higher than the foreground extinction, given in the PGC. The reason for this is that the galaxies in our sample have high amount of gass and dust. Ho IX is the smallest galaxy in the sample with a shortage of bright stars. For this reason its color functions are too complicated and the total extinction to Ho IX appears worse defined.

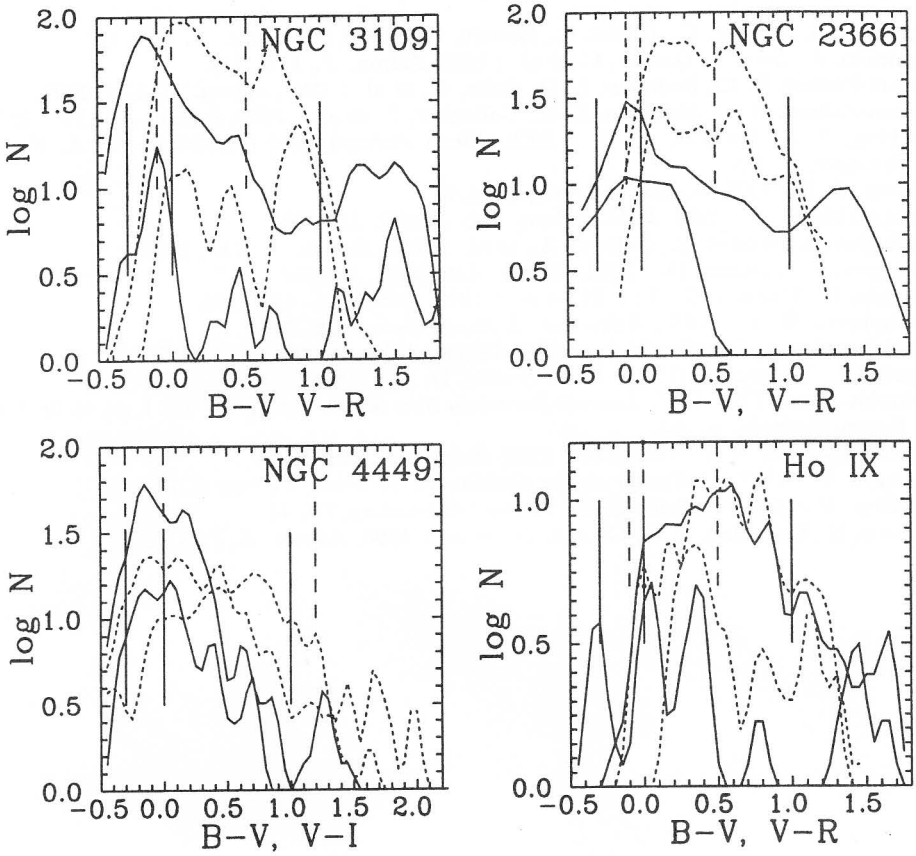

Fig. 1: Differential distributions of the stellar colors (color functions, CFs) on the CMDs, established with color index step 0.05 in two magnitude intervals for each color system. The intervals are given in Table 2. The solid curves correspond to the V band and the dashed - to the R band (for NGC 4449 – to the I band). The vertical lines (solid and dashed, respectively) show the adopted true mean color indexes of the unreddened sequences of OB stars, blue He burning and red He burning stars in V and R (or I) bands, given in Table 1. The well pronounced local maximums of the CFs are interpreted as counterparts to the corresponding sequences of bright stars and their shifts to the right are used for extinction estimations.

4. CONCLUSIONS

In this paper we check the possibility to estimate the total extinction to the resolved stellar population of dwarf galaxies using the sequences of OBS, BHS and (uncertainly) RHS. This approach may be useful in the cases of large foreground extinction, as in the case of the galaxies belonging to IC 342/Maffei complex. The accuracy of the presented method for extinction estimation is ~ 0.2 mag. For small galaxies, like Ho IX, the accuaracy of the method is lower.

References

Aparicio, A., Gallart, C., Choisi, C., Bertelli, G. : 1996, *Astrophys. J.*, **469**, L97.
Aparicio, A., Sera, J., Gallart, C. et al. : 1995, *Astron. J.*, **110**, 212.
Dohm-Palmer, R. C., Skillman, E. D., Saha, A., et al. : 1997, *Astron. J.*, **114**, 2527.
Dohm-Palmer, R. C., Skillman, E. D., Gallagher, J., et al. : 1998, *Astron. J.*, **116**, 1227.
Drilling, J. S., Landolt, A. U. : 2000, *Allen's Astrophysical Quantities*, ed. A. N. Cox, Springer, p. 388.
Flower, P. J. : 1977, *Astron. Astrophys.*, **54**, 31.
Fitzpatrick, E. L. : 1999, *Publ. Astron. Soc. Pacific*, **111**, 63.
Gallagher, J., Tolstoy, E., Colo, A. A., et al. : 1998, *Astron. J.*, **115**, 1869.
Georgiev, T., Bomans, D. : 2002, *Astron. Astrophys.*, in print.
Griggio, L., Marconi, G., Tosi, M. et al. : 1993, *Astron. J.*, **105**, 894.
Humphreys, R. M. : 1978, *Astrophys. J. Suppl. Series*, **38**, 309.
Karachentsev, I., Drozdovski, I. : 1998, *Astron. Astrophys. Suppl.*, **131**, 1.
Lynds, R., Tolstoy, E., O'Neil, E. J., Hunter, D. A. : 1998, *Astron. J.*, **116**, 146.
Schmidt-Kaler, Th. : 1965, *Landolt-Bornstein New Series*, Group VI, vol. I, ed. H. H. Voigt, Berlin, Springer, p. 284.
Schulte-Ladbeck, R. E., Hopp, U. : 1998, *Astron. J.*, **116**, 2886.
Straizys, V. : 1977, *Multicolor stellar photometry*, Mokslas, Vilnius, p. 100.
Straizys, V. : 1987, *Bulletin of the Vilnius Observatory*, **78**, 43.
Tolstoy, E., Gallagher, J. S., Cole, A. A., et al. : 1998, *Astron. J.*, **116**, 1244.

Publ. Astron. Obs. Belgrade No. 73 (2002), 149 - 152 *Poster*

THE HYPERLEDA PROJECT EN ROUTE TO THE ASTRONOMICAL VIRTUAL OBSERVATORY

V. GOLEV[1], V. GEORGIEV[2] and PH. PRUGNIEL[3]

[1] *Department of Astronomy and Astronomical Observatory of the St. Kliment Okhridski University of Sofia, P.O.Box 36, BG-1504 Sofia, Bulgaria*
E-mail : valgol@phys.uni-sofia.bg

[2] *Department of Astronomy and Astronomical Observatory of the St. Kliment Okhridski University of Sofia, P.O.Box 36, BG-1504 Sofia, Bulgaria*
E-mail : vladimir@phys.uni-sofia.bg

[3] *CRAL Observatoire Astronomique de Lyon(CNRS: UMR 142), F-69561 St-Genis-Laval Cedex, France*
E-mail : prugniel@obs.univ-lyon1.fr

Abstract. HyperLeda (**Hyper-L**inked **E**xtragalactic **D**atabases and **A**rchives) is aimed to study the evolution of galaxies, their kinematics and stellar populations and the structure of Local Universe. HyperLeda is involved in catalogue and software production, data-mining and massive data processing. The products are serviced to the community through web mirrors. The development of HyperLeda is distributed between different sites and is based on the background experience of the LEDA and Hypercat databases. The HyperLeda project is focused both on the European ***iAstro*** colaboration and as a unique database for studies of the physics of the extragalactic objects.

1. INTRODUCTION

Most of the data from ground-based observatories, and virtually all data from observatories in space, are now carefully collected and preserved for posterity. The volume of data available in the archives is exploding exponentially. Modern ground-based telescopes like the VLT are able to produce around 10 Tb/year whereas the space missions typically produce 10-100 Tb. Besides the quantity, the quality of the data description also improves drastically. Most of these archives are at least partly accessible on-line, but the great diversity of user-interfaces and data management systems limit their use, and attempting to use information from two or more archives together can be exceedingly difficult.

Many people have realized that some form of integrated access is desirable, and that, if powerful data mining facilities were also provided, the scientific gains could be enormous. The name given to this vision is "The Virtual Observatory" (VO). It is worth emphasizing just a couple of positive factors for VO:

⋆ Moore's Law is on our side: computer power, memory size, and disc capacity still seem to be doubling every 18 months.

⋆ Astronomical institutions throughout the world seem extremely willing to collaborate with each other, and to make their services freely available.

Thus a number of collaborations have been formed in support of this aim, and among these is COST 283 or ***iAstro*** (`http://www.iAstro.org`, see Murtagh *et al.*, 2002) which was reported earlier at this meeting (Golev *et al.*, 2002). The HyperLeda project is supposed to play both an important role in ***iAstro*** collaboration and as a unique database for studies of the physics of the extragalactic objects.

2. Objectives of HyperLeda

The HyperLeda project is driven by two astronomical objectives (Prugniel *et al.*, 2002): the study of

- the distribution of galaxies in the Local Universe (distance scale, luminosity function, environment), and
- the evolution of the stellar populations in nearby galaxies.

The principal need for these projects is an access to multi-parametric whole sky samples with extended documentation of the biases.

HyperLeda is based on the background experience of two databases, available through the web: LEDA (see `http://leda.univ-lyon1.fr`), containing homogenized information for nearly three million galaxies, and HYPERCAT (`http://www-obs.univ-lyon1.fr/hypercat`).

The scientific goals are the study of the evolution of galaxies and their environments, their kinematics, stellar population, and nuclear activity, determination of distances and the structure of the Local Universe. The project is focused on the nearby universe, considering it as the reference to investigate the cosmic evolution. Evolutionary studies will be based both on the use of archived data and on the new observations that can be achieved within reasonable amount of telescope time (Prugniel *et al.*, 2001).

HyperLeda develops and maintains a set of tools related to data-mining, massive data processing, data gathering (mainly from published literature and catalogues) homogenization of information and its distribution through web. HyperLeda will allow the external user an access to high quality catalogues, and specialized pipeline to customize the parameterization. Web interfaces from several different sites (mirrors) provide the fastest access to anywhere. Besides the reference data, taken from the astronomical literature and data centers, HyperLeda will make it possible to extract the astronomical information from archives such as DENIS for example.

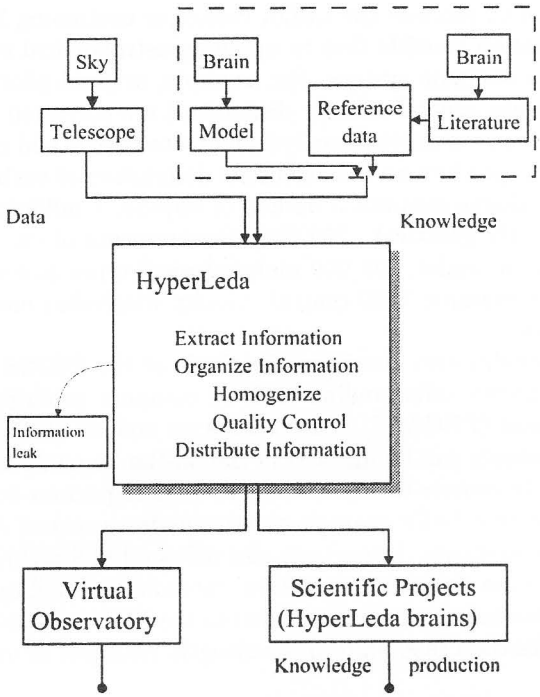

Fig. 1: Information flows in HyperLeda

3. HyperLeda features

HyperLeda implies a collaboration between CRAL Observatoire Astronomique de Lyon, Observatoire de Paris (GEPI), Astronomical Observatory of St. Kliment Okhridski University of Sofia and Sternberg Astronomical Institute at Moscow State University. Solutions proposed by HyperLeda consist in:

(1) Producing 'raw' parameters catalogues compiled from the literature.

(2) Homogenizing these parameters.

(3) Offering on-the-fly functionality to process the data.

(4) Distributing the data through the WEB.

Information flows in the HyperLeda project are shown in Fig. 1. For the different parameters of interest in the frame of our scientific objective we are collecting data from the literature. Each parameter, or group of parameters, is maintained independently by the astronomers contributing to the project. The literature is systematically searched and relevant measurements are converted into an uniform format (eg. by converting the units). These catalogues are automatically asynchronously gathered in the data-flow control center and are checked for consistency. In particular, designation of the galaxies is controlled and cross-identified.

The raw parameters, together with a parameterized description of the measurements in each dataset (series of measurements), are publicly distributed. The raw

catalogues are used to produce the LEDA catalogue containing homogenized parameters. Homogenization consists first in applying astronomical recipes to set all the measurements in a common system. For example, original photometry is converted into Johnson-Cousins, central velocity dispersions are corrected to a standard aperture, and so on. Then, a statistical analysis allows to rescale and combine the different datasets in order to produce an homogeneous description of each galaxy.

The LEDA catalogue contains 3 million of objects, 1 million of them are of confirmed nature (mostly galaxies). 250 000 measurements of cz, 3 million fluxes, diameters and position angles, 225 000 morphological types and several less frequent parameters, as for example 7200 central velocity dispersion measurements or 2000 kinematical profiles.

HyperLeda provides also access to the pixels of the DENIS survey and remote access to other surveys, offers online tools to compute evolutive synthetic spectra of stellar populations (PEGASE) and contains an archive of reference data in FITS format. These resources can be injected in the on-the fly analysis pipeline.

The possibility to process the data on the fly is an important feature of HyperLeda. One of the purposes may be for example to re-normalize a central velocity dispersion in a fiducial or metric aperture. HyperLeda also offers a FITS archive (yet in Hypercat) fed with reference data (images and spectra) intended for calibration, modelling and simulation. The processing pipeline attached to the FITS archive allows to customize the extraction of the data (e.g. shift in wavelength, resample or measure line strength indices).

For example, the pipeline editor command

http://astro.uni-sofia.bg/hypercat/fG.cgi?n=11&z=p&c=i&o=fa:LH_ELODIE/00081

will get as a result the science observation of HD019445 - extracted scan spectrum of exposure 3600 s. Archived data were flat-field corrected , wavelength resampled and flux calibrated above atmosphere.

In the future we will develop the possibility to customize the recipes of data homogenization (ie. give the user the possibility to define his own parameterization) and weighting of individual datasets. The main goal is to make HyperLeda services widely available and easily accessible (possibly) in the framework of some of the ongoing big VO projects.

References

Golev, V., Tsvetkov, M., Murtagh, F., Egret, D. *et al.* : 2002, *Publ. Astron. Obs. Belgrade*, this volume.

Murtagh, F. *et al.*: 2002, *Toward an International Virtual Observatory – Scientific Motivation, Roadmap for Development and Current Status*, ESO/ESA/NASA/NSF Astronomy Conference, June 10 - 14, 2002, Garching, Germany, in print.

Prugniel, Ph. *et al.*: 2002, *Toward an International Virtual Observatory – Scientific Motivation, Roadmap for Development and Current Status*, ESO/ESA/NASA/NSF Astronomy Conference, June 10 - 14, 2002, Garching, Germany, in print.

Prugniel, Ph. *et al.*: 2001, *Mining the Sky, eds. A.J. Banday, S.Zaroubi, & M.Bartelmann*, ESO Astrophysics Symposia, Berlin: Springer – Verlag.

Publ. Astron. Obs. Belgrade No. 73 (2002), 153 - 157 *Poster*

RADIAL VELOCITIES OF B-STARS TOWARDS THE GALACTIC ANTI-CENTER

Yu. GORANOVA, Ts. GEORGIEV, L. ILIEV, I. STATEVA, and N. TOMOV
Institute of Astronomy, Bulgarian Academy of Sciences
72 Tsarigradsko Shosse, 1784 Sofia, Bulgaria
E-mail goranova@astro.bas.bg

Abstract. Radial velocities have been determined for a sample of 22 stars of B2-B9 type situated towards the Galactic anti-center. The observations were carried out with the Coudé spectrograph of the 2m RCC telescope at Rozhen NAO in 2000-2001. This research is a part of an initial program aimed at studying the spiral structure of the Milky Way galaxy.

1. BACKGROUND

The spiral structure of distant galaxies can be traced by the distribution of young bright stars and emission line nebulae, the distribution of atomic and molecular gas, the spatial location of dust matter, as well as via pulsar radio emission. Unfortunately, the spiral pattern of our own Galaxy is much less obvious due to our obscured view from within the Galactic dusty disk.

The observed large-scale spiral features can in many cases be explained in frames of the density wave theory (Lin & Shu 1964) by regarding the arms as density perturbations in the galaxy disk. One of the main parameters in this theory is the arm gravitational potential, as far as it determines the strength and location of the density wave. In galactocentric polar coordinates (R, θ) the potential V_s of the main two-fold spiral at time t can be presented with

$$V_s(R,\theta,t) = A\cos[2\frac{\log(R/R_\odot)}{\tan(i)} - 2(\theta - \theta_0 - t\Omega_p)], \quad (1)$$

where Ω_p is the pattern angular speed, and θ_0 defines the phase at the solar radius $R_\odot$ at $t = 0$. The spiral is assumed to be logarithmic with pitch angle i, and amplitude A (Grosbøl 1997).

Spatial distribution of young Galactic OB-stars show clear evidence that they are in spiral arms (Drimmel et al. 1999), therefore their exact location can in principle be used to determine the parameters of the density wave. However the direct observations of density perturbations associated with the spiral arms are difficult due to a correlation between extinction and population effects in these regions (Grosbøl & Patsis 1998).

B-stars are relatively bright and that makes them ones of the most suitable optical tracers of the Milky Way spiral pattern. Late B5-B9 stars have well calibrated photometric properties hence their photometric distances can be derived accurately even in a field with a significant interstellar extinction. By means of spectroscopic observations their radial velocities can be derived and the velocity field can be constructed. Stars in the directions towards the Galactic center and anti-center are a special case. If their effective temperatures are determined from the photometry one can study the relation between radial velocity and age of stars as a function of the distance.

This paper is based on observations collected at the National Astronomical Observatory of Bulgaria. We present 24 CCD spectra of 22 B-stars located in an area of 10x10 square degrees around the direction to the Galactic anti-center. Radial velocities have been derived. The results are listed in Table 1, and the spectra obtained are plotted in Fig. 1.

2. OBSERVATIONS AND DATA REDUCTION

The observational program was carried out with the 2-m RRC telescope of Rozhen NAO during 13 nights from November 2000 to February 2001. The observations were obtained using a Coudé spectrograph equipped with a SITe 1024x1024 CCD. The dispersion was 8.3 Å mm^{-1}. The characteristics of the spectrograph are described in details in Kolev & Tomov (1996). The CCD-spectra were obtained in the spectral region λ 4810–5030 Å. A Th-Ar lamp was used for the wavelength calibration. A total of 24 spectra with exposures of 15 min each were obtained. The mean S/N ratio was about 100. Two reference stars were observed for the radial velocity zero-point determination.

All data reductions (bias subtraction, flat-field correction, wavelength calibration, continuum normalization, Earth motion corrections), as well as the line position determination were done with the ESO-MIDAS system.

As a reference for the line identification synthetic spectra were used. The synthetic spectrum for each of the studied stars was generated under the SYNTH-code (Piskunov 1992). The adopted atmospheric parameters were derived from the published Strömgren *uvbyβ* photometry (Hauck & Mermilliod 1998). The laboratory wavelengths were taken from the VALD-database (Piskunov et al. 1995).

In order to measure the line position each identified spectral feature was fitted with a Gaussian profile.

3. DISCUSSION OF THE RESULTS

Radial velocities have been determined for a sample of 22 B2-B9 stars by using the classical method of individual measurements of spectral lines. The heliocentric corrections were applied. The mean redial velocities were derived for Fe II, S II, Cr II lines. The zero-point was determined from IAU standards for each night, when the reference stars were observed.

The main characteristics and results for the program stars are summarized in Table 1. The stars are presented with their HD-identifiers. Apparent magnitudes m_V, spectral types, as well as the remarks about multiplicity and peculiarity are taken from the SIMBAD database. The effective temperature $T_{\rm eff}$ and the surface

Table 1: Characteristics and results for the program stars.

Star	m_V [mag]	Sp. type	$T_{\rm eff}$ [°K]	$\log g$	Comments	V_r [km/s]	σ	n
HD 34761	8.5	B8	9600	4.0	-	-18.8	3.6	4
HD 34762	6.3	B9IV	16000	3.3	SB	25.7	3.0	3
HD 35132	8.3	B9	-	-	EB, β Lyr-type	30.5	2.4	3
HD 35239	5.9	B9III	11000	3.2	-	-9.3	-	1
HD 35600	5.7	B9Ib	11000	1.9	-	0.2	1.0	5
HD 37098	5.6	B9IV-V	11000	4.5	double/multiple	37.7	7.8	5
						39.3	13.3	9
HD 37367	5.9	B2IV-V	9000	4.3	variable	23.1	4.5	5
HD 37519	5.9	B9.5III-IV	9000	3.6	p	-6.6	13.7	3
						-8.8	5.8	3
HD 38009	8.1	B9	10000	4.0	-	-28.5	2.0	4
HD 38062	8.5	B9	-	-	-	-6.1	11.5	4
HD 38306	7.7	B9	-	-	double star	16.7	-	1
HD 38450	8.0	B9	10000	3.8	-	7.4	6.4	4
HD 38909	8.3	B3II-III	11000	4.3	-	28.1	2.4	4
HD 39939	8.1	B9	-	-	-	-23.1	13.5	4
HD 40163	8.2	B9	-	-	double/multiple	-57.8	9.8	3
HD 40589	6.0	B9Iab	12000	1.8	double system	14.1	1.1	6
HD 40996	7.3	B9	9000	3.5	-	21.1	3.5	4
HD 41251	8.5	B9	-	-	variable	-6.3	1.2	6
HD 41269	6.1	B9	11000	3.5	-	8.8	5.2	8
HD 41600	7.0	B9	-	-	double/multiple	-31.5	2.9	5
HD 41638	7.8	B9	-	-	-	4.2	3.7	5
HD 41639	8.4	B9	-	-	-	27.2	-	1

gravity $\log g$, used for the synthetic spectra generation, are given in the fourth and fifth columns. The last three columns present the determined radial velocities V_r with their rms σ and the number n of the lines used for the radial velocities measurement. Obtained spectra are plotted in Fig. 1.

Main difficulties in determining the B-stars radial velocities come from the small number of the prominent lines. The obtained precision depends on the projected rotational velocity $v \sin i$ and the number of the lines measured. Inaccuracies came generally from the binaries/multiples and the possible peculiarities of the star.

Except for HD 37098 and HD 37519 the observations were performed only once. The results for these two stars show an accuracy sufficient for our purposes. An improvement of the precision can be obtained by using a cross-correlation method with synthetic spectra (see eg. Grenier et al. 1999).

Here we report the preliminary results for radial velocities of 22 B-stars situated in the direction to the Galactic anti-center. A total of 24 stellar spectra were examined. The observations were collected in a spectral region around H_β. In order to improve the statistics of the mean radial velocity obtained, we intend to extend our studies in other spectral regions. The present work is a part of an initial program aimed at studying the spiral structure of our Galaxy.

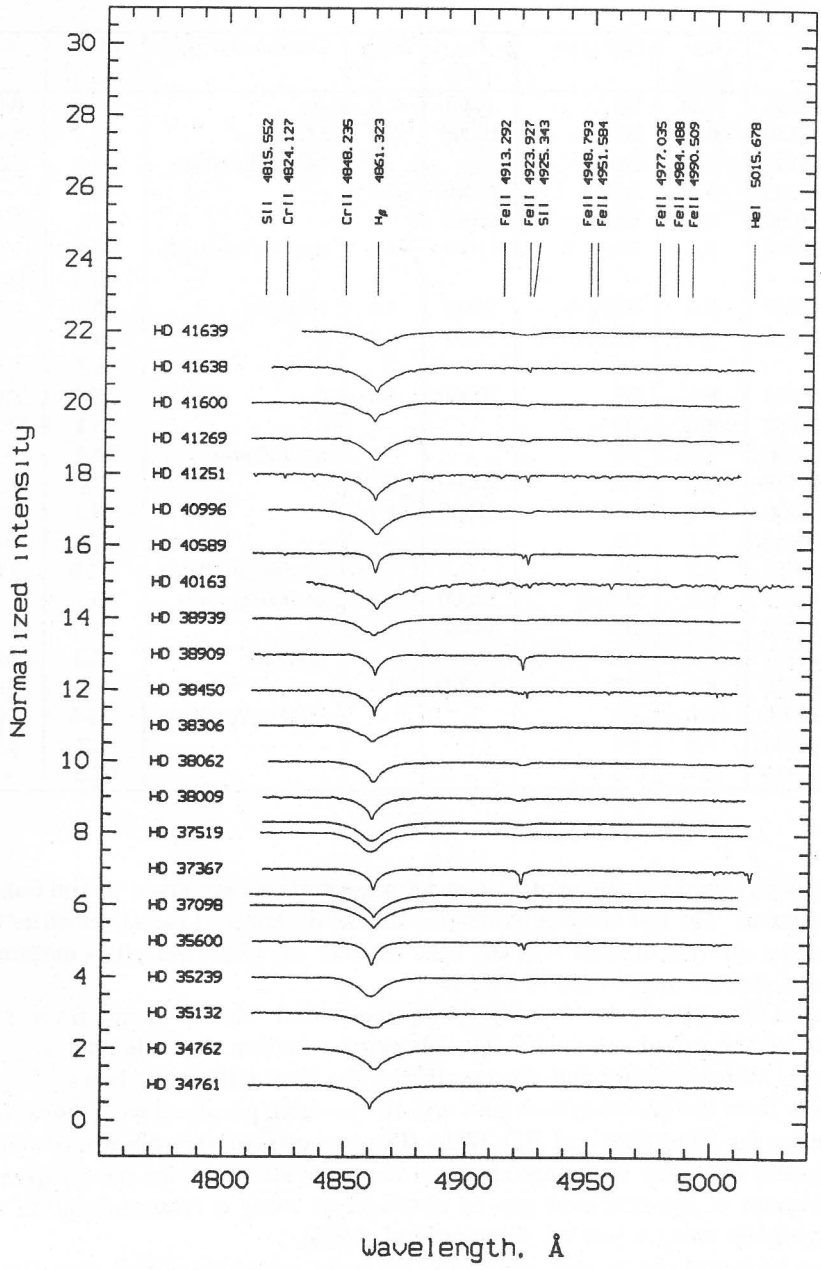

Fig. 1: Plot of the normalized spectra of the studied 22 B2-B9 stars. The identified spectral features of the H_β-line, as well as of the lines of Fe II, S II and Cr II ions are shown. The spectra are ordered with respect to the increasing of their HD-identifiers.

Acknowledgements. This research was made by using the SIMBAD database operated at CDS Strasbourg, France and the VALD database accessible via VALD-EMS Vienna, Austria.

References

Drimmel, R., Smart, R. L., and Lattanzi, M. G. : 1999, *Modern Astromrtry and Astrodynamics, eds. R. Dvorac, H. F. Haupt, K. Wodnar*, Austrian Acad. of Sci., Vienna.

Grenier, S., Burnage, R., Faraggiana, R., Gerbaldi, M., Delmas, F., Gomez, A. E., Sabas, V., and Sharif, L. : 1999, *Astron. Astrophys. Suppl.*, **135**, 503.

Grosbøl, P.J. : 1997, *Wide Field Spectroscopy, eds. E. Kontizas et al.*, ESO A4-8, **18**, 177.

Grosbøl, P. J., Patsis, P. A. : 1998, *Astron. Astrophys.*, **306**, 840.

Hauck, B., Mermilliod, M. : 1998, *Astron. Astrophys. Suppl.*, **129**, 431.

Kolev, D., Tomov, T. : 1996, in *Proc. of 100th Anniversary of the Sofia Univ. Obs., eds. Maslev K., Kurtev R.*, Sofia, Bulgaria, p. 65.

Lin, C. C., Shu, F. H. : 1964, *Astrophys. J.*, **140**, 646.

Piskunov, N. : 1992, in *Stellar Magnetism, eds. Yu. Glagolevskij and I. Romanyuk*, Nauka, St. Petersburg.

Piskunov, N., Kupka, F., Ryabchikova, T., Weiss, W. and Jeffrey, C. : 1995, *Astron. Astrophys. Suppl.*, **112**, 525.

Vallée, J. P. : 1995, *Astron. J.*, **454**, 119.

Publ. Astron. Obs. Belgrade No. 73 (2002), 159 - 162 *Poster*

ESTIMATED NUMBER OF FIELD STARS TOWARDS THE LOCAL GROUP GALAXY IC10: MODELS AND OBSERVATIONS

R. G. KURTEV

Department of Astronomy, Sofia University, James Bourchier Ave. 5, BG-1164 Sofia, Bulgaria
E-mail kurtev@phys.uni-sofia.bg

Abstract. It is very important to know the distribution in magnitude and color of the field stars from the Galaxy towards the different extragalactic objects. In this work are compared real photometrical data with the model predictions. The observational $B-V, V$ color-magnitude diagram for the area of 5.6×5.6 arcmin situated 30 arcmin north of the center of the galaxy IC 10 is compared with synthetic color-magnitude diagrams based on the model of the Milky Way galaxy (Robin & Creze 1986). Model with appropriated reddening $A_V = 1.2$ mag/kpc describes in the best way the observations. Despite the relatively good result there is about 20% more model stars. This is a significant difference when we talk about the luminosity function or IMF for instance. In these cases we have to get "a comparison field" near to the object of research.

1. INTRODUCTION

It is very important to know the distribution in magnitude and color of the field stars from our Galaxy towards the star clusters or the resolved Local Group Galaxies with low galactic latitudes. It is obviously necessary to check the level of field star contamination before discussing the detailed structure of the color-magnitude diagrams and the stellar content of the stellar systems. The purpose of this work is to compare real data ("CCD comparison field") on the distribution in color and in apparent magnitude with the model predictions (Robin & Creze 1986). The chosen area is near to the Local Group Galaxy IC 10 (30 arcmin north of the galaxy center) and situated very close to the galactic plane ($b = -3.34°$, $l = 118.97°$) and the foreground contamination is significant. This model can be used for simulations of the galactic stellar populations in any directions in photometric bands from U to K as well as radial velocity and proper motion distributions. It may help for preparing observations, for evaluating the galactic stellar contamination in extragalactic studies or in star cluster fields.

2. OBSERVATIONS AND DATA REDUCTION

A set of BV frames of the area around the Local Group Galaxy IC 10 was obtained with CCD Photometrics camera attached to the 2-m Ritchey-Chretien telescope of the

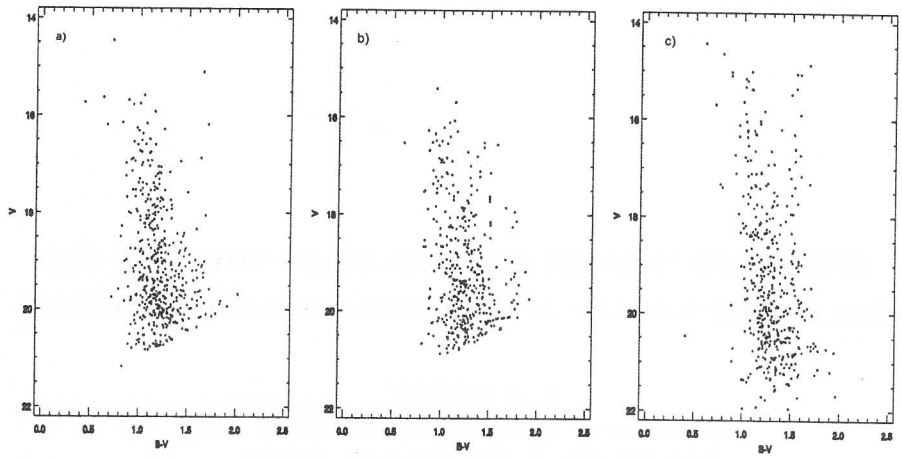

Fig. 1: a) Synthetic $(B-V, V)$ color-magnitude diagram obtained for the Model 1 ($A_V = 1.1$mag/kpc; b) for the Model 2 ($A_V = 1.2$mag/kpc.; c) Observed $(B-V, V)$ color-magnitude diagram obtained for the area around the galaxy IC 10. Only stars with photometric errors larger than 0.15 mag in both filters are plotted.

Bulgarian National Astronomical Observatory "Rozhen" on 15/16 September 1999. The exposure time of the images was 900 sec. The observing area was $5.6' \times 5.6'$. The seeing during these observations was excellent for Rozhen: $1.2''$ with stable and very good photometric conditions. The IRAF data reduction package was used to carry out the basic image reductions and the flat field correction. The Landolt (1992) standards PG0231 and PG2213 were taken before and after the observations. The transformation equations to the standard Johnson BV system are:

$$\begin{aligned} V &= 1.013v + 0.139(B-V) - 0.345X - 1.866 \\ B-V &= 1.028(b-v) - 0.203X - 0.308 \end{aligned}$$

where b, v are instrumental magnitudes, B, V are the standard ones and X is the airmass.

The stellar photometry of the frames was performed with the point-spread function fitting routine ALLSTAR available in DAOPHOT (Stetson 1993). The final photometry list contains 429 stars. The zero-point errors of the transformations to the standard BV system are 0.04 mag.

3. RESULTS

In the model predictions a mean diffuse extinction of 0.7 mag/kpc in V band is recommended for intermediate and high latitude fields. It may be modified. Because of the very low galactic latitude of the observed field this default value does not lead to a reliable result. Five different values of A_V have been used as model input parameters – $0.8, 0.9, 1.0, 1.1$ and 1.2 mag/kpc. The best coincidence of the model and the observations is at $A_V = 1.1$ mag/kpc and $A_V = 1.2$ mag/kpc. We will

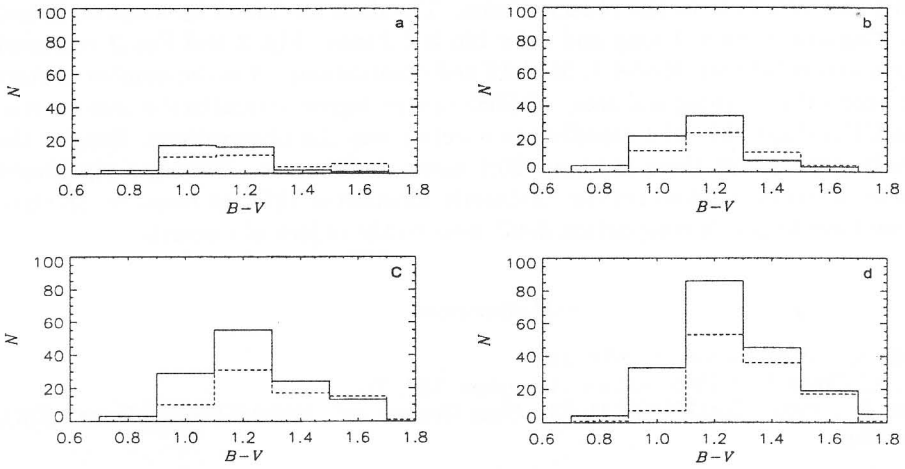

Fig. 2: Comparison between Model 1 (thick line) and observations (dashed line) within intervals by V: a) 16.5 – 17.5; b) 17.5 – 18.5; c) 18.5 – 19.5; d) 19.5 – 20.5

call the models with these extinctions Model 1 and Model 2 respectively. The output star list of Model 1 contains 480 stars within the intervals $14.0 < V < 21.5$ and $0.3 < B - V < 2.0$. In Model 2 the stars are 396 within $15.0 < V < 21.0$ and $0.5 < B - V < 2.0$.

Color-magnitude diagram (CMD) of Model 1 is given in Fig. 1a, CMD of Model 2 in Fig. 1b and observed CMD in Fig. 1c.

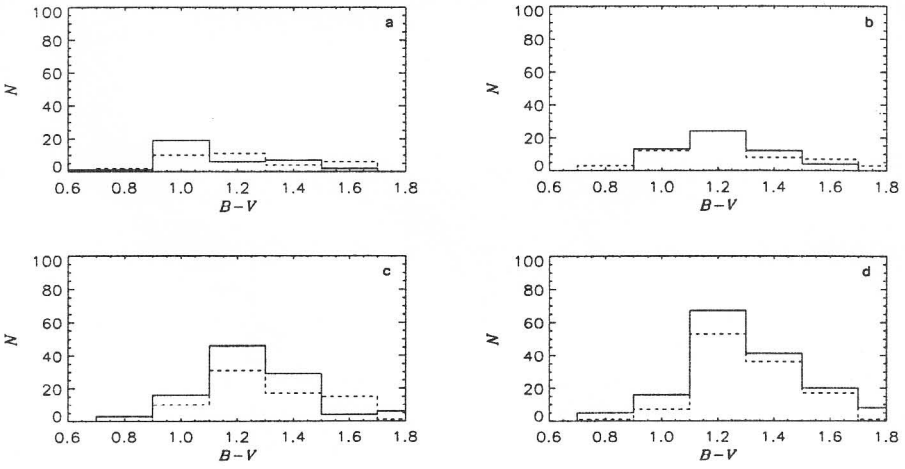

Fig. 3: Comparison between Model 2 (thick line) and observations (dashed line) within intervals by V: a) 16.5 – 17.5; b) 17.5 – 18.5; c) 18.5 – 19.5; d) 19.5 – 20.5

Star counts are made in the intervals $16.5 < V < 20.5$ and $0.6 < B - V < 1.8$ because most of the stars are there. The sample is to be complete to, at least, $V = 21.0$. Within these new boundaries there are 423 stars in Model 1, 353 stars in

Model 2 and 276 stars in the observed area. The data are bined by magnitude and color. Magnitude bin is 1 mag and color bin is 0.2 mag. Fig. 2 and Fig. 3 represent the comparison between Model 1, Model 2 and observations. N is the number of stars within interval $V = 1$mag and area of 0.0087 square degrees (equal to the area covered by the CCD chip). Model 2 describes in a better way the observations. Despite the relatively good result there is about 20% more model stars. This is a significant difference when we want to get the luminosity function or IMF for instance. In these cases we have to get "a comparison field" near to the object of research.

References

Landolt, A. : 1992, *Astron. J.*, **104**, 340.
Robin, A., Crézé, M. : 1986, *Astron. Astrophys.* **157**, 71.
Stetson, P. : 1993, "DAOPHOT II: The Next Generation", MIDAS Users' Manual, ESO, Garching.

Publ. Astron. Obs. Belgrade No. 73 (2002), 163 - 166 *Poster*

UB STELLAR PHOTOMETRY AROUND THE ASSOCIATION OB 81 IN M 31: NEW OB ASSOCIATIONS

R. G. KURTEV

Department of Astronomy, Sofia University, James Bourchier Ave. 5, BG - 1164 Sofia, Bulgaria
E-mail kurtev@phys.uni-sofia.bg

Abstract. We present *UB* stellar photometry in a field centered on the stellar complex OB81 in the Southern part of the Andromeda galaxy. We investigate the stellar content of this area. The automatized search for OB associations was carried out using the friend-of-friends algorithm of Battinelli (1991). The van den Bergh's "association" OB 81 practically covers the substantial part of the spiral arm. The "new" associations have smaller sizes and look like bright cores within this "association". The mean size of 89 ± 11 pc is comparable with the mean size of the OB associations in LMC – 60pc, SMC – 70 pc and M33 – 60 pc, confirming the idea that the size of the associations does not depend on the morphological type of the galaxy.

1. Introduction

The stellar content investigations of the Local Group galaxies allow us to study in fine details the star formation history of these systems. They also provide important verification information for the stellar evolution theory. The Andromeda galaxy (M 31) is the closest spiral galaxy similar in size and structure to our galaxy – the Milky Way. It is therefore very important to study and compare the stellar populations in both galaxies. There are some large-scale CCD surveys of M 31 (Magnier et al. 1993; Haiman et al. 1994 and others) investigating separate small areas of this galaxy (Massey, Armandroff & Conti 1986; Hunter et al. 1996; Magnier et al. 1997; Veltchev et al. 1999). All of them are in *UBV* passbands. Large-scale *U* and *B* plates obtained with the 2-m Ritchey-Chretien telescope of the Rozhen Observatory (Bulgaria) were searched by Efremov et al. (1987) for new resolved star groups and for independent delineation of the boundaries of the known groups in M 31. Two hundred and ten groups were detected as real O-associations with the mean diameter of 80 pc. The main goal of this study is to outline the new OB associations in an approximately small area covering the association OB81 in spiral arm S4 using the objective method of Battinelli (1991).

2. Observations and data reduction

A set of UB frames of the area in the spiral arm S4 of Andromeda galaxy was obtained with CCD Photometrics camera attached to the 2-m Ritchey-Chretien telescope of the Bulgarian National Astronomical Observatory "Rozhen" on 6/7 August 2000. The exposure time of the images was 900 sec. The observing area was $5.6' \times 5.6'$ and covered the area centered on the association OB 81. The seeing during these observations was rather good than excellent: $1.5-1.8''$, but with stable and very good photometric conditions. The IRAF data reduction package was used to carry out the basic image reductions and the flat field correction. The Landolt (1992) standards were taken before and after the observations. The transformation equations to the standard Johnson UB system are:

$$\begin{aligned} B &= 1.012b + 0.032(U-B) + 0.023(U-B)^2 - 0.056X - 2.556 \\ U-B &= 1.156(u-b) - 0.021(u-b)^2 - 0.054X - 3.126 \end{aligned}$$

where b, u are instrumental magnitudes, UB are standard ones and X is the airmass.

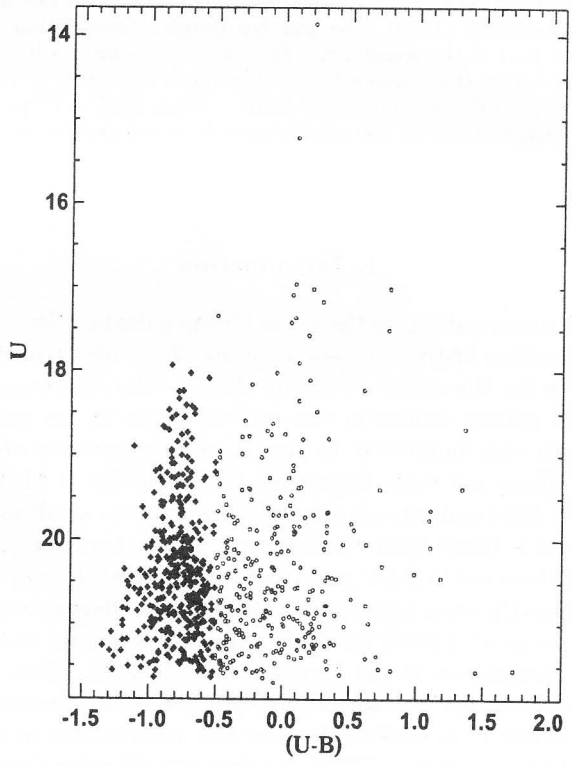

Fig. 1: $(U-B, U)$ color-magnitude diagram obtained for the area around the association OB 81 in M 31. Only stars with photometric errors larger than 0.15 in all filters are plotted.

The stellar photometry of the frames was performed with the point-spread function fitting routine ALLSTAR available in DAOPHOT (Stetson 1993). Complete details of the data reduction and analysis may be found in Georgiev et al. (1999). The stars with values of DAOPHOT CHI > 2 and those with formal errors from the PSF fitting greater than 0.15 mag are rejected so the final photometry list contains 687 stars. The zero-point errors of the transformations to the standard UB system are 0.04 mag.

3. Results

Figure 1 represents the $(U-B), U$ color-magnitude diagram (CMD). To construct this CMD only the stars with photometric errors not larger than 0.15 in both filters have been selected. The mean feature is distinctive plume of luminous blue stars in the Andromeda galaxy (black crosses) mixed with the foreground stars of the Milky way mostly with $U - B > 0$.

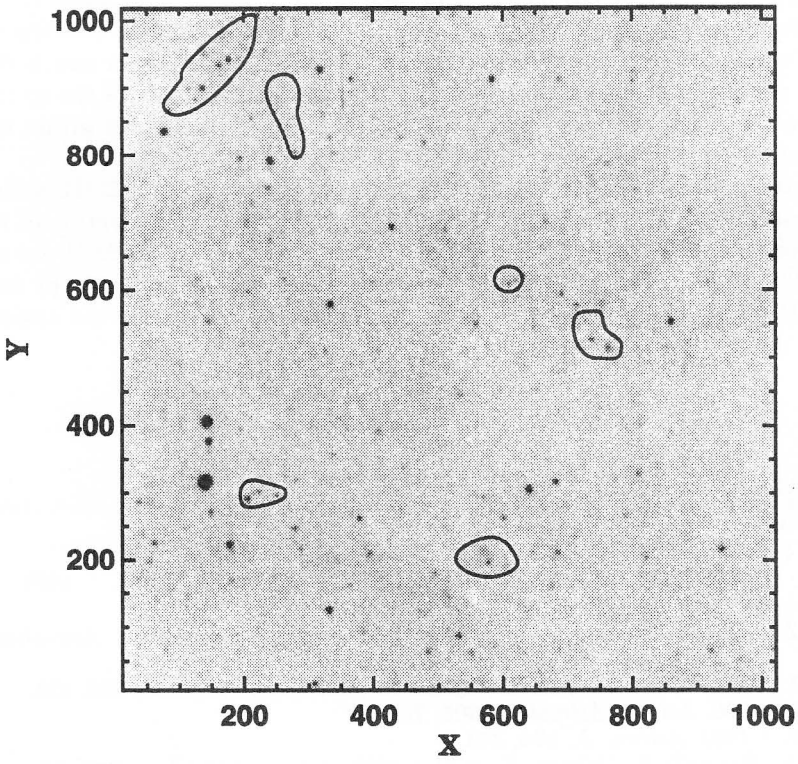

Fig. 2: Map of the associations in observational area outlined by Battinelli (1991) algorithm.

The automatized search for OB associations was carried out using the method of Battinelli (1991) (so called friend-of-friends algorithm). The bright blue stars from the main sequence in M 31 were selected by strong photometric criterion by magnitude $(18 < U < 22)$ and color $((U - B) < -0.5)$. In the most cases friend-of-friends algorithm selects the minimum number of 4 OB stars in some clump in order to have

Table 1: Mean sizes and bright OB members in the new associations

Name	X	Y	size(pc)	bright OB members
A1	740	530	87	6
A2	580	192	83	8
A3	256	854	91	9
A4	224	292	76	5
A5	153	937	134	15
A6	610	604	65	5

a "real" association. We put in our case the same minimum number of stars.

The map of the association boundaries resulting from the automatized search is shown in Fig. 2. The X, Y coordinates in pixels, the mean size of the associations in pc and number of bright OB members in each of them are given in Table 1.

The friend-of-friends algorithm selects 6 associations with sizes between 65 and 137 pc (with accepted true distance modulus of 24.2). The mean size is 89 ± 11 pc. The association OB 81 practically covers the substantial part of the spiral arm. The "new" associations have smaller sizes and look like bright cores within van den Bergh's associations.

Comparing M 31 with the Magellanic Clouds, M 33 and NGC 6822 (Bresolin et al. 1998, Ivanov 1996, Vetchev et al. 1999) we can see that the distribution of the OB associations is similar with peak between 40 and 80 pc. Those in M 31 are slightly larger – 90pc. The mean size is comparable with LMC – 60pc, SMC – 70 pc and M33 – 60 pc (Bresolin et al. 1998), confirming the idea that the size of the associations does not depend on the morphological type of the galaxy.

References

Battinelli, P. : 1991, *Astron. Astrophys.*, **244**, 69.

Bresolin, F., Kennicutt, Jr., Ferrareze, L., Gibson, B., Graham, J., et al. : 1998, *Astron. J.*, **116**, 119.

Efremov, I., Ivanov, G., Nikolov, N. : 1987, *Astrophys. Space Sci.*, **135**, 119.

Georgiev, L., Borissova, J., Rosado, M., Kurtev, R., Ivanov, G., et al. : 1999, *Astron. Astrophys. Suppl. Series*, **134**, 21.

Haiman, Z., Magnier, E., Battinelli, P., Lewin, W., et al. : 1994, *Astron. Astrophys.*, **290**, 371.

Hunter, D., Baum, W., O'Neil, Jr., E., Lynds, R. : 1996, *Astrophys. J.*, **468**, 633.

Ivanov, G. : 1996, *Astron. Astrophys.*, **305**, 708.

Landolt, A. : 1992, *Astron. J.*, **104**, 340.

Magnier, E., Batinelli, P., Haiman, Z., et al. : 1993, *Astron. Astrophys.*, **278**, 36.

Magnier, E., Hodge, P., Battinelli, P., Lewin, W., Van Paradijs, J. : 1997, *Mon. Not. Roy. Astron. Soc.*, **292**, 490.

Massey, P., Armandroff, T., Conti, P. : 1986, *Astron. J.*, **92**, 1305.

Stetson, P. : 1993, "DAOPHOT II: The Next Generation", MIDAS Users' Manual, ESO, Garching.

Veltchev, T., Nedialkov, P., Ivanov, G. : 1999, *Rev. Mex. Astron. Astrophys.*, **35**, 13.

Publ. Astron. Obs. Belgrade No. 73 (2002), 167 - 172 *Poster*

ION CHARACTERISTICS TO THE 667.82 nm He I SPECTRAL LINE SHAPE

V. MILOSAVLJEVIĆ AND S. DJENIŽE

Faculty of Physics, University of Belgrade, P.O.B. 368, Belgrade, Serbia, Yugoslavia

Abstract. Ion characteristics of the 667.82 nm He I spectral line profiles have been investigated at electron densities between 4.4×10^{22} and 8.2×10^{22} m^{-3} and electron temperatures between 18 000 and 33 000 K in plasmas created in five various discharge conditions using a linear, low-pressure, pulsed arc as an optically thin plasma source operated in a helium-nitrogen-oxygen gas mixture. On the basis of the observed asymmetry of the line profiles we have obtained their ion broadening parameters (A) caused by influence of the ion microfield on the line broadening mechanism and also the influence of the ion dynamic effect (D) on the line shape. Our A and D parameters represent the first data obtained experimentally by the use of the line profile deconvolution procedure. We have found stronger influence of the ion contribution to this He i line profile than the semiclassical theoretical approximation provides.

1. Introduction

Helium atoms and ions are present in many kinds of cosmic light sources and their radiation is very useful for astrophysical plasma diagnostical purposes (Griem 1974, 1997). In plasmas with electron densities (N) higher than 10^{21} m^{-3}, where the Stark effect begins to play an important role for the He I spectral lines broadening, knowledge of the Stark broadening characteristics is necessary. A significant number of theoretical and experimental studies are devoted to the He I Stark FWHM (full-width at half intensity maximum, W) investigations (Lesage & Fuhr 1999, and references therein). The aim of this work is to present measured Stark broadening parameters of the 667.82 nm ($2p\ ^1P^0_1$ - $3d\ ^1D_2$ transition) neutral helium (He I) spectral line at (18 000 - 33 000) K electron temperatures (T) and at electron densities of $(4.4 - 8.2)\times10^{22} m^{-3}$. Using a deconvolution procedure described by Milosavljević & Poparić (2001) we have obtained, for the first time, on the basis of the observed line profile asymmetry, the ion contribution to the line shape from the quasistatic ion (parameter A) and ion dynamic effect (coefficient D) (Griem 1974, Barnard et al. 1974, Bassalo et al. 1982) and, also, the separate electron (W_e) and ion (W_i) contributions to the total Stark width (W_t). As a plasma source we have used a linear, low-pressure, pulsed arc operated in five various discharge conditions. Our measured W_t, W_e, W_i and A values have been compared to all available theoretical and experimental data.

2. Experiment

The modified version of the linear low pressure pulsed arc (Djeniže et al. 1998, 2002) has been used as a plasma source. The working gas was helium - nitrogen - oxygen mixture (90% He + 8% N_2 + 2% O_2). The tube geometry used and the corresponding discharge conditions are presented in Table 1 in Milosavljević and Djeniže (this proceedings).

Spectroscopic observation of spectral lines was made end-on along the axis of the discharge tube described in details in Djeniže (2002).

The line profiles were recorded by a step-by-step technique using a photomultiplier (EMI 9789 QB and EMI 9659B) and a grating spectrograph (Zeiss PGS-2, reciprocal linear dispersion 0.73 nm/mm in the first order) system. The instrumental FWHM of 8 pm was obtained by using narrow spectral lines emitted by the hollow cathode discharge.

The plasma reproducibility was monitored by He I lines radiation and, also, by the discharge current using the Rogowski coil signal (it was found to be within ±5%). Using the double plasma length method, described in Milosavljević (2001), an absence of self-absorption was found in the case of the investigated line profiles.

The plasma parameters were determined using standard diagnostic methods. Thus, the electron temperature was determined from the ratios of the relative line intensities of four N III spectral lines (409.74 nm, 410.34 nm, 463.42 nm and 464.06 nm) to the 463.05 nm N II spectral line with an estimated error of ±10%, assuming the existence of LTE (Griem 1974). All the necessary atomic data were taken from NIST (2002) and Glenzer et al. (1994). The electron density decay was measured using a well-known single wavelength He-Ne laser interferometer technique (with 1.5 mm laser beam diameter) for the 632.8 nm transition with an estimated error of ±9%. The electron densities and temperatures, obtained at the moment when the line profiles were analyzed, are presented in Table 1 in Milosavljević and Djeniže (this proceedings).

3. Numerical procedure for deconvolution

The proposed function for various line shapes, Eq. (1) is of the integral form and includes several parameters. Some of these parameters can be determined in separate experiments, but not all of them. Furthermore, it is impossible to find an analytical solution for the integrals and methods of numerical integration should be applied. This procedure, combined with the simultaneous fitting of several free parameters, requires a number of computer-supported mathematical techniques.

$$K(\lambda) = K_o + K_{\max} \int_{-\infty}^{\infty} exp(-t^2) \cdot \left[\int_0^{\infty} \frac{H_R(\beta)}{1 + \left(2\frac{\lambda - \lambda_o - \frac{W_G}{2\sqrt{\ln 2}} \cdot t}{W_e} - \alpha \cdot \beta^2\right)^2} \cdot d\beta \right] \cdot dt. \quad (1)$$

Here K_o is the baseline (offset) and K_{max} is the maximum of intensity (intensity for $\lambda=\lambda_o$) (Milosavljević and Poparić 2001). $H_R(\beta)$ is an electric microfield strength distribution function of normalized field strength $\beta=F/F_o$, where F_o is the Holtsmark field strength. A ($\alpha=A^{4/3}$) is the static ion broadening parameter as a measure of the relative importance of ion and electron broadenings. R is the ratio of the mean

Table 1: Line Broadening characteristics of the He I 667.82 nm spectral line. Measured: total Stark FWHM (W_t^{exp} in pm within ±12% accuracy), electron Stark width (W_e^{exp} in pm within ±12% accuracy), ion Stark width (W_i^{exp} in pm within ±12% accuracy), static ion broadening parameter (A^{exp}, dimensionless within ±15% accuracy) and ion dynamic coefficient (D^{exp}, dimensionless within ±20% accuracy) at a given electron temperature (T in 10^3 K) and electron density (N in $10^{22}m^{-3}$). Ref presents the values given in this work (Tw) and those used from other authors: K, (Kelleher 1981); P, (Pérez et al. 1991); M, (Mijatović et al. 1995); Ga, (Gauthier et al. 1981); VK, (Vujičić and Kobilarov 1988). The index G, BCW and DSB denote theoretical data taken from Griem (1974), Bassalo et al. (1982) and Dimitrijević and Sahal-Bréchot (1990), respectively at a given T and N.

T	N	W_t^{exp}	W_e^{exp}	W_i^{exp}	A^{exp}	D^{exp}	Ref.	W_e^G	W_e^{BCW}	W_e^{DSB}	W_i^{DSB}	A^G	A^{BCW}
33.0	6.1	481	298	183	0.459	1.18	Tw	397	345	358	170	0.282	0.309
31.5	8.2	628	370	258	0.498	1.12	Tw	533	467	502	226	0.300	0.328
30.0	6.7	512	315	197	0.474	1.17	Tw	439	389	402	181	0.282	0.306
28.0	4.4	337	216	121	0.420	1.27	Tw	290	257	266	117	0.252	0.265
18.0	5.0	361	240	121	0.413	1.26	Tw	358	323	323	124	0.249	0.271
20.9	1.03	98			0.171	1.74	K						
30.1	3.2	231					P						
19.3	0.25	22					M						
20.0	10.0	960					Ga						
26.0	7.1	620					VK						

distance between the ions to the Debye radius, i.e. the Debye shielding parameter and W_e is the width (FWHM) of the $j_{A,R}$ profile (Griem 1974).

For the purpose of the deconvolution iteration process we need to know the value of K function (1) as a function of λ for every group of parameters (K_{max}, λ_o, W_e, W_G, R, A). The function $K(\lambda)$ is in integral form and we have to solve a triple integral in each step of the iteration process of varying the above group of parameters. The first integral in the K function is the microfield strength distribution function, $H_R(\beta)$, the second one is the $j_{A,R}(\lambda)$ function and the third is the convolution integral of a Gaussian with a plasma broadened spectral line profile $j_{A,R}(\lambda)$ (denoted by $K(\lambda)$ in Eq. (1)). None of these integrals has an analytic solution and they must be solved using numerical integration (Milosavljević and Poparić 2001, Milosavljević 2001).

After numerical integration the fitting procedure itself can be started. For Eq. (1), the fitting procedure will give the values for W_G, W_e, λ_o, R, A and K_{max}.

This sophisticated deconvolution method, which allows the direct determining of all six parameters by fitting theoretical K-profile (1), to experimental data, requires a sufficient number of experimental points per line, and small statistical errors.

4. Results and discussion

The plasma-broadening parameters (W_t, W_e, W_i, A, D) of the recorded line profiles at measured N and T values obtained by our deconvolution procedure are presented in Table 1 together with the results of other authors. Various theoretical (G, BCW, DSB) predictions of the W_e, W_i, and A are also given. For the normalization of the A^G and A^{BCW} values to our electron density the $N^{1/4}$ numerical factor (Griem 1974) was used.

In order to make the comparison between measured (W_t^{exp}) and calculated (W_t^{th})

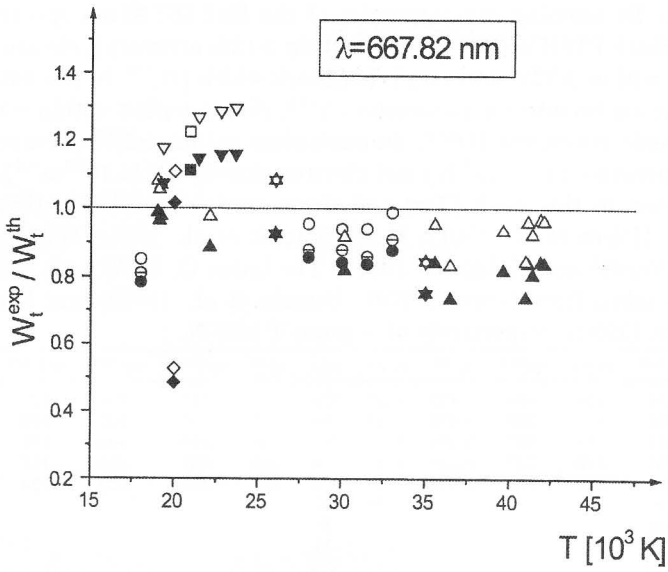

Fig. 1: Ratios of the experimental total Stark FWHM (W_t^{exp}) to the various theoretical (W_t^{th}) predictions vs. electron temperature for λ= 667.82 nm. ○, ◇, ▽, △, □ and ✡ represent our experimental data and those from Gauthier et al. (1981), Mijatović et al. (1995), Pérez et al. (1991), Kelleher (1981), and Vujičić and Kobilarov (1988), respectively. Filled, empty and half divided symbols represent the ratios related to the theories taken from Griem (1974), Bassalo et al. (1982) and Dimitrijević and Sahal–Bréchot (1990), respectively.

total (electron + ion) width values easier, the dependence of the ratio W_t^{exp}/W_t^{th} on the electron temperature is presented graphically in Fig. 1 for the researched line.

The W_t^G (Griem 1974) and W_t^{BCW} (Bassalo et al. 1982) values are calculated using Eq. (226) from Griem (1974) with the W_e and A values predicted by the G (Griem 1974) and BCW (Bassalo et al. 1982) theoretical approaches, respectively. The W_t^{exp}/W_t^{th} ratios related to the Dimitrijević and Sahal–Bréchot (1990) data have been calculated only for our experimental values. Namely, for the W_i^{DSB} calculations it is necessary to know the helium ion concentration connected to the plasma composition. We have performed this for our discharge conditions only.

It turns out that our W_e^{exp} and W_i^{exp} are the first separate experimental electron and ion Stark width results obtained by using our deconvolution procedure (Milosavljević and Poparić 2001). Our W_e^{exp} results are smaller than the G approximation for all the investigated lines. The two approximations (BCW and DSB), in the case of the 667.82 nm line, provide smaller W_e values than the G approximation, but they are also higher than ours. It pointed out that the W_e values calculated by Freudenstein and Cooper (1978) and Dimitrijević and Konjević (1986), for the 667.82 nm line, exceed all other W_e data presented in Table 1.

Inspecting Fig. 1 one can conclude that the Griem (1974) W_t values lie above all experimental and theoretical data except the results from experiments reported by Mijatović et al. (1995) and Kelleher (1981). This is clear at higher electron temperatures (see Fig. 1). Theoretical W_t values presented by Bassalo et al. (1982) lie about 10% - 30% below Griem's values. The W_t values (W_e + W_i) presented by Dimitrijević and Sahal-Bréchot (1990) agree with ours (W_t^{exp}) to within 3% – 18%.

We have found a clear contribution of the ion influence to the line broadening due to the quasistatic ion effect expressed with the ion broadening parameter (A). Our A^{exp} values are the first data obtained directly by the use of the line deconvolution procedure. They are higher than what the G and BCW approaches yield by about 40% and 34%, respectively. Furthermore, we have found that the ion dynamic effect, expressed as the D coefficient, multiplies the quasistatic ion contribution by about 1.2 for the 667.82 nm line. It should be pointed out that we have found good agreement between our W_i^{exp}/W_t^{exp} and theoretical W_i^{DSB}/W_t^{DSB} (Dimitrijević and Sahal-Bréchot 1990) ratio values. These are 37.5% (30.5%). As can be seen, this agreement is within the estimated experimental accuracies (± 12%) of the W_i^{exp} and W_t^{exp} values. One can conclude that the ion contribution to the total line width increases with the upper-level energy of the transition and plays a more important role than what the G and BCW approximations provide.

5. Conclusion

Using a line deconvolution procedure (Milosavljević and Poparić 2001, Milosavljević 2001) we obtained, on the basis of precisely recorded He I spectral line profile, their Stark broadening parameters: W_t, W_e, W_i, A and D. We found that the ion contribution to the line profile plays a more important role than the semiclassical approximation provides, which must be taken into account in the use of this He I line for plasma diagnostical purposes according to the estimations made by the semiclassical perturbation formalism (Dimitrijević and Sahal-Bréchot 1990).

Acknowledgements. This work is a part of the project "Determination of the atomic parameters on the basis of the spectral line profiles" supported by the Ministry of Science, Technologies and Development of the Republic of Serbia. S. Djeniže is grateful to the Foundation "Arany János Közalapitvány" Budapest, Hungary.

References

Barnard, A. J., Cooper, J., Smith, E. W. : 1974, *J. Quant. Spectrosc. Radiat. Transfer*, **14**, 1025.

Bassalo, J. M., Cattani, M., Walder, V. S. : 1982, *J. Quant. Spectrosc. Radiat. Transfer*, **28**, 75.

Dimitrijević, M. S., Konjević, N : 1986, *Astron. Astrophys.*, **163**, 297.

Dimitrijević, M. S., Sahal–Bréchot, S. : 1990, *Astron. Astrophys. Suppl. Ser.*, **82**, 519.

Djeniže, S., Milosavljević, V., Srećković, A. : 1998, *J. Quant. Spectrosc. Radiat. Transfer*, **59**, 71.

Djeniže, S., Milosavljević, V., Dimitrijević, M. S. : 2002, *Astron. Astrophys.*, **382**, 359.

Freudenstein, S. A., Cooper, J. : 1978, *Astrophys. J.*, **224**, 1079.

Gauthier, J. C., Geindre, J. P., Goldbach, C., Grandjouan, N., Mazure, A., Nollez, G. : 1981, *J. Phys. B*, **14**, 2099.

Glenzer, S., Kunze, H. J., Musielok, J., Kim, Y., Wiese, W. : 1994, *Phys. Rev. A*, **49**, 221.
Griem, H. R. : 1974, *Spectral Line Broadening by Plasmas*, (New York: Acad.Press).
Griem, H. R. : 1997, *Principles of Plasma Spectroscopy*, (Cambridge: Univ.Press).
Kelleher, D. E. : 1981, *J. Quant. Spectrosc. Radiat. Transfer*, **25**, 191.
Lesage, A., Fuhr, J. R. : 1999, *Bibliography on Atomic Line Shapes and Shifts (April 1992 through June 1999)*, Observatoire de Paris.
Mijatović, Z., Konjević, N., Ivković, M., Kobilarov R. : 1995, *Phys. Rev. E*, **51**, 4891.
Milosavljević, V., Poparić, G. : 2001, *Phys. Rev. E*, **E63**, 036404.
Milosavljević, V. : 2001, *PhD Thesis*, University of Belgrade, Faculty of Physics, Belgrade (unpublished).
NIST 2002 - *Atomic Spectra Data Base Lines* - http://physics.nist.gov.
Pérez, C., de la Rosa, I., de Frutos, A. M., Mar, S. : 1991, *Phys. Rev. A*, **44**, 6785.
Vujičić, B. T., Kobilarov, R. : 1988, 9th Int. Conf. Spect. Line Shapes, Contributed papers, Nicholos Copernicos University press, Toru Poland A18.

Publ. Astron. Obs. Belgrade No. 73 (2002), 173 - 179 *Poster*

CONTRIBUTION OF ION TO THE ASTROPHYSICAL IMPORTANT 471.32 nm He I SPECTRAL LINE BROADENING

V. MILOSAVLJEVIĆ and S. DJENIŽE

Faculty of Physics, University of Belgrade, P.O.B. 368, Belgrade, Serbia, Yugoslavia

Abstract. Ion contribution of the astrophysical important Stark broadened 471.32 nm He I spectral line profiles have been measured at electron densities between $4.4\,10^{22}$ and $8.2\,10^{22}$ m^{-3} and electron temperatures between 18 000 and 33 000 K in plasmas created in five various discharge conditions using a linear, low-pressure, pulsed arc as an optically thin and reproductive plasma source operated in a helium-nitrogen-oxygen gas mixture. On the basis of the observed asymmetry of the line profiles we have obtained their ion broadening parameters (A) caused by influence of the ion microfield and also the influence of the ion dynamic effect (D) to the line shape. Our A and D parameters represent the first data obtained experimentally by the use of the line profile deconvolution procedure. We have found stronger influence of the ion contribution to this He I line profiles than the semiclassical theoretical approximation provides. This can be important for some astrophysical plasma modelling or diagnostics.

1. Introduction

After hydrogen, helium is the most abundant element in the universe. The 471.32 nm ($2p\ ^3P^0_{2,1}$ - $4s\ ^3S_1$ transition) neutral helium (He I) spectral line are the most investigated in the helium spectrum. This line has been used by various investigations of the radiation emitted by cosmic light sources like: white dwarfs, variables, supergiants and galaxies (Rupke et al. 2002, Bergeron et al. 2002, Peimbert et al. 2002, Thuan et al. 2002, Bresolin et al. 2002, Benjamin et al. 2002, Drissen et al. 2001, Cuesta and Phillips 2000). Therefore, the use of this He I spectral line for diagnostical purposes in astrophysics understands the knowledge of its line profile characteristics. A significant number of theoretical and experimental works has been dedicated to the He I Stark FWHM (full-width at half intensity maximum, W) investigations (Lesage and Fuhr 1999, and references therein). The aim of this work is to present the measured Stark broadening parameters of the He I 471.32 nm spectral line at (18 000 - 33 000) K electron temperatures (T) and at $(4.4 - 8.2)\,10^{22}$ m^{-3} electron densities (N). The used T values are typical for many cosmic light sources. Using a deconvolution procedure described by Milosavljević and Poparić (2001) we have obtained, for the first time, on the basis of the observed line profile asymmetry, the ion contribution to the line shape expressed due to the quasistatic ion (parameter A) and ion dynamic effect (coefficient D) (Griem 1974, Barnard et al. 1974, Bassalo et al. 1982) and, also, the separate electron (W_e) and ion (W_i) contributions to the total Stark width (W_t). As a

plasma source we have used a linear, low-pressure, pulsed arc operated in five various discharge conditions. Our measured W_t, W_e, W_i and A values have been compared to all available theoretical and experimental data.

2. Experiment

The modified version of the linear low pressure pulsed arc (Djeniže et al. 1998, 2002) has been used as a plasma source. The working gas was helium - nitrogen - oxygen mixture (90% He + 8% N_2 + 2% O_2). The used tube geometry and corresponding discharge conditions are presented in Table. 1.

Table 1: Various discharge conditions. C-bank capacity, U-bank voltage, H-plasma length, Φ-tube diameter, P-filling pressure. N and T denote electron density and temperature, respectively obtained at a 25^{th} μs after the beginning of the discharge when the line profiles were analyzed.

C (μF)	U (kV)	H (cm)	Φ (mm)	P (Pa)	N (10^{22}m^{-3})	T (K)
8	4.5	6.2	5	267	6.1	33000
14	4.2	14.0	25	267	8.2	31500
14	3.4	14.0	25	267	6.7	30000
14	2.6	14.0	25	267	4.4	28000
14	1.5	7.2	5	133	5.0	18000

Spectroscopic observation of spectral lines was made end-on along the axis of the discharge tube described in details in Djeniže (2002).

The line profiles were recorded by a step-by-step technique using a photomultiplier (EMI 9789 QB and EMI 9659B) and a grating spectrograph (Zeiss PGS-2, reciprocal linear dispersion 0.73 nm/mm in the first order) system. The instrumental FWHM of 8 pm was obtained by using narrow spectral lines emitted by the hollow cathode discharge.

The plasma reproducibility was monitored by the He I (501.56 nm, 388.86 nm and 587.56 nm) lines radiation and, also, by the discharge current using the Rogowski coil signal (it was found to be within ±5%). Using the double plasma length method, described by Milosavljević (2001), the correction of the line profiles was performed in order to eliminate the influence of self-absorption on the line shapes.

The plasma parameters were determined using standard diagnostics methods. Thus, the electron temperature was determined from the ratios of the relative line intensities of four N III spectral lines (409.74 nm, 410.34 nm, 463.42 nm and 464.06 nm) to the 463.05 nm N II spectral line with an estimated error of ±10%, assuming the existence of the LTE (Griem 1974). All the necessary atomic data were taken from NIST (2002) and Glenzer et al. (1994). The electron density decay was measured using a well known single wavelength He-Ne laser interferometer technique for the 632.8 nm transition with an estimated error of ±9%. The electron densities and temperatures, obtained at the moment when the line profiles were analyzed, are presented in Table 1.

3. Numerical procedure for deconvolution

The proposed functions for various line shapes, eq. (1) is of the integral form and include several parameters. Some of these parameters can be determined in separate experiments, but not all of them. Furthermore, it is impossible to find an analytical solution for the integrals and methods of numerical integration to be applied. This procedure, combined with the simultaneous fitting of several free parameters, causes the deconvolution to be an extremely difficult task and requires a number of computer supported mathematical techniques. Particular problems are the questions of convergence and reliability of deconvolution procedure, which are tightly connected with the quality of experimental data.

$$K(\lambda) = K_o + K_{max} \int_{-\infty}^{\infty} exp(-t^2) \cdot [\int_0^{\infty} \frac{H_R(\beta)}{1 + (2\frac{\lambda - \lambda_o - \frac{W_G}{2\sqrt{\ln 2}} \cdot t}{W_e} - \alpha \cdot \beta^2)^2} \cdot d\beta] \cdot dt \quad (1)$$

Here K_o is the baseline (offset) and K_{max} is the maximum of intensity (intensity for λ=λ_o) (Milosavljević and Poparić 2001). $H_R(\beta)$ is an electric microfield strength distribution function of normalized field strength β=F/F_o, where F_o is the Holtsmark field strength. A (α=$A^{4/3}$) is the static ion broadening parameter as a measure of the relative importance of ion and electron broadenings. R is the ratio of the mean distance between the ions to the Debye radius, i.e. the Debye shielding parameter and W_e is the electron width (FWHM) in the $j_{A,R}$ profile (2).

For the purpose of deconvolution iteration process we need to know the value of K function (1) as a function of λ for every group of parameters (K_{max}, λ_o, W_e, W_G, R, A). The function K(λ) is in integral form and we have to solve a triple integral in each step of iteration process of varying the above group of parameters. The first integral in the "K" function is the micro field strength distribution function, $H_R(\beta)$ the second one is the $j_{A,R}(\lambda)$ function eq. (2) and the third is the convolution integral of a Gaussian and a plasma broadened spectral line profile $j_{A,R}(\lambda)$, denoted by K(λ) equation (1). All these integrals have no analytic solution and must be solved using the numerical integration.

$$j_{A,R}(\lambda) = j_o + j_{max} \cdot \int_0^{\infty} \frac{H_R(\beta)}{1 + (2\frac{\lambda - \lambda_o}{W_e} - \alpha \cdot \beta^2)^2} \cdot d\beta \quad (2)$$

The most difficult integral to deal with is the micro field strength distribution function, because this is a multidimensional integral. Straightforward manner would be the estimates of multidimensional integral by Monte Carlo method of integration. The numbers of random samples of points must be large in order to achieve satisfactory accuracy. That would lead to the increased processor time (Milosavljević 2001).

In general, the base line K_o in functions (1) is a function of wavelength. In many cases it is nearly constant, or linear function.We have included in our procedure the fitting of background by cubic polynomial, as independent step, in order to prepare experimental data for the main deconvolution procedure.

The upper limits of numerical conditionality of this method are minimum twenty experimental points per line (the border of line is $(-3/2 \cdot W_e + \lambda_o < \lambda < +3/5 \cdot W_e + \lambda_o)$,

where W_e is electron FWHM), and maximal statistical indeterminacy in intensity is 5% at every experimental point. Poor experimental measurements weaken the conditionality of the system of equations, and lead to non-applicability of this method. This has been concluded by testing the sensitivity of the algorithm by generating random statistical noise with Gaussian distribution in every point involved in theoretical profiles.

4. Results and discussion

The plasma broadening parameters (W_t, W_e, W_i, A, D) obtained by our deconvolution procedure of the recorded line profile at a measured N and T values are presented in Table 2 together with other author's results. Various theoretical (G, BCW, DSB) predictions of the W_e, W_i, and A are also given. By the normalization of the A^G and A^{BCW} values to our electron density the well known $N^{1/4}$ numerical factor (Griem 1974) was used.

Table 2: Measured line broadening characteristics of the 471.32 nm spectral line. Total Stark FWHM (W_t^{exp} in pm within ±12% accuracy), electron Stark width (W_e^{exp} in pm within ±12% accuracy), ion Stark width (W_i^{exp} in pm within ±12% accuracy), static ion broadening parameter (A^{exp}, dimensionless within ±15% accuracy) and ion dynamic coefficient (D^{exp}, dimensionless within ±20% accuracy) at a given electron temperature (T in 10^3 K) and electron density (N in $10^{22}\mathrm{m}^{-3}$). Here Tw present the values given in this work and those used from other authors: RS, Roder and Stampa (1964); K, Kelleher (1981); B, Berg et al. (1962); W, Wulff (1958); Gr, Griem et al. (1962); L, Lincke (1964); P, Pérez et al. (1991); M, Mijatović et al. (1995).The index G, BCW and DSB denote theoretical data taken from Griem (1974), Bassalo et al. (1982) and Dimitrijević and Sahal – Bréchot (1990), respectively at a given T and N.

T	N	W_t^{exp}	W_e^{exp}	W_i^{exp}	A^{exp}	D^{exp}	Ref.	W_e^G	W_e^{BCW}	W_e^{DSB}	W_i^{DSB}	A^G	A^{BCW}
33.0	6.1	542	371	171	0.343	1.0	Tw	554	483	398	95	0.146	0.162
31.5	8.2	713	481	232	0.368	1.0	Tw	740	648	533	125	0.157	0.175
30.0	6.7	595	407	188	0.352	1.0	Tw	603	528	430	99	0.150	0.166
28.0	4.4	372	261	111	0.317	1.0	Tw	394	341	281	65	0.136	0.151
18.0	5.0	403	286	117	0.335	1.0	Tw	428	370	319	69	0.142	0.161
16.5	1.7				0.20*		RS						
20.9	1.03	96			0.095	1.36	K						
20.0	13.0	1400					B						
30.0	3.2	290					W						
30.0	2.6	300					Gr						
22.7	9.3	91					L						
30.2	3.23	295					P						
19.3	0.25	23					M						

In order to make the comparison among measured (W_t^{exp}) and calculated (W_t^{th}) total (electron + ion) width values easier, the W_t^{exp}/W_t^{th} dependence on the electron temperature is presented graphically in Figure 1 for the investigated lines.

The G (Griem 1974) and BCW (Bassalo et al. 1982) W_t values are calculated using the Eq.(226) from Griem (1974) with the W_e and A values predicted by the G and BCW theoretical approaches, respectively. The W_t^{exp}/W_t^{th} ratios related to the Dimitrijević and Sahal-Bréchot (1990) (DSB) data have been calculated only for our experimental values. Namely, for the calculations of the W_i^{DSB} it is necessary to know the helium ion concentration connected to the plasma composition. We have performed this for our discharge conditions only.

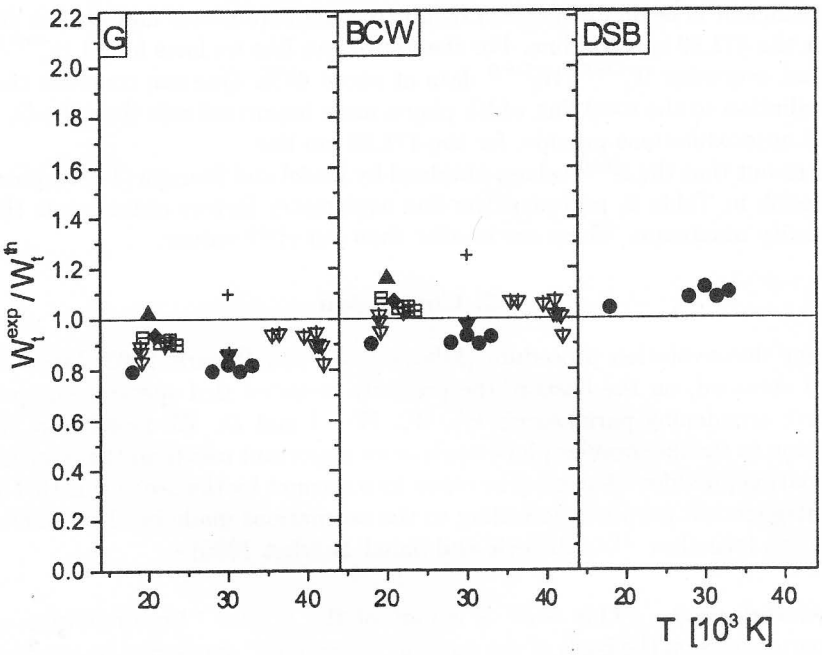

Fig. 1: Ratios of the experimental total Stark FWHM (W_t^{exp}) to the various theoretical (W_t^{th}) predictions vs. electron temperature for the He I 471.32 nm line. ○, +, ◇, △, ▽+, ▽and+ represent our experimental data and those from Griem et al. (1962), Kelleher (1981), Berg et al. (1962), Wulff (1958), Lincke (1964), Pérez et al. (1991) and Mijatović et al. (1995), respectively. G, BCW and DSB represent the ratios related to the theories taken from Griem (1974), Bassalo et al. (1982) and Dimitrijević and Sahal - Bréchot (1990), respectively.

It turns out that our W_e^{exp} and W_i^{exp} are the first separated experimental electron and ion Stark width data obtained by using our deconvolution procedure. Our W_e^{exp} data are smaller than the G, BCW and DSB approximations provide for the investigated lines. Approximations BCW and DSB provide smaller W_e values than the G approximation.

By the inspection of the Figure 1 one can conclude that Griem's (1974) W_t values lie above most of the experimental values and also above BCW and DSB theoretical data. Theoretical W_t values presented by Bassalo et al. (1982) lie about 10% - 15% below Griem's values. The W_t values ($W_e + W_i$) presented by Dimitrijević and Sahal-Bréchot (1990) agree with ours (W_t^{exp}) within 3% - 10% (on average).

We have found evident contribution of the ion influence to the line broadening due to the quasistatic ion effect expressed with the ion broadening parameter (A). Our

A^{exp} values are the first data obtained directly by the use of the line deconvolution procedure. They are higher than the G and BCW approaches provide at about 135% and 110%, respectively. We have found that the ion dynamic effect, expressed due to the D coefficient is negligible ($D \simeq 1$) by our plasma parameters and plasma composition for the 471.32 spectral line. For the 471.32 nm line we have found W_i^{exp}/W_t^{exp} values that overvalue W_i^{DSB}/W_t^{DSB} data at about 65%. One can conclude that the ion contribution to the total line width play a more important role than the G, BCW and DSB approximations provide, for the 471.32 nm line.

It turns out that the A^{exp} values, obtained by Rodel and Stampa (1964), presented with asterisk in Table 2, represent the line asymmetry factors obtained at the line half intensity maximum. These are smaller than our A^{exp} values.

5. Conclusion

Using line deconvolution procedure (Milosavljević and Poparić 2001, Milosavljević 2001) we obtained, on the basis of the precisely recorded He I spectral line profiles, their Stark broadening parameters: W_t, W_e, W_i, A and D. We found that the ion contribution to the line profiles plays much more important role than the semiclassical approximation provides what must be taken into account by the use of this He I line to plasma diagnostical purposes according to the estimations made by the semiclassical perturbation formalism (Dimitrijević and Sahal-Bréchot 1990).

Acknowledgments. This work is a part of the project "Determination of the atomic parameters on the basis of the spectral line profiles" supported by the Ministry of Science, Technologies and Development of the Republic of Serbia. S. Djeniže is grateful to the Foundation "Arany János Közalapitvány" Budapest, Hungary.

References

Barnard, A. J., Cooper, J., Smith, E. W. : 1974, *J. Quant. Spectrosc. Radiat. Transfer*, **14**, 1025.

Bassalo, J. M., Cattani, M., Walder, V. S. : 1982, *J. Quant. Spectrosc. Radiat. Transfer*, **28**, 75.

Benjamin, R. A, Skillman, E. D., Smits, D. S. : 2002, *Astrophys. J.*, **569**, 288.

Berg, H. F., Ali, A. W., Lincke, R., Griem, H. R. : 1962, *Phys. Rev.*, **125**, 199.

Bergeron, P., Liebert, J. : 2002, *Astrophys. J.*, **566**, 1091.

Bresolin, F., Gieren, W., Kudritzki, R.-P., Pietvzyński, G., Przybilla, N. : 2002, *Astrophys. J.*, **567**, 277.

Cuesta, L., Phillips, J. P. : 2000, *Astrophys. J.*, **543**, 754.

Dimitrijević, M. S., Sahal−Bréchot, S. : 1990, *Astron. Astrophys. Sup. Ser.*, **82**, 519.

Djeniže, S., Milosavljević, V., Srećković, A. : 1998, *J. Quant. Spectrosc. Radiat. Transfer*, **59**, 71.

Djeniže, S., Milosavljević, V., Dimitrijević, M. S. : 2002, *Astron. Astrophys.*, **382**, 359.

Drissen L., et al. : 2001, *Astrophys. J.*, **546**, 484.

Glenzer, S., Kunze, H. J., Musielok, J., Kim, Y. K., Wiese, W. L. : 1994, *Phys. Rev. A*, **49**, 221.

Griem, H. R. : 1974, *Spectral Line Broadening by Plasmas*, (New York: Acad.Press).

Griem, R. H., Baranger, M., Kolb, A. C., Oertel, G. : 1962, *Phys. Rev.*, **125**, 177.

Kelleher, D. E. : 1981, *J. Quant. Spectrosc. Radiat. Transfer*, **25**, 191.

Lesage, A., Fuhr, J. R. : 1999, *Bibliography on Atomic Line Shapes and Shifts (April 1992 through June 1999)*, Observatoire de Paris.

Lincke, R. : 1964, *PhD Thesis*, University of Maryland (unpublished).
Mijatović, Z., Konjević, N., Ivković, M., Kobilarov, R. : 1995, *Phys. Rev. E*, **51**, 4891.
Milosavljević, V., Poparić, G. : 2001, *Phys. Rev. E*, **63**, 036404.
Milosavljević, V. : 2001, *PhD Thesis*, University of Belgrade, Faculty of Physics, Belgrade (unpublished).
NIST : 2002 - *Atomic Spectra Data Base Lines* - http://physics.nist.gov.
Peimbert, A., Peimbert, M., Luridiana, V. : 2002, *Astrophys. J.*, **565**, 668.
Pérez, C., de la Rosa, I., de Frutos, A. M., Mar, S. : 1991, *Phys. Rev. A*, **44**, 6785.
Popović, L. Č., Dimitrijević, M. S., Tankosić, D. : 1999, *Astron. Astrophys. Supp. Ser.*, **139**, 617.
Roder, O., Stampa, A. : 1964, *Z. Physik.* **178**, 348.
Rupke, D. S., Veilleux, S., Sanders, D. B. : 2002, *Astrophys. J.*, **570**, 588.
Thuan, T. X., Lecavelier des Etangs A., Izotov, Y. : 2002, *Astrophys. J.*, **565**, 941.
Wulff, H. : 1958, *Z. Phys.*, **150**, 614.

Publ. Astron. Obs. Belgrade No. 73 (2002), 181 - 190 *Poster*

RED SUPERGIANTS IN M 31: EXTINCTION, METALLICITIES AND GAS-TO-DUST RATIO

PETKO NEDIALKOV and TODOR VELTCHEV
Department of Astronomy, University of Sofia, James Bourchier 5, Sofia 1164, BULGARIA
E-mail japet@phys.uni-sofia.bg
E-mail cirene@phys.uni-sofia.bg

Abstract. We derived individual extinction values for selected red supergiant (RSGs) candidates in M31 with broadband photometry. Taking into account their position on the colour-magnitude diagram and using a probability method, the metallicity of each star was estimated. In the range 2-15 kpc the ratio [O/H] is nearly constant. The derived individual extinctions and pencil beams values from three different gas maps (Westerbork HI, VLA HI and IRAM CO(1→0)-line survey) were used to obtain gas-to-dust ratio in M 31. For the 9 most luminous stars both the ratios $N(HI)/2\,E_{B-V}$ and $N(HI + H_2)/2\,E_{B-V}$ are not very different from those in the Milky Way. Significant fractions outside the expected range of Galactic atomic gas-to-dust ratio are obtained for $\sim 1/3$ of the sample using Westerbork and for $\sim 1/2$ of the sample - using VLA maps. The ratios are overestimated for objects located high above the midplane of M 31 and underestimated - due to resolution effects, - for several RSGs coinciding with small HI clouds.

1. INTRODUCTION

The available broadband photometry for RSGs in nearby galaxies offers a good opportunity for the derivation of their extinction through the Q-method. On a colour-colour diagram containing $(V - I)$ colour, these objects are distinctly separated from the foreground dwarfs and the position of the zero-absorption line allows unambiguous determination of their true colour. The aim of our work is to obtain individual extinctions and metallicities for RGSs in M 31 that can be used to study the gas-to-dust ratio.

2. THE SAMPLES AND THE DEREDDENING PROCEDURE

The main source of objects for the present study is the large catalog with BVRI photometry of Magnier et al. (1992). The diagrams $(B - V)$ vs. $(V - I)$ (Fig. 1) and $(V - R)$ vs. $(V - I)$ (Fig. 2) clearly show the red end of the foreground dwarfs sequence whose scatter increases with the V magnitude. The zero-absorption line for supergiants was composed as a strip encompassing the Geneva evolutionary tracks (Lejeune & Schaerer 2001) for masses in the typical range of 9-25 $\mathcal{M}_\odot$. In both Figures, the thin lines designate the borders of the strip and the thick one - its center.

We adopted the Galactic value of the total-to-selective-extinction ratio $R_V = 3.1$ leading to a slope of the reddening vector as plotted in the lower left corners. Then the true colour of each star is calculated through the Q-method for 9 different sets of colour values corresponding to the central point, the corners and the size-centers of its photometric error box, and for the two borders and central line of the zero-absorption line strip: 27 values in total. The error of the true colour is obtained as arithmetic mean of its minimum and maximum value. However, the position and photometric errors of some objects below the strip do not allow derivation of plausible values in all 27 cases. We chose RSG candidates that allow at least 9 dereddenings with the adopted slope: 64 on diagram $(B-V)$ vs. $(V-I)$ (Fig. 1) and 35 on diagram $(V-R)$ vs. $(V-I)$ (Fig. 2). To the common objects was ascribed a colour excess that is the average value obtained from both diagrams. Finally we have 69 RSG candidates of the catalog of Magnier et al. (1992) with reliably determined true colours and extinction. Five of them turn out to be very luminous and were excluded from the study of the metallicity gradient and gas-to-dust ratio in the galaxy (see next section).

The second source for RSG candidates is a list of red stars in M 31 of Massey (1998). His BVR photometry is of higher precision and we supplemented it - after a cross-identification, - only with an I magnitude from the catalog of Magnier et al. (1992). Thus further 37 objects were selected (not included in the first sample) appropriate for dereddening through our procedure both on the diagram $(B-V)$ vs. $(V-I)$ and/or $(V-R)$ vs. $(V-I)$.

3. EXTINCTION AND METALLICITY OF THE RSG-CANDIDATES IM M 31

The derived individual extinctions A_V for the RSGs are not high and vary from 0.2 to 2.2. Their lower limit is close to the foreground extinction toward M 31 of $E_{B-V} = 0.062$ (Schlegel et al. 1998). The assumed distance modulus is 24.47 (Stanek & Garnavich 1998). As shown in Fig. 3, the absolute magnitudes of most RSG candidates fall into the range $-5 > M_V > -7$ (initial masses 12-21 $\mathcal{M}_\odot$) which supports the claim that there is a lack of luminous RSGs in the Andromeda galaxy (Berkhuijsen & Humphreys 1989, Massey 1998). There are five exceptions with true colours $(V-I)_0 \sim 2.0$, located in an area where the evolutionary tracks for more massive stars reach their turning point to the blue. These very luminous objects from the catalog of Magnier et al. (1992) are most likely affected by blending which is pointed out as a problem of this photometry. The evolutionary tracks of the RSGs on the colour-magnitude diagram and their lifetimes turn out to depend essentially on the star's metallicity Z (see e.g. Salasnich, Bressan & Chiosi 1999). Thus the probabilities to "meet" in a fixed area a RSG with given Z vary significantly which enables us to estimate the individual metallicity via a simple 'bullets-method' (Fig. 4). The location of a star on the diagram M_V vs. $(V-I)$ is determined by its error box which is crossed through by tracks for different sets of initial masses $\mathcal{M}$ and Z. We calculated approximate tracks in the mentioned range of 9-25 $\mathcal{M}_\odot$ with step $\Delta\mathcal{M} = 1$ as functions of $\mathcal{M}$ and Z using the analytic formulae of Hurley, Pols & Tout (2000). The initial stellar mass is out of scope of this work and we consider Z as the sole parameter. If each track is divided by points of one and the same, fixed timestep, the number of points N_{Z_i} for metallicity Z_i ('bullets of type Z_i') in the

error box would be a measure for the probability that the stellar metallicity is Z_i:

$$p_i = N_{Z_i}/N$$

where N is the total number of points in the error box. Then the estimates of the individual metallicity and its error are given by:

$$Z = \sum_i p_i Z_i$$

$$\sigma_Z = \sqrt{\frac{\sum_i N_{Z_i} Z_i^2 - Z^2}{N}}$$

The total metallicity Z was transformed to $[O/H]$ assuming relative element abundances as derived by Anders & Grevesse (1989) for the solar photosphere. The obtained values are plotted vs. the galactocentric distance of the RSGs in Fig. 5. There is no evidence for a steep metallicity gradient in M 31 in the range $10' - 70'$ (2-15 kpc). For comparison are drawn the gradients of Smartt et al.(2001) (-0.018 dex kpc^{-1}) and Galarza, Walterbos & Braun (1999) (-0.06 dex kpc^{-1}) used two different abundance calibrations for the *H II* regions. Our result becomes clearer if we require stronger criteria concerning the dereddening procedure: at least 18 plausible dereddenings of 27 possible and at least 4 plausible dereddenings to each border and to the central line of the zero-absorption strip (see Fig. 1 and 2). We then obtain a subsample with highly reduced scatter of abundance estimates vs. galactocentric distance (filled symbols, Fig. 5). Up to angular distances of $\sim 30'$, there may be a slight positive gradient [O/H]. In the region between $30'$ and $65'$ (7–15 kpc) the stellar metallicity varies in a wide range above the predicted values with the same scatter like in the abundance studies mentioned above. This may indicate that objects with different metallicities are present even at a fixed galactocentric distance. One possible explanation is the enrichment of the protostellar matter due to ongoing active star formation and consequent supernova explosions. Recently this ring of active star formation has been a subject of intensive research (e.g. Pagani et al. 1999).

4. GAS-TO-DUST RATIO IN M 31

The new CO(1→0) map (Guelin et al. 2000) with a spatial resolution of 23 $''$ at λ 2.6 mm combined with the available *H I* maps of M 31 yields excellent opportunities for detailed study of the total gas-to-dust ratio. Here we mean by 'dust' the derived individual extinction values for the RSGs. Because of the poor statistics (106 extinction estimates) it is not possible to construct an extinction map. For the atomic hydrogen we took pencil beam column densities at λ 21 cm from 2 different maps: Westerbork with an angular resolution of $24 \times 36''$ (Brinks & Shane, 1984) and VLA with a resolution of 10 $''$ (Walterbos & Braun, 1992). As the VLA map does not cover a large part of the SW half of M 31 and further only the extinctions of 55 objects falling in both maps are considered. We converted CO-intensity to molecular hydrogen column density $N(H_2)$ using a constant X_{CO} conversion factor (Strong & Mattox 1996) since the metallicity is nearly constant with radius. The total column density $N(HI + 2\,H_2)$ is obtained as the sum of both components, multiplied by a factor 1/2 assuming that the stars on the average are located at the midplane of the galaxy. The relationships 'atomic gas-dust' and 'total gas-dust' are illustrated in Fig. 6 and Fig.

7, respectively. A constant gas-to-dust ratio in M 31 would yield a good correlation like in the Milky Way (cf. Fig. 2 in Bohlin et al. 1978) which is not the case here. One of the explanations could be a gas-to-dust ratio depending on the galactocentric distance. But the observed large spread is most probably due to another reason: the varying fraction of the gas density (not exactly 1/2) associated with the dust – stars located in the front part or in the back of the disk yield deviations from the corresponding line. To diminish the latter effect we divide our sample in 3 different groups on the diagram $H\,I$ vs. E_{B-V} (Fig. 6): objects within (filled triangles), above (open squares) and below (open circles) the expected range of the Galactic ratio. The most luminous objects (large open squares) with a single exception due to resolution problems (see below) turn out to be members of the first group. The single criterion $M_V < -6$. immediately improves the correlations for limited samples in magnitude used here since such stars can be seen even under larger column densities of the gas. On the other hand, the presence of objects with overestimated gas-to-dust ratio (open squares; the typical deviating case) is explained with their high location above the galactic midplane. The objects within the expected range of Galactic atomic gas-to-dust ratio are most appropriate for a study of total gas-to-dust ratio (Fig. 7). This group is obviously larger in number using the Westerbork data (left hand panel, 60% of the sample). Following Bohlin et al. (1978), one should expect that adding of the molecular gas fraction will tighten the 'total gas-dust' correlation. This effect is not seen in Fig. 7, however. One notes that the VLA data (right hand panel) have less scatter around the line corresponding to the Galactic total gas-to-dust ratio. That leads us to a third reason for decreasing the expected correlation: the angular resolution of the $H\,I$ maps. Direct comparison in Fig. 6 between Westerbork (left hand panel) and VLA (right hand panel) column densities shows a scale difference of ~ 2. A natural explanation may be that the ISM in M 31 consists predominantly of small clouds not well resolved on the Westerbork map. Indeed, the RGSs lying below the expected strip (open circles in the left hand panels) are located in such small clouds with underestimated column density on $24 \times 36''$ resolution map.

The calculated estimates of the gas-to-dust ratios based on the data for 9 most luminous RSGs (8 on the right hand panels) are summarized in Table 1. It is intriguing that the values of Lequeux (2000) for the outermost part of M 31 are significantly higher while the canonical Galactic values (Bohlin et al. 1978) are confirmed by our results. For further details, comments and discussion see our forthcoming paper.

Acknowledgments. We thank Elly M. Berkhuijsen for a fruitful discussion and the valuable comments on the manuscript. This research was partially supported by contract Nr. F-825/1998 with the National Science Foundation, Ministry of Education and Sciences, Bulgaria.

Table 1: Gas-to-Dust Ratios in M 31 and in the Milky Way

	$< N(HI)/2E_{B-V} >$ [10^{21} atoms cm^{-2} mag^{-1}]	$< N(HI+2H_2)/2E_{B-V} >$ [10^{21} atoms cm^{-2} mag^{-1}]
Westerbork	1.4 ± 0.4	3.4 ± 1.1
VLA	5.7 ± 1.9	5.9 ± 2.0
M 31 (Lequeux 2000)	$11.0 \div 14.5$	—
Milky Way (Bohlin et al. 1978)	4.8 ($1.5 \div 14.5$)	5.8 ($3.3 \div 10$)

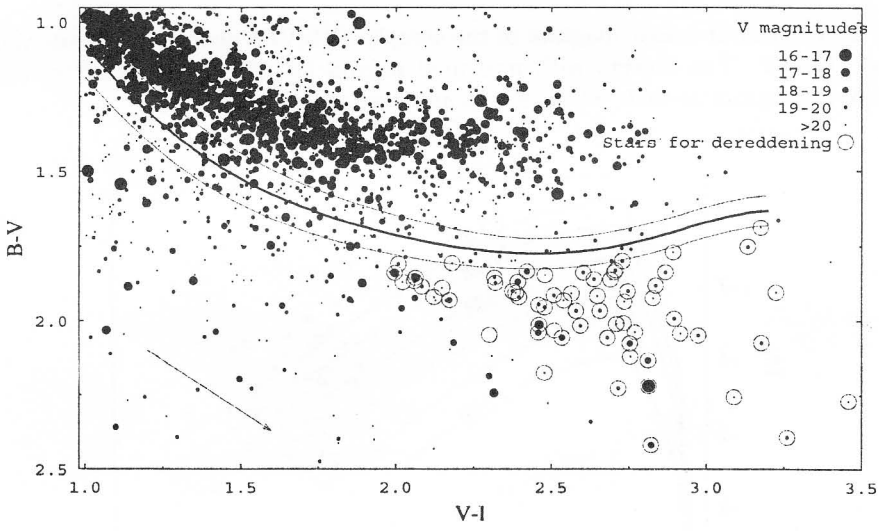

Fig. 1: The colour-colour diagram of the sample with BVI photometry from Magnier et al. (1992). The pointsizes correspond to different V magnitude intervals. In the lower left is shown the direction of the reddening vector (R_V =3.1). The strip delineated with solid lines gives the location of the zero-absorption line (see text). The stars appropriate for our dereddening procedure are plotted with open circles.

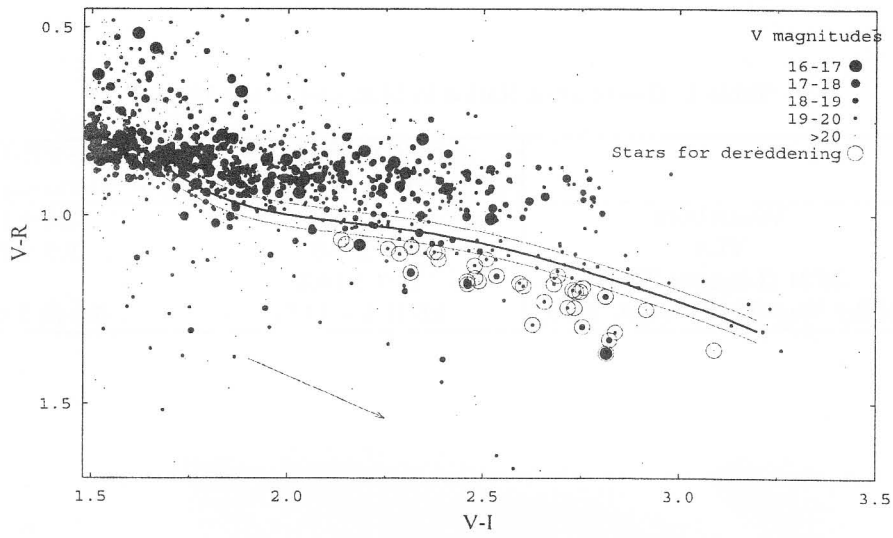

Fig. 2: The colour-colour diagram of the sample with VRI photometry from Magnier et al. (1992). The objects with measured magnitude in B are plotted on the (B-V)/(V-I) diagram as well. The symbols are the same as in Fig. 1.

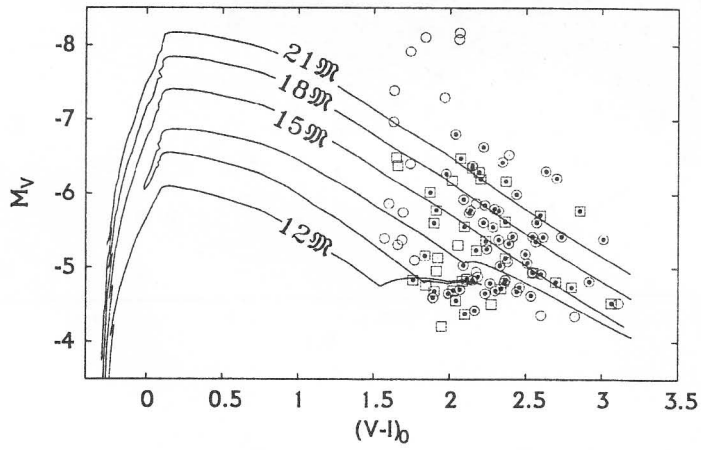

Fig. 3: The dereddened RSG-candidates from Magnier et al. (1992) (circles) and Massey (1998) (squares) on the colour-magnitude diagram. The evolutionary tracks for 12, 15, 18 and 21 solar masses and $Z = 0.02$ (solid lines) are plotted. The filled symbols are the subsample selected for study of the metallicity gradient and the gas-to-dust ratio.

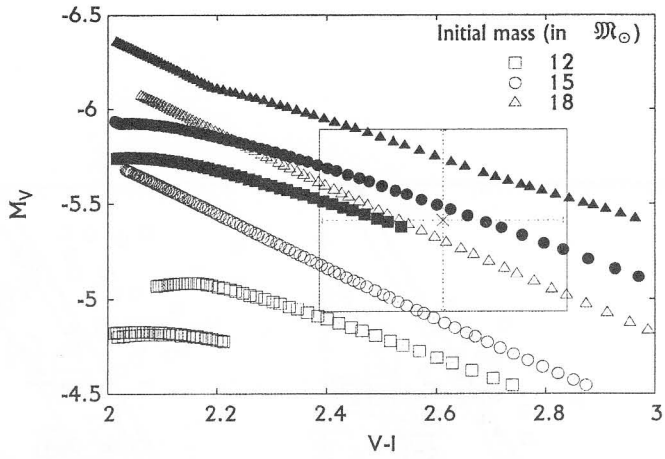

Fig. 4: The 'bullets-method' for estimation of star's metallicity. A set of evolutionary tracks for metallicities $Z = 0.012$ (filled symbols) and $Z = 0.02$ (open symbols) and three different initial masses (squares, circles and triangles) are given. The error bars in colour and absolute magnitude determine the area for counting the points of equal timesteps for given Z (see text).

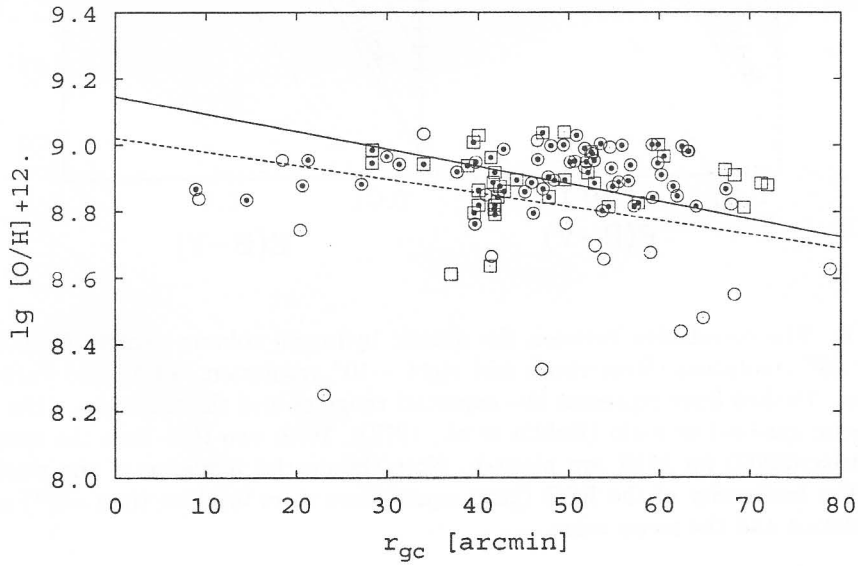

Fig. 5: Metallicity of individual stars in M31 (in units of oxygen abundance) versus their galactocentric distance. The symbols are the same as in Fig. 3. The mean abundance gradients derived by Galarza, Walterbos & Braun (1999) (solid line) and Smartt et al. (2001) (dashed) are plotted for comparison.

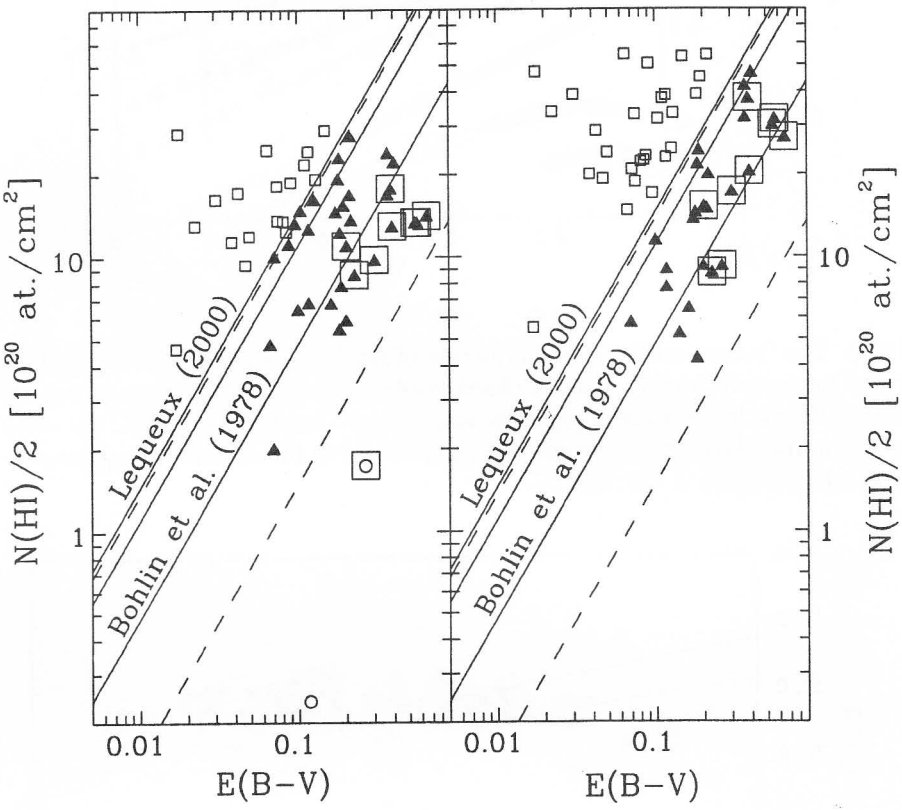

Fig. 6: The correlation between the atomic hydrogen column density N(HI)(left - 24 × 36″ resolution, Westerbork and right - 10″ resolution, VLA) and extinction E_{B-V}. Dashed lines represent the expected range of and the thick one - the mean Galactic gas-to-dust ratio (Bohlin et al., 1978). With two thin lines the results of Lequeux (2000) for M 31 are plotted. Note the crucial influence of the resolution and the luminosity of the RSG (large squares are stars brighter than -6^m) on the correlation and the mean value.

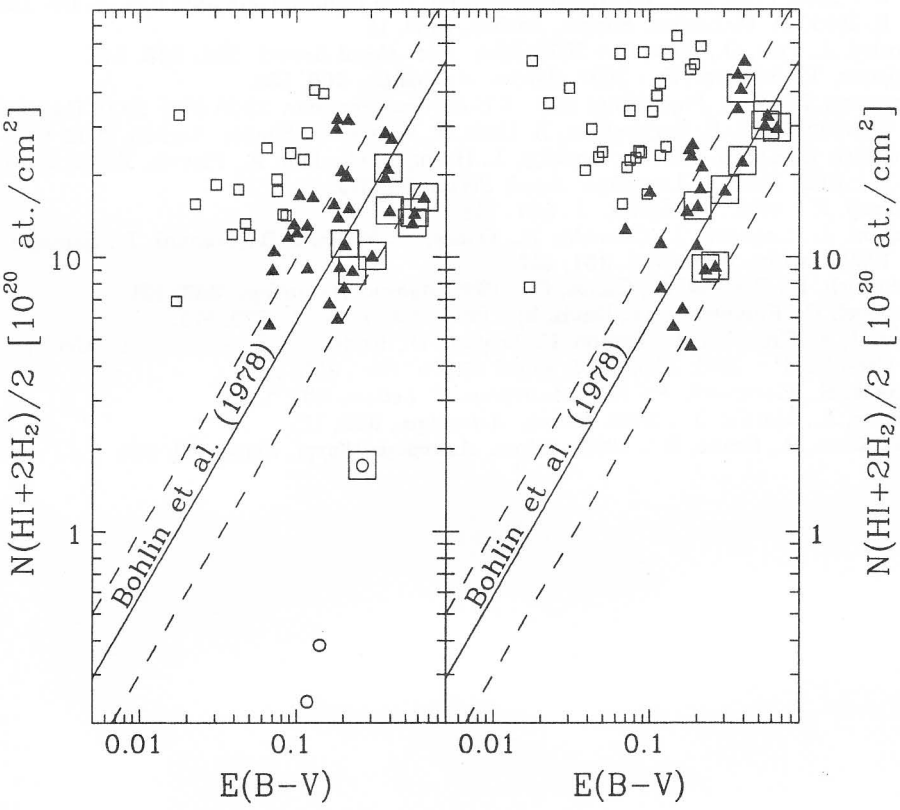

Fig. 7: The same as in Fig. 6, but for the half of the hydrogen total column density. The molecular fraction was added, assuming constant X(CO) conversion factor (Strong & Mattox, 1996). Note the absence on both the right hand panels of open circles corresponding to stars, embedded in unresolved small clouds.

References

Anders, E., Grevesse, N. : 1989, *Geochim. Cosmochim. Acta*, **53**, 197.
Berkhuijsen, E., Humphreys, R. : 1989, *Astron. Astrophys.*, **214**, 68.
Bohlin, R., Savage, B., Drake, J. : 1978, *Astrophys. J.*, **224**, 132.
Brinks, E., Shane, W. : 1984, *Astron. Astrophys.*, **55**, 179.
Galarza, V., Walterbos, R., Braun, R. : 1999, *Astron. J.*, **118**, 2775.
Guelin, M., Nieten, C., Neininger, N., Muller, S., Lucas, R., Ungerechts, H., Wielebinski, R. : 2000, *Proc. 232. WE-Heraeus Seminar*, Bad Honnef, Germany; Eds. E. Berkhuijsen, R. Beck, R. Walterbos. Shaker, Aachen, 2000, 15.
Hurley, J., Pols, O., Tout, C. : 2000, *Mon. Not. Royal Astron. Soc.*, **315**, 543.
Lejeune, T., Schaerer, D. : 2001, *Astron. Astrophys.*, **366**, 538.
Lequeux, J.: 2000, *Proceedings 232. WE-Heraeus Seminar*, 22-25 May 2000, Bad Honnef, Germany; Eds. E. Berkhuijsen, R. Beck, R. Walterbos. Shaker, Aachen, 2000, 63.
Magnier, E., Lewin, W., van Paradijs, J., Hasinger, G., Jain, A., Pietsch, W., & Truemper, J. : 1992, *Astron. Astrophys. Suppl. Series*, **96**, 379.
Massey, P. : 1998., *Astrophys. J.*, **501**, 153.
Pagani, L., Lequeux, J., Cesarsky, D., Donas, J., Milliard, B., Loinard, L., Sauvage, M. : 1999, *Astron. Astrophys.*, **351**, 447.
Salasnich, B., Bressan, A., Chiosi, C. : 1999, *Astron. Astrophys.*, **342**, 131.
Schlegel, D., Finkbeiner, D., Davis, M.: 1998, *Astrophys. J.*, **500**, 525.
Smartt, S., Crowther, P., Dufton, P., Lennon, D., Kudritzki, R., Herrero, A., McCarthy, J., Bresolin, F. : 2001, *Mon. Not. Royal Astron. Soc.*, **325**, 257.
Stanek, K., Garnavich, P.: 1998, *Astrophys. J. Letters*, **503**, L131.
Strong, A., Mattox, J. : 1996, *Astron. Astrophys.*, **308**, L21.
Walterbos, R., Braun, R. : 1992, *Astron. Astrophys. Suppl. Series*, **92**, 625.

Publ. Astron. Obs. Belgrade No. 73 (2002), 191 - 194 *Poster*

REMARKS ON THE MASS DISTRIBUTION IN STELLAR SYSTEMS

SLOBODAN NINKOVIĆ[1]

[1] *Astronomical Observatory, Volgina 7, 11160 Belgrade-74, Yugoslavia*
E-mail sninkovic@aob.bg.ac.yu

Abstract. A general consideration of mass distribution in stellar systems is presented.

1. General

It is rather well known that in the modern approach, the starting point in the study of the mass distribution within a stellar system is the observed profile. The alternative consisting of ascribing a given theoretically based profile to the stellar system under study belongs to the past. As an example one can mention Plummer's (e. g. 1915) papers where a particular theoretically based density law (Schuster's polytrope) was attributed to the observed globular clusters. However, a number of papers originating mainly from the middle of the twentieth century clearly indicated the importance of introducing empirical density laws (e. g. de Vaucouleurs, 1948; King, 1962). The modern equipment, doubtlessly, enables a sophisticated treatment of observational data, in particular to obtain a satisfactory trend between the observational points. In this way one has nowadays many empirical profiles (surface density is ment) which rather well reflect the real mass distribution within a class of stellar systems, i. e. concrete stellar systems (e. g. Dehnen, 1993 and references therein). However, one must take into account that the region of a stellar system available to the observations is limited, in other words there are always points evading a direct evidence. In such a situation the only way of obtaining the surface density is to calculate it by using the fitting formulae (model). Then one can have unusual outcomes: a model used for the purpose of fitting the observational results can result in an infinite space density at the system centre, or likewise this can be the case with both the surface density and the space one. For instance, Dehnen's model (mentioned above), except one special case, yields infinite values at the centre for both densities. On the other hand de Vaucouleurs' model (also mentioned above), though yielding a finite central surface density, results in an infinite central space density! No matter what kind of physical meaning is ascribed to such results, it is clear that they cannot be realistic. For example, one may consider the possibility of a massive central black hole. Then the main result would be its mass. However, as very well known, the mass value for a black hole clearly determines its radius and, as a consequence, it follows that the

black-hole density is finite! There are also other disadvantages of models yielding central singularities, for instance, though the total mass is finite, the total potential energy can be infinite (e. g. Tremaine et al., 1994).

Problems can also arise when the outer boundary is studied. Usually for the purpose of avoiding the well-known difficulties it is assumed that the stellar system under study is isolated, i. e. that the density in the surrounding space is zero. In order to make this presentation clear enough the present author will take into consideration the example of a spherically symmetric stellar system. In such a situation there is the very clear notion of the maximal apocentric distance. Obviously, its amount must be finite, but it need not be specified. The latter case corresponds to a model with an infinite limiting radius of the (stellar) system. In the reverse case, i. e. if the limiting radius is finite, it must be equal to the maximal apocentric distance. Then, as a consequence, the density on the inner side of the outer sphere (that of the radius equal to the limiting one) must be non-zero, i. e. there will be a discontinuity. Some authors (e. g. Casertano, 1983; even the present author was once among them - e. g. Ninković, 1992) reject such a possibility. However, there is no reason to be afraid of this discontinuity, it is practically the consequence of the artificial assumption that the surrounding space is empty.

Therefore, the present author's position is that the outer boundary of a stellar system in a model of it can be both finite and infinite, but that in the former case the discontinuity at the outer boundary is unavoidable, whereas in the latter one a model is meaningful only if it yields finite values for both the total mass and the total potential energy. Thus in this, latter, case the boundary discontinuity vanishes since the system density reaches zero in the infinity. Perhaps it may seem that the same line of reasoning is valid for the central density, i. e. that an infinite central density merely means that the central-density value in a given model is not specified (in other words it can always exceed a given limit), but in addition to the difficulties indicated above, there are also ones concerning the computer programming in the presence of a central singularity (say the orbits), not to speak about the velocity distribution, for instance how to understand an isotropic velocity distribution extending to the centre when due to the central density singularity the orbits of individual stars cannot include the centre itself. The existence of a central density singularity can be justified to some extent for the case of a central black hole since then the gravitational potential in the immediate surroundings of the centre is that of point mass. However, as already remarked, the black-hole mass determines its radius, in other words since the mass must be finite, as a consequence the black-hole density (central density) will be finite. In addition, clearly, for the case of point-mass potential highly eccentric orbits of zero angular momentum are excluded. Consequently, in the immediate surroundings of the centre the velocity distribution can be hardly isotropic.

2. Some concrete proposals

In an earlier paper (Ninković, 1998) the present author considered a special case of the generalised Schuster density law. In particular, for the space density the following formula is borne in mind

$$\rho(r) = \frac{\rho(0)}{[1 + (r/r_c)^2]^{i/2}} , \qquad (1)$$

where r is the distance to the centre of the stellar system under study (assumed to be spherically symmetric), ρ is its space density, r_c is a constant parameter (system scale length or core radius), i being a non-negative integer. As easily seen, the case $i = 5$ corresponds to the classical Schuster density law. However, from the empirical point of view the special cases $i = 2$, $i = 3$ and $i = 4$ are of more interest. As indicated in the mentioned paper (Ninković, 1998), the first of them corresponds to the quasi-isothermal-sphere case applied most frequently for the purpose of describing the mass distribution anticipated in the dark-matter subsystems of galaxies, the second one ($i = 3$) is sufficiently close to the King (1962) mass distribution usually anticipated in globular clusters, whereas the last one, in view of the recent results (more precisely, density dependence of $\rho(r) \propto r^{-4}$ in outer parts - e. g. Dehnen, 1993), might be applicable to the ellipsoids of elliptical galaxies, i. e. to the bulges of spiral ones.

It should be emphasized that formula (1) has an advantage that the corresponding surface density is very easily obtainable analytically. The concrete expressions can be found in the mentioned paper (Ninković, 1998). More clearly, the expressions of both kinds - those concerning the space density and those concerning the surface one - contain algebraic functions only. This, however, need not be the case with other quantities of interest: the potential, the mean velocity squares, etc. The exception is the classical Schuster case ($i = 5$) where, if one remains in the framework of the isotropic velocity distribution, all these functions are algebraic and easily obtainable. Therefore, of interest might be alternative formulae where one has, for instance, for the potential an expression consisting of algebraic functions and which can be easily related with family (1). Such a case is with a family of potential formulae considered by Kuzmin and his disciples. Here the corresponding potential formula is given in its most general case, i. e.

$$\Pi(r) = \frac{G\kappa\mathcal{M}}{a + [b^2 + (\kappa r)^2]^{1/2}} , \qquad (2)$$

where r is, as earlier, the distance to the centre of the stellar system under study, Π is its potential, G is the gravitation constant, $\mathcal{M}$ is the total mass of the system, a, b and κ are the system parameters, the former two are the scale lengths, and the latter one is dimensionless. The Schuster classical model is a special case of (2) when $a = 0$, $\kappa = 1$. If a is different from zero, the density dependence in the outer parts is also $\rho(r) \propto r^{-4}$ (for details Ninković, 2001 and the references therein).

In the same paper (Ninković, 2001) one finds the common case of (1) and (2) for $i = 4$ (in (1)) and $\kappa = 1$ (in (2)). The use of two additional dimensionless parameters in (2) (ratio a/b and κ) offers new possibilities. For instance, the interesting special case of (1) - $i = 4$ - yields a nearly constant density within the central part, without a cusp (about this term e. g. Dehnen, 1993). However, if the observations indicate a cuspy mass distribution for a stellar system, then the special case $i = 4$ of (1) requires amendments in order to improve the fit. One way is to introduce an additional subsystem (say, a nucleus) or a formula containing more parameters, but realistic, i. e. interpreting the cusp not by means of a central singularity, but through a prominent maximum at the centre. This is possible by using (2) allowing κ to be arbitrarily large, but, nevertheless, finite. Then, as some preliminary studies of the present author show, the maximum on the circular-velocity curve will be realistic, i. e. it will occur for some value of the ratio r/b greater than zero. On the other

hand, for some models having central singularity this maximum can reach the centre, itself, or even cease to exist for steeper density slopes. A typical example is the family considered, for instance, by Dehnen (1993).

A few words may be said concerning the special case of (1) $i = 3$. It has been already compared to the King (1962) case. It should be said that, if the space density is treated correctly, one also obtains a critical value where the surface one vanishes regardless of the existence of the discontinuity at the boundary mentioned above. As indicated by the present author (Ninković, 1998), this case has already been applied to star clusters, the field of very frequent application of King's (1962) density formula.

References

Casertano, S.: 1983, *Mon. Not. R. Astron. Soc.*, **203**, 735.
de Vaucouleurs, G.: 1948, *Ann. Astrophys.*, **11**, 247.
Dehnen, W.: 1993, *Mon. Not. R. Astron. Soc.*, **265**, 250.
King, I.: 1962, *Astron. J.*, **67**, 471.
Ninković, S.: 1992, *Astron. Nachr.*, **313**, 83.
Ninković, S.: 1998, *Serb. Astron. J.*, **158**, 15.
Ninković, S.: 2001, *Serb. Astron. J.*, **164**, in press.
Plummer, H. C.: 1915, *Mon. Not. R. Astron. Soc.*, **76**, 107.
Tremaine, S., Richstone, D. O., Byun, Y.-I., Dressler, A., Faber, S. M., Grillmair, C., Kormendy, J. and Lauer, T. R.: 1994, *Astron. J.*, **107**, 634.

Publ. Astron. Obs. Belgrade No. 73 (2002), 195 - 199 *Poster*

SEARCH FOR UNDETECTED STAR CLUSTERS IN OUR GALAXY IN THE 2MASS DATABASE

P. PESSEV[1], V.D. IVANOV[2], J. BORISSOVA[3]

[1] *Department of Astronomy, Sofia University, Bulgaria*

[2] *ESO, Chile*

[3] *Institute of Astronomy, Bulgarian Academy of Sciences, Sofia, Bulgaria*

Abstract. A simple and robust method, based on stellar surface density was proposed in order to search for undetected star clusters in our Galaxy on the base of the 2MASS catalogue. The zone of the sky of galactic latitude between -80 and -40 degree was choosen to test the method. As a result we identify approx. 30% of suspected cluster candidates. Careful check of the remaining objects show that most of them are asterisms.

1. Introduction and Motivation

The known Galactic globular clusters (GC) are less than 150 (Harris 1996). The majority of them were discovered through optical searches, biased against highly obscured objects. Since the Galaxy is estimated to have 160±20 GCs (Harris 1991), a certain number of them may still be hidden behind the Galactic disk. On the other hand, according to the latest numerical predictions approximately 50 star clusters are expected to be found towards the galactic center (Portegies et al, 2001).

The Two Micron All Sky Survey (2MASS) offers an opportunity to carry out a search for missed GCs because it covers the Galactic Plane in near-infrared wavelengths where the extinction is almost ten times smaller in comparison with the optical part of the spectrum (e.g. Rieke & Lebofski 1985). The abundant dust found throughout this region obscures both Galactic and extragalactic sources. The 2MASS provides the first views in three near-infrared bands (J, H and K_S) of the entire populations of sources–ranging from galaxies in the Zone of Avoidance to stars and clusters in the Milky Way–across a significant fraction of the sky.

The purpose of this paper is to present the searching criterion for undetected star clusters and the first results for the zone of the sky of galactic latitude between -80 and -40 degrees.

2. Search Algorithm

A simple and robust method, based on stellar surface density was chosen for this project. It was implemented as a set of C codes in order to carry out the process automatically – a necessity dictated by the vast amount of data that have to be processed.

The first step was to divide 2MASS point source catalog into spatial bins. We chose square bins, to minimize the computational demands. The bin size is a free parameter, to allow searches of structures of different angular sizes on the sky. For each bin we store the total number of stars, the K_S-band luminosity function, and the distribution of stars along $J - K_S$ color.

We also select and store the "red" objects in each bin, for further analysis. We use an adaptive definition for them: (i) a polinomial separating the stellar locus from non-stellar point sources on the $[K_S, (J - K_S)]$ CMD was determined based on a inspection of star-dominated fields; (ii) for each bin the polinomial is given an offset relative to the median K_S-band magnitude, and the median $J - K_S$ color of the bin.

The result from the first step is a 2-dimensional distribution of stars on the sky. Next, we search for peaks in this 2-D histogram. For each bin we calculate the background level and its standard deviation σ from the average number of stars in the neighbouring bins. Finally, we store for future inspection and identification the "peaks" of the 2-D distribution that deviate by more than 3σ from the background value.

3. Results and Discussion

To verify our search algorithm and to explore the parametric space of the search parameters – namely the bin size and overdensity – we selected a region of the sky with low concentration of globular clusters: $0 \leq$ R.A. $\leq$ 24 hr and Dec ≤ -40 degr, far from the Galactic center.

A map of the region is given in Fig. 1. The known CGs are indicated by open circles.

The field yielded 149 cluster candidates. A search in SIMBAD databases allowed us to identify only 42 of them. In Fig. 2 are shown histograms of standard deviation σ and number of stars in the selected bins. Solid lines are for cluster candidates, dotted lines indicate the "known" objects.

Analysis of Fig. 2 shows that 28% of cluster candidates are identified. Only 2% of them have $\sigma \leq 4$ and N_{star} (number of stars in the bin) more than 150. The careful check of these cluster candidates shows, that they are usually situated in very reach fields in Magelanic Clouds and Galaxy. We exclude them from future analysis and prepare list of so-called "most probable candidates". They are given in Table 1. The coordinates given in Columns 2 and 3 represent the center of the bins.

The above selected star cluster candidates were checked in Simbad on R plates. Ten of them which are situated in dense and crowded fields are examined on J,H,K Quick View images. Another 7 clusters are identified as LMC clusters. The remaining cluster candidates are probably asterisms, except 5 candidates which could be star clusters. The coordinates of their centers are given in Table 2.

Further analysis of the color-magnitude diagrams and follow-up observations are necessary to confirm the status of star cluster candidates given in Table 2.

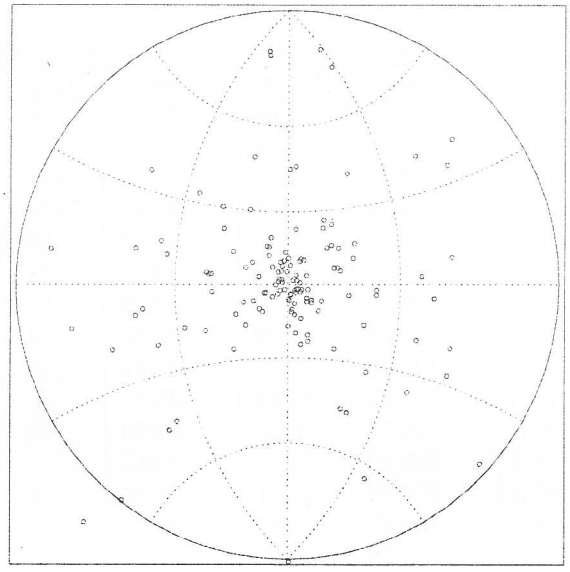

Fig. 1: Map of the test field. The known Galactic GCs are indicated as open circles.

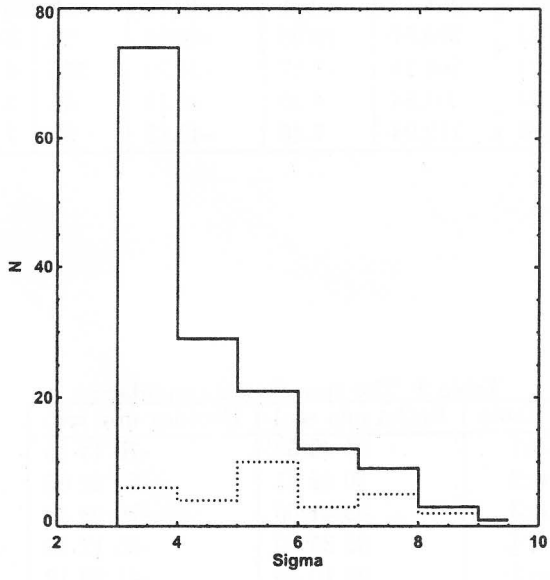

Fig. 2: Histograms of standard deviation σ and number of stars in the bins. Solid lines are for cluster candidates, dotted lines indicate the "known" objects.

Table 1: The coordinates of the selected objects

Name	Ra(deg)	Ra(ha)	Dec(deg)	N_{star}	σ
obj1	84.54	5.64	-71.54	78	3
obj2	85.38	5.69	-70.38	123	3
obj3	77.71	5.18	-70.21	113	3
obj4	85.79	5.72	-69.63	120	4
obj5	126.87	8.45	-59.87	58	6
obj6	129.62	8.64	-59.87	71	5
obj7	131.45	8.76	-59.29	95	6
obj8	128.95	8.59	-55.37	114	9
obj9	132.29	8.81	-48.12	245	5
obj10	342.12	22.80	-46.87	46	6
obj11	98.70	6.58	-41.70	48	5
obj12	289.62	19.30	-41.62	88	5
obj13	277.79	18.51	-41.37	158	5
obj14	102.45	6.83	-41.29	59	6
obj15	115.20	7.68	-41.29	109	6
obj16	104.79	6.98	-41.04	65	6
obj17	297.87	19.85	-41.04	46	5
obj18	119.29	7.95	-40.87	149	7
obj19	112.95	7.53	-40.79	99	7
obj20	105.62	7.04	-40.70	59	6
obj21	296.79	19.78	-40.70	54	5
obj22	299.37	19.95	-40.54	55	5
obj23	268.16	17.87	-40.29	358	6
obj24	103.54	6.90	-40.12	48	5
obj25	112.04	7.46	-40.12	89	7

Table 2: The star cluster candidates

Name	Ra(ha min sec)	Dec(deg min sec)
cc1	05 42 39	-70 14 18
cc2	10 42 41	-62 32 02
cc3	05 41 06	-70 23 33
cc4	08 35 30	-55 12 13
cc5	08 10 49	-41 20 12

4. Acknowledgments

This publication makes use of data products from the Two Micron All Sky Survey, which is a joint project of the University of Massachusetts and the Infrared Processing and Analysis Center/California Institute of Technology, funded by the National Aeronautics and Space Administration and the National Science Foundation. This research was supported in part by the Bulgarian National Science Foundation grant under contract No.F-812/1998 with the Bulgarian Ministry of Education and Sciences. J.B. thanks Mr. Borissov for financial support.

References

Harris, W. : 1991, *Ann. Rev. Astron. Astrophys.*, **29**, 543.
Harris, W. : 1996, *Astron. J.*, **112**, 1487.
Rieke, G. H., Lebofski, M. J. : 1985, *Astrophys. J.*, **288**, 618.
Portegies, Z., Simon, F., Makino, J., McMillan, St., Hut, P. : 2001, *Astrophys. J.*, **546**, 101.

Publ. Astron. Obs. Belgrade No. 73 (2002), 201 - 206 *Poster*

THE S4 SPIRAL ARM IN M 31
GALAXY - INFRARED VERSUS OPTICAL

GEORGI POPOV[1], PETKO NEDIALKOV[2], ILIJA ROUSSEV[3] and TODOR VELTCHEV[2]

(1) Faculty of Physics, University of Plovdiv, Tsar Asen 24, Plovdiv 4000, BULGARIA
(2) Department of Astronomy, University of Sofia, James Bourchier 5, Sofia 1164, BULGARIA
(3) Center for Space Environment Modeling, 1414 Space Research Building, The University of Michigan, Ann Arbor, MI 48109-2143, USA
E-mail goro_popov@hotmail.com
E-mail japet@phys.uni-sofia.bg
E-mail ilr@vortex.engin.umich.edu
E-mail eirene@phys.uni-sofia.bg

1. INTRODUCTION

The spiral arms of M 31 have been a subject of extensive studies over the last two decades in the Department of Astronomy at the University of Sofia (Ivanov & Golev 1984, Ivanov 1984, Georgiev & Ivanov 1985, Kurtev & Ivanov 1986, Nikolov & Tasheva 1989, Nedialkov & Ivanov 1999, Veltchev et al. 1999, Kurtev 2002). The fragment of the spiral arm S4 along the major axis is extremely interesting region because the existing wealth of data on the stellar content as well on the hydrogen (atomic and molecular) and PAH dust emission (Lequeux 2000) offers an excellent opportunity to discover the fine details of star formation history (Chernin et al. 1995) in this Local Group galaxy. We describe here a technique to obtain continuous maps of the stellar populations, and present some preliminary results.

2. TECHNIQUE

The discrete distribution of the stars presents a significant difficulty while trying to compare the spatially distributed parameters of stellar populations with continuous radio or mid-infrared maps.

This problem prompted us to convolve the discrete stellar distributions with Gaussian filters. Our approach has multiple advantages:

1. It takes into account both the number and the apparent magnitudes of the observed stars.

2. The convolution allows us to obtain a continuous picture of the surface brightness from which the background and foreground contamination can be subtracted easily.

3. It alleviates the blending problem which affects severely the individual extinction estimates.

4. The comparison with other 2-dimensional distributions is straightforward.

5. The investigation of the various hierarchical structures (clusters, OB associations, young star complexes and dust clouds), is simplified since they all are defined as regions encompassed by isophotes of constant surface brightness or lines of constant color.

The individual stars were treated as δ-functions. We implemented Gaussian filters with standard deviation $\sigma = 20''$, cut-off levels of 3σ and peak values of $10^{-0.4 \times \mathrm{magnitude}}/(\mathrm{pixel\ size})^2$, and the pixels size is $2''$.

3. DATA

We used archival near-infrared and optical photometry for a $20' \times 20'$ field, centered at $\alpha(2000) = 0^{\mathrm{h}}\,40^{\mathrm{m}}\,40^{\mathrm{s}}$ and $\delta(2000) = 40°\,39'\,30''$ (see Lequeux 2000).

The JK photometry of 277 stars was taken from the *Two Micron All Sky Survey* (2MASS) and was selected as follows: $\mathrm{K} > 12.6^{\mathrm{m}}$ and $\mathrm{J} - \mathrm{K} > 1.2^{\mathrm{m}}$. The comparison with a nearby field of equal area well outside the boundaries of M 31 and at the same Galactic latitude indicates a contamination of less than 15% (Fig. 1). The optical photometry (BV) was compiled from the catalog of Magnier et al. (1992), imposing criteria: $\mathrm{V} > 16.5^{\mathrm{m}}$ and $\mathrm{B} - \mathrm{V} < 0.4^{\mathrm{m}}$. It consists of 1473 stars. As seen in Fig. 3, the foreground contamination is negligible.

The color and magnitude criteria described above were designed to select massive stars. Indeed, Figs. 2 and 4 show that the majority of objects in our sample is located inside the boundaries of the classical "OB associations" as delineated by van den Bergh (1966).

4. RESULTS

1. Several subgroups of enhanced surface brightness within the stellar complexes are detected and the brightest of them have typical sizes of $\sim 60''$ (~ 200 pc).

2. The spiral arm S4 is much more prominent and tighter in the K-band (Fig. 5) than in the optical (Fig. 6), suggesting that the near infrared wavebands are more reliable for tracing of the spiral arms.

3. There exists a well defined offset between the ridge of the gas arm and the surface brightness in K, especially strong in the region of OB 78, and between the inner side of OB 82 and OB 81.

4. The association OB 79 has no gas and relatively few RGS candidates, yet it is extremely reach of OB stars, probably indicating a recent burst of star formation.

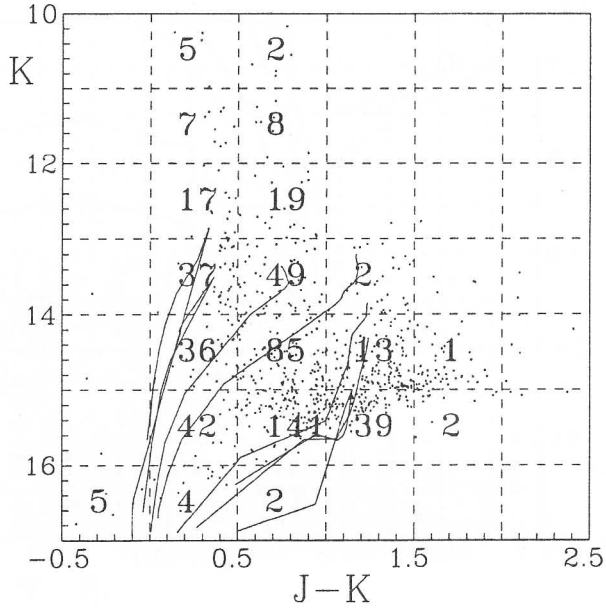

Fig. 1: All stars with JHK photometry from 2MASS catalog within the selected area. The number of predicted (foreground+background) contamination objects is shown in several bins.

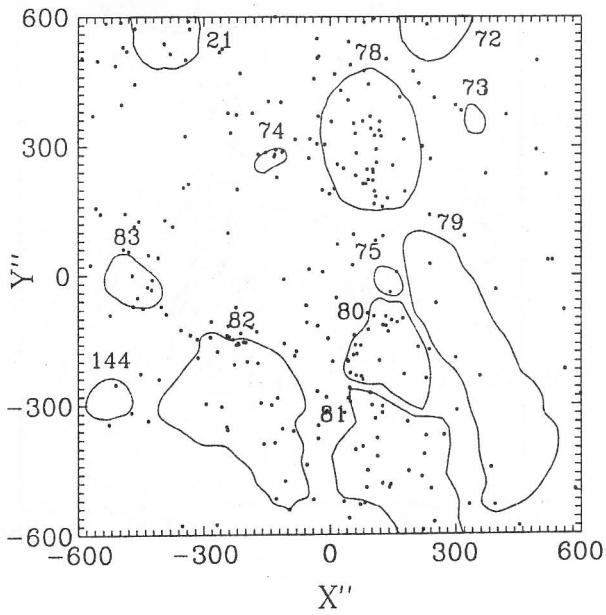

Fig. 2: Red supergiants candidates within the same area with the outlined boundaries of the OB associations (van den Bergh, 1964).

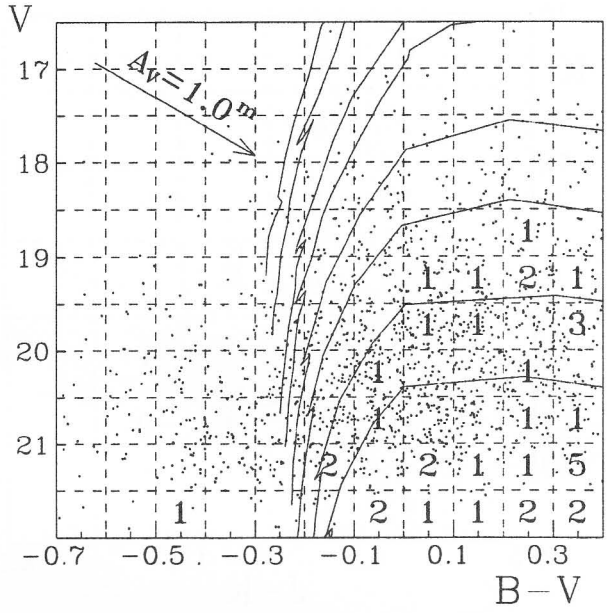

Fig. 3: Blue stars from the catalog of Magnier et al. (1992) within the selected area.

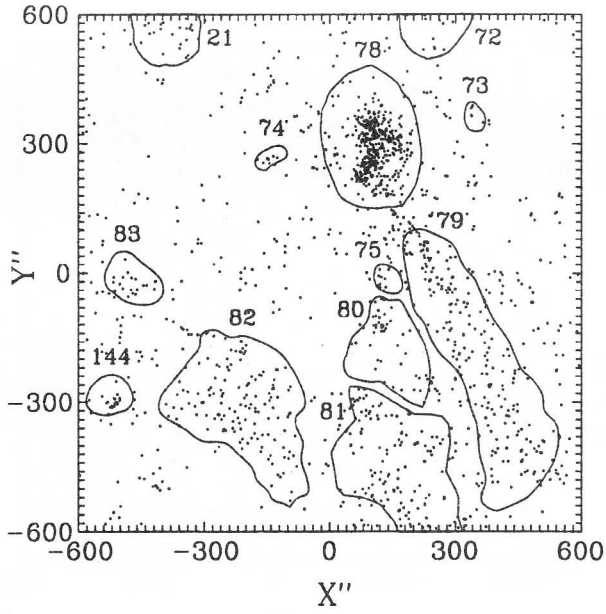

Fig. 4: The positions of the stars from Fig. 3 with the outlined boundaries of the OB associations (van den Bergh, 1964).

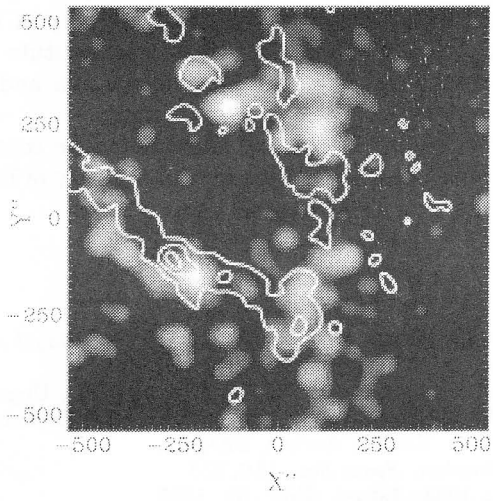

Fig. 5: A grey-scale surface brightness map in K-band, obtained after convolution of the stars from Fig. 2 with 2D gaussians (st. dev. = 20″). The values of μ_K vary from 20.2^m (white) to 24.1^m per square arcsec (black). The contours indicate the CO($1 \rightarrow 0$) line intensity from the map of Guelin et al. (2000). Levels are from 2 to 17 K km/s in steps of 5 K km/s.

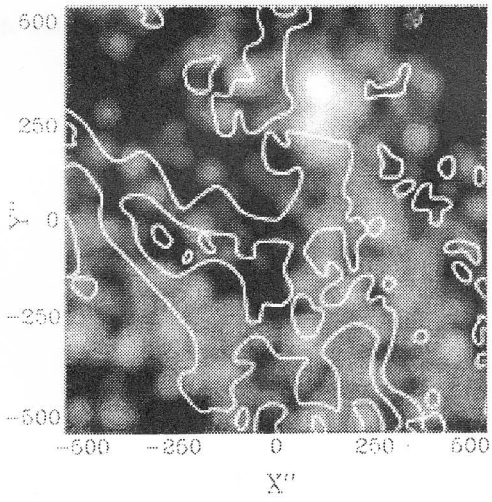

Fig. 6: A grey-scale surface brightness map in B-band, obtained after convolution of the stars from Fig. 4 with 2D gaussians (st. dev. = 20″). The values of μ_B vary from 23^m (white) to 30^m per square arcsec (black). The contours indicate the 21 cm H I line integrated intensity from data in Brinks & Shane (1984). Levels are from 1500 to 3000 K km/s in steps of 500 K km/s.

Acknowledgments. This publication makes use of data products from the *Two Micron All Sky Survey*, which is a joint project of the University of Massachusetts and the Infrared Processing and Analysis Center/California Institute of Technology, funded by the National Aeronautics and Space Administration and the National Science Foundation.
P. N. and T. V. acknowledge the partial support by the contract Nr. F- 825/1998 with the Bulgarian National Science Foundation, Ministry of Education and Sciences.

References

Chernin, A., Efremov, Yu., Voinovich, P.: 1995, *Mon. Not. Royal Astron. Soc.*, **275**, 313.
Georgiev, Ts., Ivanov, G.: 1985, *Astron. Letters*, **11**, 73.
Guelin, M., Nieten, C., Neininger, N., Muller, S., Lucas, R., Ungerechts, H., Wielebinski, R.: 2000, *Proc. 232. WE-Heraeus Seminar*, Bad Honnef, Germany; Eds. E. Berkhuijsen, R. Beck, R. Walterbos. Shaker, Aachen, 2000, 15.
Ivanov, G.: 1984, *Astrophys. Space Sci.*, **110**, 357.
Ivanov, G., Golev, V.: 1984, *Astron. Tsir.*, Nr. 1352.
Kurtev, R., Ivanov, G.: 1986, *Astron. Tsir.*, Nr. 1435.
Kurtev, R.: 2002, *UB stellar photometry around the association OB81 in M31* (this symposium).
Lequeux, J.: 2000, *Proc. 232. WE-Heraeus Seminar*, Bad Honnef, Germany; Eds. E. Berkhuijsen, R. Beck, R. Walterbos. Shaker, Aachen, 2000, 63.
Magnier, E., Lewin, W., van Paradijs, J., Hasinger, G., Jain, A., Pietsch, W., Truemper, J.: 1992, *Astron. Astrophys. Suppl. Series*, **96**, 379.
Nedialkov, P., Ivanov, V.: 1999, *Astron. Astrophys. Trans.*, **17**, 367.
Nikolov, N., Tasheva, R.: 1990, *Astrophys. Space Sci.*, **170**, 257.
van den Bergh, S.: 1964, *Astrophys. J. Suppl. Series*, **9**, 65.
Veltchev, T., Nedialkov, P., Ivanov, G.: 1999, *Rev. Mex. Astron. Astrofis.*, **35**, 13.

Publ. Astron. Obs. Belgrade No. 73 (2002), 207 - 210 *Poster*

THE PROBLEM OF THE Fe II TEMPLATE IN AGNs

L. Č. POPOVIĆ, M. S. DIMITRIJEVIĆ, M. DAČIĆ, A. KUBIČELA[1]

[1]*Astronomical Observatory, Volgina 7, 11160 Belgrade, Yugoslavia*
E-mail lpopovic@aob.aob.bg.ac.yu

Abstract. In order to make a template for fitting and subtracting the Fe II emission lines in the H_β wavelength range, we applied an approximate relation for the Fe II line relative intensities as a function of temperature. Using the obtained relative intensities we fitted the H_β wavelength range of several AGNs. We found a good fit of the redshelf of H_β with our Fe II template.

1. Introduction

The Fe II template offers a handly tool in studying the warm emitting gas in Broad Line Regions (BLRs) of active galactic nuclei. Several papers were published to study the Fe II template in UV and optical regions (see e.g. Vestergaard and Wilkes 2001, and references therein). One of the frequently investigated problem is the Fe II template in the H_β wavelength range, since the template contributes to the red wing of H_β and before an analysis of the H_β line profile is made, the template has to be subtracted (see e.g. Popović et al. 2001).

The aims of this paper are: 1) to estimate the contribution of Fe II template to the red part of H_β wavelenght range; 2) to find a suitable intensity ratio of Fe II template which can be used for subtraction of redshelf from H_β line.

2. Observations

We use HST observations obtained with the Space Telescope Imaging Spectrograph (STIS), covering the wavelength range 2900-5700 Å for three AGNs 3C120, Mrk 493 and I Zw1. The grating G430L, was used to cover the observed spectral range as a whole. The dispersion of the spectra was 2.747 Å/pixel. The spectra were reduced by the HST team. We transform the wavelength scale to zero redshift taking into account the cosmological red-shifts of the observed AGNs (e.g. Véron-Cetty and Véron 2000). After that we estimate and subtract the continuum, taking as the reference wavelengths: 3750 Å, 3900 Å, 4050 Å, 4200 Å, 4450 Å, 5100 Å, and 5600 Å.

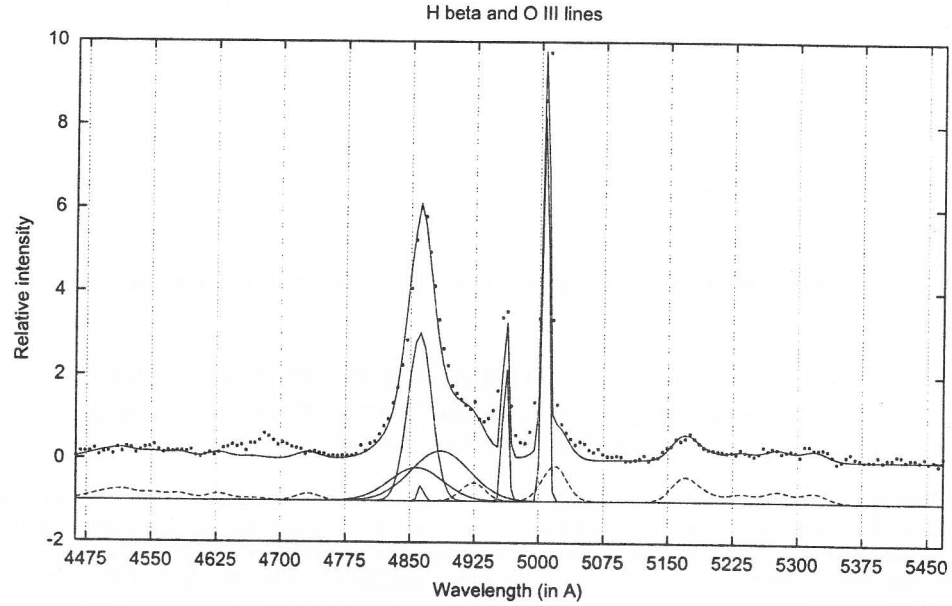

Fig. 1: The wavelength range of 3C 120 H_β line fitted with Fe II template and Gaussian functions for H_β and [OIII] lines. The dots represent observations, and the solid line the best fit. The Gaussian components and Fe II template decomposition are presented at the bottom (dashed line).

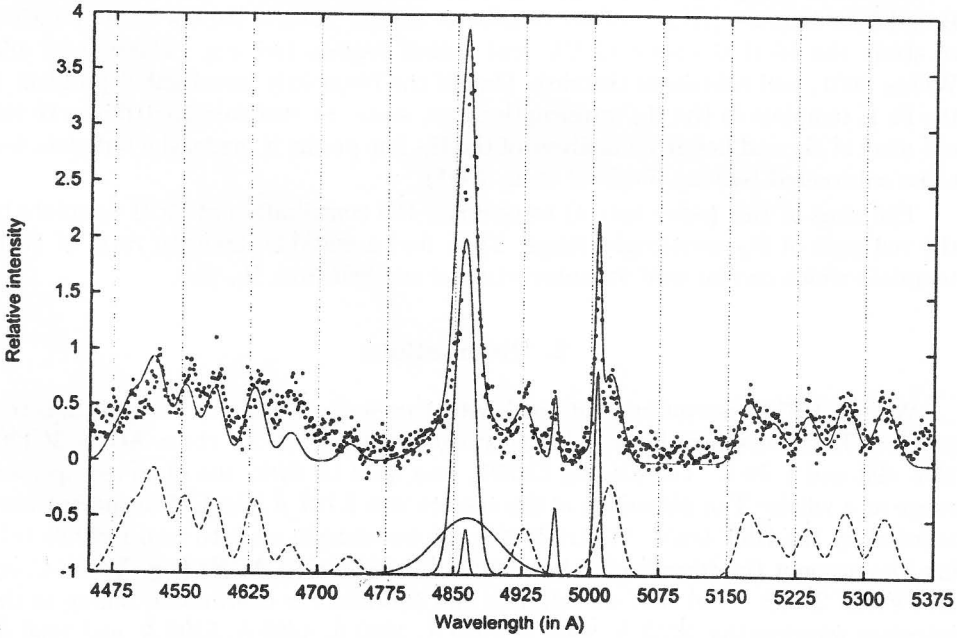

Fig. 2: The same as in Fig. 1, but for Mrk 493.

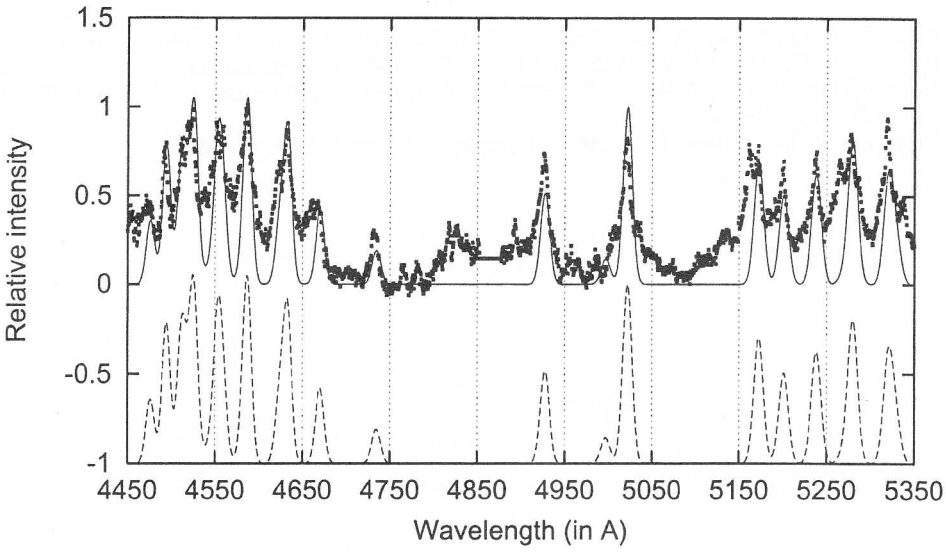

Fig. 3: The same as in Fig. 1, but for I Zw1

3. The intensity ratio of Fe II template

First we have indentified the Fe II lines which are present in the spectra of I Zw 1 and we found that the three types of transitions are present, where the lower levels are $3d^5 4s^2\ ^6S$, $3d^6(^3F2)4s\ ^4F$ and $d^6(^3G)4s\ ^4G$.

We selected the lines from these three types, assuming that the intensity ratio within the transitions which have the same lower level is

$$\frac{I_1}{I_2} = (\frac{\lambda_2}{\lambda_1})^3 \frac{f_1}{f_2} \cdot \frac{g_1}{g_2} \cdot e^{-(E_1 - E_2)/kT},$$

where I_1 and I_2 are intensities of the lines, λ_1 and λ_2 are transition wavelengths, f_1 and f_2 are oscillator strengths, g_1 and g_2 are the corresponding statistical weights, E_1 and E_2 are energies of upper levels, k is the Boltzman constant and T is the electron temperature.

We have assumed that each of lines can be represented by a Gaussian with the width and shift (w and d) and for all Fe II lines w/λ and d/λ are the same. It means that all Fe II lines from template originate from the same region with the same kinematical properties. The results of our fit are shown in Figs. 1-3.

4. Conclusion

As one can see from Figs. 1-3, our approximation for Fe II template in the H_β wavelength range can satisfactorily fit the template and can be used for subtracting the template from the red wing of Sy 1 and QSO H_β lines. The detailed discussion will be given elsewhere (Popović et al. 2002).

References

Popović, L. Č., Stanić, N., Kubičela, A., Bon, E.: 2001, *Astron. Astrophys.*, **367**, 780.
Popović, L. Č., Dimitrijević, M.S. and Dačić, M.: 2002, in preparation.
Véron-Cetty, M.-P. and Véron, P.: 2000, *A Catalogue of Quasars and Active Galactic Nuclei*, Sci. Report 19.
Vestergaard, M., Wilkes, B.J.: 2001, *Astrophys. J. Suppl. Series*, **134**, 1.

Publ. Astron. Obs. Belgrade No. 73 (2002), 211 - 214 *Poster*

THE SPECTRAL LINE SHAPES OF MRK 1040 AND SMALL NEIGHBOURING GALAXY

L. Č. POPOVIĆ[1], E. BON[1], D. ILIĆ[1]
[1]*Astronomical Observatory, Volgina 7, 11000 Belgrade, Yugoslavia*
E-mail lpopovic@aob.bg.ac.yu
E mail ebon@aob.bg.ac.yu
E-mail dilic@aob.bg.ac.yu

Abstract. The spectra of Mrk 1040 and UGC 01935 were observed with Isaac Newton Telescope (INT) on January 24 and 25 at the same time (both object were in the slit). We have analyzed the H_β and H_α emission line shapes and shifts of these two Active Galactic Nuclei (AGNs).

1. Introduction

Mrk 1040 is a Seyfert 1 galaxy (z=0.016) (Reynolds et al. 1995), with a companion galaxy UGC 01935 distant about 20" to the north along the minor axis (Colbert et al. 1996). The compact object is clasified as S01 type G.

In this paper we present our observations of H_α and H_β emission line spectral regions of these galaxies.

2. Observation and data reduction

Mrk1040 and UGC 01935 were observed with 2.5 m Isaac Newton Telescope at La Palma, in the period between 21th and 25th of January. The observation contained Balmer series of emission lines. We observed the spectra around H_α

and H_β line of both objects within the same slit. The slit was 1". The Intermediate Dispersion Spectrograf (IDS) and the 235 camera in combination with the R1200y greating were used.

Each set of observations contained 3 spectra with exposure time of 1400 sec. CuNe and CuAr lamps were used for wavelength calibration. Reduction of data was performed using IRAF and DIPSO software packages.

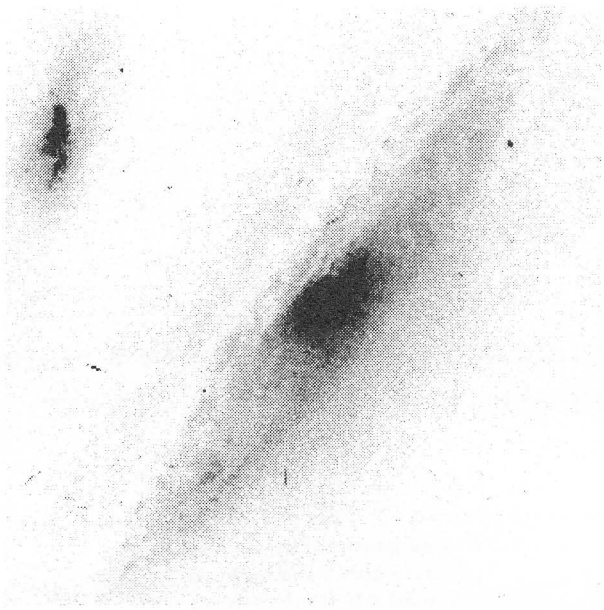

Fig. 1: Mrk 1040 and UGC 01935 photo from Palomar 48-inch Schmidt telescope (Ref. NED)

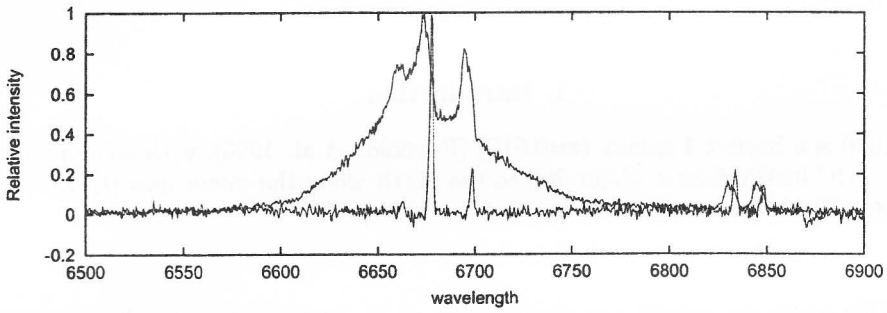

Fig. 2: Comparison of $H\alpha$ line of MRK 1040 and UGC 01935

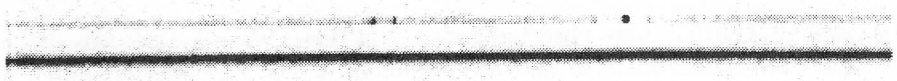

Fig. 3: Spectra around $H\alpha$ line of Mrk1040 and UGC 01935 within the same slit

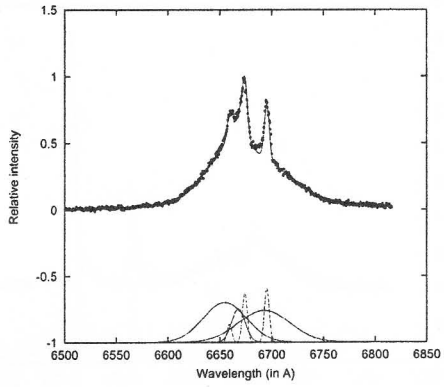

Fig. 4: Decomposition of the H_α line. The dots present observation and solid line is the best fit obtained by Gaussian decomposition. The Gaussian components are shown at the bottom of the figure

Mrk1040: The H_α can be decomposed into four Gaussian components; three broad ones and one narrow. Narrow component has the same width (w) and shift (z) as N II lines $\frac{w}{\lambda} = 0.0005$ ($w = 150\frac{km}{s}$), and $z = 0.01697$. The three broad Gaussian components have parameters: a) blueshifted with respect to cosmological redshift $w = 1350\frac{km}{s}$, $z = 0.014$; b) central $w = 430\frac{km}{s}$, $z = 0.016$; c) redshifted with respect to cosmological redshift $w = 1620\frac{km}{s}$, $z = 0.0198$.

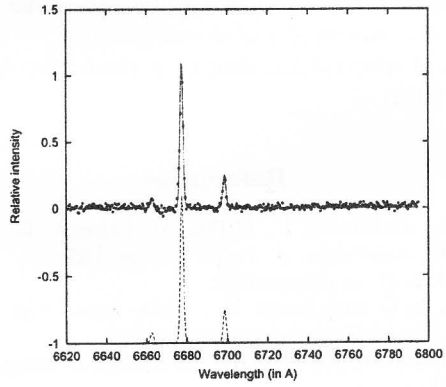

Fig. 5: The same as in Fig. 4. but for the UGC 01935 H_α line

UGC 01935: The $H\alpha$ and N II lines have the same redshift and width and can be represented by one Gaussian component with parameters: $w = 50\frac{km}{s}$, $z = 0.0175$. Weak apsorbtion lines at the $z = 0.0169$ from Mrk 1040 are present.

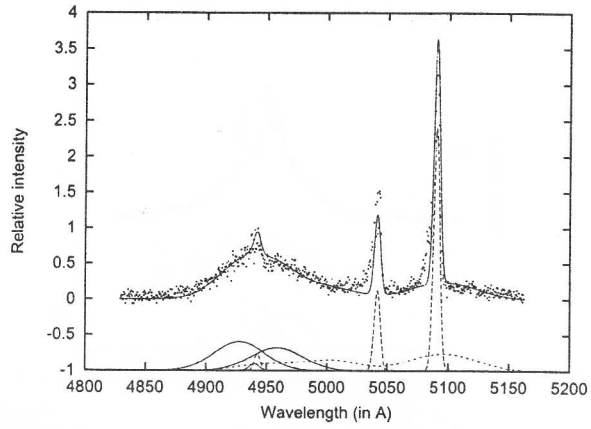

Fig. 6: The same as in Fig. 4. but for the H_β profile of Mrk 1040. The dashed complex line at the bottom represents combination of Fe II complex

3. Results

As one can see in Fig 2. the redshift of the UGC 01935 is higher ($z = 0.0175$) than that of Mrk 1040. Using their redshift and assuming that $H_0 = 50\frac{km}{s}/Mpc$, $\Omega_0 = 1$, we obtained that the distance between these galaxies is about 3.4 Mpc. The line shape of MRK 1040 H_α is typical for Sy 1 galaxy, while line width of UGC 01935 H_α is characteristic for LINERs.

As one can see from Figs 4-6 the H_β and H_α lines of Mrk 1040 are very complex and can be decomposed into three broad components, while the lines of UGC 01935 can be represented by one narrow Gausian component.

Detailed discussion of spectral line shapes of these two objects will be given elsewhere (Popović et al. 2002)

References

Colbert, J. M., Baum, A., Gallimore, F., O'Dea, P., Lehnert, D., Tsvetanov, I., Mulchaey, S., Caganoff, D. : 1996, *Astrophys. J. Suppl. Series*, **105**, 75.

Popović, L. Č, Bon, E., Ilić, D. in preparation.

Reynolds, C. S., Fabian, A. C. and Inoue, H. : 1995, *Mon. Not. Roy. Astron. Soc.*, **276**, 1311.

NED : 1994. - The Digitized Sky Survey: 102 CD-ROMs of images compressed by a factor of 10., 1994. DSS, 1, 0.

Publ. Astron. Obs. Belgrade No. 73 (2002), 215 - 218 *Poster*

COULD THE SHAPE OF Mrk 205 Fe Kα LINE BE EXPLANED BY MICROLENSING EFFECT?

L. Č. POPOVIĆ[1] and P. JOVANOVIĆ[1]
[1] *Astronomical Observatory, Volgina 7, 11160 Belgrade, Yugoslavia*
E-mail lpopovic@aob.bg.ac.yu
E-mail pjovanovic@aob.bg.ac.yu

Abstract. We discuss the unusual shape of Mrk 205 Fe Kα line in the light of microlensing influence of a caustic from the galaxy NGC 4319. The shape of the Fe Kα line may be described as disc emitted line deformed by microlensing effect of a star with mass less than 0.2 $M_\odot$ from the NGC 4319 star disc. In the paper we discuss the two scenarious of line variation, if the microlensing effect is present.

1. Introduction

The objects Mrk 205 and NGC 4319 are interesting, because their nuclei are close each other. Mrk 205 is a low redshifted (z=0.071), low luminosity quasar ($M_V = -23$) located only about 0.7′ away from the center of the nearby spiral galaxy NGC 4319 (z=0.00468). In many papers the possibility of their physical connection was discussed (Burbridge 1996, Bubridge and Hoyle 1996, Arp 1998). On the other side, Baryshev & Ezova (1998) and Bukhmastova (2001) explained the appearance of quasar-galaxy pairs (as Mrk 205 - NGC 4319) by theorizing that distant AGNs experienced mesolensing by globular clusters in the halos of more nearby galaxies.

The quasar is viewed through the outer disc of the galaxy (Bahcall et al. 1992, Bowen & Blades 1993). The shape of UV and optical lines are typical for quasars and Sy 1 galaxies (Bahcall et al. 1992, Corbin & Boroson 1995), while it has an unusual weak UV bump (McDowell et al. 1989), indicating that the thermal disc emission is hidden in extreme UV. Recent observations with XMM-Newton have revealed a remarkable Fe K_α line profile (Reeves et al. 2001). The profile can be resolved into a narrow component located at 6.4 KeV and a broad component at 6.7 KeV which is inconsistent with the relativistic profile expected from the inner accretion disc (Fabian et al. 1989) assumed to be present in majority of Active Galactic Nuclei (AGNs) (Nandra et al. 1997). In the paper Reeves et al. (2001) it was suggested that the broad component at 6.7 KeV is 'most likely' originating from X-ray reflection off the surface of a highly ionised accretion disc.

Concerning the fact that the Mrk 205 is viewed through the outer disc of the NGC 4319, the microlensing effect of stars from the outer disc can influence on the emission line shape. Recently (Popović et al 2001ab, 2002ab) considered the influence

of microlensing on the spectral line profile generated by a relativistic accretion disc in the Schwarzschild geometry, finding that significant changes in the line profile can be induced by microlensing. The scope of these studies has been the region where the broad X, UV and optical lines are generated. However, microlensing detection should be much more favourable in the tiny region generating the X-Ray radiation (Popović et al. 2001b, 2002ab). Thus it seems clear that the Fe Kα line can be strongly affected by microlensing and recent observations of two lens systems seem to support this idea (Oshima et al. 2001, Chartas et al. 2002).

In this paper we are going to discuss the unusual Mrk 205 Fe K$_\alpha$ line profile (Reeves et al. 2001) considering the possibility that such line profile is due to microlensing effects caused by a star from the foreground galaxy NGC 4319.

2. Results

Influence of the microlensing effect on a line generated by a relativistic accretion disc rotating around a Black Hole (BH) is analyzed in paper Popović et al. (2002a), where the ray tracing method (Bao et al. 1994, Bromley et al.1997, Fanton et al. 1997, Čadež et al. 1998) for line profile calculation were used.

2. 1. ESTIMATION OF THE CAUSTIC PARAMETERS

To model the unusual Mrk 205 Fe K$_\alpha$ line shape first we calculated the Einstein Ring Radius (ERR) expressed in gravitational radii (GM/c^2) for different masses of the lens which belongs to the NGC 4319 using the relation

$$\eta_0 = \sqrt{\frac{4GM_{ml}}{c^2} \cdot \frac{D_s D_{ds}}{D_d}}, \tag{1}$$

where G is the gravitational constant, M_{ml} is the mass of the lens, and D_s, D_d and D_{ds} are the angular distances between observer – source, observer – deflector and deflector source, respectively. The distances can be calculated using the relation (Grogin & Narayan 1996)

$$D(z_i, z_j) = \frac{2c}{H_0} \frac{(1 - \Omega_0 - G_i G_j)(G_i - G_j)}{\Omega_0^2 (1 + z_i)(1 + z_j)^2} \tag{2}$$

where H_0 is the Hubble constant and z_i, z_j are the redshifts, here we suppose that H_0=50, and Ω_0=1. The factors $G_{i,j}$ are

$$G_{i,j} = \sqrt{1 + \Omega_0 z_{i,j}} \tag{3}$$

Finally, for the case of Mrk 205 and NGC 4319 we obtained the relation between the ERR (in gravitational radii) and mass of deflector (in Solar masses) as

$$\eta_0 = 6476\sqrt{M_{ml}}. \tag{4}$$

The ERRs for three masses of deflector are given in Table 1. As one can see from the Table 1, very small objects (about 0.001 M$_\odot$) have enough ERR to cover a big part of X-ray accretion disc (order of hundred gravitational radii).

Table 1: The mass of lenses and corresponding ERR in gravitational radii for the case of Mrk 205 and NGC 4319

M_{ML} ($M_\odot$)	0.001	0.01	1
ERR (R_g)	204	647	6476

For further calculation we accepted the parameters of caustic (Popović et al. 2002a): $\beta = 1$, $A_0 = 1$ and we tested the line profile shape changing the position of the caustic as well as the ERR.

2. 2. MODELING OF MRK 205 FE K_α LINE

In order to compare the modeled profile with the observed one, we took observations from Reeves et al. (2001). First we subtracted the continuum as was proposed in Reeves et al. (see their Fig. 2), after that we compared our calculated profile with the observed one. We accepted that narrow line located at 6.4 KeV (rest frame) is arising from a neutral matter distant from the black hole (Reeves et al. 2001), and we modeled only the broad component with the peak at 6.7 keV.

First we started from the parameters of the emitting disc proposed by Reeves et al. (2001): $i = 45°$, $R_{out} = 1000\ R_g$ and emissivity of $p = -2.5$, but we found the best fit with following parameters: $i = 40°$, $R_{inn} = 10\ R_g$, $R_{out} = 500\ R_g$, p=-2.5. The location of caustic is at $X_c = -90$, $Y_c = 0$ and that ERR is about 2800 R_g that corresponds to a star with mass less than 0.2 Solar masses. In Figure 1. the comparison of the observed line profile with the calculated one is presented. As we can see from that figure, the model of an accretion disc plus microlensing effects of a star from NGC 4319, can describe the broad component of Mrk 205 Fe K_α line.

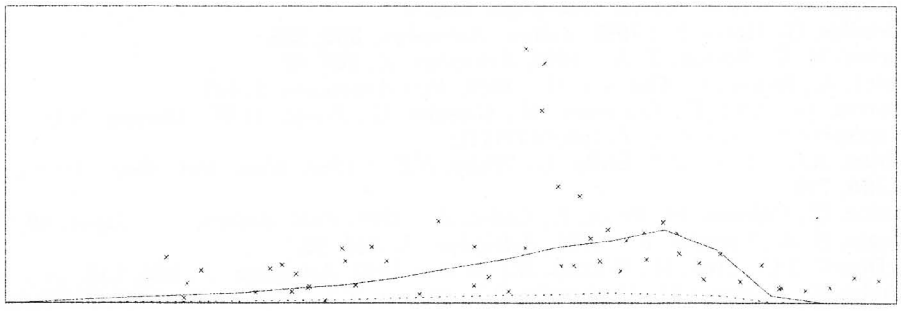

Fig. 1: The fit (solid line) of observed data (x-x-x) with the XMM-Newton (EPIC MOS and PN detectors) in comparison with the undisturbed disc line (dashed).

Moreover, we calculated the line profile in future if the MLE influence is present. The line profile would change in two ways, depending on the caustic motion direction. If caustic would cross from the approaching to the receding part of the disc the line would arise in intensity and peak of the line would move to the approaching side. After the caustic crosses the central part, the peak would move to the receding part and line would again become weaker. On the other side, if the movement of the caustic

is from the receding to the approaching side, the line would change very slowly, and peak would move to the red part of the line, but not as dramatically as in the previous case.

3. Discussion and Conclusion

We considered the possibility that the unusual line profile of Mrk 205 Fe K_α line is caused by microlensing effect of a star from the NGC 4319 stellar ring, and we found:

1) That small objects (of the order of 0.001 $M_\odot$) from the NGC 4319 stellar ring can produce significant changes in Mrk 205 Fe K_α line profile.

2) That the unusual shape of Mrk 205 Fe K_α line can be modeled by emission of an accretion disc with parameters $i = 40°$, $R_{inn} = 10\ R_g$, $R_{out} = 500\ R_g$ p=-2.5 which emission is deformed by a caustic from the NGC 4319 stellar disc. We found that the location of the caustic is at $X_c = -90$, $Y_c = 0$ and that ERR is 2800 R_g corresponding to a star with the mass less than 0.2 Solar masses.

3) That if the unusual Fe K_α profile is due to MLE influence we can expect the two scenarios of the line variation depending on caustic motion direction. An extended discussion about this will be published elsewhere (Popović et al. 2002b)

References

Arp, A. : 1998, *Quasars, Red-shifts and Controversies*, Cambridge Univ. Press, Cambridge.

Bahcall, J.N., Jannuzi, B.T., Schneider, D.P., Harig, G.F., Jenkins, E.B. : 1992, *Astrophys. J.*, **398**, 495.

Bao, G., Hadrava, P., Ostgaard, E. : 1994, *Astrophys. J.*, **435**, 55.

Baryshev, Yu.V., Ezova, Yu. L. : 1998, *Astron. Zh.*, **74**, 497.

Bowen, D.V., Blades, J.C. : 1993, *Astrophys. J.*, **403**, L55.

Bromley, B.C., Chen, K., Miller, W.A. : 1997, *Astrophys. J.*, **475**, 57.

Bukhmastova, Yu.V. : 2001, *Astron. Zh.*, **78**, 675.

Burbidge, G. : 1996, *Astron. Astrophys.*, **309**, 9.

Burbidge, G., Hoyle, F. : 1996, *Astron. Astrophys.*, **309**, 335.

Corbin, M. C., Borson, T. A. : 1996, *Astrophys. J.*, **107**, 69.

Čadež, A., Fanton, C., Calivani, M. : 1998, *New Astronomy*, **3**, 647.

Chartas, G., Agol, E., Eracleous, M., Garmire, G., Bautz, M.W., Morgan, N.D. : 2002, accepted to *Astrophys. J.*, (ph/0112112).

Fabian, A.C., Rees, M.J., Stella, L., White, N.E. : 1989, *Mon. Not. Roy. Astron. Soc.*, **238**, 729.

Fanton, C., Calivani, M., Felice, F., Čadež, A. : 1997, *Publ. Astron. Soc. Japan*, **49**, 159.

Grogin, N. A., Narayan, R. : 1996, *Astrophys. J.*, **464**, 92.

McDowell, J.C., Elvis, M., Wilkers, B.J. et al. : 1989, *Astrophys. J.*, **345**, L13.

Nandra, K., George, I.M., Mushotzky, R.F., Turner, T.J., Yaqoob, T. : 1997, *Astrophys. J.*, **477**, 602

Oshima, T., Mitsuda, K., Fujimoto, R., Iyomoto, N., Futamoto, K. et al. : 2002, *Astrophys. J.*, **563**, L103.

Popović, L.Č., Mediavilla, E.G., Muñoz, J. : 2001a, *Astron. Astrophys.*, **378**, 295.

Popović, L.Č., Mediavilla, E.G., Muñoz, J., Dimitrijević, M.S., Jovanović, P. : 2001b, *Serb. Aston. J.*, **164**, 53 (Also, presented on GLITP Workshop on Gravitational Lens Monitoring, La Laguna, Canary Islands, Spain).

Popović, L.Č., Mediavilla, E.G., Jovanović, P., Muñoz, J. : 2002, *Astron. Astrophys.*, in press.

Popović, L.Č., Jovanović, P. : 2002, *New Astronomy*, in press.

Reeves, J.N., Turner, M.J.L., Pounds, K.A., O'Brien, P.T., Boller, Th., Ferrando, P., Kendziorra, E., Vercellone, S. : 2001, *Astron. Astrophys.*, **365**, L134.

Publ. Astron. Obs. Belgrade No. 73 (2002), 219 - 230 *Poster*

PROBING THE EXTINCTION LAW AND GAS-TO-DUST RATIO M31 VIA GLOBULARS BEHIND THE DISK

A. S. SAVCHEVA[1] and S. V. TASSEV[2]

[1] *Massachusetts Institute of Technology, Cambridge, MA 02142, USA*
E-mail savcheva@mit.edu

[2] *Sofia University, 5 James Bourchier st., Sofia 1164, Bulgaria*
E-mail sv3t@club26.com

Abstract. We use the Catalogue of M31 Globular Clusters and Globular Clusters Candidates, compiled by Barmby (2000), containing 400 M31 globular clusters and candidates. We reduce this list to a sample of 41 globular clusters that have: (i) UBVRIK photometry, (ii) HI data, (iii) reliable [Fe/H] and (iv) reliable extinction as determined by us. For determining the intrinsic colours we used the evolutionary synthesis models for globular clusters by Kurth *et al.* (1999). The mean total-to-selective ratio in M31 in terms of the analytical formula by Cardelli *et al.* (1989) is found to be R_V 2.7 ± 0.2. Using data from 21 cm observations of M31 we got the HI column densities and obtained $N(HI)/Av \sim 9 \times 10^{20}$ atoms cm^{-2} mag^{-1} but varying with the radius, indicating possible supersolar metallicity toward the centre of M 31 galaxy.

1. Introduction

The understanding of true opacities in galactic disks is extremely important because of its impact on various extragalactic problems. An accurate knowledge of the reddening in the galactic disks is very helpful in building gas-and-dust distributions and stellar statistics.

M31 is one of the most studied galaxies because of its proximity. Its distance of only 0.7 Mpc allows precise spectroscopy and photometry of M31 globular clusters. Several hundred globulars is a very promising number not only for comprehensive statistical studies but also for a search for objects lying behind the greatest curtain on the sky.

The globulars in M31 have been used to test the quality of the models, assuming Galactic extinction law (Ivanov & Nedialkov, 1997). Here we assume that the models are correct and check the variance of the extinction law in M31. Recently, Nedialkov & Veltchev (1999) derived a mean gas-to-dust ratio in M 31 in star-formation regions

somewhat larger (3.8) than the canonical Galactic value (3.1). In this paper we present a study of M31 globular cluster system, which helps us to derive the M31 extinction law as well as accurate gas-to-dust ratios. We combine reliable spectroscopically determined metallicities with UBVRIK photometry to obtain the absorption distributions and to test the reddening law in M31. We also obtain $N(HI)/A_V$ using HI column densities from Brinks & Shane (1984).

2. Data

In this work all observational parameters of the globular clusters are obtained from the *Catalogue of M31 Globular Clusters and Globular Cluster Candidates*, compiled by P. Barmby (version from February, 2000). Originally, the catalogue contained about 400 globulars, having photometry data, determined [Fe/H] and coordinates. The first step was to select the objects with spectroscopically determined [Fe/H] and reliable photometry in at least UBVRIK bands.

In order to use model colours from Kurth *et al.* (1999) we had to convert the catalogue data for [Fe/H] into Z. We did this assuming that solar abundance ratios can be applied to M31 responsibly. This assumption, based on the Padova Group (1999) exact values, leads to

$$[Fe/H] = \lg(Z/X) + 1.596548 \tag{1}$$

Taking into consideration the following two simple relations

$$X = 1 - Y - Z = 0.77 - 3.25Z \tag{2}$$

$$Y = 0.23 + 2.25Z \tag{3}$$

The final conversion formula for Z comes to be

$$Z = \frac{0.77.10^{[Fe/H]-1.596548}}{3.25.10^{[Fe/H]-1.596548} + 1} \tag{4}$$

3. M31 Extinction Law

3. 1. MODEL COLOURS AND EXTINCTIONS

After we determine Z we can obtain the intrinsic colours of the globular clusters using the evolutionary model colours from Kurth (1999). Unfortunately, we had model colours for only six values of Z for which the authors calculated the temporal evolution of the UBVRIK colours. We performed interpolation in Z to determine how the colours of our clusters evolve with age. In Fig. 1 B-V is given as a function of Z and log t.

Using the photometry data from the catalogue and the model colours we obtain the following extinctions: $E_{X-Y} = (X-Y) - (X-Y)_0$, where $(X-Y)$ is $(U-B)$, $(B-V)$, $(V-R)$, $(V-I)$, $(V-K)$. Since for a given Z the model colours are calculated for 34 different ages, we actually get 34 different extinctions in each colour. This result accounts for the fact that different ages means different spectral distributions amounting to age-dependent reddening.

3. 2. ABSORPTION AND A_λ/A_V

In the previous section we determined E_{X-Y} which allows us to determine A_λ (where λ is the centre of the pass band) since $E_{X-Y} = A_X - A_Y$. These expressions give us 34 values for A_λ depending on the age of the cluster. At the same time we obtain A_V using the relation

$$A_V = E_{B-V}.R_V \tag{5}$$

Here R_V is a free parameter that gives one of the forms of the extinction law. Firstly, we do not assume any particular value for R_V. Instead, we vary it from 2.0 to 6.5 with a step of 0.1. When entered into equation (5) and the 34 possible different values for E_{B-V} have been taken into account we get a set of 1564 values for A_V.

The above derived A_λ/A_V we compare with the average R_V-dependent extinction law from Cardelli *al.* (1989) which is in the form

$$\langle A_\lambda/A_V \rangle = a(x) + b(x)/R_V \tag{6}$$

Here $a(x)$ and $b(x)$ are functions of λ^{-1}, where λ is the centre of the pass band in the Cousins photometric system. It is important to consider the spectral dependence of the parameters which the authors deal with by giving two expressions for $a(x)$ and $b(x)$ for the infrared and optical.

1)For the Infrared $0.3\mu m^{-1} \leq x \leq 1.1\mu m^{-1}$

$$a(x) = 0.574x^{1.61} \qquad \text{and} \qquad b(x) = -0.527x^{1.61} \tag{7}$$

2)In the Optical $1.1\mu m^{-1} \leq x \leq 3.3\mu m^{-1}$ and $y = x - 1.82$

$$a(x) = 1 + 0.17699y - 0.50447y^2 - 0.02427y^3 + 0.72085y^4 + \\ +0.01979y^5 - 0.77530y^6 + 0.32999y^7 \tag{8}$$

$$b(x) = 1.41438y + 2.28305y^2 + 1.07233y^3 - 5.3843y^4 - \\ -0.62251y^5 + 5.30260y^6 - 2.09002y^7 \tag{9}$$

We vary R_V in the same limits as before. We obtain the extinction law in two independent ways and get two sets of points depending on the age of the clusters and varying with the free parameter R_V. By comparing the two extinction laws we determine the error distribution as a function of age and R_V. In Fig. 2 is shown the plot of A_λ/A_V versus λ^{-1} for two globulars, corresponding to three different ages (including the one with smallest residual) and extinction law parametrized for total-to-selective ratio R_V equal to 2.7 and 5.4 respectively.

Using the smallest residuals along the A_λ/A_V axis (see Fig. 2) as a criterion for determining R_V and the ages of the clusters, we obtain a mean R_V of 2.72 (Fig. 5), which well corresponds to the polarimetry results (Martin & Shawl, 1979) of previous studies. Notably, there are several clusters in our selection with a few extrema in the error corresponding to different ages and R_V (Fig. 3 and Fig. 4), which might be reasonably interpreted either as young and bright objects behind the disk or as old ones in front with small extinction.

It is particularly interesting to look at the A_V histogram (Fig. 5), where one can notice a slightly bimodal nature of the distribution. Our selection is based on the presence of HI data in these lines of sight (Fig. 6). The sample of objects we use is selected by this criterion and hence the A_V distribution shows mostly clusters behind the disk. The large measured values for A_V suggest that most clusters lie behind the M31 disk. Considering this, we can say that this A_V distribution probably reflects the presence of clusters in front of the disk as well as some behind.

Although we do not have many clusters between us and the M31 plane (observationally), the sample that we have is statistically significant to build R_V distribution depending on the distance between the cluster and the centre of the galaxy R, as well as to study the gas-to-dust ratio in M31 (Section 4).

3. 3. AGES

Minimal error between the two extinction laws (as discussed in the previous section), gives also the ages of the clusters. The histograms of the obtained ages and corresponding R_V and A_V are shown on Fig. 6. Using this method we found several candidates for young clusters which are visible to us because they lie along lines of sight with smaller absorption. The more unlikely option is that these clusters are located in average absorption region but are intrinsically brighter. However, we think that the used technique might not be that sensitive with respect to the age. In fact in the error bar we can virtually have clusters with any age (Fig. 3).

4. A_V and the Gas-to-Dust Ratio

Using the values for A_V we obtained above and the HI column densities, determined by Brinks & Shine (1984) from 21cm radio observations, we derived the gas-to-dust ratio in M31. We give the positions of the sample clusters on the map of atomic hydrogen, provided also by Brinks & Shane (1984) in Fig. 6. The corresponding R_V and A_V are shown in Fig. 7, and a histogram of the obtained gas–to–dust ratios - in Table 1. and their distribution in Fig. 8. The two dashed lines on the plot in Fig. 7 bound the region of the plot where the Galactic gas-to-dust ratios vary. On the plot the triangles represent globulars typical for M31 and the circles are objects with smaller N(HI)/Av $\sim 9 \times 10^{20}$ atoms cm^{-2} mag^{-1} than the average for the Milky Way N(HI)/Av $\sim 15 \times 10^{20}$ atoms cm^{-2} mag^{-1} . From the column densities and calculated A_V we obtain N(HI) vs. A_V. It is convenient to use this data to plot $N(HI)/A_V$ versus distance to the centre (Fig. 9). Our plot is a confirmation of the

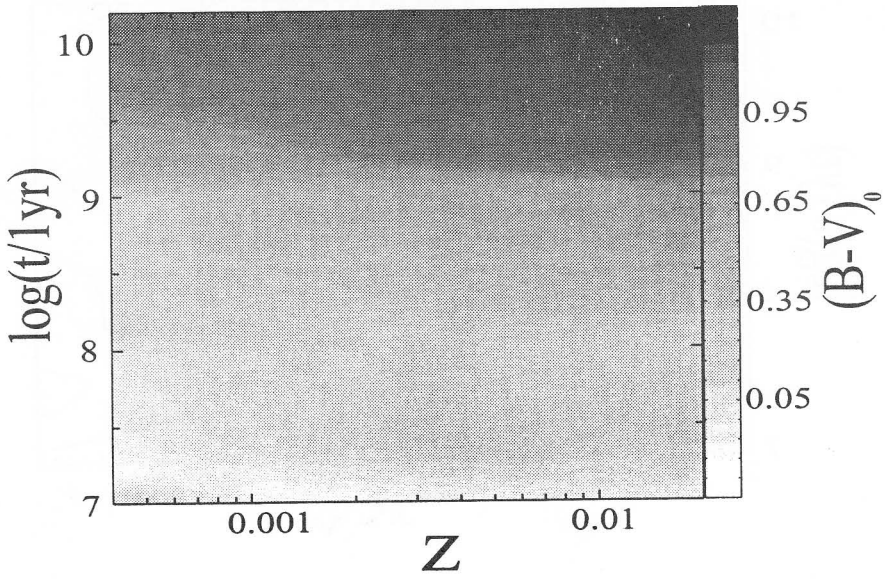

Fig. 1: Intrinsic $(B - V)_0$ color of globular cluster as function of metallicity and age.

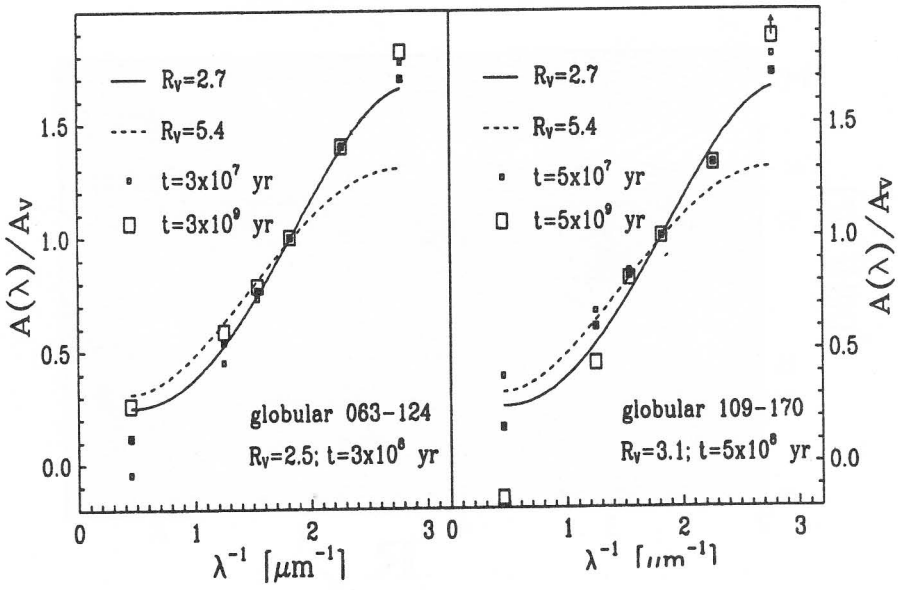

Fig. 2: Example of extinction law (CCM) optimization for two with fixed metallicity - 063-124 (right) and 109-170 (left).

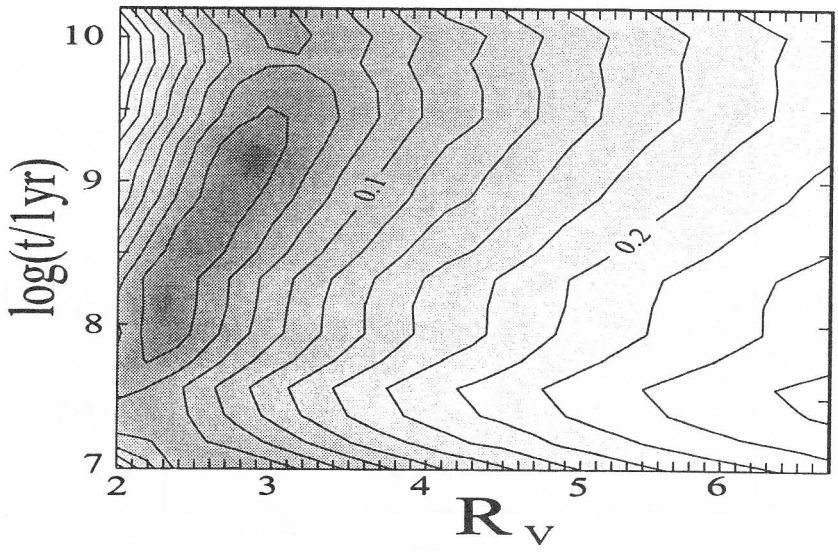

Fig. 3: R.M.S. of the residuals from the extinction curves as a function of the total-to-seelective extinction ratio (X-axis) and age (Y-axis). Typical example (cluster 109-170 from Fig. 2) of residuals with a few minima. Note the weak dependence of r.m.s. on the age.

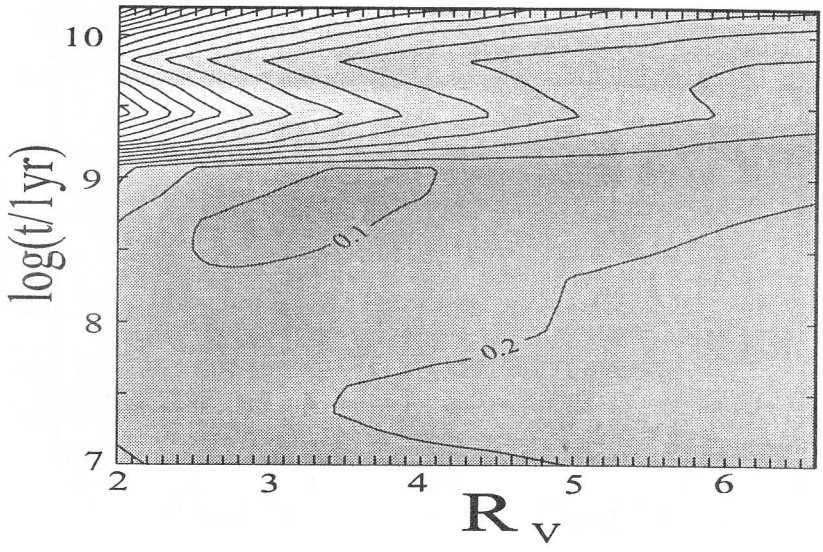

Fig. 4: Same as Fig. 3. Typical example (cluster 063-124 from Fig. 2) of residuals with well defined minimum.

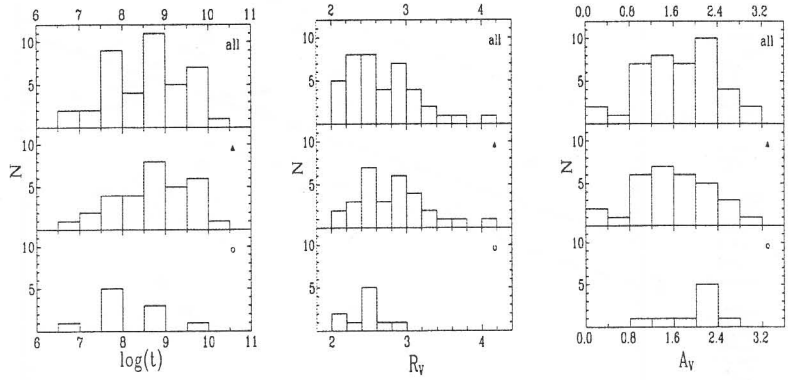

Fig. 5: Distribution by age (left), extinction (middle) and total-to-selective ratio (right) for 43 globulars, candidates to lie behind the disk of M31.

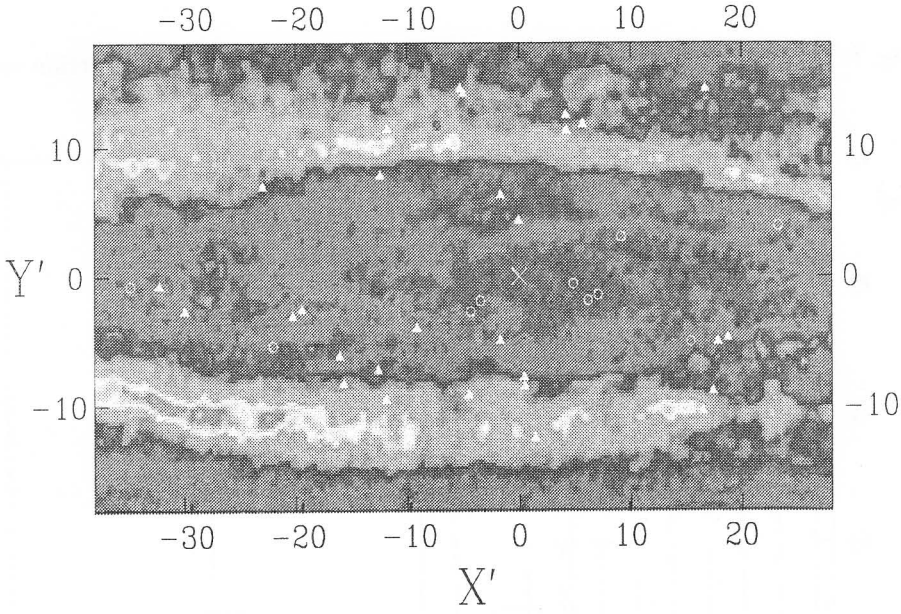

Fig. 6: Rectangular coordinates of the 43 globulars (relative to the galaxy centre), candidates to lie behind the disk of M31 galaxy. 33 globulars indicating "Galactic" gas-to-dust ratios are represented with filled white triangles and the rest - with white open circles. The positions are superimposed over the HI map (Brinks & Shane, 1984).

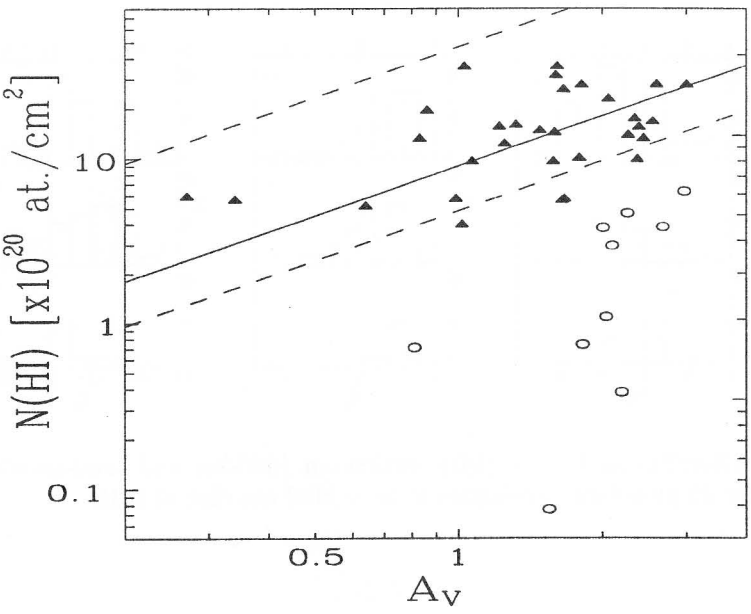

Fig. 7: HI column densities (Brinks & Shane, 1984) versus derived extinction values.

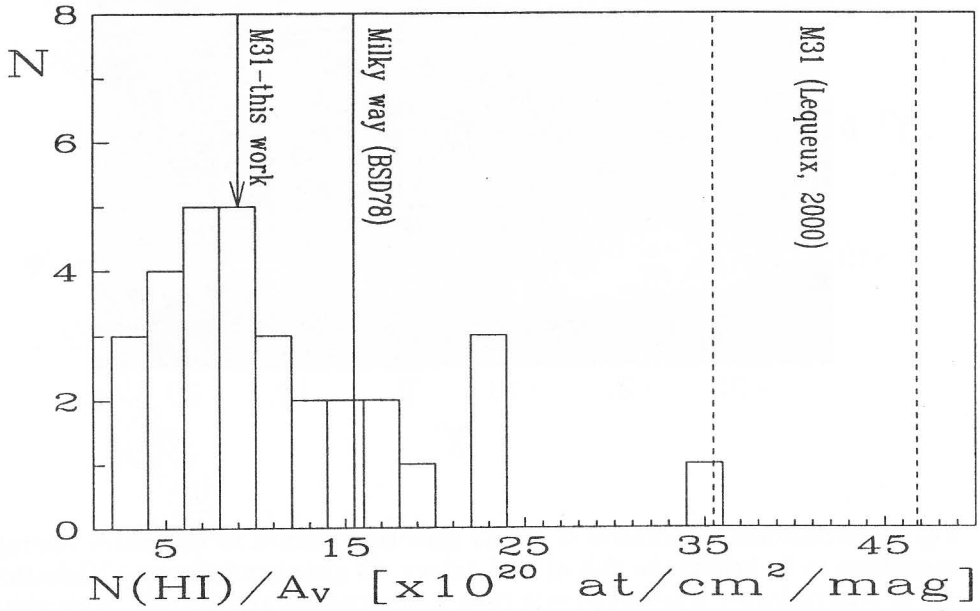

Fig. 8: Distribution by atomic gas-to-dust ratio for 33 globulars.

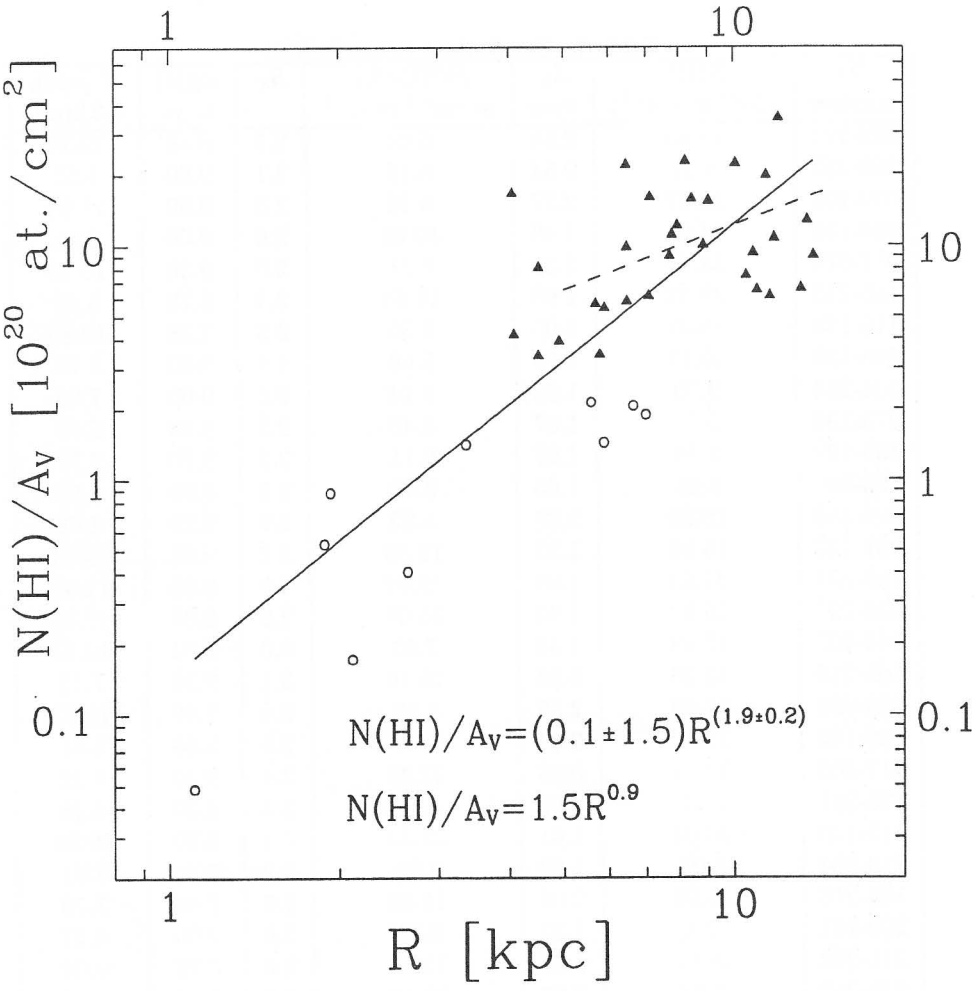

Fig. 9: Radial distribution of the atomic gas-to-dust ratio as derived for 33 (triangles) and 10 (open circles) globulars. The dashed line represents the gradient as determined by Braun & Walterbos (1999) for 6 HII regions in M31. The solid line represents a power law fit, indicating possible central hypermetallicity.

Table 1: Gas-to-dust ratios in M31

ID number	N(HI) (10^{20} at cm^{-2})	A_V *mag*	N(HI)/A$_V$ at cm^{-2} mag^{-1}	R_V	log(t) t, yr	R [kpc], 0.2 kpc/$''$
063-124	16.86	2.55	6.61	2.5	8.48	13.21
206-257	5.21	0.64	8.15	3.1	9.60	4.52
039-101	13.97	2.27	6.16	2.3	9.90	11.65
094-156	14.91	1.48	10.08	2.9	9.00	8.85
017-070	14.49	1.59	9.11	2.9	9.30	13.88
185-235	26.32	1.66	15.86	2.4	8.78	8.45
116-178	28.07	3.00	9.36	2.3	7.78	10.86
068-130	10.17	1.79	5.69	4.1	9.60	5.70
204-254	9.70	1.58	6.14	2.8	9.00	7.09
073-134	5.77	1.67	3.46	2.3	8.48	5.80
135-192	9.74	1.07	9.11	3.2	9.70	7.71
153-000	5.65	1.65	3.43	2.9	8.85	4.51
096-158	10.00	2.37	4.22	2.9	8.70	4.08
061-122	15.69	1.22	12.86	3.7	9.85	13.54
180-231	31.88	1.60	19.92	2.8	9.00	11.43
235-297	36.14	1.03	35.09	2.9	8.30	12.50
044-107	17.59	2.34	7.52	2.0	7.84	10.54
161-215	13.36	0.83	16.10	3.1	9.30	7.12
038-098	15.59	2.39	6.52	2.4	7.48	11.03
093-155	13.34	2.44	5.47	2.6	7.85	5.91
217-269	19.72	0.86	22.93	3.4	9.30	8.22
228-281	5.77	0.99	5.83	3.3	9.30	6.48
117-176	36.04	1.61	22.39	3.1	8.60	10.09
213-264	4.03	1.02	3.95	2.2	9.30	4.91
165-218	23.03	2.06	11.18	2.6	7.48	7.79
209-261	12.38	1.25	9.91	2.6	9.00	6.47
211-262	28.06	1.81	15.50	2.6	7.78	9.04
229-282	5.98	0.27	22.16	2.7	8.30	6.46
239-000	28.15	2.60	10.83	2.2	7.00	11.83
178-229	5.70	0.34	16.76	3.5	10.04	4.06
174-226	16.09	1.32	12.19	2.9	9.60	7.96

result obtained by Braun and Walterbros (1992) for galactocentric gas-to-dust ratio gradient. Moreover, our result is consistent with Braun's - the 6 points they use for compare well with ours. Comparing the lines in Fig. 9 (the dashed line is from Braun and Walterbros 1992) one can see that the slope of our line is greater. This can be explained considering the fact that in our sample we also have clusters close to the centre, which may imply higher metallicity of the inner parts of the dust component of the disk. Table 2 summarizes what we determined for the clusters of our sample in terms of gas-to-dust ratios, ages, R_V.

Finally, we made a histogram of $N(HI)/A_V$ and compared it with those of other authors (Fig. 8). It is assuring that our $N(HI)/A_V$ distribution contains reasonable values for the Milky Way. The fact that we observe a peak at slightly lower values N(HI)/Av $\sim 9 \times 10^{20}$ atoms cm^{-2} mag^{-1} was already discussed but the distribution pattern we see suggests that our clusters are located in sampling varying with distance $N(HI)/A_V$. We compare our results for M31 gas-to-dust with the values for the Milky Way - data from Bohlin *et al.* (1978) and another estimate for M31, obtained by Lequeux (2000). Our value for the gas-to-dust ratio is probably less from that Lequeux gives because of the different technique used in determining $N(HI)/A_V$. He uses primarily UV data and having in mind the probable dust properties in terms of composition and size, it is completely understandable why Lequeux (2000) obtains three times larger gas-to-dust ratio then we do.

5. Conclusions

This work addresses several different problems. First, we determined the absorption in M31 disk at different radii. This was achieved by obtaining extinctions and appropriate values of the free parameter R_V for all 41 M31 clusters we study. Second, by comparing our extinction law with the average extinction law given by Cardelli *et al.* (1989), we estimated the ages of the clusters. At this point we found several candidates for young clusters but we don't assert it since we think that our method might not be very sensitive to the age. And finally, using column densities of HI (Brinks & Shane, 1984) we obtained a gas-to-dust ratios for M31, close to that in the Milky Way. We derive power law dependence of N(HI)/Av at the distance to the centre much steeper than those previously found (Braun & Walterbos, 1992; Nedialkov *et al.*, 2000) which may reflect the supersolar metallicity near the M 31 centre. Recently, Davidge (2001) suggested that the brightest stars in the bulges of M 31 and the Milky Way belong to an old, metal-rich population and they are bright not because of small age, but because of high metallicity. In the near future we intend to test a richer sample of globulars in M 31 because the number of clusters with known metallicities is already above 200 (Perrett *et al.*, 2000).

References

Barmby, P., Huchra, J.: 2000, *Astron. J.*, **119**, 727.
Barmby, P.: 2000, http://cfa-www.harvard.edu/~pbarmby/m31gc/m31gc.html.
Bohlin, R., Savage, B., Drake J.: 1978, *Astrophys. J.*, **224**, 132.
Braun, R., Walterbos, R.: 1992, *Astrophys. J.*, **386**, 120.
Brinks, E., Shane, W.: 1984, *Astron. Astrophys. Suppl. Series*, **55**, 179.
Cardelli, J., Clayton, G., Mathis, J.: 1989, *Astrophys. J.*, **345**, 245.
Davidge, T.: 2001, *Astron. J.*, **122**, 1386.
Ivanov, V., Nedialkov, P.: 1997, *Proceedings of IV Congress of the Euro-Asian Astronomical Society*, Moscow, p.2.
Kurth, O., Fritze, U.: 1999, *Astron. Astrophys. Suppl. Series*, **138**, 19.
Lequeux, J.: 2000, *The interstellar medium in M 31 and M33*, Eds.: E. M. Berkhuijsen, R. Beck, R. A. Walterbos, Germany, Aachen, 98.
Martin, R., Shawl, S.: 1978, *Astrophys. J*, **231**, L57.
Nedialkov, P., Veltchev, T.: 1999, Study of the extinction law in M 31 and selection of red supergiants, astro-ph/9911262.
Nedialkov, P., Berkhuijsen, E., Nieten, Ch., Haas, M.: 2000, *The interstellar medium in M 31 and M 33*, Eds.: E. M. Berkhuijsen, R. Beck, R. A. Walterbos, Germany, Aachen, 98.
Perrett, K., Bridges, T., Hanes, D., Irwin, M., Brodie, J., Carter, D., Huchra, J., Watson, F. G.: 2002, *Astron. J.*, **123**, 2490.

Publ. Astron. Obs. Belgrade No. 73 (2002), 231 - 246 *Poster*

R-BAND PHOTOMETRIC PROFILES OF 120 EDGE-ON NORTHERN GALAXIES

O. I. STANCHEV, Ts. B. GEORGIEV, and Yu. B. GORANOVA
Institute of Astronomy, Bulgarian Academy of Sciences
72 Tsarigradsko Shosse, 1784 Sofia, Bulgaria
E-mail stanchev@astro.bas.bg

Abstract. The major and minor axis profiles of 120 late type edge-on galaxies, observed with the 6-m telescope in the R band, are presented. Only 7 of them ($\sim 6\%$) show exponential shapes, 99 ($\sim 83\%$) have well pronounced truncation below 24 mag/arcsec^2 and 13 ($\sim 11\%$) are intermediate, with weak truncation below 25 mag/arcsec^2. A brief survey of the possible explanation of the truncation effect is given. The major-axis sizes and axial ratios at 25 mag/arcsec^2, as well as the respective Tully–Fisher relations are presented. The "edge-on" TF relations may be used as raw distance estimators, having relative standard errors $25 - 33\%$.

1. INTRODUCTION

The investigation of the distribution of stars in galaxies is very important for elucidation of their structure and evolution. Surface photometry provides information about the space distribution of stars in the galactic bulges and disks, if galaxies under various projection angles (inclinations, i) are compared. In this sense the edge-on galaxies, having $i \approx 90°$, are very valuable. They show the galactic structures perpendicular to the galactic plane and give possibility to disentangle the components that have different scale parameters. In addition, due to the line-of-sight integration, one can follow the light distribution to large distances from the center. One very interesting fact is that most of the edge-on galaxies show strong truncation of their major axes profiles. Here we present and discuss a uniform system of profiles and sizes of such galaxies.

2. THE PROFILES AND THEIR CLASSIFICATION

In this work we use the smoothed profiles of 120 northern edge-on galaxies, derived from the isophote maps of Karachentsev et al. (1992). The sample is selected from the reprints of the POSS by the criterion "axial ratio on blue photographs $a/b > 7$ and contains almost all such galaxies with major axis $2 < a < 8$ arcmin. Observations had been carried out with the 6-m telescope with CCD-camera attached to the focal reducer in 1988–1990. The photometry has been performed in red bandpass, close to the R-system of Cousins ($\lambda_{\rm eff} \approx 6500$ Å). Using the table of Karachentsev et al.

(1992), we list the basic data on the galaxies, as well as the parameters derived by us in Table 1, as follows:

– UGS – galaxy number in the Uppsala General Catalogue;
– V – radial velocity in km/s, with respect to the Local Group (this work);
– W – 21 cm FWHM line-width in km/s;
– m_{24}^0 – extinction corrected magnitude (R) within the isophote 24 mag/arcsec^2 (this work);
– α_{25} – angular radius in arcsec along the major axis at 5 mag/arcsec^2 (this work);
– α_{25}/b_{25} – apparent aspect ratio at 25 mag/arcsec^2 (this work);
– M – absolute magnitude of the galaxy, calculated with m_{24}^0 (this work);
– A – galaxy linear diameter in kpc, corresponding to $2\alpha_{25}$;
– PT – profile type: e – exponential, t – truncated, i – intermediate;
– WP – warp presence (w);
– HP – halo presence (h).

Most of the large late-type disk galaxies, which are visible edge-on, show strong deviation from the expected exponential brightness shape, i.e. their photometric profiles seem to be truncated. A statistical study of this truncation may pose interesting constraints on galaxy formation theory. For example, if the truncation were also present in the mass distribution, it would have important dynamical consequences at the discs outer edges. From this point of view we classified empirically the shapes of the major axis profiles of the sample galaxies in *three types* - exponential, truncated and intermediate:

– *Exponential profiles* with long quasi-linear parts up to 25–26 mag/arcsec^2 have 7 galaxies ($\sim 6\%$).

– *Truncated profiles* with strong decrease of the surface brightness below 24 mag/arcsec^2 have 99 galaxies ($\sim 83\%$).

– *Intermediate profiles* with linear part and weakly pronounced truncation after 25 mag/arcsec^2 have 13 galaxies ($\sim 11\%$).

One galaxy (UGC 9556) has been classified as peculiar (see Sect. 3).

Examples of the profiles are shown in Fig. 1. Figure 5 presents the smoothed profiles of all 120 edge-on galaxies from the sample.

The truncations (cut-offs) are placed at low surface brightness levels, as it is seen from the profiles in Fig. 1. These cut-offs are not infinitely sharp edges, but rather regions where the radial exponential scale length suddenly decreases from several kpc to less than ~ 1 kpc.

There are many suggestions as to the causes of such cut-off effects at the edges of the disks of most edge-on galaxies. For example, Bottema (1995) suggests that tidal interactions between neighboring galaxies may be the cause of sharp disk truncation in individual galaxies. Another possible explanation of the truncations is that star formation has ceased at that position due to the low H I density (Fall & Efstathiou 1980; van der Kruit & Searle 1981). But in scenario with slow disk formation (Larson 1976) the truncation radius might be the radius where the disk formation time equals the present age of the galaxy formation mechanisms.

Generally, we must include both intrinsic physical processes and projection effects due to the positions of spiral arms with respect to the line-of-sight. The importance of the latter effects can be assessed observationally, since in this case one would expect an asymmetry in either of the truncations themselves on either side of the galaxy.

Table 1: Some basic data on the sample of 120 edge-on galaxies

UGC	V	W	m^0_{24}	α_{25}	$(\alpha/b)_{25}$	M	A	PT	WP	HP
231	841	210	12.70	141.3	6.9	-17.96	18.59	e		
290	758	100	15.99	49.6	4.6	-14.46	5.90	i	w	
418	4438	382	13.64	63.05	4.19	-20.27	36.91	t		
485	5238	359	13.57	77.4	4.8	-20.74	54.76	t	w	
507	5277	455	13.17	73	3.5	-21.07	49.90	t	w	h
542	4508	368	13.04	61.7	2.9	-20.96	37.72	t		h
711	1978	202	13.96	113.15	7.05	-18.12	28.58	e		
1400	5536	963	11.73	87.8	2.8	-22.70	65.42	t		h
1650	4585	235	15.41	36.4	3.2	-18.63	22.67	e		
1839	1535	142	14.46	65.3	4.4	-16.98	12.28	t	w	h
1867	5195	281	13.97	62.6	5.4	-20.36	44.42	t		
1970	1915	228	13.60	70.1	3.5	-18.59	18.56	t		h
2092	6120	452	13.72	96.9	4.2	-20.83	76.50	t		h
2101	5835	500	13.36	64.5	3.9	-21.20	50.91	t		h
2370	2162	194	14.62	67.8	7.7	-17.94	21.34	t		
2411	2546	312	13.07	140.3	10.6	-19.85	52.11	i		
3326	4085	528	12.91	111.2	6.2	-21.02	65.81	t		
3365	5150	537	12.64	66	3.5	-21.73	47.74	t		h
3425	4057	419	12.94	138	4.4	-20.96	80.38	i		h
3474	3633	360	12.97	75.1	4.3	-20.72	39.86	t		
3489	5455	475	13.65	65.9	5.3	-20.79	49.40	t	w	
3539	3305	312	13.98	67	4	-19.49	32.08	t		h
3597	5958	-	13.45	61.3	3.5	-21.19	50.41	e	w	
3697	3136	262	12.99	107.6	9.95	-20.43	50.29	t	w	
3782	2269	336	12.56	115.4	4.9	-20.19	39.71	t	w	
3879	4797	250	14.56	67	3.9	-19.64	45.05	i	w	
3959	3109	425	12.28	119	4.6	-21.08	54.19	i	w	h
4043	3401	419	13.46	73.5	3.9	-20.09	36.46	t		
4148	736	135	15.67	54.9	5.2	-15.28	8.24	t	w	
4257	4164	243	14.66	69.4	5.2	-19.28	41.24	t	w	
4259	3832	397	13.09	64.7	3.4	-20.72	36.20	t		h
4277	5459	575	13.13	122	4.4	-21.35	93.00	i		h
4278	563	180	12.50	146.3	6.5	-18.11	18.82	t		h
4550	2068	264	13.76	84.2	3.6	-18.89	27.70	t		h
4704	596	129	14.32	120.8	5.25	-16.38	16.17	i	w	
4719	5116	542	13.13	80.9	4.9	-21.22	58.14	t	w	
4961	1578	324	12.67	111.3	4.8	-19.53	29.63	t		
5173	6237	491	13.64	86.9	5.4	-21.14	75.91	t	w	h
5203	1551	190	14.22	79.9	5.4	-18.01	21.56	t	w	
5210	4441	304	14.19	66	4.2	-19.90	42.16	t	w	
5341	7568	607	13.85	97.3	7	-21.31	101.28	t		
5389	6980	352	14.55	65.6	5.5	-20.42	62.86	t		
5452	1342	200	13.59	79.65	4.5	-18.29	18.37	t	w	
5495	8249	569	13.55	81.9	3.3	-21.78	92.72	t	w	h
5537	3756	288	14.40	80.25	5	-19.40	44.85	i		h
5662	1324	173	14.18	102.6	6.9	-17.69	23.53	e	w	
5687	3563	258	14.27	66.6	4.2	-19.45	35.72	t	w	
5741	1391	325	12.46	95.3	3.8	-19.61	24.01	t		h

Table 1: (continued)

UGC	V	W	m^0_{24}	α_{25}	$(\alpha/b)_{25}$	M	A	PT	WP	HP
6080	2180	190	14.97	59	4.06	-17.79	20.42	t		
6116	1134	304	12.31	125.6	5.3	-19.41	26.83	t		
6483	3891	324	13.74	56.2	3.6	-20.12	32.20	t		
6497	6324	384	14.74	63.8	4.9	-20.02	55.45	t		
6594	1040	171	14.05	79.2	4.2	-17.60	16.38	t	w	
6667	978	176	13.47	100.6	5.8	-17.97	18.87	t	w	
6686	6546	402	13.77	89	5.4	-21.12	81.83	t	w	
6774	2417	228	14.05	57.8	4.6	-18.90	21.75	i	w	
6802	1256	139	14.16	70.2	4.2	-17.66	15.75	t	w	
7001	1507	196	13.55	84.15	5.3	-18.74	23.37	t	w	h
7153	2606	264	14.28	67.7	4.8	-18.83	27.54	t		
7170	2444	210	14.11	87.6	5.7	-18.92	34.34	t	w	
7222	931	232	12.02	138	4.1	-19.31	24.60	t		h
7279	1978	208	14.33	73	5.2	-18.46	25.56	t		h
7291	226	218	12.43	106.4	4.3	-18.04	12.78	t		h
7301	712	131	14.39	53.3	4.7	-16.60	8.15	t	w	
7313	2131	214	13.86	68.3	4.6	-19.04	25.13	t		
7321	409	210	12.99	160.3	10.5	-17.48	19.29	t		
7387	1733	256	13.91	72	5.3	-18.74	23.57	t		h
7403	2541	363	12.70	112.6	4.1	-20.54	48.70	t		h
7459	525	189	13.84	72.7	4.6	-16.50	8.26	t	w	
7513	995	280	12.21	124.2	4.9	-19.68	28.76	t		
7522	1428	310	12.70	87.7	4.7	-19.69	25.50	t		h
7607	4226	278	14.67	104.25	6.3	-19.47	68.05	t		h
7617	6972	436	14.06	80.1	5.2	-20.92	77.14	t	w	h
7687	1733	144	14.02	81.4	4.4	-18.66	27.12	t		
7725	1759	151	13.55	80.4	3.8	-19.16	27.13	e	w	
7774	526	190	13.78	97.8	5.6	-16.82	12.51	t		
7808	7273	520	13.91	98.9	5.3	-21.26	103.44	i		
7993	4789	366	14.27	65.7	4.9	-19.99	45.38	t	w	
7999	4761	442	13.22	64.4	4.2	-21.00	43.39	t		
8025	6316	513	13.33	63.3	4.4	-21.47	56.00	t		
8146	669	162	13.44	99.9	5	-17.68	16.19	t		
8286	407	179	12.01	159.9	5.3	-18.62	20.72	t		
8463	4647	-	12.65	82.5	4.3	-21.65	58.04	t		h
8115	2049	256	13.08	67.5	4.3	-19.63	22.71	t		
9127	2883	570	11.85	131.9	6.8	-21.63	63.57	t		
9242	1440	187	13.63	136.5	10.1	-18.77	39.95	i	w	
9249	1365	147	14.46	69	4.7	-18.08	21.58	t		
9422	3310	314	13.93	62.2	5.3	-19.76	33.05	t		
9431	2237	330	12.93	99.5	5.2	-20.10	38.75	t		
9556	2292	230	14.88	45	4.1	-18.12	17.39	i		h
9568	2138	418	12.49	110.4	3.5	-20.41	40.60	t		h
9760	2015	144	14.91	94.05	5.8	-18.16	37.51	t		
9780	5178	335	14.04	71.5	4	-20.48	55.55	t	w	h
9856	2491	218	14.62	90	4.8	-18.64	39.11	t		h
9948	2612	536	12.37	94.2	4	-20.88	40.78	t	w	
9977	1912	247	13.35	111.6	5.9	-19.65	42.98	t		h

Table 1: (continued)

UGC	V	W	m^0_{24}	α_{25}	$(\alpha/b)_{25}$	M	A	PT	WP	HP
10227	9026	600	13.84	74	5	-21.77	95.10	t	w	
10288	2045	352	12.69	146.9	5.3	-20.40	58.88	i		h
10297	2306	224	13.98	67.5	4.4	-19.25	28.98	t		
11132	2828	339	13.85	65.5	3.7	-19.60	31.19	t	w	
11230	7103	400	14.57	65.25	4.4	-20.52	65.84	t		
11301	4500	491	12.69	88.1	6	-21.59	61.40	t	w	
11394	4236	365	13.47	71.25	5.1	-20.68	46.70	t	w	
11411	7438	396	14.19	69	4.3	-20.99	72.67	t	w	
11838	3478	250	14.08	66	5.2	-19.57	34.30	t		h
11841	5989	535	12.90	98.4	6.9	-21.81	83.26	t		
11859	3014	306	14.18	74.6	5	-19.18	33.96	e		h
11893	5564	619	13.18	78.1	3.9	-21.37	61.55	t		
11964	1399	170	14.75	64.4	5.8	-17.25	15.65	t	w	
11994	4872	404	13.03	64.9	4	-21.24	45.04	t		
12001	4269	534	12.84	71.6	4	-21.18	44.16	t		
12190	7263	577	13.54	71.6	4.7	-21.52	71.19	t	w	h
12281	2567	260	13.34	105.1	6.6	-19.62	39.81	t		
12411	8656	571	13.25	54.4	5.4	-22.17	64.15	t		
12423	4838	486	13.08	114.4	4.9	-21.10	76.13	i		h
12430	3676	225	13.54	81.75	5.3	-20.13	42.90	t	w	
12452	4960	314	14.01	69	4.2	-20.22	46.90	t	w	h
12506	2385	345	13.47	88	4.4	-19.32	30.78	t		
12693	4952	220	14.79	58.5	5	-19.46	40.15	t	w	
12900	6803	458	14.09	71.25	4.75	-20.77	64.91	t	w	

3. SOME PECULIARITIES

We find weak halos in 40 ($\sim$ 33%) of the examined galaxies. The most prominent of them – UGC 5495 – is shown in Fig. 2 (left panel).

Many galaxies, including our own, show large-amplitude warps in the outer parts of their disks. Departures from the ideal symmetry involve warps, tilts, corrugations, differential ellipticity, vertical convection with the halo, etc. Flaring, even if it does not break the ideal disk symmetry, may again be considered a perturbative effect. These features are not large but are common. Their study may provide clues to understanding the nature of galaxies and the intergalactic medium.

We noticed warping features in 47 of our 120 sample galaxies ($\sim$ 39%). Figure 2 (right panel) presents image of an S-shaped edge-on galaxy – UGC 3697.

We also have one galaxy – UGC 9556 – with profile, showing big bulge and long exponential periphery as it appears in Fig. 3. It is possible, that these peculiarities in the profile shape are due to bad photometric calibration.

4. TULLY–FISHER RELATIONS

The Tully–Fisher (TF) relations are important tools for distance estimation in the

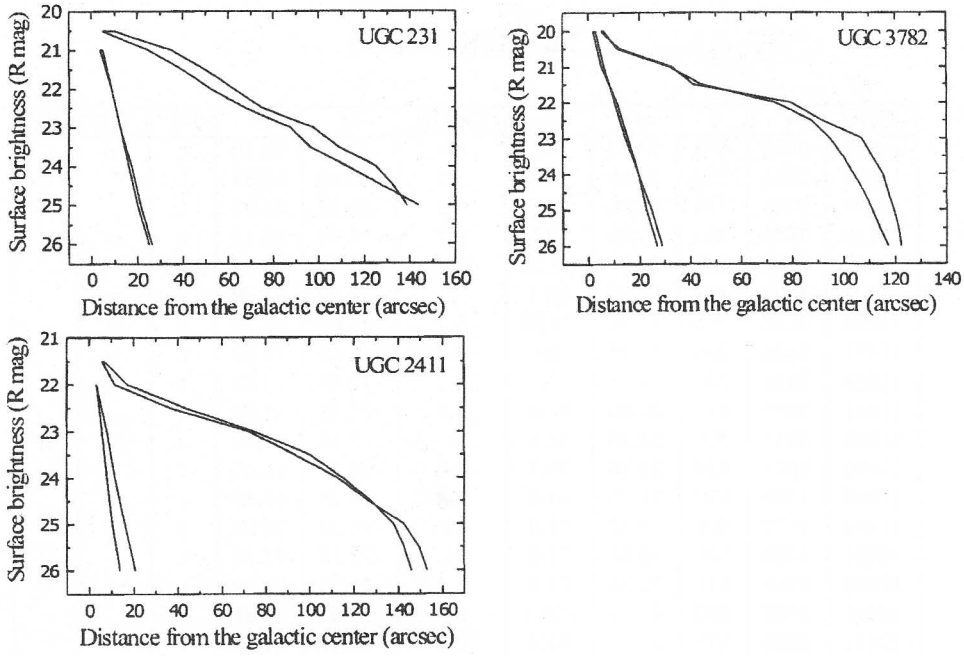

Fig. 1: Photometric profiles of UGC 231 (exponential, the left top panel), UGC 3782 (truncated, the right top panel) and UGC 2411 (intermediate, the bottom panel).

Universe. Due to the errors of the inclination estimation, the corrections of the observed sizes or magnitudes of the galaxies to face-on view increases the scatter of the relations. However, in the special case of edge-on galaxies these corrections may be omitted. Then we must expect that the "edge-on" Tully–Fisher relations for the later giant galaxies must be narrower than the usual ones.

Figure 4 (left panel) presents the TF relations between the absolute magnitude M and the 21 cm FWHM linewidth W (km/s) for 107 galaxies. Because of the absence of data on W, two galaxies (UGC 3597 and UGC 8463) are not included in this relation. Moreover, we consider the galaxies UGC 290, UGC 4148, UGC 7301 and UGC 7459 with $M > -16$ mag, as probably nearby dwarfs. They are excluded, too. Besides, the galaxies UGC 3425, UGC 7607, UGC 7774, UGC 9127, UGC 11301, and UGC 11411 are also excluded because of their bad frames. The galaxy UGC 1400 does not participate in the relation because in PGC it is classified as a "multiple" galaxy.

The absolute magnitude M was calculated from the equation

$$M = m^0{}_{24} - 25 - 5 \lg V + 5 \lg H_0. \qquad (1)$$

Using the relations $A_R = 0.57 A_B$ and $m^0_{24} = m_{24} - A_R$, m^0_{24} in Eq. (1) is the extinction corrected red (R) magnitude within the isophote of 24 mag/arcsec^2. We use the data about A_B from the Revised Flat Galaxy Catalogue of Karachentsev et al. (1999) and the Lyon/Meudon Extragalactic Database (LEDA). $H_0 = 75$ km s^{-1} Mpc^{-1} is the adopted Hubble constant. V is the radial velocity in (km/s)

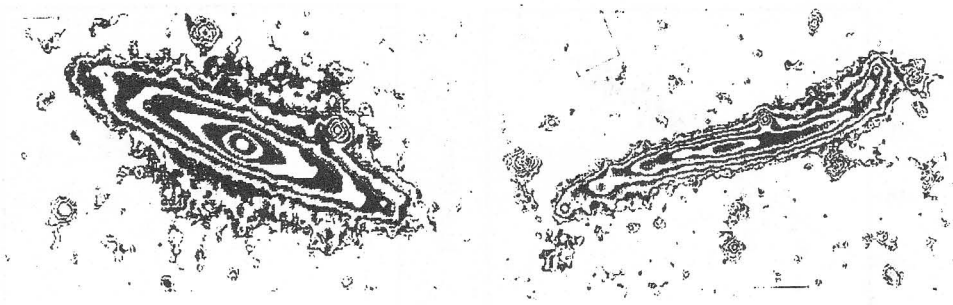

Fig. 2: The isophote maps of UGC 5495 (left panel) and the warped galaxy UGC 3697 (right panel)

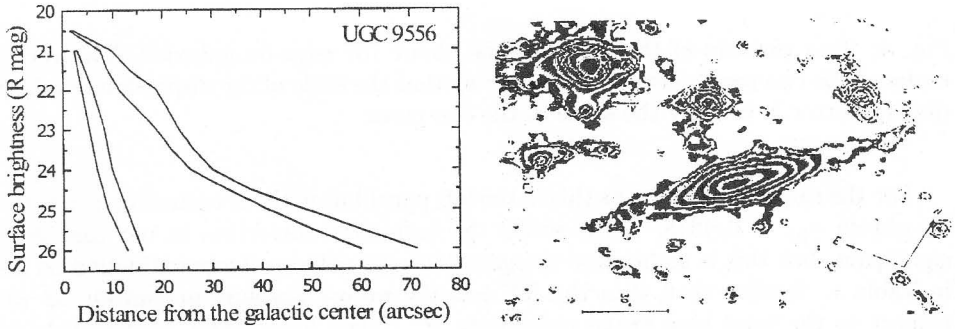

Fig. 3: Photometric profile of UGC 9556 (left panel) and its isophote map (right panel)

corrected from heliocentric to Local Group, through a method recommended by the NASA/IPAC Extragalactic Database, based on the work of Karachentsev & Makarov (1996). Figure 4 (right panel) presents the TF relation between the linear diameter A (kpc) and W (km/s) for the same 107 galaxies. Here the same galaxies as these in the previous TF relation are excluded. We calculate the linear diameter of an observed galaxy from the equation

$$A_{25} = 2a_{25}\frac{V}{H_0}1000, \tag{2}$$

where α_{25} is the galaxy angular radius along the major axis at 25 mag/arcsec^2 converted in radians.

In Fig. 4 (left panel) the data are fitted with the line

$$M = \begin{array}{l} -3.13 - 6.70\lg W, \\ \pm 0.64 \pm 0.26 \end{array} \qquad \sigma_M = 0.4771,$$

and for Fig. 4 (right panel) – with the line

$$\lg A = \begin{array}{l} -0.91 + 1.00\lg W, \\ \pm 0.17 \pm 0.07 \end{array} \qquad \sigma_{\lg A} = 0.1237.$$

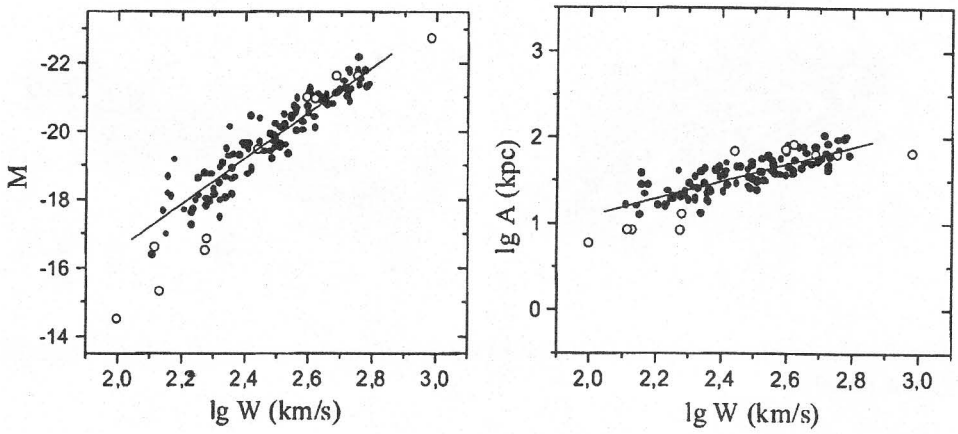

Fig. 4: Two variants of the TF relations about 107 edge-on galaxies. The vertical scales of the two panels are set in such a way that the scale of the dispersion in relative distance error is visually the same in the two cases.

For the same TF relation as this in the left panel but without extinction correction, we obtain $\sigma_M = 0,4818$. As it seems the extinction correction in our case is not significant, but this is so because the galaxies have not very large extinction as seen in Table 1. Besides that, if in this TF relation we use absolute magnitude M with respect to the total blue visual magnitude B_t^0 (taken from RFGC and LEDA, and corrected for extinction) instead of with respect to the visual magnitude in R-light, then we could obtain $\sigma_M = 0.6593$.

Let us compare the two TF relations as distance estimators. The distance modulus standard errors are $\sigma_\mu = \sigma_M = 0.48$ mag and $\sigma_\mu = 5\sigma_{\lg A} = 0.62$ mag, respectively. The corresponding relative distance errors are $10^{\sigma_\mu/5}$, i.e. $25 - 33\%$, respectively.

A previous investigation of 117 galaxies of the present sample, based on less accurate data, shows badly defined TF relations. The scatters of the relations of type (1) in the B-band and (2) in the R band are $0.75 - 0.85$ mag (relative distance error is $40 - 50\%$) (Georgiev 1992). In the present paper we use more accurate CCD data and because of this the scatters of the TF relations grow down ~ 1.5 times.

5. CONCLUSIONS

We show that 83% of the studied edge-on galaxies have strongly truncated major axis profiles. Because of their large apparent sizes a few edge-on galaxies (NGC 891, NGC 4244, NGC 5907, etc.) with known truncated profiles are not included in the discussed sample. Another homogenous sample of southern edge-on galaxies is investigated by Pohlen et al. (2000). Applying our classification for the galaxies in this sample, we found that 28 of them have truncated profiles and only 3 galaxies (ESO 319-026, ESO 578-025 and ESO 583-008) may be considered as belonging to the intermediate type. Therefore, the standard exponential disk model must be revised. Generally, we conclude that $\sim 90\%$ of the disk edge-on galaxies have truncated profiles. Further we show that the "edge-on" TF relations may be used as raw distance estimators, having

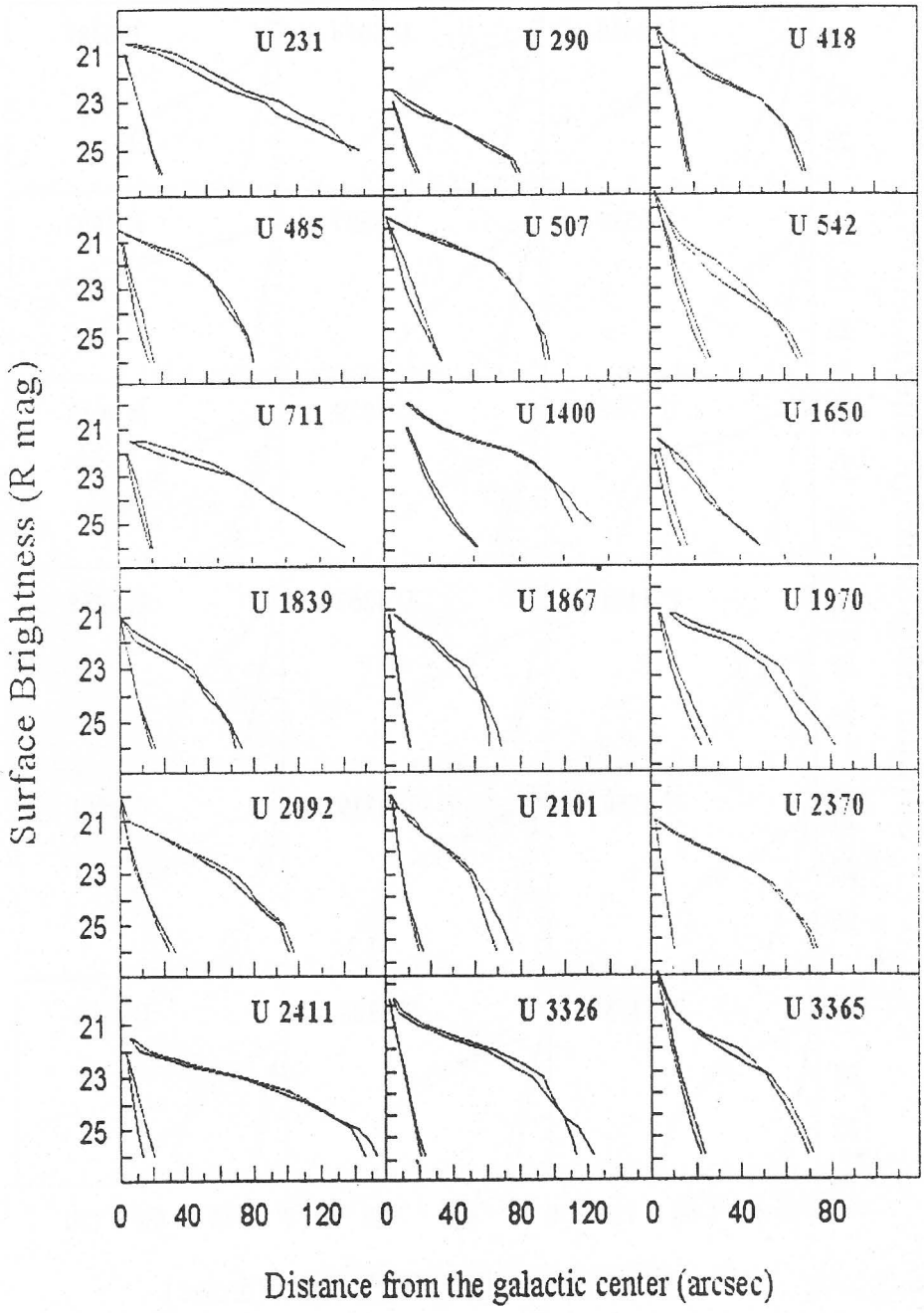

Fig. 5: Smoothed photometric profiles for the sample of 120 edge-on galaxies.

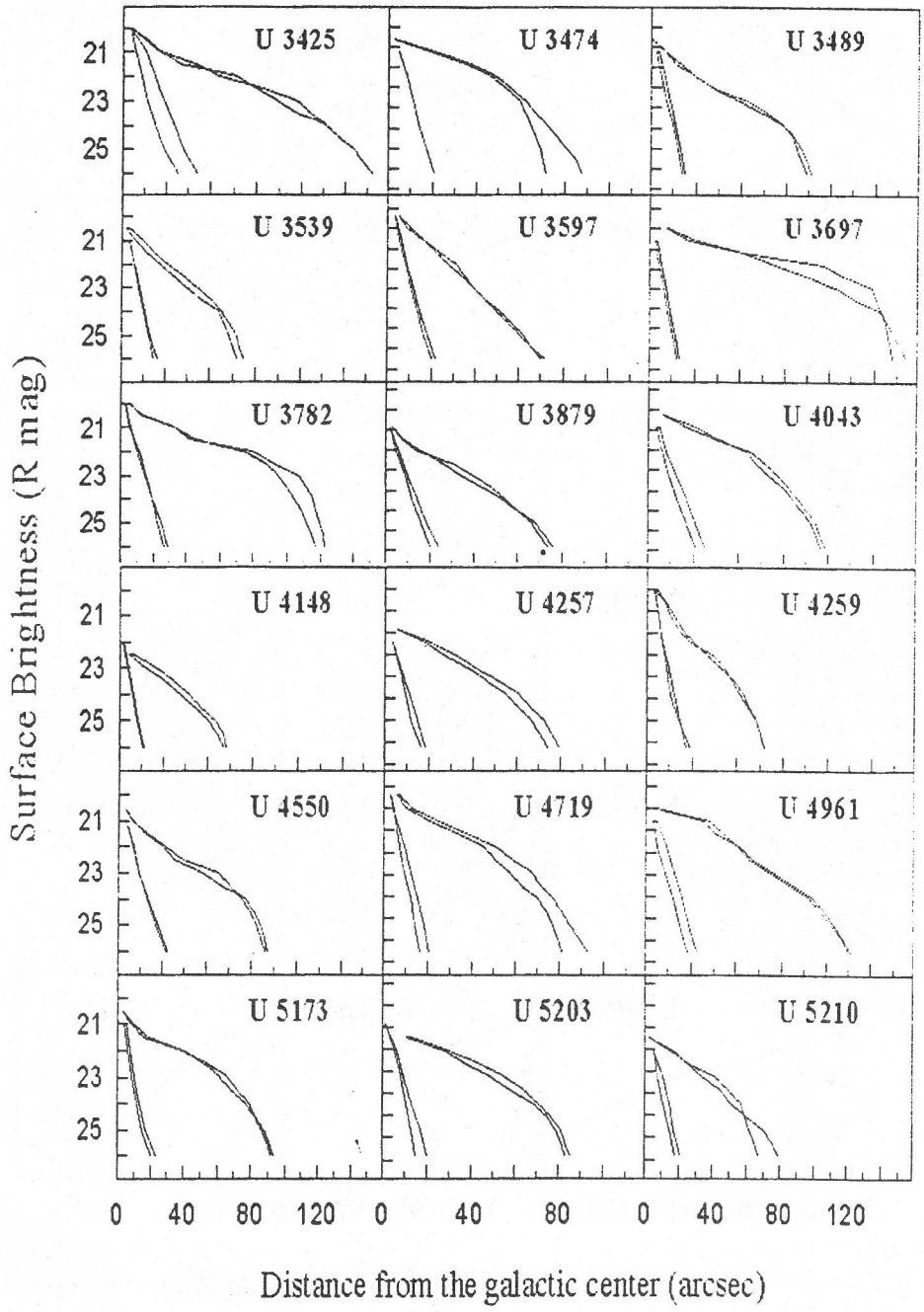

Fig. 5: (continued)

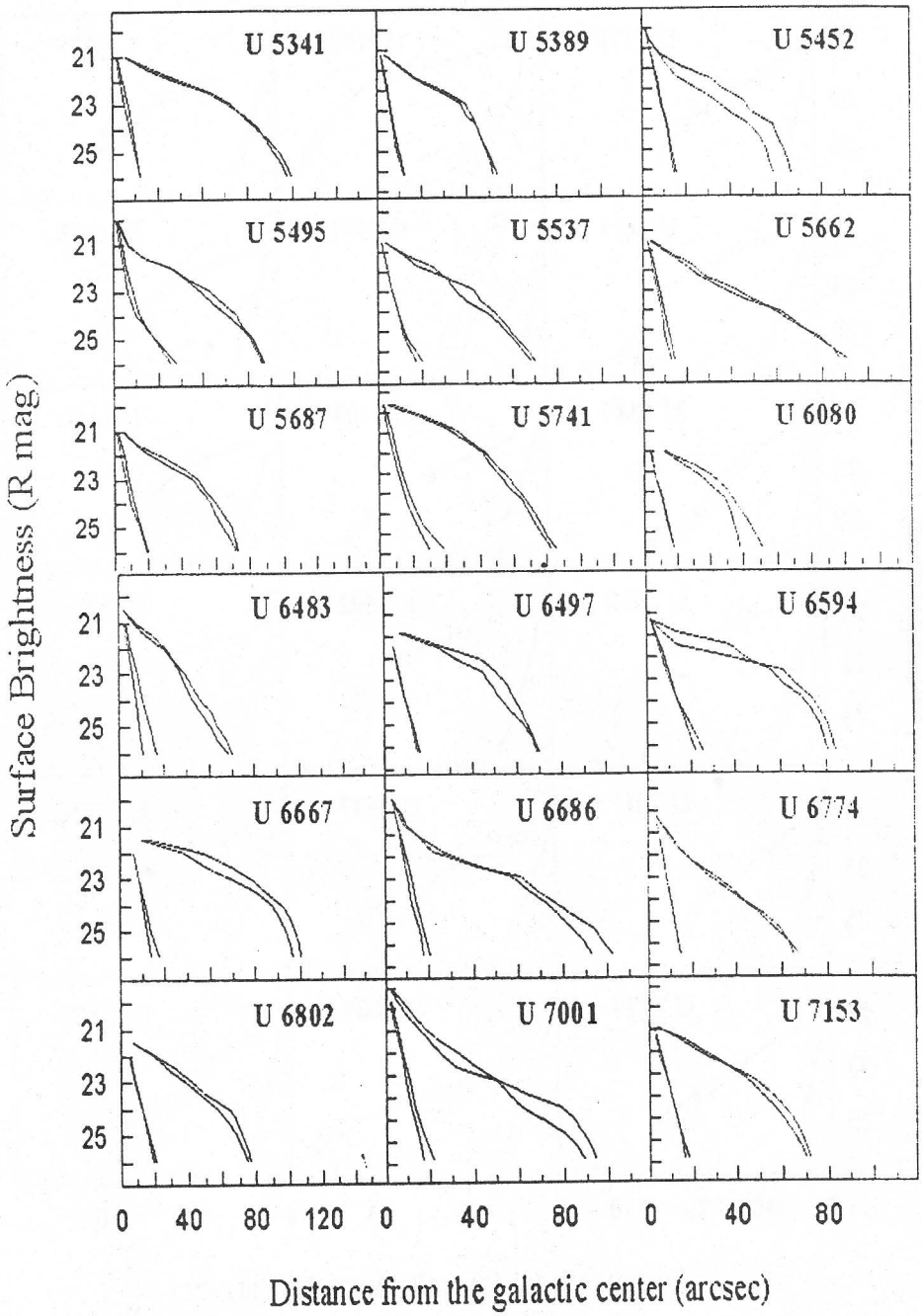

Fig. 5: (continued)

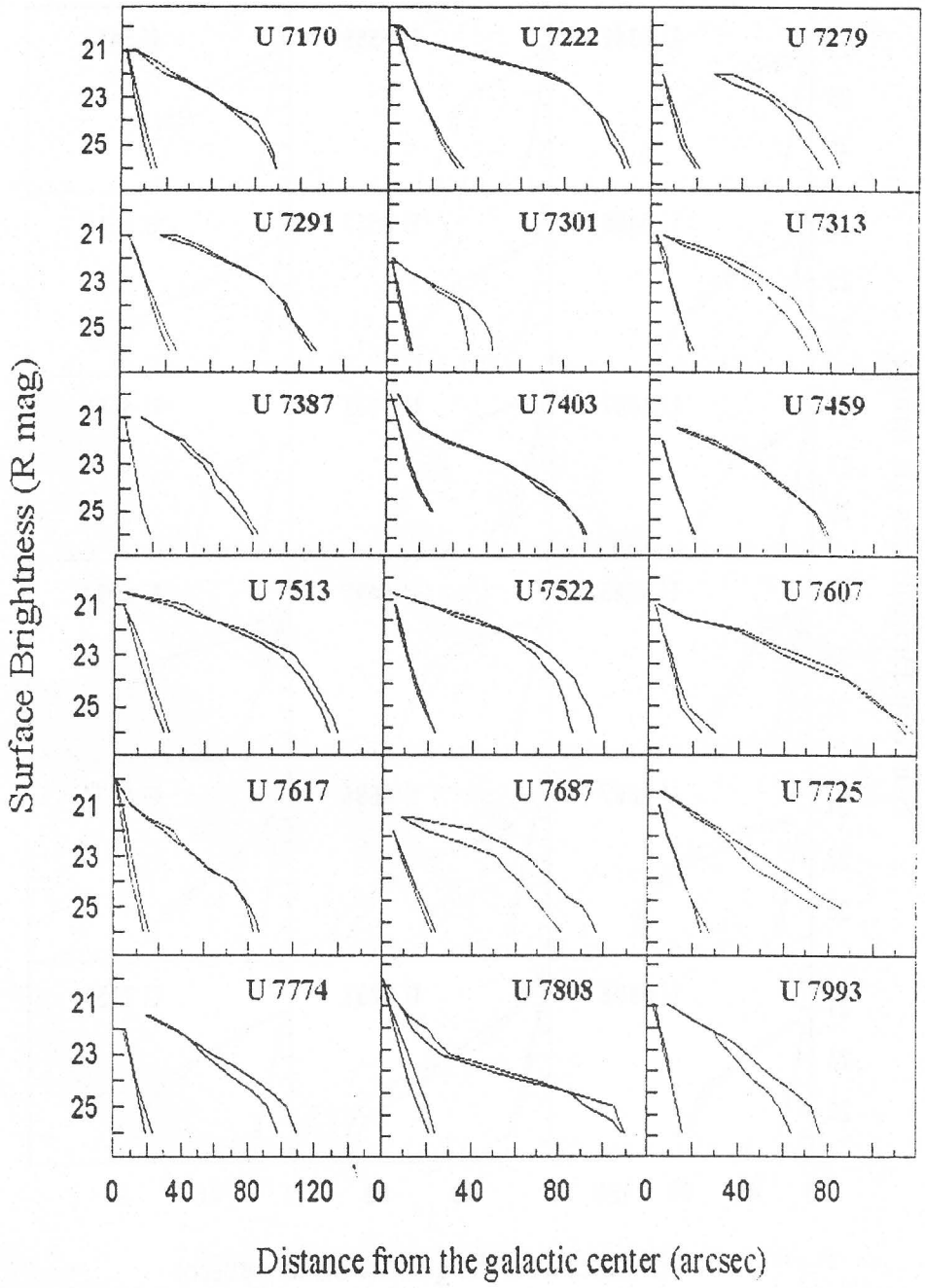

Fig. 5: (continued)

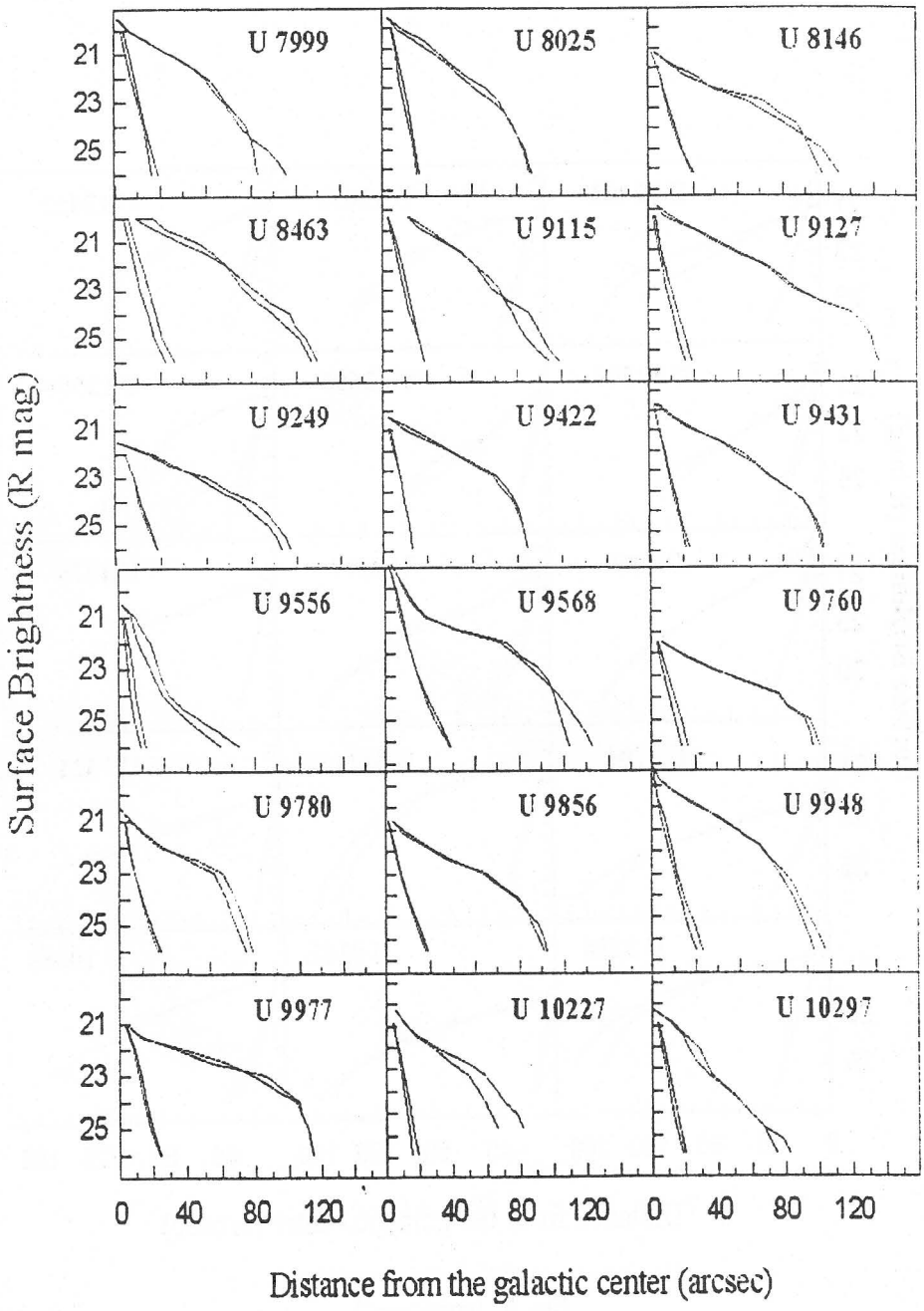

Fig. 5: (continued)

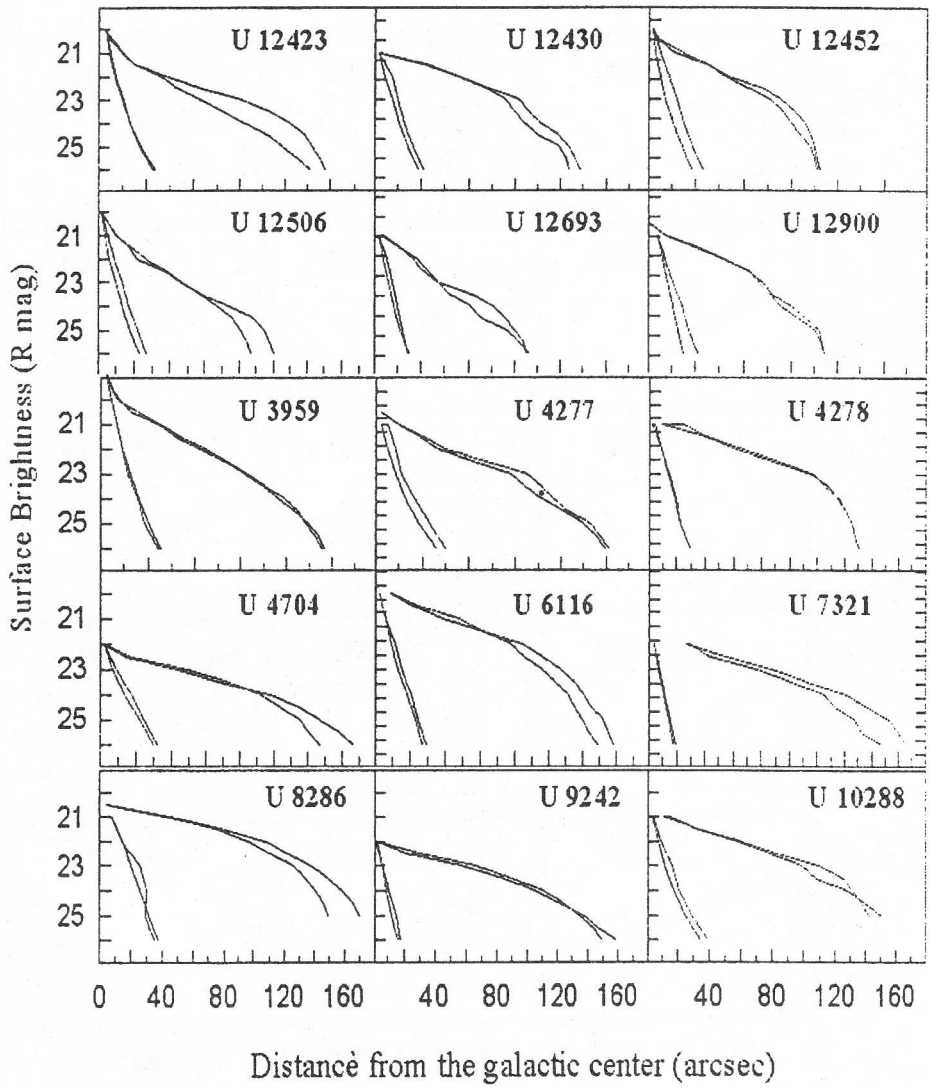

Fig. 5: (continued)

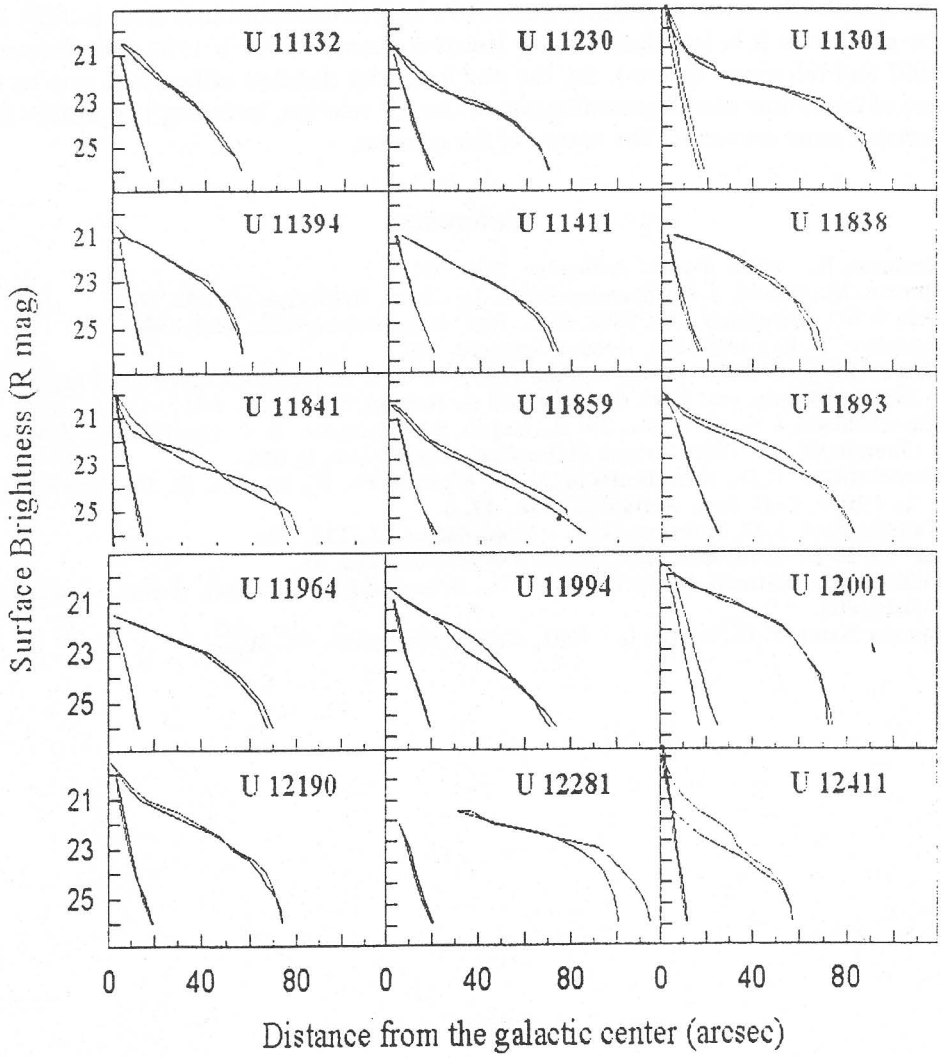

Fig. 5: (continued)

relative standard errors about 30%.

Generally, the scatter of the TF relations arises from four main sources – errors in the measurements of the parameters, uncertainties associated with the corrections applied to them, variance of the galactic properties and the Malmquist bias of the sample. The mean apparent scatter of the I band TF relation, in the case of galaxies in clusters, is typically about 0.4 mag (Bureau et al. 1996). It is known also, that in the scatter for the small galaxies exceeds 0.5 mag (relative distance error is 30%) and for giant ones it is less than 0.3 mag (relative distance error is 15%) (see Giovanelli 1997 and references therein). So, the way for better distance estimations may be the use of multidimensional generalization of the TF relation, including parameters that account more accurately the nature of the galaxies.

References

Bottema, R. : 1995, *Astron. Astrophys.*, **295**, 605.

Bureau, M., Mould, J. R., Staveley-Smith, L. : 1996, *Astrophys. J.*, **463**, 60.

Fall, S. M., Efstathiou, G. : 1980, *Mon. Not. Royal Astron. Soc.*, **193**, 189.

Georgiev, T. B. : 1992, *Sov. Astron. Lett.*, **18**, 299.

Giovanelli, R. : 1997, *Galaxy scalling relations, ESO astrophysics symposia*, Proc. of the ESO workshop, eds. L. N. da Costa and A. Renzini, Sprnger, p. 146.

Karachentsev, I. D., Georgiev, Ts. B., Kajsin, S. S., Kopylov, A. I., Ryadchenko, V. P., and Shergin, V. S. : 1992, *Astron. Astrophys. Transactions*, **2**, 256.

Karachentsev, I. D., Karachentseva, V. E., Kudrya, Yu. N., Sharina, M. E., Parnovsky, S. L. : 1999, *Bull. Spec. Astrophys. Obs.*, **47**, 5.

Karachentsev, I. D, Makarov, D. A. : 1996, *Astron. J.*, **111**, 794.

Larson, R. B., 1976, *Mon. Not. Royal Astron. Soc.*, **176**, 31.

Pohlen, M., Dettmar, R. J., Luetticke, R., Schwarzkopf, U. : 2000, *Astron. Astrophys.*, **144**, 405.

van der Kruit, P. C., Searle, L. : 1981, *Astron. Astrophys.*, **95**, 105.

Publ. Astron. Obs. Belgrade No. 73 (2002), 247 - 255 *Poster*

ON THE LARGE-SCALE PERIODICITY IN THE SPATIAL DISTRIBUTION OF RICH CLUSTERS OF GALAXIES

K. Y. STAVREV

Institute of Astronomy, Bulgarian Academy of Sciences, 72 Tsarigradsko Shosse Blvd., BG-1784 Sofia, Bulgaria
E-mail kstavrev@skyarchive.org

Abstract. In a study of the large voids in the spatial distribution of Abell/ACO clusters of galaxies in the Northern Galactic Hemisphere we have analysed the variations with redshift of the number density of clusters in a large solid angle (galactic latitude $b \geq +30°$) and to a limiting redshift $z \sim 0.2$, as well as the spatial distribution of large voids to $z \leq 0.14$. Two samples of clusters (1) with measured redshifts and (2) with measured or photometrically estimated redshifts have been used. While the first sample shows two maxima in the number density distribution at $z \sim 0.03$ and $z \sim 0.07$–0.08, known from previous studies, the second one shows also a well defined third maximum at $z = 0.12$–0.14 which coincides roughly with the third of the peaks in the number of galaxies towards the North Galactic Pole discovered by Broadhurst et al. (1990). The analysis of the spatial void distribution suggests the presence at $z \sim 0.07$–0.08 of a giant 2-D structure, composed of several known superclusters. We propose an explanation of the third density maximum at $z = 0.12$–0.14 as a combined effect of (1) the systematic overestimate of m_{10} – the magnitude of the tenth brightest cluster member – in Abell's catalogue which has affected our estimated redshifts, and (2) the presence in the redshift range 0.12–0.14 of another giant 2-D structure. The existence of the two large-scale structures is in agreement with a quasi-periodic distribution of the rich clusters of galaxies with a period $\Delta z \sim 0.05$.

1. INTRODUCTION

Using deep pencil-beam redshift surveys of galaxies in direction to the North and South Galactic Poles to $z \lesssim 0.3$ Broadhurst et al. (1990, hereafter BEKS) discovered a surprising regularity in the redshift distribution with most galaxies lying in discrete peaks with roughly equal separation of 128 h^{-1} Mpc (hereafter $H_0 = 100\,h$ km s^{-1} Mpc^{-1}). This unexpected result was later confirmed by the same authors on the basis of new 1-D surveys directed away off the galactic poles (Koo et al. 1993), as well as by other authors who used more or less deep samples of galaxies at different locations on the celestial sphere (Ettori et al. 1997, Vettolani et al. 1997, Drinkwater et al. 2000). Periodicity with a smaller characteristic scale has been also found in the redshift distribution of galaxies in the Hubble Deep Field (Williams et al. 1996) for the redshift range $z = 0.3$–1.1 (Cohen et al. 2000).

Strong evidence for the apparently periodic distribution of galaxies, as well as an explanation of this phenomenon, came from the analysis of wide-angle cluster sam-

ples. Bahcall (1991) was the first to show that the observed peaks in the redshift distribution of galaxies originate from the intersections of the narrow-beam surveys with the regions of known extended superclusters. Thus, the regularity in the distribution of galaxies is consistent with a description of the large-scale structure of the Universe as a network of superclusters and large voids with a typical mean separation of $\sim$ 100–150 h^{-1} Mpc. The structural reality of the peaks in BEKS survey has been confirmed also by Tully et al. (1992) and Guzzo et al. (1992) on the basis of deeper samples of rich clusters of galaxies. The former authors show that the periodicity maxima deliniated by BEKS coincide with giant structures composed of rich clusters which span over several hundred h^{-1} Mpc in directions orthogonal to the supergalactic plane (i.e. parallel to the galactic plane). Let us note that similar huge structure (stratum) with dimension $\sim$ 500 h^{-1} Mpc and roughly parallel to the galactic plane has been detected earlier by Kopylov et al. (1988) in the distribution of rich Abell clusters (richness class $R \geq 2$) towards the northern galactic cap at $z = 0.16$–0.18.

As some authors have shown, the existence of regularity in the distribution of galaxies with a characteristic scale $\gtrsim$ 100 h^{-1} Mpc leads to the appearance of a local peak in the power spectrum and to an oscillating correlation function. E.g. Einasto et al. (1997a, 1997b) obtain a power spectrum for the Abell clusters of galaxies with a well defined peak at a wavenumber $k = 0.05\ h$ Mpc^{-1}, corresponding to a wavelength of 120 h^{-1} Mpc, and an oscillating correlation function with regularly spaced secondary maxima and minima with a period of the oscillations 115 h^{-1} Mpc. This regularity is in contradiction with the standard theory of large-scale structure formation which predicts random distribution of the galaxies and clusters of galaxies on large scales. The origin of a large-scale periodicity can be explained by barionic acoustic oscillations during the early stages of the evolution of the Universe. However, as Eisenstein et al. (1998) have shown such an explanation requires too large baryon fraction in disagreement with the big bang nucleosynthesis constraints. To overcome the difficulties encountered in the frames of the standard structure formation scenario Kirilova & Chizhov (2000) propose a completely different mechanism of non-gravitational origin producing baryon density perturbations during the inflationary stage of the Universe which evolve into baryonic shells devided by vast underdence regions.

Up to now several of the nearest peaks in BEKS redshift distribution have been identified with large structures (superclusters, walls). As shown by Bahcall (1991) the first two northern and the first two southern peaks coincide with known superclusters from the catalogue of Bahcall & Soneira (1984, hereafter BS). The first northern peak ($z \sim 0.02$) is due to the Coma and Hercules superclusters (BS10, BS15) which form an extended flat structure in the distribution of galaxies, called "the Great Wall" (Geller & Huchra 1989). The second northern peak ($z \sim 0.08$) corresponds to the Corona Borealis supercluster (BS12). The first southern peak ($z \sim 0.02$) originates from the Perseus-Pisces supercluster (BS19), and the second southern peak ($z \sim 0.06$) is due to several superclusters (BS1–3, BS20). Tully et al. (1992) and Guzzo et al. (1992) have identified the third southern maximum at $z \sim 0.11$ with the Sculptor supercluster (Seitter et al. 1989).

In this paper we present some new evidence for the structural reality of the second and third northern peaks in the redshift distribution observed by BEKS. We show on the basis of the analysis of deeper and more complete samples of rich clusters of

galaxies that these peaks indicate the existense of huge 2-D structures composed of rich clusters extending roughly parallel to the galactic plane and separated by large voids. This result is consistent with the existence of a large-scale regularity in the spatial distribution of clusters of galaxies.

2. THE CLUSTER SAMPLES

We use two samples of rich clusters (richness class $R \geq 1$) from the catalogues of Abell (Abell 1958) and ACO (Abell, Corwin & Olowin 1989; hereafter ACO). The samples are limited in the Northern Galactic Hemisphere. The redshift data for the clusters have been compiled from four sources (Lebedev & Lebedeva 1996; NASA/IPAC Extragalactic Database; Slinglend et al. 1998; Andernach & Tago 1998). Details on the compilation of the redshift data and the preparation of the cluster samples are given in Stavrev (2000).

The first sample (sample AR/L) contains only clusters with spectroscopically measured redshifts. The number of objects in this sample for a limiting redshift $z \leq 0.2$ and a limiting galactic latitude $b \geq +30°$ is 486.

In order to increase the completeness of the first sample at larger distances we form a second sample (sample ARE/L) in the same spatial volume ($z \leq 0.2$, $b \geq +30°$) which in addition to the clusters with spectroscopically measured redshifts contains also clusters with photometrically estimated redshifts for which there are no spectroscopic measurements so far. For this purpose we use the calibration equation

$$\begin{array}{rcl} \log z & = & \underset{\pm 829}{-4.5372} + \underset{\pm\, 50}{0.2132}\, m_{10} \end{array}$$

from Kalinkov, Stavrev & Kuneva (1985), where m_{10} is the magnitude of the 10th brightest cluster member estimated by Abell (1958). Let us note that the photometrically estimated cluster redshifts may have large errors (20–30%). Sample ARE/L contains 1040 clusters.

3. ANALYSIS OF THE NUMBER DENSITY DISTRIBUTION OF CLUSTERS

Fig. 1 shows the variations of the spatial density of the number of clusters (in units $10^{-6}\ h^3\ \mathrm{Mpc}^{-3}$) as a function of the redshift for both analysed samples. The vertical lines in Fig. 1 correspond to the first four peaks in the number of galaxies discovered towards the North Galactic Pole by BEKS. The first two peaks are shown separately for the deep samples of galaxies (dotted line) and the bright samples (dashed-dotted line) used by BEKS (see their Fig. 1 a and b).

As it is seen in Fig. 1, the density distribution for the first sample AR/L (spectroscopically measured redshifts, solid line) fluctuates in the redshift range 0.01–0.09 around a mean level of about $6\ 10^{-6}\ h^3\ \mathrm{Mpc}^{-3}$, i.e. in agreement with the estimate by Bahcall & Cen (1993) for the mean spatial density of the $R \geq 1$ Abell/ACO clusters. Therefore, we accept that sample AR/L is fairly complete for $z \leq 0.09$. In this range the spatial number density of clusters shows two well defined maxima at $z =$ 0.02–0.04 and $z =$ 0.07–0.08 which coincide well with the first two northern peaks in BEKS redshift distribution of galaxies, and correspond, as already pointed out in Sect. 1, to the Great Wall and to the Corona Borealis supercluster, respectively. In

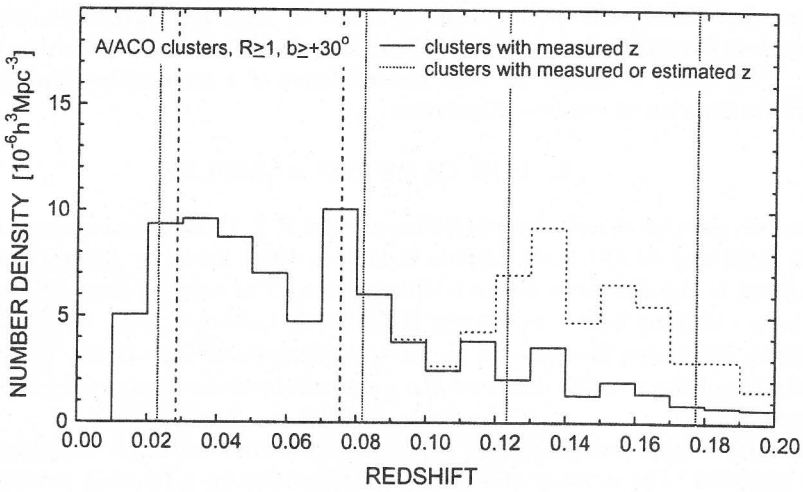

Fig. 1: Spatial number density of clusters as a function of redshift for Abell/ACO clusters of richness class $R \geq 1$ and galactic latitude $b \geq +30°$ (1) with measured redshifts (solid line), and (2) with measured or photometrically estimated redshifts (dashed line). The vertical lines correspond to the first four peaks in the number of galaxies discovered towards the North Galactic Pole by Broadhurst et al. (1990) according to the deep (dotted line) and bright (dashed-dotted line) galaxy samples used by them

the next redshift range, for $z = 0.09$–0.14, the number density of clusters with measured redshifts drops by about 50% because of the incompleteness of sample AR/L at larger distances. However, what makes impression is that the density in this range remains at the same mean level (although with some variations), showing no visible trend with the distance. For $z > 0.14$ the spatial density of clusters becomes very low due to the strong incompleteness of sample AR/L in this redshift range.

The number density distribution for the second sample ARE/L (measured or estimated redshifts, dashed line in Fig. 1) shows that the distribution function is identical with that for sample AR/L up to $z = 0.09$ and differs only slightly from it in the redshift range 0.09–0.12, while for $z > 0.12$ the difference is significant. As it is seen in Fig. 1, after the addition of the clusters with photometrically estimated redshifts a deep minimum in the number density of clusters is outlined at $z = 0.10$–0.11, followed by a high maximum for $z = 0.12$–0.14. This maximum coincides well with the third of the peaks in the number of galaxies in BEKS survey.

A similar strong density enhancement in the distance range 300–450 h^{-1} Mpc is known from the investigation of Scaramella et al. (1991) for a sample of rich ($R \geq 1$) Abell clusters, about 45% of which with estimated redshifts, and has been explained by these authors as an effect of the systematic overestimate of m_{10} for the distant clusters in Abell's catalogue. Such systematic errors do exist in this catalogue, as pointed out by Abell et al. (1989). However, in spite of the large errors introduced by the clusters with photometrically estimated redshifts the reality of the maximum at $z = 0.12$–0.14 cannot be definitely ruled out. An argument in support of this is the behaviour of

the number density function for sample AR/L in the redshift range 0.09–0.14. As already pointed out, there is almost no decline in the density with redshift in this range. This fact can be easily explained if a real density enhancement of clusters at z = 0.12–0.14 is assumed. Another, independent argument is the peak in the number of galaxies at these redshifts detected by BEKS. Therefore, we suggest that the density maximum at z = 0.12–0.14 is a combined effect of (1) the systematic overestimate of m_{10} in Abell's catalogue, which has affected our photometrically estimated redshifts, and (2) the presence at that redshift range of a real giant 2-D structure similar to the Great Wall and the dominant planes and orthogonal structures suggested by Tully et al. (1992) and Einasto M. et al. (1997).

Let us also note that the fourth northern peak of BEKS shown in Fig. 1 at $z = 0.17$–0.18 probably indicates another giant structure more since it coincides by distance with the huge stratum composed of $R \geq 2$ Abell clusters discovered by Kopylov et al. (1988) in the redshift range 0.16–0.18.

If we accept that the Great Wall and the suggested three more distant giant structures are located at redshifts 0.02–0.03, 0.07–0.08, 0.12–0.14, and 0.16–0.18, respectively, then the quasi-regularity in the distribution of rich clusters is characterized by a period $\Delta z \sim 0.05$.

4. ANALYSIS OF THE SPATIAL VOID DISTRIBUTION

The samples AR/L and ARE/L (with somewhat modified limits: $b \geq +20°$, $z \leq$ 0.16) have been used in Stavrev (2000) for identification of the large voids (diameter $D \geq 50\ h^{-1}$ Mpc) in the spatial distribution of galaxy clusters in a volume limited by galactic latitude $b \geq +30°$ and redshift $z \leq 0.14$ (distance $r \leq 420\ h^{-1}$ Mpc). (These limits concern the coordinates of the void centres.)

Fig. 2 shows cross-sections of the spatial distribution of the identified voids for both samples. A 3-D coordinate system centred in the Galaxy with axes x and y lying in the galactic plane and directed to points with galactic coordinates $l = 0°$, $b = 0°$ and $l = 90°$, $b = 0°$, respectively, and axis z directed to the North Galactic Pole, is used. Fig. 2 (a and b) present the two central cross-sections perpendicular to the galactic plane, along the x and y axes, respectively, for the voids in the distribution of the clusters from sample AR/L, and Fig. 2 (c and d) show the same but for sample ARE/L. Voids are marked with their serial numbers in the corresponding void catalogues described in Stavrev (2000). The cross-sections contain also the corresponding distributions of the clusters (filled circles) surrounding the voids (in slices 10 h^{-1} Mpc thick).

All cross-sections in Fig. 2 show that a large zone of enhanced number density of the clusters which is not intersected by large voids exists at a distance of 200–250 h^{-1} Mpc from the galactic plane. This zone is best outlined in Fig. 2 a and can be traced also in the adjacent cross-sections for $y \neq 0$ and $x \neq 0$ (not shown here). It is roughly parallel to the galactic plane (i.e. perpendicular to the supergalactic plane) with dimensions $\sim 300 \times 150\ h^{-1}$ Mpc along the x and y axes, respectively. This feature corresponds to the second maximum in the density distribution of Abell/ACO clusters at redshift $z = 0.07$–0.08 (see Fig. 1), as well as to the second northern peak in the number of galaxies in BEKS survey, and most probably indicates the presence of a giant 2-D structure similar to the Great Wall and to the giant structures suggested by Tully et al. (1992) and Einasto M. et al. (1997).

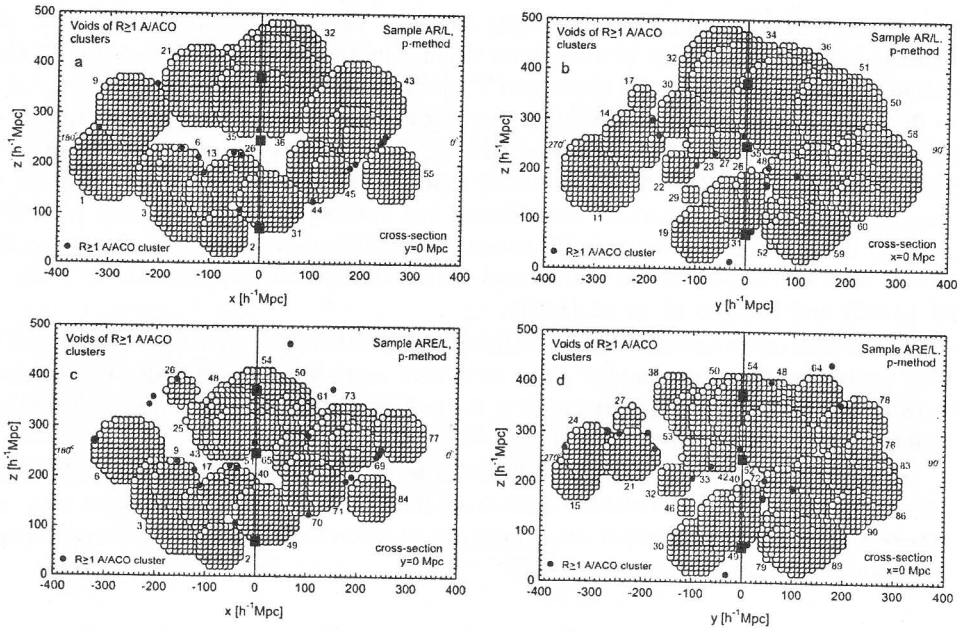

Fig. 2: Central cross-sections in the $x - z$ plane (left panel) and $y - z$ plane (right panel) of the spatial distribution of voids: a and b) voids of $R \geq 1$ Abell/ACO clusters with measured redshifts (sample AR/L), c and d) same as a and b but for clusters with measured or photometrically estimated redshifts (sample ARE/L). Voids are marked with their serial numbers from the corresponding void catalogues. The coordinate system is centred in the Galaxy with axes x and y directed to $l = 0°$, $b = 0°$ and $l = 90°$, $b = 0°$, respectively, and axis z directed to the North Galactic Pole. The distribution of clusters is shown by filled circles for slices 10 h^{-1} Mpc thick. The filled squares along the galactic axis correspond to the first three northern peaks in the redshift distribution of galaxies discovered by Broadhurst et al. (1990)

As we pointed out in Sect. 1, the second northern peak in the number of galaxies from BEKS survey was attributed by Bahcall (1991) most of all to the Corona Borealis supercluster. However, the dense zone which separates the large voids in Fig. 2 contains several more superclusters. We have identified this zone also in the spatial distribution of galaxies for a combined sample extracted from the Center for Astrophysics Redshift Catalogue (ZCAT, Huchra et al. 1992) and the MX Northern Abell Cluster Redshift Survey (Slinglend et al. 1998), shown in Fig. 3 for 19 879 galaxies in the Northern Galactic Hemisphere. A denser clumpy layer roughly parallel to the galactic plane can be seen in Fig. 3 a (shown by a horizontal arrow) at a distance $\sim$ 200–250 h^{-1} Mpc. It is composed of separate concentrations of galaxies elongated along the line-of-sight due to the finger-of-God effect. (Many of the "fingers" represent Abell clusters from the MX redshift survey.) These concentrations correspond (from left to right) to the Ursa Major, Draco, Boötes, and Corona Borealis superclusters (shown by vertical arrows). The layer borders on its nearest side with a less populated layer which contains the large void in Boötes.

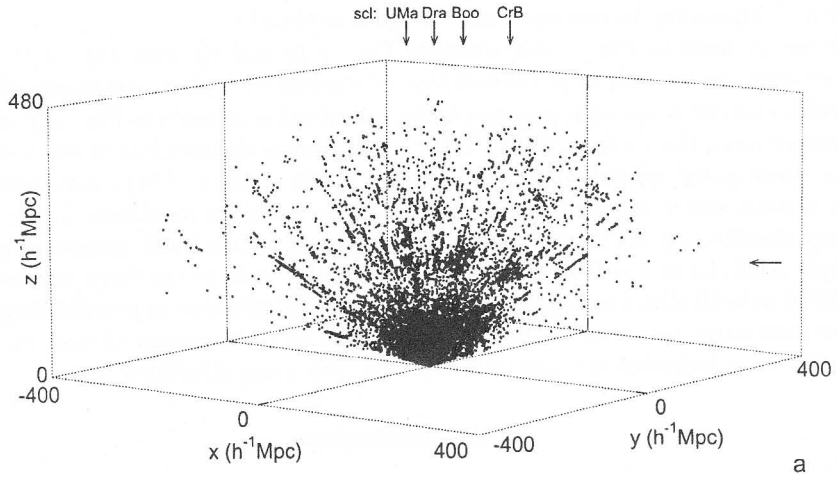

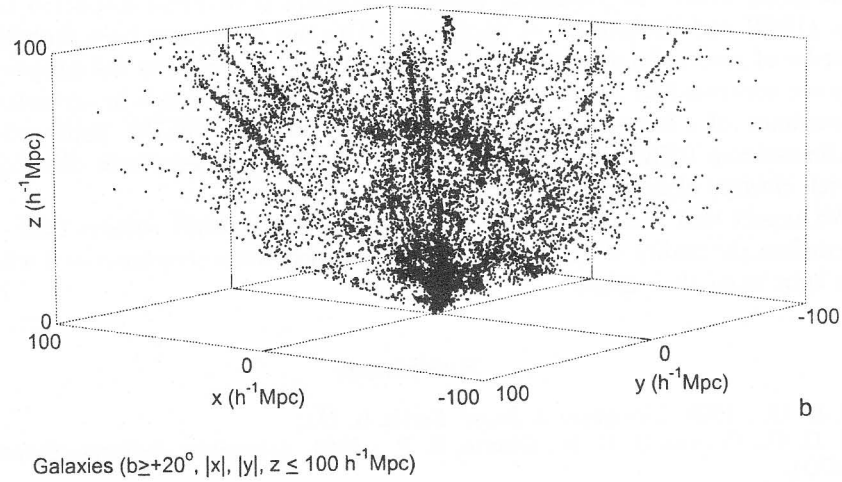

Fig. 3: Spatial distribution of the galaxies from the CfA Redshift Catalogue and the MX Northern Abell Cluster Redshift Survey, shown as perspective graphs with a coordinate system as in Fig. 2 for: a) 19 879 galaxies with galactic latitude $b \geq +20°$ and redshift $z \leq 0.16$, and a view point at $l \approx 320°$, $b \approx +18°$; the horizontal arrow and the vertical arrows show the positions of the superclusters in UMa, Dra, Boo, and CrB; b) galaxies to $|x|, |y|, z = 100\ h^{-1}$ Mpc and a view point at $l \approx 140°$, $b \approx +18°$

The distribution of galaxies in Fig. 3 b presents in more detail the nearer part of the distribution in Fig. 3 a (to 100 h^{-1} Mpc) seen from a view point opposite to that in Fig. 3 a. The Great Wall which corresponds to the first northern maximum

in BEKS redshift distribution is well outlined as a giant flat structure at a distance $\sim 80\ h^{-1}$ Mpc roughly perpendicular to the line-of-sight.

If we go back to Fig. 2 and compare Fig. 2 (c and d) with Fig. 2 (a and b), respectively, we see that after the addition of clusters with photometrically estimated redshifts another dense zone appears in the distribution of voids in Fig. 2 (c and d) at a distance along the z axis $\sim 400\ h^{-1}$ Mpc. This zone is situated just at the boundaries of the investigated spatial volume limited to a depth of $420\ h^{-1}$ Mpc and therefore its more distant side is not defined. It corresponds to the third maximum in the number density distribution of clusters with measured or photometrically estimated redshifts (sample ARE/L) at $z = 0.12$–0.14 (see Fig. 1) and is near to the third northern peak in BEKS redshift distribution. In spite of the uncertainties due to possible large errors in the estimated distances to the clusters, as well as to boundary effects, we suggest that this zone indicates another, more distant, flat giant structure.

5. Conclusions

The results from the analysis of the redshift distributions of rich Abell/ACO clusters in the Northern Galactic Hemisphere (Sect. 3), as well as of the spatial distribution of large voids of rich Abell/ACO clusters (Sect. 4), suggest the existence at redshifts 0.7–0.8 and 0.12–0.14 of giant two-dimensional structures, similar to the Great Wall and to the giant structures (dominant plane, orthogonal structures) suspected by Tully et al. (1992) and Einasto M. et al. (1997). The two structures have dimensions of the order of several hundred h^{-1} Mpc and are roughly parallel to the galactic plane. They are separated by large voids of rich clusters. This picture is in agreement with the existence of a large-scale regularity in the galaxy distribution, indicated by the one-dimensional BEKS survey, and is consistent with a quasi-periodic distribution of the rich clusters of galaxies with a period $\Delta z \sim 0.05$.

We expect that the results from the new extensive redshift surveys (2dF, SDSS) will confirm the reality of the two suggested extremely large structures and will throw more light upon their origin.

References

Abell, G. O. : 1958, *Astrophys. J. Suppl. Series*, **3**, 211.

Abell, G. O., Corwin, H. G. Jr., Olowin, R. P. : 1989, *Astrophys. J. Suppl. Series*, **70**, 1 (ACO).

Andernach, H., Tago, E. : 1998, *Large Scale Structure: Tracks and Traces*, eds. V. Müller et al., World Scientific Press, Singapore, p. 147.

Bahcall, N. A. : 1991, *Astrophys. J.*, **376**, 43 (BS).

Bahcall, N. A., Cen, R. : 1993, *Astrophys. J.*, **407**, L49.

Bahcall, N. A., Soneira, R. M. : 1984, *Astrophys. J.*, **277**, 27.

Broadhurst, T. J., Ellis, R. S., Koo, D. C., Szalay, A. S. : 1990, *Nature*, **343**, 726 (BEKS).

Cohen, J. G., et al. : 2000, *Astrophys. J.*, **538**, 29.

Drinkwater, M. J., et al. : 2000, *Astron. Astrophys.*, **355**, 900.

Einasto, J., et al. : 1997a, *Nature*, **385**, 139.

Einasto, J., et al. : 1997b, *Mon. Not. Roy. Ast. Soc.*, **289**, 801.

Einasto, M., Tago, E., Jaaniste, J., Einasto, J., Andernach, H. : 1997, *Astron. Astrophys. Suppl. Ser.*, **123**, 119.

Eisenstein, D. J., Hu W., Silk, J., Szalay, A. S. : 1998, *Astrophys. J.*, **494**, L1.

Ettori, S., Guzzo, L., Tarenghi, M. : 1997, *Mon. Not. Roy. Ast. Soc.*, **285**, 218.

Geller, M. J., Huchra, J. P. : 1989, *Science*, **246**, 897.
Guzzo, L., Collins, C. A., Nichol, R. C., Lumsden, S. L. : 1992, *Astrophys. J.*, **393**, L5.
Huchra, J. P., Geller, M. J., Clemens, C. M., Tokarz, S. P., Michael, A. : 1992, *Bull. Inform. CDS*, **41**, 31.
Kalinkov, M., Stavrev, K., Kuneva, I. : 1985, *Astron. Nachr.*, **306**, 283.
Kirilova, D. P., Chizhov, M. V. : 2000, *Mon. Not. Roy. Ast. Soc.*, **314**, 256.
Koo, D. C., Ellman, N., Kron, R. G., Munn, J. A., Szalay, A. S., Broadhurst, T. J., Ellis, R. S.: 1993, *Observational Cosmology*, eds. G. Chincarini et al., ASP Conf. Ser., vol. **51**, p. 112.
Kopylov, A. I., Kuznetsov, D. Yu., Fetisova, T. S., Shvartsman, V. F. : 1988, *Large Scale Structures of the Universe*, eds. J. Audouze et al., p. 129.
Lebedev, V. S., Lebedeva, I. A. : 1996, *A compilation of redshifts of clusters of galaxies, electronic version 1996.0.*
Scaramella, R., Zamorani, G., Vettolani, G., Chincarini, G. : 1991, *Astron. J.*, **101**, 342.
Seitter, W. C., Ott, H. A., Duemmler, R., Schuecker, P., Horstmann, H. : 1989, *Morphological Cosmology*, eds. P. Flin, H. W. Duerbeck, Lecture Notes in Physics, vol. **332**, p. 3.
Slinglend, K., Batuski, D., Miller, C., Haase, S., Michaud, K., Hill, J. M. : 1998, *Astrophys. J. Suppl. Series*, **115**, 1.
Stavrev, K. Y. : 2000, *Astron. Astrophys. Suppl. Ser.*, **144**, 323.
Tully, R. B., Scaramella, R., Vettolani, G., Zamorani, G. : 1992, *Astrophys. J.*, **388**, 9.
Vettolani, G. et al. : 1997, *Astron. Astrophys.*, **325**, 954.
Williams, R. E., et al. : 1996, *Astron. J.*, **112**, 1335.

Publ. Astron. Obs. Belgrade No. 73 (2002), 257 - 263 *Poster*

RED SUPERGIANTS IN M 33 GALAXY

O. VASSILEV[1], L. VASSILEVA[2], G. IVANOV[1] and D. VASSILEV[3]

(1) Department of Astronomy, University of Sofia,James Bourchier 5, Sofia 1164, Bulgaria

(2) Institute of Astronomy, Bulgarian Academy of Sciences, 72 Tsarigradsko chaussèe, BG – 1784 Sofia, Bulgaria

(3) Department of Informatics, Sofia University, James Bourchier Ave. 5, BG – 1164 Sofia, Bulgaria

E-mail ovassilev@tenzor-bg.com

E-mail lubav@astro.bas.bg

E-mail ivanov@phys.uni-sofia.bg

E-mail dvasilev@ucc.uni-sofia.bg

Abstract. In the present work the spatial distribution of the red supergians in M 33 galaxy is discussed. The observational data exhibit stellar groups of high stellar density. The smallest 60 groups with stellar density corresponding to signal-to-noise ratio $S/N > 5$ have a mean size of 8.1″ ($\approx$ 30 pc). They are real stellar associations in M33. The size of the largest stellar groups found in M33 is of about 200″ ($\sim$ 0.8 kpc) and is typical for a stellar complex.

1. OBSERVATIONAL DATA AND RED SUPERGIANTS SAMPLES

We applied an approach, proposed by Popov et al. (2002), to obtain a continuous picture of the spatial distribution of the brightest stars in M 33 galaxy. Their JHK photometry is published in the *Two Micron All Sky Survey* (2MASS). The initial sample of stars was selected using a square field with a width of 1.5° and centered on M 33 nucleus (Table 1). Figure 1 illustrates the differences between the stellar populations, occupying areas of equal angular size outside the boundaries of the galaxy (Fig. 1a) and within its effective diameter (Fig. 1b). Several hundreds of stars have been detected (Table 2) at the red end of the evolutionary tracks (Lejeune et al. 1997); they are most probably red supergiants (RSGs) in the mass range of 12-20 $M_{\odot}$. Figure 2 clearly shows the location of the stellar disk cut off along the major axis: a = 32′ at ($S/N < 3$). It is natural to set a limit K > 13^{m} since brighter stars should belong to the Milky Way (Fig. 1) - the total number of objects in the sample with this single restriction (Sample 1) is denoted as N_1. Another sample is a subsample of Sample 1 and contains stars selected by criterion $J - K > 1.1$ which leads to even stronger S/N ratio and also testifies that the stellar disk ends at $a \approx 30'$ along the major axis (see Fig.3). Further we take into consideration only a sample of

Table 1: General information on M 33 galaxy

Center's (nucleus) coordinates (de Vaucouleurs & Leach 1981):
$\alpha(2000) = 01^h33^m50.89^s$
$\delta(2000) = +30°39'36.7''$
Fundamental observables (RC3):
$D25 = 35.4'$
$(a/b) = 1.698$
$a_{eff} = 13.5'$
Positional angle P. A. = 23°
Inclination angle i = 54.3°
Distance modulus (Lee et al. 2002):
$m - M = 24.52^m$
Foreground extinction (Schlegel et al. 1998):
$E_{B-V} = 0.135$
$E_{J-K} = 0.072$; $A_K = 0.050$

$N_2 = 1650$ stars populating the whole area 1.5° × 1.5° and constrained by conditions: $K > 13^m$ and $J - K > 1.1$ (Sample 2).

2. SURFACE BRIGHTNESS AND COLOUR MAPS

The individual J and K magnitudes of the stars with rectangular coordinates X and Y, relative to M 33 center, represented by δ-functions, were convoluted with 2D gaussians ($\sigma = 50''$), cut-off level at 3σ. Their contribution to the surface brightness in each pixel is calculated by: $\mu = -2.5\log(10^{-0.4\,m}/(\text{pixel size})^2)$. The chosen scale of $5''$/pixel gives an image of 1020 × 1020 pixels after removal of $150''$ strips from both sides in X and Y in order to avoid edge effects. The adopted foreground surface brightnesses μ_1 (Sample 1) and μ_2 (Sample 2) are given in Table 3. For their calculation we used a hexagonal grid consisting of about 200 independent measurements of the foreground surface brightness.

The choice of $\sigma = 50''$ conditioned by our intent to recover the grand design features of M 33. We expected to find structures not smaller than $150''$ (~ 0.6 kpc at the distance of M 33), i.e. stellar complexes or spiral arms of 1/2 arm width.

3. THE MAIN RESULTS

1. The spiral pattern of M 33 is delineated as area with high density of RSGs (Fig. 3) and with surface brightness μ_2 (in K passband) larger than 23 mag.arcsec^{-2} (Fig. 4).

2. The spiral structure is patchy - there were detected several regions of enhanced surface brightness, especially in the central region ($15'' \times 15''$). Their size of about $200''$ (~0.8 kpc) is typical of a stellar complex (Fig. 4).

3. A pair of dusty arms is visible on $(J-K)$ color map (Fig. 5). They surround the central region of maximal K-surface brightness. Assuming the mean $< J - K >= 1.2$

to be the true color for a red supergiant and $< J-K >$=1.8 at the ridges of the dusty arms, a value of $A_V = 3.$ could be derived which reflects 1/2 of the optical depth of the disk: 1.086 $\tau_V = 2$ A_V. A rough estimate of the vertical optical depth in the dusty arms is obtained: $\tau_B = 4.5$, with preliminary correction for inclination (factor $a\ cos(i)$) and postulating $A_B = 1.331$ A_V. The disk of M 33 seems to be optically thick at least at the rigdes of its spiral arms - like in the case of other nearby spiral galaxy M 31 (Nedialkov & Ivanov 1999).

4. An impressive coincidence exists between the K-band surface brightness map and the H-alpha emission map (Fig. 6). This indicates that the RSGs and their progenitors OB stars (not visible in IR) are well mixed in the space and the star formation in M 33 disk has been a continuous process over the last 10 Myr.

Table 2: Foreground contamination in the field of M 33 galaxy derived from counts in elliptical rings of one and the same area of 200 arcmin^2. The expected number of MW stars is $N_1 = (138 \pm 12)$ for Sample 1, and $N_2 = (15 \pm 4)$ Sample 2.

a'	N_1	cont. %	N_2	cont. %
12.6	819	16.8	431	3.5
16.4	451	30.6	214	7.0
19.4	367	37.6	180	8.3
22.0	309	44.7	118	12.7
24.4	239	57.7	79	19.0
26.5	188	73.4	48	31.3
28.5	177	78.0	48	31.3
30.3	159	86.8	34	44.1
32.0	156	88.5	35	42.9
33.7	130	106.2	16	93.8
35.3	162	85.2	20	75.0
36.8	138	100.0	21	71.4
38.2	140	98.6	13	115.4

Table 3: Adopted foreground surface brightnesses in [mag.arcsec^{-2}] in J and K passbands: μ_1 for Sample 1 and μ_2 for Sample 2.

Band	μ_1	μ_1 $(S/N = 5)$	μ_2	μ_2 $(S/N = 5)$
J	24.7 ± 0.6	24.0	28.7 ± 1.0	27.5
K	24.0 ± 0.4	23.1	27.3 ± 0.9	26.1

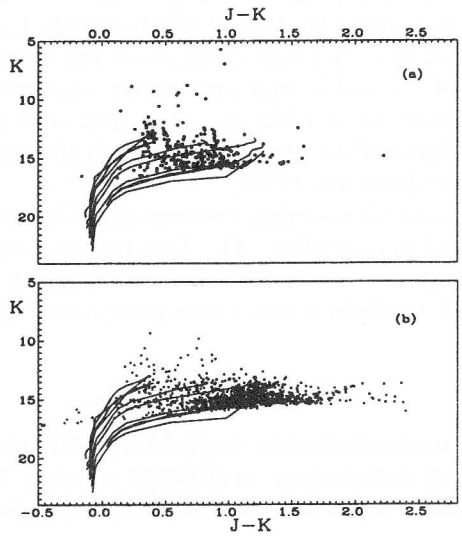

Fig. 1: Colour-magnitude diagrams K vs. $J-K$ for areas of equal angular size in: (a) foreground field, and (b) within the effective diameter of M 33. Note the strong crowding of RSGs at $K = 13^m - 16^m$ and $J-K = 1.2^m$. The evolutionary tracks (solid lines) for stars with initial mass between 12-60 $M_\odot$ are also shown.

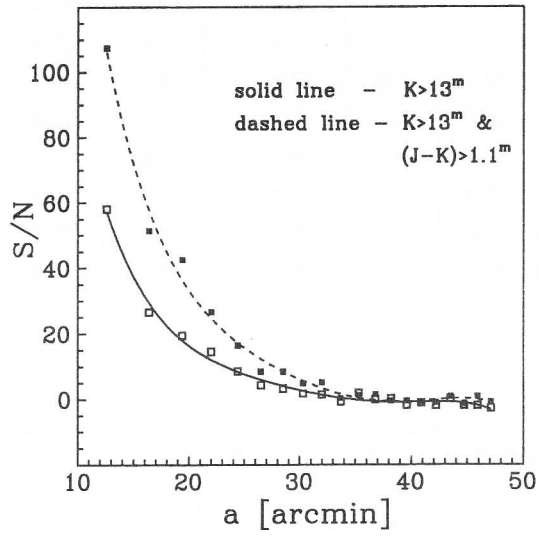

Fig. 2: The signal-to-noise ratio versus major axes of elliptical rings of one and the same area: 200 arcmin^2.

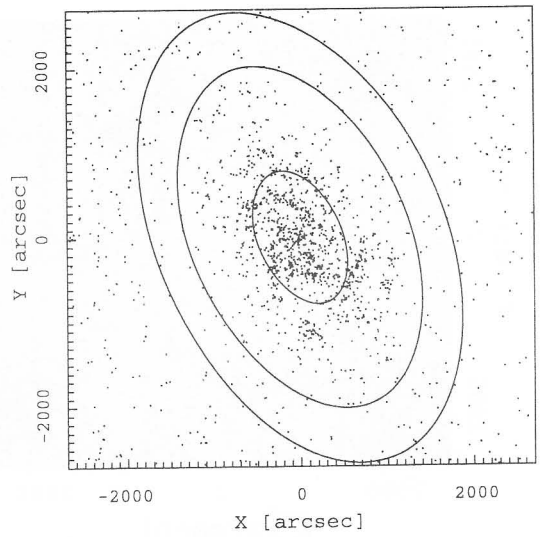

Fig. 3: Program field and spatial distribution of the stars (filled circles) from Sample 2 ($K > 13^m$ and $J - K > 1.1^m$). The size of the smallest ellipse corresponds to the effective diameter along the major axis, that of the intermediate - to D25, and the outermost ellipse encompasses an area, equal to the area outside of it.

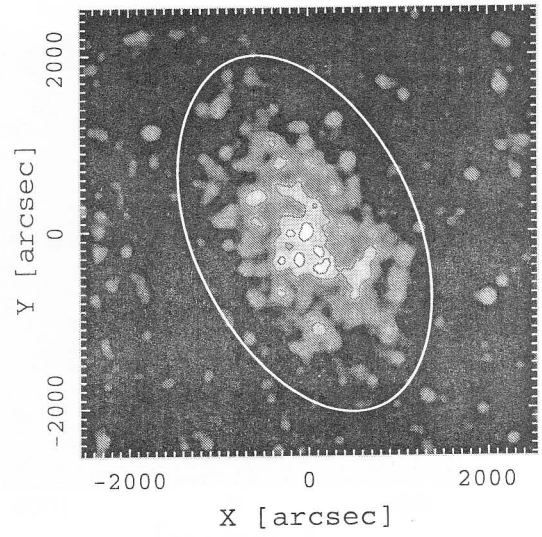

Fig. 4: Gray-scale representation of the surface brightness in K-band. The inner isophote corresponds to $\mu_K = 22$ mag arcsec^{-2} and the outer - to $\mu_K = 24$ mag arcsec^{-2} . The gray scale reaches $\mu_K = 24.5$ mag arcsec^{-2} (black). The diameter of the white ellipse is D25′.

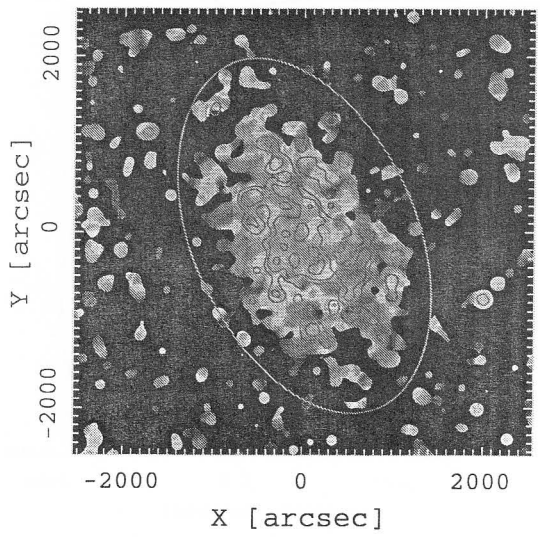

Fig. 5: A false colour map in $(J-K)$ with superimposed isophote μ_K = 23 mag arcsec^{-2}. The bluest end is at $(J-K) = 0.8^m$ in violet and the reddest end - at $(J-K) = 2.3^m$ in red. Note the prominent spiral pattern in green $(J-K = 1.8)$ indicating the dusty arms.

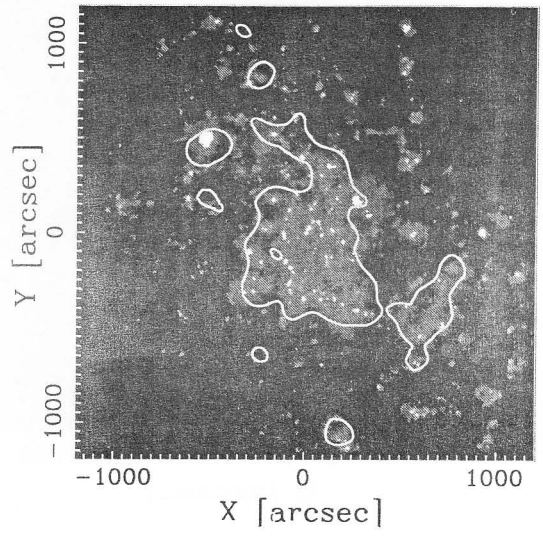

Fig. 6: The surface brightness isophote $\mu_K = 23$ mag arcsec^{-2}, superimposed on grey-scale H-alpha map within the inner area $2400'' \times 2400''$ of the program field (Fig. 3).

4. DISCUSSION

In the near future we intend to:
1. Correlate the surface brightness in IR with its estimates in optical passbands and H-alpha.
2. Resolve the stellar associations in M 33 via convolution with gaussians of different widths.
3. Study the B/R and WR/R ratio as a function of the galactocentric distance and metallicity and also their variation in the OB associations.
4. Derive precise extinction values from the individual colors of the RSGs.

Acknowledgments

This publication makes use of data from the *Two Micron All Sky Survey*, which is a joint project of the University of Massachusetts and the Infrared Processing and Analysis Center/California Institute of Technology, funded by the National Aeronautics and Space Administration and the National Science Foundation.
O. V. and G. I. acknowledge the partial support by the contract Nr. F-825/1998 with the Bulgarian National Science Foundation, Ministry of Education and Sciences.

References

de Vaucouleurs, G., Leach, R.: 1981, *Publ. Astron. Soc. Pacific*, **93**, 190.
de Vaucouleurs, G., de Vaucouleurs, A., Corwin, H. Jr., Buta, R., Paturel, G., Fouque, P.: 1991, *Third reference catalog of Bright galaxies (RC3)*, Heidelberg, Springer.
Lee, M., Kim, M., Sarajedini, A., Geisler, D., Gieren, W.: 2002, *Astrophys. J.*, **565**, 959.
Lejeune, T., Cuisinier, F., Buser, R.: 1997, *Astron. Astrophys. Suppl. Series*, **125**, 229.
Nedialkov, P., Ivanov, V.: 1999, *Astron. Astrophys. Trans.*, **17**, 367.
Popov, G., Nedialkov, P., Roussev, I., Veltchev, T.: 2002, (this meeting).
Schlegel, D., Finkbeiner, D., Davis, M.: 1998, *Astrophys. J.*, **500**, 525.

AUTHOR INDEX

LIST OF PARTICIPANTS

Ana Borisova - Institute of Astronomy, Bulgarian Academy of Sciences, Bulgaria
e-mail: ana@skyarchive.org

Anelia Staneva – Sofia University, Bulgaria,
e-mail: avesta@phys.uni-sofia.bg

Daniela Andreeva - Institute of Space Research, Bulgarian Academy of Sciences, Bulgaria
e-mail: danvasan@astro.bas.bg

Dimitar Vassilev - Sofia University, Bulgaria
e-mail: dvasilev@ucc.uni-sofia.bg

Dragomir Olević – Astronomical Observatory-Belgrade, Serbia
e-mail: dolevic@aob.bg.ac.yu

Edi Bon - Astronomical Observatory-Belgrade, Serbia
e-mail: ebon@aob.bg.ac.yu

Endrik Kruegel - Max Planck MPIfR - Bonn, Germany
e-mail: p309ekr@mpifr-bonn.mpg.de

Galin Borisov - Institute of Astronomy, Bulgarian Academy of Sciences, Bulgaria
e-mail: gborisov@astro.bas.bg

Georgi Ivanov - Sofia University, Bulgaria
e-mail: ivanov@phys.uni-sofia.bg

Hristo Lukarski - Institute of Space Research, Bulgarian Academy of Sciences, Bulgaria
e-mail: loukarski@astro.bas.bg

Ivan Yankulov - Sofia University, Bulgaria

Jordanka Borissova - Institute of Astronomy, Bulgarian Academy of Sciences, Bulgaria
e-mail: yura@haemimont.bg

Lubomir Iliev - Institute of Astronomy, Bulgarian Academy of Sciences, Bulgaria
e-mail: liliev@astro.bas.bg

Katya Tsvetkova - Institute of Astronomy, Bulgarian Academy of Sciences, Bulgaria
e-mail: katya@skyarchive.org

Konstantin Stavrev- Institute of Astronomy, Bulgarian Academy of Sciences,Bulgaria
e-mail: kstavrev@skyarchive.org

Krasimira Yankova - Institute of Space Research, Bulgarian Academy of Sciences, Bulgaria
e-mail: f7@space.bas.bg

Luba Vassileva - Institute of Astronomy, Bulgarian Academy of Sciences, Bulgaria
e-mail: lubav@astro.bas.bg

Lubomir Iliev - Institute of Astronomy, Bulgarian Academy of Sciences, Bulgaria
e-mail: liliev@astro.bas.bg

Luka Popović - Astronomical Observatory-Belgrade, Serbia
e-mail: lpopovic@aob.bg.ac.yu

Maria Dimitrova - Institute of Space Research, Bulgarian Academy of Sciences, Bulgaria
e-mail: maria@space.bas.bg

Marusja Bachvarova - Institute of Space Research, Bulgarian Academy of Sciences, Bulgaria
e-mail: marusjab@yahoo.com

Milan Dimitrijević - Astronomical Observatory-Belgrade, Serbia
e-mail: mdimitrijevic@aob.bg.ac.yu

Milcho Tsvetkov - Institute of Astronomy, Bulgarian Academy of Sciences, Bulgaria
e-mail: tsvetkov@skyarchive.org

Miodrag Dacic - Astronomical Observatory-Belgrade, Serbia
e-mail: dacic@aob.bg.ac.yu

Oleg Vassilev - Sofia University, Bulgaria
e-mail: ovassilev@tenzor-bg.com

Orlin Stanchev - Institute of Astronomy, Bulgarian Academy of Sciences, Bulgaria
e-mail: stanchev@astro.bas.bg

Petko Nedialkov – Sofia University, Bulgaria
e-mail: japet@phys.uni-sofia.bg

Predrag Jovanović - Astronomical Observatory-Belgrade, Serbia
e-mail: pjovanovic@aob.bg.ac.yu

Radostin Kurtev – Sofia University, Bulgaria
e-mail: kurtev@phys.uni-sofia.bg

Renada Konstantinova-Antova - Institute of Astronomy, Bulgarian Academy of Sciences, Bulgaria
e-mail: antovi@astro.bas.bg

Rossitsa Ivanova – Veliko Tarnovo, Bulgaria

Rumen Bogdanovski - Institute of Astronomy, Bulgarian Academy of Sciences, Bulgaria
e-mail: R.Bogdanovski@astro.bas.bg

Slobodan Ninković - Astronomical Observatory-Belgrade, Serbia
e-mail: sninkovic@aob.bg.ac.yu

Svetlin Fotev – Institute of Space Research, Bulgarian Academy of Sciences, Bulgaria
e-mail: sfotev:@space.bas.bg

Todor Veltchev – Sofia University, Bulgaria
e-mail: eirene@phys.uni-sofia.bg

Tsvetan Georgiev - - Institute of Astronomy, Bulgarian Academy of Sciences, Bulgaria
e-mail: tsgeorg@astro.bas.bg

Valeri Golev - Sofia University, Bulgaria
e-mail: valgol@phys.uni-sofia.bg

Vasil Popov - Institute of Astronomi, Bulgarian Academy of Sciences, Bulgaria
e-mail: vpopov@astro.bas.bg

Vladan Chelebonović – Institute of Astronomy, Serbia
e-mail: vcelebonovic@sezampro.yu

Vladimir Shkodrov - Institute of Astronomi, Bulgarian Academy of Sciences, Bulgaria
e-mail: vshkodrov@eagle.cu.bas.bg

Vojislava Protic Benisek - - Astronomical Observatory-Belgrade, Serbia
e-mail: vprotic@aob.bg.ac.yu

Yuliana Goranova - Institute of Astronomi, Bulgarian Academy of Sciences, Bulgaria
e-mail: julya_bg@astro.bas.bg

Zoran Simic - Astronomical Observatory-Belgrade, Serbia
e-mail: zsimic@aob.bg.ac.yu

Zorica Cvetković - Astronomical Observatory-Belgrade, Serbia
e-mail: mdimitrievic@aob.bg.ac.yu

Fig. 1. Participants of the III Bulgarian-Serbian Astronomical Meeting (All photos save for the photos 37 and 39 taken by Miodrag Dačić. Photos 37 and 39 are taken by Vojislava Protić Benišek). Sitting: Miodrag Dačić, Galin Borisov, Dragomir Olević. First row: Vladan Čelebanović, Jordanka Borisova, Vladimir Shkodrov, Georgi Ivanov, Milan S. Dimitrijević.

Fig. 2. Georgi Ivanov, Milan S. Dimitrijević.

Fig. 3. Vladimir Shkodrov, Georgi Ivanov, Milan S. Dimitrijević.

Fig. 4. III Bulgarian-Serbian Astronomical Meeting.

Fig. 5. Predrag Jovanović, Rumen Bogdanovski, Edi Bon.

Fig. 6. Ljubomir Iliev, Predrag Jovanović.

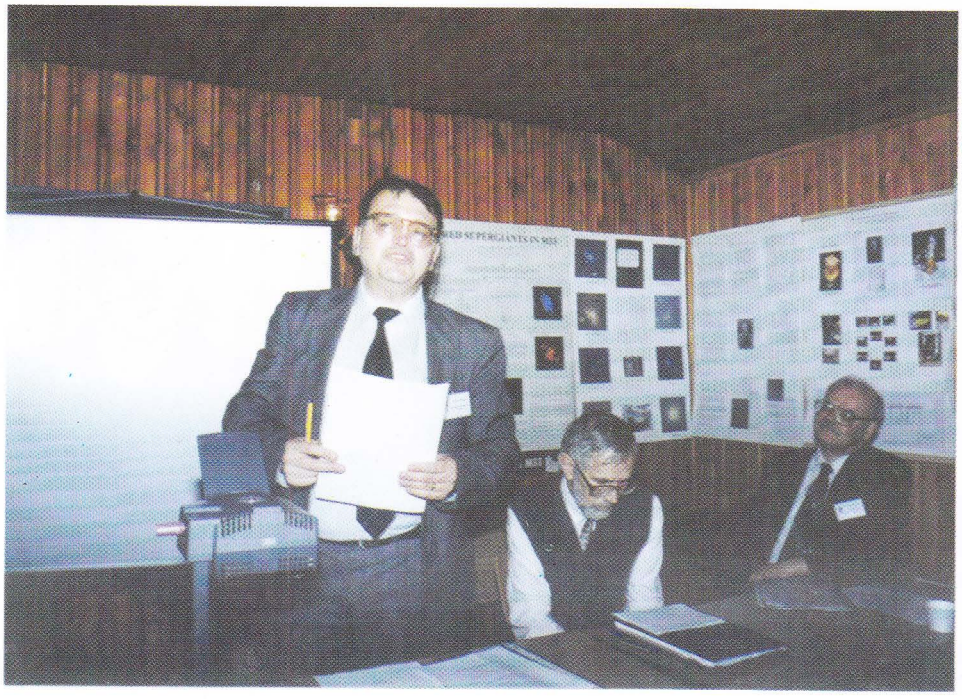

Fig. 7. Miltcho Tsvetkov, Georgi Ivanov, Milan S. Dimitrijević.

Fig. 8. Hristo Lukarski, Anelia Staneva, Tsvetan Georgiev.

Fig. 9. Slobodan Ninković, Todor Velchev, Endrik Kruegel.

Fig. 10. Valeri Golev, Miltcho Tsvetkov, Georgi Ivanov, Milan S. Dimitrijević.

Fig. 11. Luka Č. Popović, Miltcho Tsvetkov, Georgi Ivanov, Milan S. Dimitrijević.

Fig. 12. First row: Miltcho Tsvetkov, Luka Č. Popović, Radostin Kurtev, Ani Lukarska, Hristo Lukarski, Anelia Staneva.

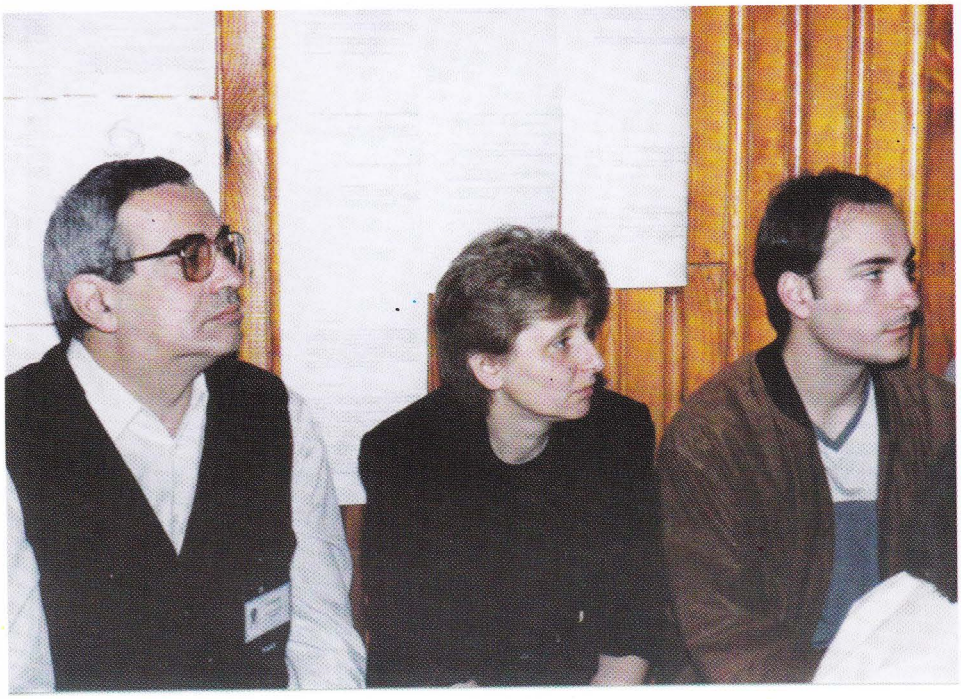

Fig. 13. Valeri Golev, Jordanka Borisova, Orlin Stanchev.

Fig. 14. Georgi Ivanov, Milan S. Dimitrijević, Miltcho Tsvetkov.

Fig. 15. Rositsa Ivanova, Georgi Ivanov, Milan S. Dimitrijević.

Fig. 16. Zorica Cvetković, Miltcho Tsvetkov.

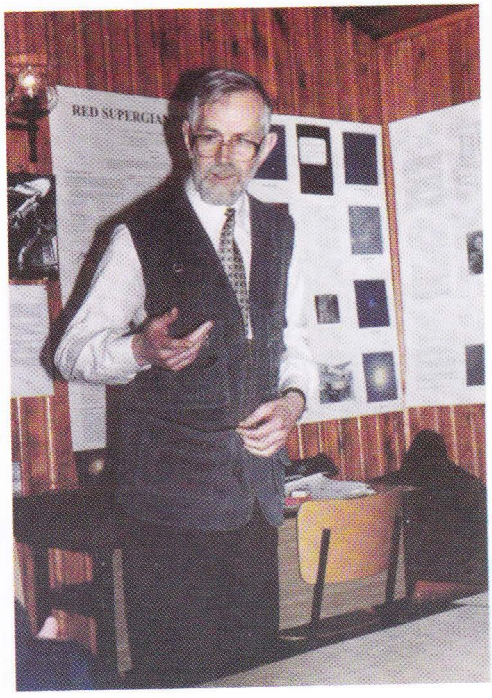

Fig. 17. Georgi Ivanov.

Fig. 18. Todor Velchev.

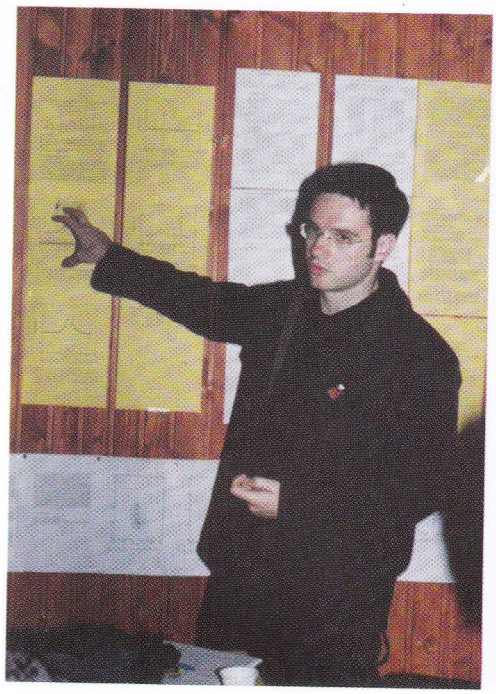

Fig. 19. Edi Bon.

Fig. 20. Radostin Kurtev.

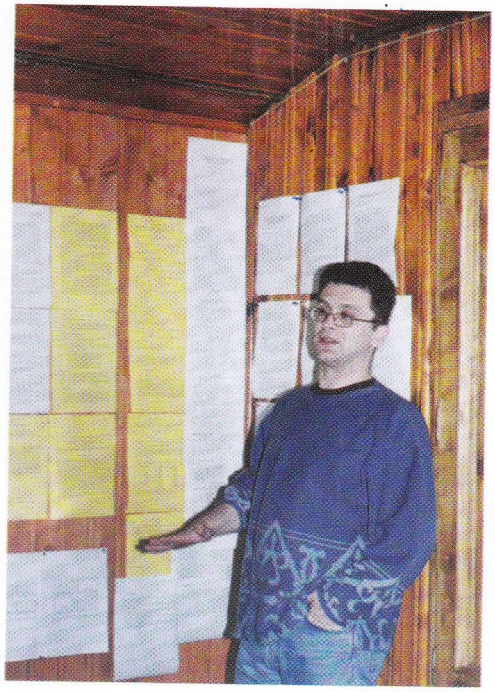

Fig. 21. Zoran Simić.

Fig. 22. Zorica Cvetković.

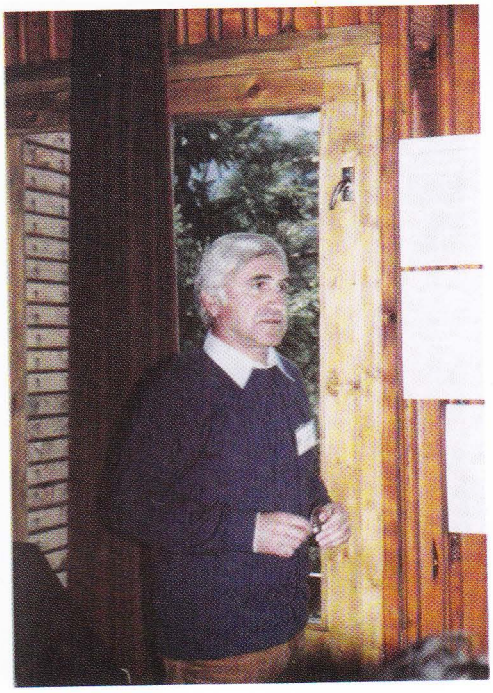

Fig. 23. Konstantin Stavrev.

Fig. 24. Maria Dimitrova.

Fig. 25. Daniela Andreeva.

Fig. 26. Jordanka Borisova.

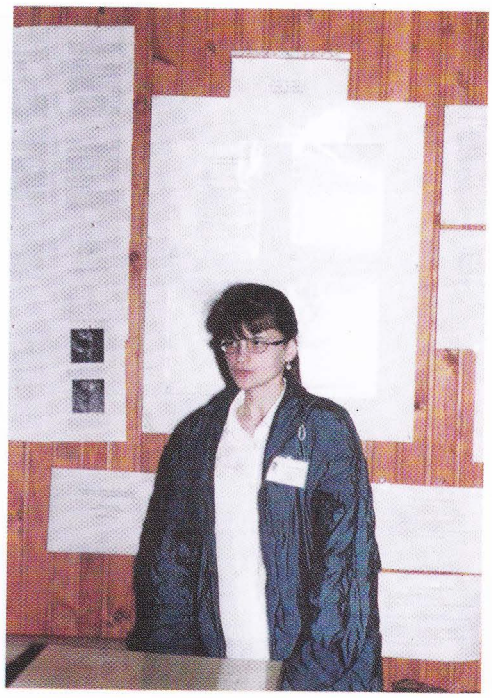

Fig. 27. Krasimira Iankova.

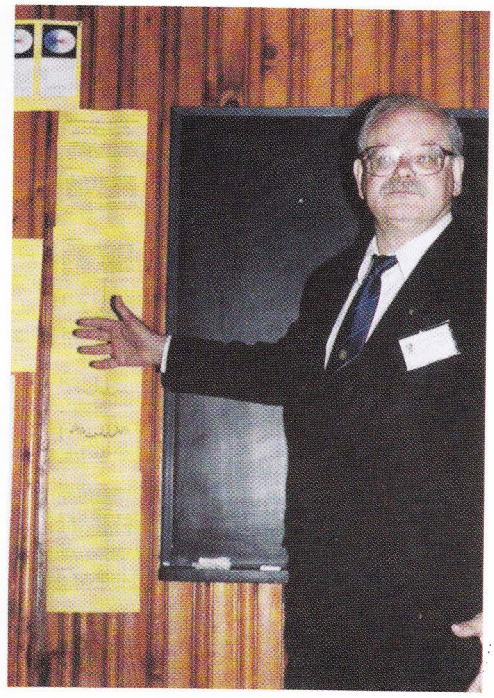

Fig. 28. Milan S. Dimitrijević.

Fig. 29. Valeri Golev, Ani Lukarska, Hristo Lukarski.

Fig. 30. Georgi Ivanov, Vladimir Shkodrov.

Fig. 31. First row: Vladan Čelebanović, Renada Antova, Ana Borisova, Katja Tsvetkova.

Fig. 32. Institute of Space Research. 15. 05. 2002. Petar Getsov, Milan S. Dimitrijević, Miodrag Dačić.

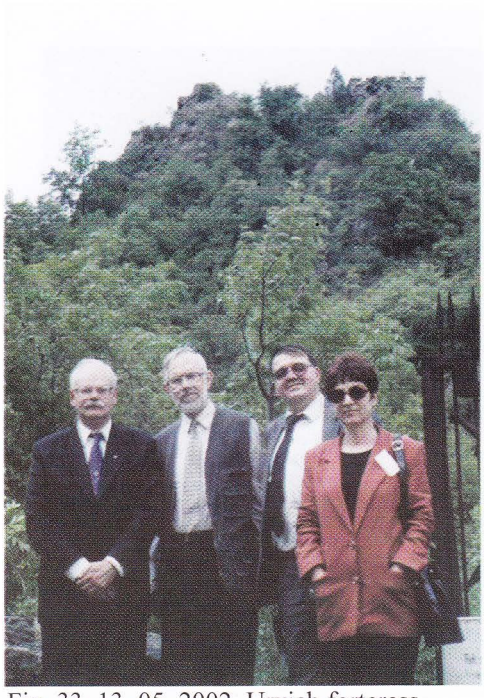

Fig. 33. 13. 05. 2002. Urvich forteress. Milan S. Dimitrijević, Georgi Ivanov, Miltcho Tsvetkov, Katja Tcvetkova.

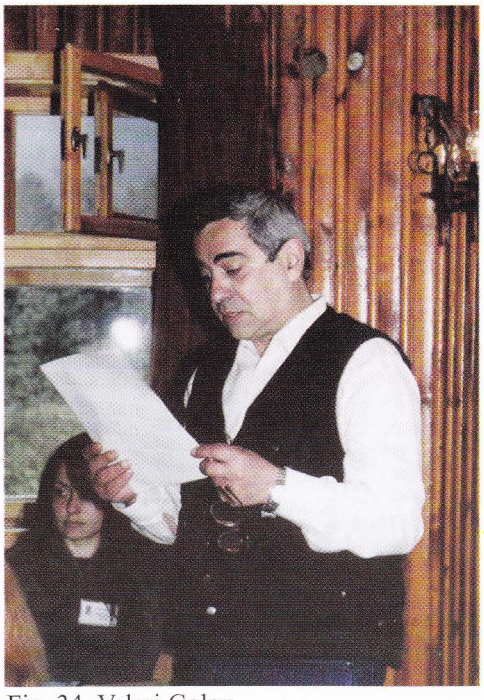

Fig. 34. Valeri Golev.

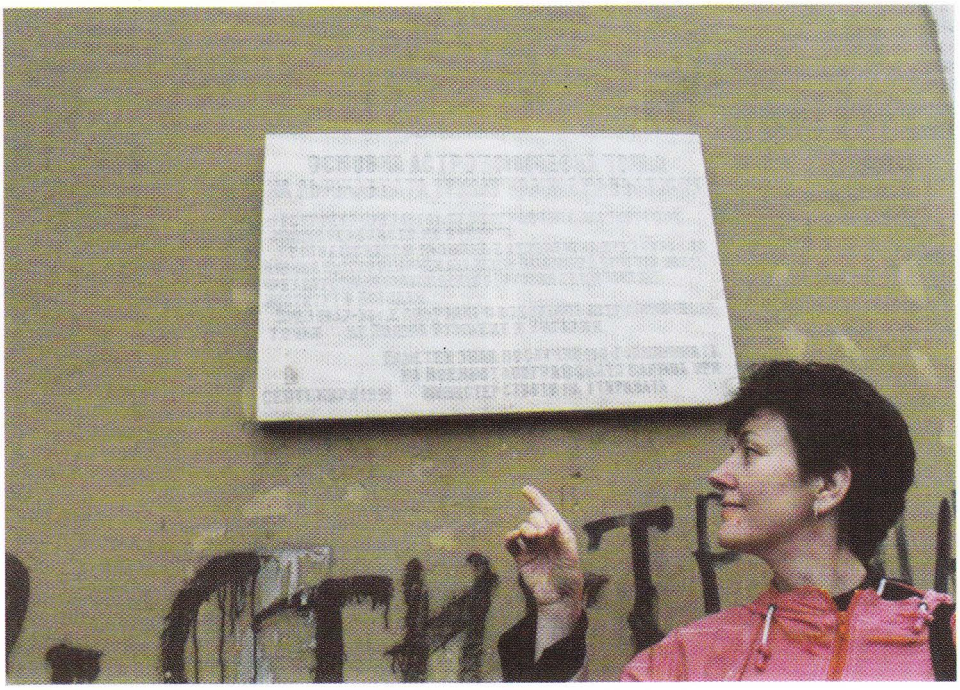

Fig. 35. Sofia 13.05.2002. Basic astronomical point of the state triangulation of Bulgaria. Zorica Cvetković.

Fig. 36. Sofia Astronomical Observatory.

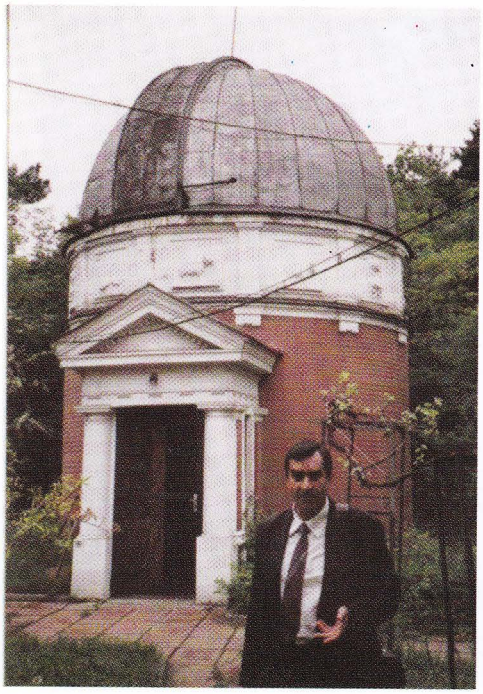

Fig. 37. Sofia Astronomical Observatory. 13. 05. 2002. Miodrag Dačić.

Fig. 38. Sofia Astronomical Observatory. 13.05. 2002. Edi Bon.

Fig. 39. Vladimir Shkodrov, Vojislava Protić-Benišek.

CIP – Каталогизација у публикацији
Народна библиотека Србије, Београд

520/524 (063) (082)
521–355 (063) (082)

BULGARIAN-Serbian Astronomical Meeting (3 ; 2002 : Gjolechitsa)
Proceedings of the Third Bulgarian-Serbian Astronomical Meeting, May 13-15, 2002, Gjolechitsa, Bulgaria / edited by G. [Georgi] Ivanov, M. [Milan] S. Dimitrijević and P. [Predrag] Jovanović. - Београд : Astronomical Observatory, 2003 (Belgrade : INKA). - 286 str., [16] listova s tablama : ilustr. ; 24 cm. - (Публикације Астрономске опсерваторије у Београду : св. 73 = Publications of the Astronomical Observatory of Belgrade, ISSN 0373-3742 ; no. 73)

Tekst na engl. i bug. jeziku. - Tiraž 300.
- Bibliografija uz svaki rad.

ISBN 86-80019-01-1
1. Ivanov, Georgi
a) Астрономија - Зборници b) Astrofizika - Zbornici
COBISS.SR-ID 105052172